AFRRI REPORTS

October
November
December

1986

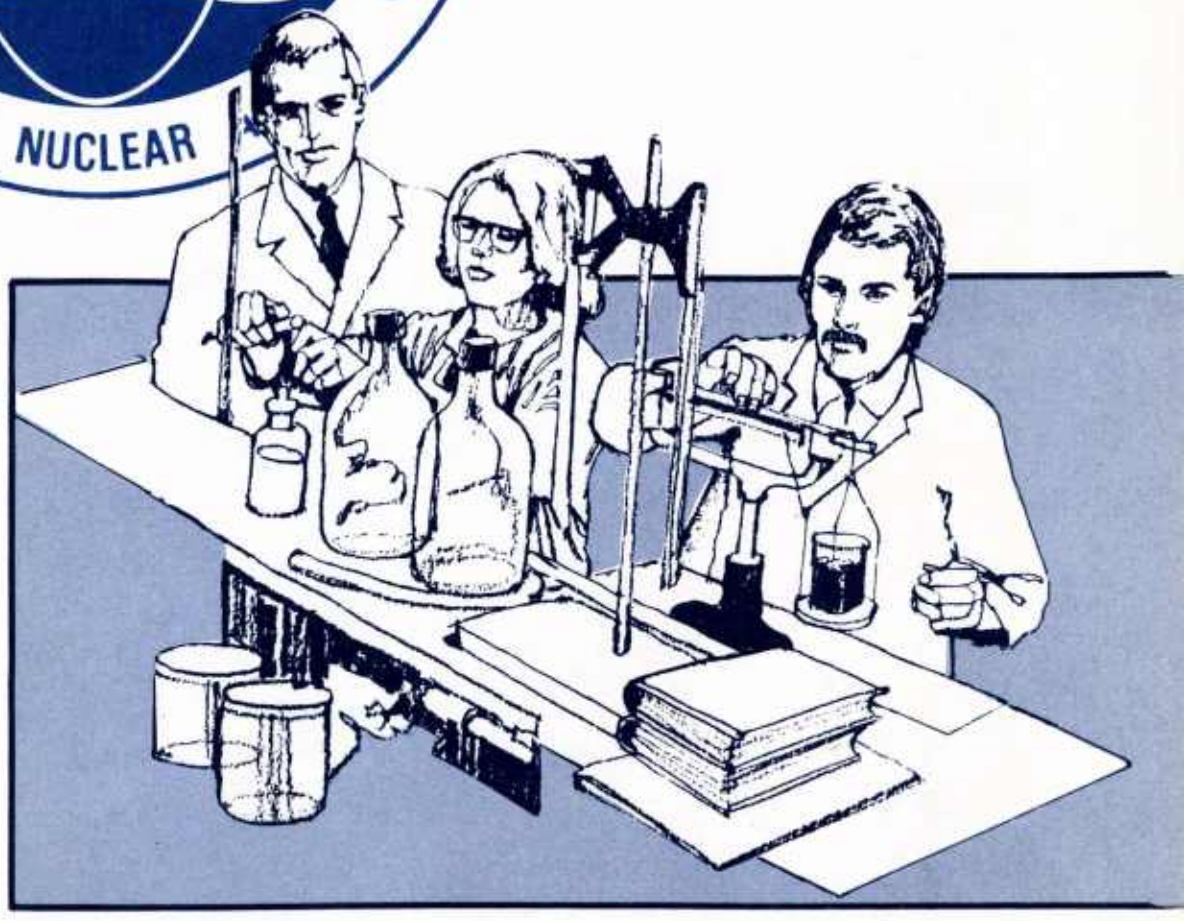

Defense Nuclear Agency

Armed Forces Radiobiology Research Institute

Bethesda, Md 20814-5145

DISTRIBUTION LIST UPDATE

This mailer is provided to enable DNA to maintain current distribution lists for reports. We would appreciate your providing the requested information.

☐ Add the individual listed to your distribution list.

☐ Delete the cited organization/individual.

☐ Change of address.

NAME: _____

ORGANIZATION: _____

OLD ADDRESS	CURRENT ADDRESS
_____	_____
_____	_____
_____	_____

TELEPHONE NUMBER: ( ) _____

SUBJECT AREA(s) OF INTEREST:

_____ _____

_____ _____

_____ _____

DNA OR OTHER GOVERNMENT CONTRACT NUMBER: _____

CERTIFICATION OF NEED-TO-KNOW BY GOVERNMENT SPONSOR (if other than DNA):

SPONSORING ORGANIZATION: _____

CONTRACTING OFFICER OR REPRESENTATIVE: _____

SIGNATURE: _____

CUT HERE AND RETURN

Director
Defense Nuclear Agency
ATTN: [redacted] TITL
Washington, DC 20305-1000

Director
Defense Nuclear Agency
ATTN: [redacted] TITL
Washington, DC 20305-1000

UNCLASSIFIED

SECURITY CLASSIFICATION OF THIS PAGE

REPORT DOCUMENTATION PAGE

1a. REPORT SECURITY CLASSIFICATION UNCLASSIFIED	1b. RESTRICTIVE MARKINGS
2a. SECURITY CLASSIFICATION AUTHORITY	3. DISTRIBUTION/AVAILABILITY OF REPORT Approved for public release; distribution unlimited.
2b. DECLASSIFICATION/DOWNGRADING SCHEDULE	
4. PERFORMING ORGANIZATION REPORT NUMBER(S) SR86-34 through SR86-52, and TR86-3	5. MONITORING ORGANIZATION REPORT NUMBER(S)
6a. NAME OF PERFORMING ORGANIZATION Armed Forces Radiobiology Research Institute 6b. OFFICE SYMBOL (If applicable) AFRRI	7a. NAME OF MONITORING ORGANIZATION
6c. ADDRESS (City, State and ZIP Code) Defense Nuclear Agency Bethesda, Maryland 20814-5145	7b. ADDRESS (City, State and ZIP Code)
8a. NAME OF FUNDING/SPONSORING ORGANIZATION Defense Nuclear Agency 8b. OFFICE SYMBOL (If applicable) DNA	9. PROCUREMENT INSTRUMENT IDENTIFICATION NUMBER
8c. ADDRESS (City, State and ZIP Code) Washington, DC 20305	10. SOURCE OF FUNDING NOS. PROGRAM ELEMENT NO. / PROJECT NO. / TASK NO. / WORK UNIT NO.
11. TITLE (Include Security Classification) AFRRI Reports Oct-Dec 1986	
12. PERSONAL AUTHOR(S)	
13a. TYPE OF REPORT Reprints/Technical 13b. TIME COVERED FROM _____ TO _____	14. DATE OF REPORT (Yr., Mo., Day) 15. PAGE COUNT 101
16. SUPPLEMENTARY NOTATION	
17. COSATI CODES FIELD / GROUP / SUB. GR.	18. SUBJECT TERMS (Continue on reverse if necessary and identify by block number) N/A

19. ABSTRACT (Continue on reverse if necessary and identify by block number)

This volume contains AFRRI Scientific Reports SR86-34 through SR86-52, and Technical Report TR86-3 for Oct-Dec 1986.

20. DISTRIBUTION/AVAILABILITY OF ABSTRACT UNCLASSIFIED/UNLIMITED ☐ SAME AS RPT. ☐ DTIC USERS ☐	21. ABSTRACT SECURITY CLASSIFICATION UNCLASSIFIED
22a. NAME OF RESPONSIBLE INDIVIDUAL Junith A. Van Deusen	22b. TELEPHONE NUMBER (Include Area Code) (202)295-3536 22c. OFFICE SYMBOL ISDP

DD FORM 1473, 83 APR EDITION OF 1 JAN 73 IS OBSOLETE.

UNCLASSIFIED

SECURITY CLASSIFICATION OF THIS PAGE

CONTENTS

Scientific Reports

SR86-48: Shea-Donohue, T., Steel, L., Montcalm, E., and Dubois, A. Gastric protection by sucralfate.

SR86-49: Steel, L. K., Rafferty, M. A., Wolfe, W. W., Egan, J. E., Kennedy, D. A., Catravas, G. N., Jackson, W. E., III, and Dooley, M. A. Urinary excretion of cyclic nucleotides, creatinine prostaglandin E_2 and thromboxane B_2 from mice exposed to whole-body irradiation from an enhanced neutron field.

SR86-50: Swaja, R. E., Oyan, R., Sims, C. S., and Dooley, M. A. Performance characteristics of a high-level solid-state personnel dosimetry system in pulsed radiation environments.

SR86-51: Walden, T. L., Jr., Holahan, E. V., Jr., and Catravas, G. N. Development of a model system to study leukotriene-induced modification of radiation sensitivity in mammalian cells.

SR86-52: Yang, G. L., and Swenberg, C. E. Stochastic models for cells exposed to ionizing radiation.

Technical Report

TR86-3: Dooley, M., Goodman, L. J., Zeman, G. H., Schwartz, R. B., Eisenhauer, C. M., and Blake, P. K. Ionization chamber intercomparison in mixed neutron and gamma-ray radiation fields by National Bureau of Standards and Armed Forces Radiobiology Research Institute. Armed Forces Radiobiology Research Institute, Bethesda, MD, 1986.

INT. J. RADIAT. BIOL., 1986, VOL. 50, NO. 5, 789–793

Rapid communication

Neutron-induced free radicals in oriented DNA

CARMEN M. ARROYO, ALASDAIR J. CARMICHAEL, CHARLES E. SWENBERG and LAWRENCE S. MYERS, JR

Physical Radiobiology Division, Radiation Sciences Department, Armed Forces Radiobiology Research Institute, Bethesda, Maryland 20814-5145, U.S.A.

Samples of oriented DNA containing 30 per cent water were irradiated with neutrons at 77 K. The electron spin resonance (e.s.r.) spectra obtained from these irradiated DNA samples show that the formation of radicals is different when the incident neutrons are parallel or perpendicular to the DNA helix. When the incident neutrons are perpendicular to the DNA helix the e.s.r. spectra of thymine and guanine ionic radicals (T^-, G^+) are observed. An additional e.s.r. spectrum corresponding to the hydrogen addition radical on thymine ($TH^\cdot$) is observed when the incident neutrons are parallel to DNA helix. The $TH^\cdot$ radical appears to be formed by protonation of T^-.

Indexing terms: oriented DNA, neutron radiation, electron spin resonance.

Electron spin resonance (e.s.r.) of solid-state oriented deoxyribonucleic acid (DNA) irradiated with neutrons is of interest because it offers, at low temperatures, an opportunity to study structural features of the free radicals formed in oriented macromolecular samples. In addition, it provides further information about the mechanism of radiation damage in living systems.

In previous studies, e.s.r. spectroscopy has been applied to observe the effects of γ- and u.v.-radiation on oriented DNA fibres (Gräslund *et al.* 1971, 1979, Hütterman *et al.* 1984). With u.v.-(300 ± 10 nm) and γ-radiation, a mixture of anionic free radicals on thymine (T^-) and cationic free radicals on guanine (G^+) has been reported. The e.s.r. spectra obtained in those studies depended on the orientation (parallel or perpendicular) of the fibres in the magnetic field. However, when the full u.v. spectrum is used to irradiate the oriented DNA fibres, an eight-line e.s.r. spectrum is observed in addition to the T^- and G^+ ionic bases. This additional e.s.r. spectrum corresponds to the hydrogen addition radical on thymine ($TH^\cdot$). The e.s.r. spectrum of $TH^\cdot$ is nearly isotropic (Dûlcić and Herak 1972).

In the present study, the effect of neutron irradiation on oriented DNA is reported. The results obtained are the first to show that the formation of radicals depends on the orientation of the DNA helix with respect to the incident radiation.

Oriented DNA fibres were prepared using the wet spinning technique developed by Rupprecht (1966, 1970a, b, 1979). In this method, highly polymerized calf thymus DNA (Sigma Chemical Co.) was dissolved (1 mg/ml) in a 0·4 mol dm^{-3} sodium chloride solution. This DNA solution was then passed through a spinneret into a column containing ethanol (73 per cent) and 0·4 mol dm^{-3} NaCl as a precipitating medium. The oriented fibres flow down the column and are converged by a V-shaped guide forming a film on a rotating Teflon-coated cylinder. After

drying over silica gel the films are folded into $10 \times 2 \times 2$ mm packages and equilibrated in an atmosphere containing 75 per cent relative humidity. In order to verify the reliability of our DNA samples, DNA packages provided by Dr Allan Rupprecht at the University of Stockholm were irradiated with neutrons as controls. The e.s.r. results obtained were identical. Birefringence, u.v. dichroism and X-ray diffraction studies in the control packages indicate that the DNA helical axis is oriented along the fibre axis (Gräslund *et al.* 1978). Other control experiments included the irradiation at 77 K of unoriented DNA packages identical in size and shape to the oriented DNA packages. For each irradiation, two DNA packages were transferred to a foam dewar containing liquid nitrogen, one with the DNA fibres oriented parallel and the other with the fibres perpendicular to the direction of the incident neutrons. The experiment was repeated several times, each time giving identical results. Irradiations were carried out with the TRIGA† Mark F pool type nuclear research reactor, within a cadmium–gadolinium lined exposure room designed to minimize thermal neutron fluence. Blocks of metallic bismuth surrounding the foam dewar degraded the fission neutron spectrum and attenuated the fission γ-rays. Less than 3 per cent of the dose is due to γ-contamination. A dose of 15 kGy measured using indium foils of similar size to the DNA package was delivered at a dose rate of 0·4 kGy/min. E.s.r. spectra were recorded on a Varian E-9 X-band spectrometer equipped with a E-231 rectangular cavity and at 100 kHz magnetic field modulation. The e.s.r. spectra remain virtually unchanged with the orientation of the irradiated fibres in the magnetic field and with a microwave power as low as 10 μW.

It is evident from the figure that the effect of neutron irradiation on oriented DNA fibres is different when the incident neutrons are perpendicular to the fibres or parallel to them. Figure (*a*) shows the e.s.r. spectra obtained at 77 K following neutron irradiation in the direction perpendicular to the DNA fibres. These spectra are similar to those previously attributed to $T^{\dagger}$ and $G^{\ddagger}$ (Gräslund *et al.* 1971, 1979, Hütterman *et al.* 1984). Furthermore, similar to the e.s.r. spectra obtained following γ- and 300 nm u.v.-irradiation of the fibres (Gräslund *et al.* 1971, 1979), the spectra in figure (*a*) show a magnetic field orientation dependence. When the irradiation was carried out with incident neutrons in a direction parallel to the fibres (figure (*b*)), six of the eight hyperfine lines corresponding to the TH· are observed in addition to the suggested $T^{\dagger}$ and $G^{\ddagger}$ (Shulman *et al.* 1966).

Fast neutrons interact principally by elastic collisions with nuclei in the matter. Energy is most effectively transferred to the lighter nuclei, so that in hydrogenous materials (45 per cent H for the oriented DNA package) the most important process is the ejection of fast protons. These recoil protons are scattered in all possible angles (θ) with respect to the direction of the incident neutrons with their initial energy given by $E_n \cos^2 \theta$, where E_n is the neutron energy. Therefore, the chemical reactions that occur after fast neutron irradiation are induced by high energy protons which interact with molecules causing excitation and ionization. These interactions are largest along the direction of the incident neutrons.

U.v. photolysis at 77 K and temperature-dependent studies following u.v.- and γ-irradiation of the DNA packages, indicate that TH· is a secondary radical generated by protonation of $T^{\dagger}$ (Gräslund *et al.* 1971, 1979, Hüttermann *et al.* 1984). Although in neutron irradiation of the oriented DNA fibres TH· may be formed by

† Training Research and Isotope Production General Atomic Reactor.

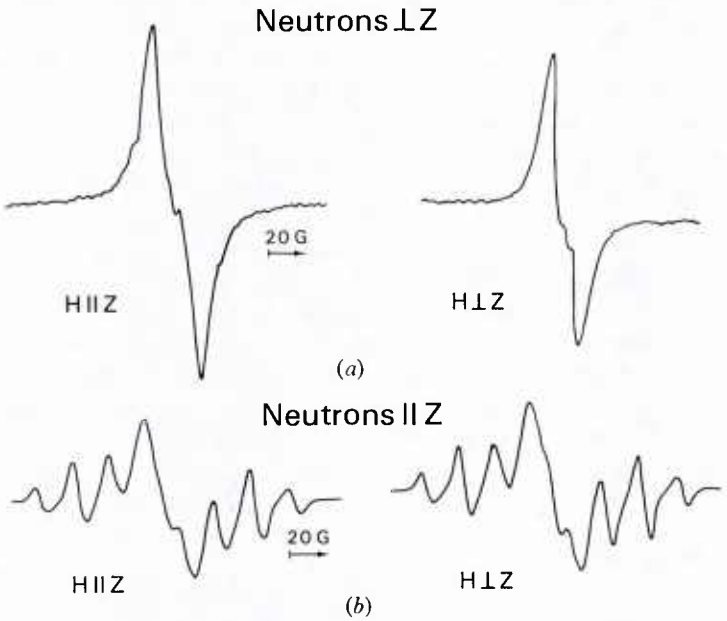

E.s.r. spectra at 77 K of neutron-induced free radical in an oriented NaDNA sample containing 30 per cent H_2O. The spectra were recorded with the magnetic field (H) of the spectrometer parallel and perpendicular to the fibre Z axis (or DNA helix) of the sample. Irradiation conditions: (*a*) incident neutrons perpendicular to the fibre Z or helix axis; (*b*) incident neutrons parallel to the fibre Z or helix axis. E.s.r. spectrometer was set at: magnetic field, 3350 G; microwave power for (*a*) 20 μW and (*b*) 0·2 mW; receiver gain for (*a*) $1{\cdot}25 \times 10^4$ and for (*b*) $2{\cdot}5 \times 10^3$.

the direct addition of a hydrogen atom to thymine, this mechanism is unlikely because hydrogen atoms would also react with other bases and the products of these reactions should be observed by e.s.r.. However, none of these products are observed in the e.s.r. spectra in the figure. Therefore, the results shown in the figure suggest that the production of $TH^{\cdot}$ occurs via proton addition to T^{-} radicals. This conclusion is supported by the observation that under the same conditions, the central portion of the e.s.r. spectrum (figure (*b*)) containing the $TH^{\cdot}$ radical is reduced by a factor of approximately 10 suggesting that the $TH^{\cdot}$ radicals originate from T^{-}.

It is of interest to compare the amount of radicals observed following neutron irradiation perpendicular to the DNA helix with those produced by neutron irradiation parallel to the DNA helix. Double integration of the first derivative e.s.r. spectra under the same conditions indicates that the amount of radicals formed are different for either neutron irradiation direction. The amount of radicals observed is lower by a factor of three when the incident neutrons are parallel to the DNA helix. It is possible that the observed difference in radical yields, for neutron irradiations parallel and perpendiculat to the DNA helix, is a consequence of differences in the macroscopic arrangement of both samples during irradiation. However, results obtained from control experiments suggest that this is unlikely. In these experiments packages of unoriented DNA, with identical size and shape to the oriented ones, were irradiated with neutrons at 77 K and their e.s.r. spectra were recorded. During irradiation, the control samples were placed in the same positions as the oriented

DNA packages with respect to the incident neutrons. Double integration of the e.s.r. spectra showed no significant differences in the area under the e.s.r. peaks and thus in free radical yield. The e.s.r. spectra of the irradiated unoriented DNA packages are similar to those shown in figure (*a*). One explanation for this observation is that for randomly oriented DNA, the neutron interactions will not occur for a sufficient distance along the DNA helix, and therefore will not produce the same effect as the neutron irradiation strictly parallel to the DNA helix (figure (*b*)).

There are two important differences in the effects produced by neutron irradiation of DNA: (1) the observed radicals are substantially less for neutron irradiation parallel versus irradiation perpendicular to the helix; and (2) the formation of $TH^{\cdot}$ occurs only when the incident neutrons are parallel to the DNA helix. A possible explanation for the observed decrease in the amount of radicals could be ion recombination (charge annihilation). High l.e.t. radiation, such as the neutron irradiation described in this work, generates multiple excitations and ionizations in the DNA molecules. However, when the neutrons pass through the stacked bases, i.e. parallel to the DNA helices, multiple ionizations close to one another may occur along each DNA molecule. The proximity of the ionizations would facilitate ion recombination, therefore, lowering the total number of radicals observed. On the other hand, an explanation for the substantially larger number of radicals observed when the incident neutrons are perpendicular to the DNA helices, is that the ionizations will be produced on different DNA molecules along the neutron paths, making it difficult for ion recombination to occur. It is also possible in this case that the ionizations occurring on the same DNA molecule are separated sufficiently to prevent their recombination.

Ion recombination can also account for the formation of $TH^{\cdot}$. It is known that ion recombination produces singlet and triplet states (Fielden and Lillicrap 1970–72), however, Buck (1960) has postulated that this process predominantly generates triplet states. Shulman and Rahn (1966) have suggested that triplet excitation can migrate through the DNA chain to the base with the lowest triplet state (thymine). Assuming this to be the case, the triplet excitation generated by ion recombination could be transferred to T^{-} giving T^{-} of sufficient energy to be protonated forming $TH^{\cdot}$. Consistent with this mechanism is the production of $TH^{\cdot}$ via protonation of T^{-} in model systems and in oriented DNA fibres by u.v. photoexcitation at 77 K (Gräslund *et al.* 1979, Sevilla *et al.* 1976).

In conclusion, ion recombination and migration of the resulting triplet excitation to T^{-} forming $TH^{\cdot}$ is consistent with the observed differences between neutron irradiation parallel and perpendicular to the DNA helix. The observation of a lower amount of radicals and of $TH^{\cdot}$ only when the incident neutrons are parallel to the DNA helix, indicates that the magnitude of damage to the target depends on the angle at which the incident particles pass through it. In addition, it suggests that high l.e.t. damage *in vivo* depends on the incident angle with respect to the helix axis of DNA.

Acknowledgment

The authors wish to thank Dr Allan Rupprecht from the University of Stockholm, Sweden for kindly providing samples of DNA packages and Dr Michael Sevilla, Oakland University, Rochester, Michigan for helpful discussions. We also would like to thank the AFRRI Reactor Staff and Dosimetry Staff for their cooperation in the radiation experiments.

References

BUCK, W. L., 1960, The origin of scintillations in organic materials. *IRE Transaction on Nuclear Science*, **7**, 11–16.

DÛLCIĆ, A., and HERAK, J. N., 1972, Radiation abstraction of hydrogen atoms in single crystals of thymine. *Journal of Chemical Physics*, **57**, 2537–2540.

FIELDEN, E. M., and LILLICRAP, S. C., 1970–72, Excited states and energy transfer in biomolecular systems. *Current Topics in Radiation Research Quarterly*, **7**, 133–180.

GRÄSLUND, A., EHRENBERG, A., RUPPRECHT, A., and STRÖM, G., 1971, Ionic base radicals in γ-irradiated DNA. *Biochimica et Biophysica Acta*, **254**, 172–186.

GRÄSLUND, A., EHRENBERG, A., RUPPRECHT, A., and STRÖM, G., 1979, U.v.-induced free radicals in oriented DNA. *Photochemistry and Photobiology*, **29**, 245–251.

GRÄSLUND, A., RUPPRECHT, A., and EHRENBERG, A., 1978, Structure of radicals from nucleic acids. *Effects of Ionizing Radiation on DNA, Physical, Chemical and Biological Aspects*, edited by J. Huttermann, W. Kohnlein and R. Teoule (Berlin: Springer-Verlag), pp. 71–79.

HÜTTERMANN, J., VOIT, K., OLOFF, H., KOHNLEIN, W., GRÄSLUND, A., and RUPPRECHT, A., 1984, Specific formation of electron gain and loss centres in X-irradiated oriented fibres of DNA at low temperatures. *Faraday Discussions Chemical Society*, **78**, 135–149.

RUPPRECHT, A., 1966, Preparation of oriented DNA by wet spinning. *Acta Chemica Scandinavica*, **20**, 494–504.

RUPPRECHT, A., 1970 a, A wet spinning apparatus and auxillary equipment suitable for preparing samples of oriented DNA. *Biotechnology and Bioengineering*, **12**, 93–121.

RUPPRECHT, A., 1970 b, Preparation by wet spinning of oriented DNA films for polarized infrared study. *Biochimica et Biophysica Acta*, **199**, 277–280.

RUPPRECHT, A., 1979, Wet spinning of hyaluronic acid preparation of oriented samples. *Acta Chemica Scandinavica*, **B33**, 779–780.

SEVILLA, M. D., FAILOR, R., CLARK, C., HOLROYD, R. A., and PETTEI, M., 1976, Electron transfer in dinucleoside phosphate anions. *Journal of Physical Chemistry*, **80**, 353–358.

SHULMAN, R. G., RAHN, R. O., PERSHAN, P. S., LONGWORTH, J. W., and EISINGER, J., 1966, Electron spin resonance of irradiated deoxyribonucleic acid. *Electron Spin Resonance and the Effects of Radiation on Biological Systems*, edited by W. Snipes (Washington, D.C.: National Academy of Sciences–National Research Council), pp. 46–80.

SHULMAN, R. G., and RAHN, R. O., 1966, Electron spin resonance of the excited triplet states of pyrimidines and purines. *Journal of Chemical Physics*, **45**, 2940–2949.

References

BUCK, W. L., 1960, The origin of scintillations in organic materials. *IRE Transaction on Nuclear Science*, **7**, 11–16.

DÛLCIĆ, A., and HERAK, J. N., 1972, Radiation abstraction of hydrogen atoms in single crystals of thymine. *Journal of Chemical Physics*, **57**, 2537–2540.

FIELDEN, E. M., and LILLICRAP, S. C., 1970–72, Excited states and energy transfer in biomolecular systems. *Current Topics in Radiation Research Quarterly*, **7**, 133–180.

GRÄSLUND, A., EHRENBERG, A., RUPPRECHT, A., and STRÖM, G., 1971, Ionic base radicals in γ-irradiated DNA. *Biochimica et Biophysica Acta*, **254**, 172–186.

GRÄSLUND, A., EHRENBERG, A., RUPPRECHT, A., and STRÖM, G., 1979, U.v.-induced free radicals in oriented DNA. *Photochemistry and Photobiology*, **29**, 245–251.

GRÄSLUND, A., RUPPRECHT, A., and EHRENBERG, A., 1978, Structure of radicals from nucleic acids. *Effects of Ionizing Radiation on DNA, Physical, Chemical and Biological Aspects*, edited by J. Huttermann, W. Kohnlein and R. Teoule (Berlin: Springer-Verlag), pp. 71–79.

HÜTTERMANN, J., VOIT, K., OLOFF, H., KOHNLEIN, W., GRÄSLUND, A., and RUPPRECHT, A., 1984, Specific formation of electron gain and loss centres in X-irradiated oriented fibres of DNA at low temperatures. *Faraday Discussions Chemical Society*, **78**, 135–149.

RUPPRECHT, A., 1966, Preparation of oriented DNA by wet spinning. *Acta Chemica Scandinavica*, **20**, 494–504.

RUPPRECHT, A., 1970a, A wet spinning apparatus and auxillary equipment suitable for preparing samples of oriented DNA. *Biotechnology and Bioengineering*, **12**, 93–121.

RUPPRECHT, A., 1970b, Preparation by wet spinning of oriented DNA films for polarized infrared study. *Biochimica et Biophysica Acta*, **199**, 277–280.

RUPPRECHT, A., 1979, Wet spinning of hyaluronic acid preparation of oriented samples. *Acta Chemica Scandinavica*, **B33**, 779–780.

SEVILLA, M. D., FAILOR, R., CLARK, C., HOLROYD, R. A., and PETTEI, M., 1976, Electron transfer in dinucleoside phosphate anions. *Journal of Physical Chemistry*, **80**, 353–358.

SHULMAN, R. G., RAHN, R. O., PERSHAN, P. S., LONGWORTH, J. W., and EISINGER, J., 1966, Electron spin resonance of irradiated deoxyribonucleic acid. *Electron Spin Resonance and the Effects of Radiation on Biological Systems*, edited by W. Snipes (Washington, D.C.: National Academy of Sciences–National Research Council), pp. 46–80.

SHULMAN, R. G., and RAHN, R. O., 1966, Electron spin resonance of the excited triplet states of pyrimidines and purines. *Journal of Chemical Physics*, **45**, 2940–2949.

Vol. 132, No. 1, 1985 BIOCHEMICAL AND BIOPHYSICAL RESEARCH COMMUNICATIONS
October 15, 1985

EVIDENCE OF de novo MEMBRANE GENERATION IN THE MECHANISM OF MAST CELL SECRETORY GRANULE ACTIVATION

Stephen P. Chock* and Elsa A. Schmauder-Chock+

Laboratory of Neurochemistry*, NINCDS, NIH, Bethesda MD. 20892
Dept. of Biology+, The George Washington University, Washington, D.C. 20052
Dept. of Experimental Hematology, Armed Forces Radiobiology Research Institute, Bethesda, MD. 20814

Received August 23, 1985

Summary - Evidence which suggests the occurrence of a rapid new membrane assembly has been observed in the secretory granules of the rat peritoneal mast cell during the early stage of granule activation. The rapid insertion of these newly generated vesicles enables the perigranular membrane of the activated granule to enlarge and expand prior to fusion with the plasma membrane and/or with the neighboring granule membranes. If the newly inserted membrane represents "specialized fusogenic membrane patches", then the presence of de novo membrane generation as an integral step in the mechanism of mast cell granule exocytosis would constitute a fail-safe mechanism in histamine release.

Overwhelming evidence has suggested that granule matrix swelling and the enlargement of the perigranular membrane are early morphological indicators of mast cell granule activation (1-3). Since excess membrane in the form of folds or inclusions has not been observed in the quiescent granule and it is known that membrane cannot stretch beyond 2-3% of its original area (4), it is necessary to consider that new membrane is generated during granule activation. Fusion of this newly generated membrane with the perigranular membrane would enable the granule to expand and the perigranular membrane to lift from the surface of the granule matrix.

By using various ultrastructural techniques, we found that: First, rapid-freezing and freeze-substitution of mast cells reveals the presence of membrane vesicles associated with activated or secreted granules. Second, purified granules after removal of their perigranular membrane can generate membrane vesicles. And third, membrane vesicles and the fusion of these vesicles with the perigranular membrane have been observed using a simultaneous activation, fixation, and membrane enhancement (SAFME) procedure.

0006-291X/85 $1.50

Based on these findings, we proposed that de novo membrane generation can occur as part of the activation process in the mechanism of mast cell granule exocytosis.

MATERIALS AND METHODS

Preparation of mast cells and mast cell granules: Rat peritoneal mast cells were purified according to Sullivan et al. (5) and mast cell granules were purified according to Kruger et al. (6). When perigranular membranes were to be removed, the washed intact granules were sedimented and resuspended in cold deionized water with gentle vortexing. The osmotically lysed granules were then pelleted by centrifugation at 1100xg for 10 min.

Specimen preparation for ultrastructural studies: For routine electron microscopy, samples were fixed in 2.5% glutaraldehyde buffered in 100 mM sodium cacodylate containing 4 mM $MgCl_2$ and osmicated in 1% osmium tetroxide made up in the same buffer. After dehydration the samples were embedded in Epon-812. For rapid-freezing and freeze-substitution, purified mast cells were placed in 7% serum albumin made up in HEPES buffered Hank's balanced salt solution and rapid-frozen and freeze-substituted in acetone containing 4% osmium tetroxide (7). For freeze-fracture, purified granules with their membranes removed, were placed in succeeding concentrations of glycerol to a final concentration of 30%. Following routine sample application procedure, specimens were fractured in a Balzers freeze-etch instrument. The replicas were cleaned in sodium hypochlorite prior to examination.

The SAFME procedure: To achieve simultaneous activation, fixation, and membrane enhancement, mast cells were fixed in 100 mM sodium cacodylate containing 4 mM $MgCl_2$, 0.5 mg/ml saponin, 2 mg/ml tannic acid and 1% glutaraldehyde pH 7 for 30 min at room temperature. After several washings with 100 mM cacodylate buffer the specimens were post-fixed in 1% osmium tetroxide before dehydration and embedding.

RESULTS AND DISCUSSION

Early evidence which suggested that mast cell granules could be the source of the new membrane stemmed from the observation of membranous "blebs" in association with activated granules as well as with purified granules (6,8). Although "blebs" are often considered an artifact of glutaraldehyde fixation, their appearance in activated granules suggests that the granules may have the potential to generate membrane. To avoid glutaraldehyde fixation artifacts, we used rapid-freezing and freeze-substitution techniques to investigate if the granule can indeed serve as the source of new membrane. As shown in Fig. 1, membrane vesicles were found in association with activated and with extruded granules in the absence of glutaraldehyde. This observation supports the concept that the granule can serve as the source of new membrane.

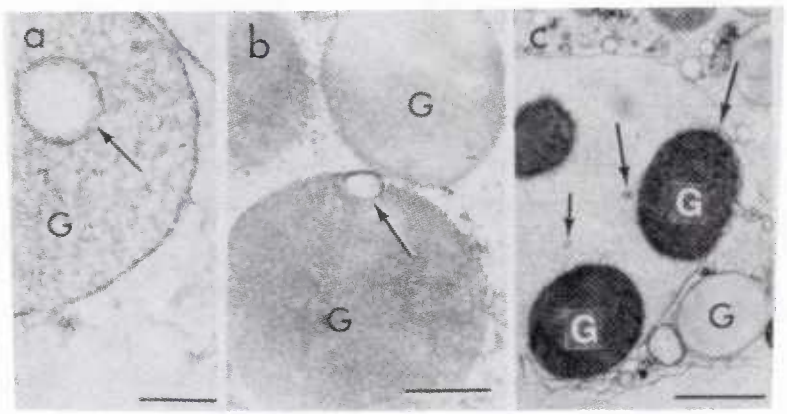

Fig. 1 Vesicles associated with spontaneously activated and released mast cell secretory granules examined using rapid-freezing and freeze-substitution technique. Vesicles (arrows) are found within the granules (G) in an early stage of activation (a and b) and in association with released granules (c). In rapid-freezing, granules in an earlier stage of activation appear less electron-dense than released granules. The bars represent 0.1 micrometer in (a and b) and 1 micrometer in (c).

To further demonstrate that the granule matrix can be the source of new membrane, mast cell granules were purified according to the method of Kruger et al. (6). Perigranular membranes were removed by osmotic shock. Incubation of the demembraned granules in deionized water can result in the formation of bilayer vesicles (referred to as "beads" in ref. 9) at the periphery of the granule matrix or in regions of water infiltration (Fig. 2). When freeze-

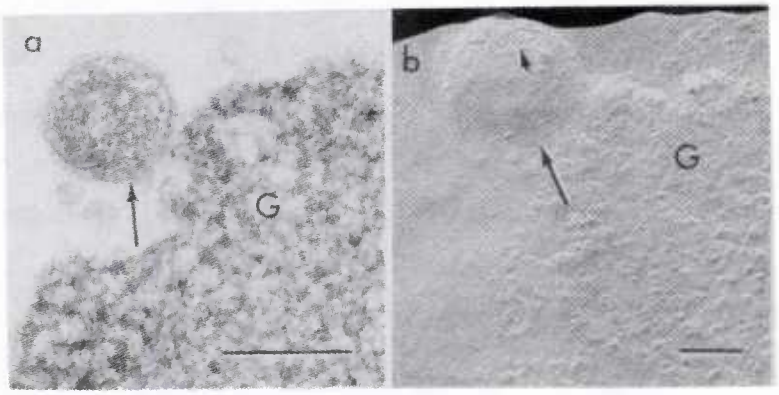

Fig. 2 Purified granules (G), after their membranes have been removed, can generate new membrane in an aqueous environment. (a) Glutaraldehyde-fixed demembraned granule showing the formation of a bilayer bead (arrow) at the periphery of the granule matrix. Frequently electron-dense materials are trapped within the beads. (b) Freeze-fracture of demembraned granule (arrow) reveals a typical bilayer fracture plane (arrowhead) containing no intramembrane particle. The bar represents 0.1 micrometer.

fractured, these newly formed beads showed the typical bilayer fracture plane (Fig. 2b). The absence of intra-membrane protein particles might suggest that the beads are newly formed membrane. During mast cell activation the infiltration of water from the cytoplasm and/or from the nucleus into the granule may result in the rapid formation of bilayer beads in the periphery of the granule matrix situated directly under the perigranular membrane. These newly generated membranes may fuse readily with the perigranular membrane causing it to expand and lift from the granule matrix.

The process of mast cell degranulation has been measured in the millisecond time range (10). The plant glycoside, saponin, was used in low concentration to activate the granules while simultaneously permeabilizing the cells to glutaraldehyde and tannic acid (SAFME procedure). A typical result obtained with the SAFME procedure is shown in Fig. 3. In this figure, membrane vesicles can be seen in the space between the granule matrix and the perigranular membrane. Some appear to be in the process of fusing with the perigranular membrane. These vesicles are not artifacts due to the presence of saponin since their presence has also been observed recently in our laboratory in granules activated by other means and in the absence of saponin. These vesicles may be a product of de novo membrane generation originating from within the granule caused by the activation of the granule by saponin. This interpretation is based on the following reasons. (1) The amorphous and electron-dense quiescent granule can be activated to form membrane vesicles (Fig. 1-3). Thus the granule is capable of serving as the source of the new membrane. (2) There are no observable membrane vesicles congregating outside the granules before or after their activation, suggesting that these membrane vesicles seen in Fig. 3 could not have originated from the cytoplasm. Furthermore, there is no known mechanism by which membrane vesicles can traverse a large membrane and reappear as vesicles on the other side of the membrane. (3) These vesicles shown in Fig. 3 could not have resulted from the process of "granule endocytosis" since the occurrence of such a process would lead to perigranular membrane shrinkage rather than the rapid expansion

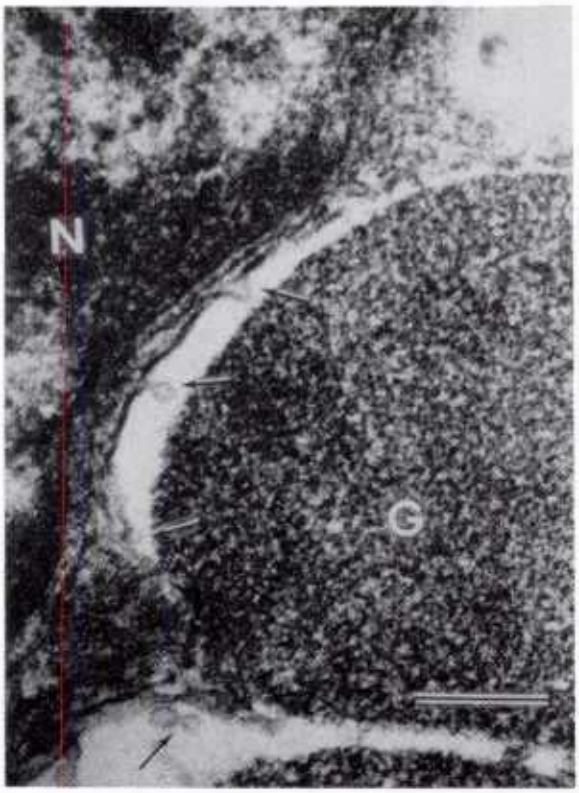

Fig. 3 de novo membrane generation induced by the SAFME procedure. Mast cell granules (G) in early stage of activation are seen near the nucleus (N). Vesicles or beads (arrows) are seen between the perigranular membranes and the granule matrices. Beads in various stages of fusion with the perigranuar membrane can also be seen. The bar represents 0.25 micrometer.

observed following activation. (4) The rapid expansion of the perigranular membrane during granule decondensation, can be accounted for by the fusion of new membrane assembled from membrane precursor elements stored in the granule matrix (9). This entropy-driven process can be very rapid since it does not involve a chemical reaction.

It is not clear if the newly inserted membrane might represent specialized fusogenic membrane patches inserted for the purpose of promoting fusion. If it were so, then the incorporation of the process of de novo membrane generation into the mechanism of secretion would constitute a fail-safe mechanism for secretion. It not only prevents accidental fusion among unactivated quiescent granules, but also assures the success of exocytosis

once the correct activating signal has been received by the granules. Since secretory granules are not known to be able to percolate or move rapidly in the cytoplasmic matrix, it is not clear how an activated granule can come into contact with the plasma membrane in order to form a pore and secrete its contents. The incorporation of the process of de novo membrane generation into the mechanism of secretion, not only enhances the chance of contact between the expanding activated perigranular membrane and the plasma membrane; but it might also assure the success of pore formation.

The evidence presented here is in agreement with the many published observations on mast cell secretion. It is also consistent with our hypothesis that de novo membrane generation occurs as part of the secretory mechanism for the mast cell. It explains how granule swelling and the lifting of the perigranular membrane can occur during exocytosis. The lifting and expansion of the perigranular membrane not only increase the probability of contact between the activated granule and the plasma membrane and/or with the adjacent granules to assure fusion, it can also result in the formation of a large exocytotic cavity to assure rapid washout of the soluble granule mediators. When the expanding perigranular membrane comes into contact with the adjacent granules, the fusion among these granules would result in the formation of a large membrane-lined common cavity before pore formation. This may be the mechanism by which granules activated deep within the cell can be released.

REFERENCES

1. Bloom, G.D. and Haegermark, O. (1965) Exptl. Cell Res. 40, 637-654.
2. Lawson, D., Raff, M.C., Gomperts, B., Fewtrell, C., and Gilula, N.B. (1977) J. Cell Biol. 72, 242-259.
3. Anderson, P., Slorach, S.A., and Uvnas, B. (1973) Acta Physiol. Scand. 88, 359-372.
4 Kwok, R. and Evans, E. (1981) Biophysical J. 35, 637-652.
5. Sullivan, T.J., Parker, K.L., Stenson, W., and Parker, C. (1975) J. Immunol. 114, 1473-1478.
6. Kruger, P.G.,Lagunoff, D.,and Wan, H.(1980) Exptl. Cell Res. 129, 83-93.
7. Heuser, J.E., Reese, T.S., Dennis, M.T., Jan, Y., Jan, L., and Evans, L. (1979) J. Cell Biol. 81, 275-300.
8. Lawson, D. (1980) in Membrane-Membrane Interactions. Gilula, N.B. (ed.) Raven Press, New York. pp 27-44.
9. Chock, S.P. and Chock, E.A. (1985) Fed. Proc. 44, 1324 (534la).
10. Douglas, W.W. (1974) Biochem. Soc. Symp. 39, 1-28.

Life Sciences, Vol. 39, pp. 1543-1547
Printed in the U.S.A.

Pergamon Journals

DOSE DEPENDENT RADIATION-INDUCED HYPOTENSION IN THE CANINE

L. G. Cockerham, J. D. Hampton, and T. F. Doyle

Physiology Department
Armed Forces Radiobiology Research Institute
Bethesda, Maryland 20814-5145

(Received in final form August 1, 1986)

Summary

Radiation-induced early transient incapacitation (ETI) is often accompanied by severe systemic hypotension. However, postradiation hypotension does not occur with equal frequency in all species and is not reported with consistency in the canine. In an attempt to clarify the differences in reported canine postradiation blood pressures, canine systemic blood pressures were determined both before and after exposure to gamma radiation of either 80 Gy or 100 Gy. Data obtained from six sham-radiated beagles and 12 radiated beagles indicated that 100 Gy, whole-body, gamma radiation produced a decrease in systemic mean blood pressure while 80 Gy, whole-body, gamma radiation did not. Analysis of this data could be consistent with a quantal response to a gamma radiation dose between 80 Gy and 100 Gy.

Radiation-induced hypotension has been implicated as the cause of early transient incapacitation (ETI) found with supralethal radiation exposure (1). However, postradiation hypotension does not occur with equal frequency in all species, having been reported to occur in monkeys and rats but not in cats and dogs (1-3). Furthermore, experimental data concerning postradiation hypotension in dogs remains confusing. Dogs exposed to 190 Gy mixed gamma-neutron radiation presented an initial (1-2 min) hypertensive phase followed by a normotensive phase after 30 min postradiation (4). Other investigators (5) found no significant differences in arterial pressure of dogs up to 48 hr following mixed gamma-neutron radiation of 15 Gy. In contrast, Cockerham et al. (6) have reported that dogs, exposed to 100 Gy, ^{60}Co radiation experienced an initial (10-15 min) hypertensive phase followed by a hypotensive phase that showed a 31% decrease below preradiation levels by 90 min postradiation.

This experiment was designed in an attempt to reconcile the differences in reports of postradiation arterial blood pressure in the canine by examining postradiation blood pressure following different dose levels of gamma radiation. A second objective is to determine if the beagle's response to radiation has an "all-or-none" point above which the animal may show a response and below which there is no measureable response.

Methods

Eighteen male beagles (Hazleton Research Animals, Cumberland, VA), 12-15 months old and weighing between 8.5 and 16.6 kg, were used in this study. The animals were divided randomly into three groups of six animals each and treated as follows: Group 1 - sham-radiated or control beagles; Group 2 - beagles exposed to 100 Gy, whole-body radiation; Group 3 - beagles exposed to 80 Gy, whole-body radiation. Food was withheld from all

0024-3205/86 $3.00 + .00

dogs for 16 hr before the experiment, but water was available ad libitum. Research was conducted according to the principles enunciated in the "Guide for the Care and Use of Laboratory Animals" prepared by the Institute of Laboratory Animal Resources, National Research Council and the animals were euthanized humanely with an i.v. injection of saturated $MgSO_4$, 1 hr after radiation.

Approximately 2 hr before radiation or sham-radiation, the animals were weighed and a foreleg was shaved to facilitate administration of anesthetic by intravenous administration of 30 mg/kg sodium pentobarbital (Nembutal). Each dog was intubated with a cuffed endotracheal tube and ventilated using a forced volume respirator to maintain a stable blood pH and oxygen tension. After insertion of the endotracheal tube, each animal was placed on a circulating water blanket to maintain body temperature between 36 and 38°C, measured rectally. A femoral arterial catheter was used to withdraw blood for blood gas determinations and to measure systemic arterial blood pressure using a Statham P23 Db pressure transducer. A systemic venous catheter was used to administer physiological saline to replace withdrawn blood and to administer maintenance doses of anesthetic.

Mean systemic arterial blood pressure (MBP) was measured for 30 min before radiation or sham-radiation and for 60 min after. After 30 min of recording, the animals were disconnected from the respirator and recording apparatus to facilitate radiation in a separate room. After radiation or sham-radiation for controls, the animals were reconnected to the respirator and recording apparatus within 4 min and measurements were continued for 60 min. At 30 and 10 min preradiation or sham-radiation, and at 6, 15, 30, 45, and 60 min postradiation or sham-radiation, blood samples were taken via the arterial catheter to monitor stability of blood pH and oxygen tension and then the respirator was adjusted accordingly. Simultaneously, body temperature was monitored and maintained with the water blanket.

Blood pressure data were grouped into 10 min intervals, measured in relation to midtime of radiation, and plotted at the middle of the interval. The Wilcoxon Rank Sum Test was used to analyze statistically the MBP data. A 95% level of confidence was employed to determine significance. Since all the animals were treated identically before radiation or sham-radiation, and since the preradiation data for the control and test animals showed no significant difference, the preradiation data were combined.

Radiation was accomplished with a bilateral, whole-body exposure to gamma ray photons from a ^{60}Co source located at the Armed Forces Radiobiology Research Institute. Dose rate measurements at depth were made with an ionization chamber placed in a tissue equivalent model. For Group 2 animals exposure was limited to a mean of 1.44 min at 73 Gy/min steady state, free-in-air. The measured midline dose rate was 66 Gy/min, producing a calculated total dose of 100 Gy, considering rise and fall of the radiation source. For Group 3 animals exposure was limited to a mean of 1.26 min at 67 Gy/min steady state, free-in-air. The measured midline dose rate was 60 Gy/min, producing a calculated total dose of 80 Gy, allowing for the rise and fall of the radiation source.

Results

Postradiation mean systemic arterial blood pressure (MBP) for the control animals, after an initial slight decrease, stabilized for the remainder of the experiment (Fig. 1). However, within 10 min postradiation, the 100 Gy radiated animals showed an initial, significant increase followed by a steady, rapid decrease in MBP. The drop in pressure reached its lowest point at the final observation, the 60 min postradiation, a level 48% below the preradiation level. When the data are examined statistically, a significant difference ($p = 0.05$) is noted between the two groups at the 10, 40, 50, and 60 min postradiation times.

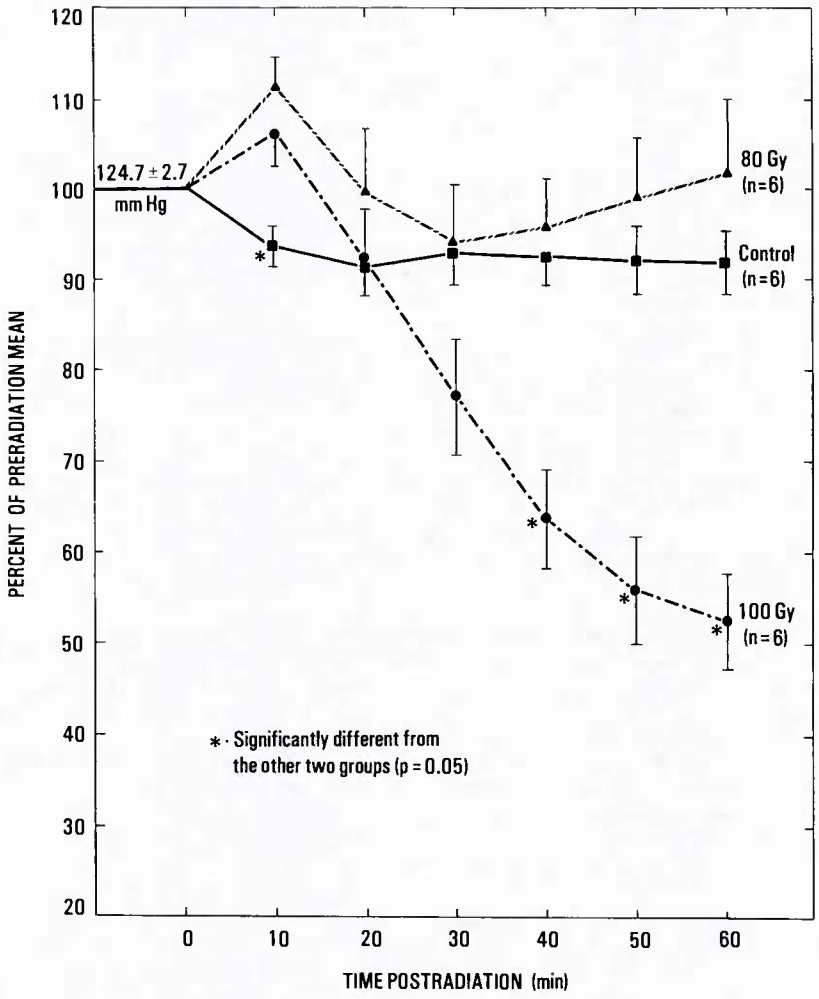

FIG. 1

Canine postradiation mean systemic blood pressure following whole body exposure to ^{60}Co, gamma radiation.

The MBP of the 80 Gy radiated animals showed an even greater increase at 10 min postradiation than did the 100 Gy radiated group. However, this increase was not significantly different from that seen in the 100 Gy radiated group while being significantly different from the control group. At no other time point was the 80 Gy radiated group significantly different from the controls. There were significant differences, however, between the 80 Gy radiated and the 100 Gy radiated animals at the 40, 50, and 60 min postradiation time points.

Discussion

Chaput et al. (2) radiated beagles with pulsed, mixed gamma-neutron radiation varying from 50 to 176 Gy and found that dogs receiving less than 100 Gy continued to perform at or near preradiation levels. Although blood pressure data were not reported in that study, data from this study shows that dogs exposed to 100 Gy, whole-body, gamma radiation displayed hypotension within 1 hr while those receiving less than 100 Gy (80 Gy), did not. Even though one measured parameter does not necessarily corroborate the other, the dose-response relationship of both parameters could be consistent with a quantal or "all-or-none" response for the beagle to a gamma radiation dose between 80 Gy and 100 Gy. Had Chaput et al. reported blood pressure data, a better comparison could be obtained.

The postradiation hypotension found in this experiment does not corroborate results reported by Kabal et al. (5), who showed no significant differences in the mean arterial pressures of radiated (15 Gy) and nonradiated animals at either 48 hr or 72 hr postradiation. This, of course, could be due to a difference of radiation dose and postradiation time of measurement.

However, this study does agree with Tubyfill et al. (4), who reported an initial hypertensive phase followed by a normotensive phase at approximately 20-30 min postradiation. After that point, however, there is some disagreement since this report displays a hypotensive phase from 30 to 60 min postradiation. Tubyfill et al displayed a hypotensive phase from 20 to 60 min, but in the head shielded group only. The other two groups, the unshielded group and the trunk shielded group, were normotensive for this period of time. The investigators offered no explanation of this significant difference nor did they give the dose rate of exposure to mixed gamma-neutron radiations. The difference in radiation (mixed gamma-neutron versus gamma only) and a possible difference in rate of exposure may account for the differences in the report by Tubyfill et al. and this study.

The initial transient hypertensive phase seen in this canine experiment may have been due to the radiation induced elevations in canine plasma histamine levels as reported earlier (7) and implicated in primate postradiation hypotension (8). The elevation of blood pressure rather than a depression may be explained by the histamine-induced release of catecholamines from chromaffin cells of the adrenal medulla, a histamine H1-receptor phenomenon (9-13). The validity of this explanation is further strengthened through the abolishment of this radiation-induced phenomenon by pretreatment with a histamine H1-receptor blocker (14).

Acknowledgements

This work was supported by Armed Forces Radiobiology Research Institute, Defense Nuclear Agency, under research Work Unit MJ 00053. The views presented in this paper are those of the authors; no endorsement by the Defense Nuclear Agency has been given or should be inferred. The authors sincerely thank Mrs. M. H. Owens for preparation of the manuscript.

References

1. D.J. MILETICH and T.A. STRIKE, Scientific Report SR70-1, Armed Forces Radiobiology Research Institute, Bethesda, MD (1970).
2. R.L. CHAPUT, R.T. KOVACIC and E.L. BARRON, Scientific Report SR72-1, Armed Forces Radiobiology Research Institute, Bethesda, MD (1972).
3. T.L. PITCHFORD, Scientific Report SR68-24, Armed Forces Radiobiology Research Institute, Bethesda, MD (1968).
4. D.L. TUBYFILL, J. THORP and D. WISE, Scientific Report SR70-4, Armed Forces radiobiology Research Institute, Bethesda, MD (1970).
5. J. KABAL, S.J. BAUM and L.J. PARKHURST, Radiat. Res. 50 528-538 (1972).

6. L.G. COCKERHAM, T.F. DOYLE, R.B. TRUMBO and J.B. NOLD, Int. J. Radiat. Biol. 45 65-72 (1984a).
7. L.G. COCKERHAM, T.F. DOYLE, M.A. DONLON and E.A. HELGESON, Aviat. Space Eviron. Med. 55 1041-1045 (1984b).
8. W.A. ALTER III, R.N. HAWKINS, G.N. CATRAVAS, T.F. DOYLE and J.K. TAKENAGA, Radiat. Res. 94 654 (1983).
9. J.H. BURN and H.H. DALE, J. Physiol. 61 185-214 (1926).
10. U.S. von EULER, Histamine: Its Chemistry, Metabolism and Physiological and Pharmacological Actions, Handbook of Experimental Pharmacology, Vol. 18, Part 1, p. 318, ed. M. Rocha e Silva, Springer-Verlag, New York (1966).
11. P. NARANJO, Histamine: Its Chemistry, Metabolism and Physiological and Pharmacological Actions, Handbook of Experimental Pharmacology, Vol. 18, Part 1, p. 179, ed. M. Rocha e Silva, Springer-Verlag, New York (1966).
12. S.B. FLYNN, B.M. JOHNSTON and D.A.A. OWEN, Br. J. Pharmac. 61 101-107 (1977).
13. G. BALFAGON, R. GALVAN and E. J. MARCO, J. Pharm. Pharmacol. 36 248-252 (1984).
14. L.G. COCKERHAM, T.F. DOYLE, M.A. DONLON and C.J. GOSSETT-HAGERMAN, Fundam. Appl. Toxicol. 5 597-604 (1985).

Biochem. J. (1986) 235, 531–536 (Printed in Great Britain)

Formation of cytosine glycol and 5,6-dihydroxycytosine in deoxyribonucleic acid on treatment with osmium tetroxide

Miral DIZDAROGLU,* Eric HOLWITT,† Michael P. HAGAN† and William F. BLAKELY†
*Center for Radiation Research, National Bureau of Standards, Gaithersburg, MD 20899, U.S.A., and †Experimental Hematology Department, Armed Forces Radiobiology Research Institute, Bethesda, MD 20814, U.S.A.

OsO_4 selectively forms thymine glycol lesions in DNA. In the past, OsO_4-treated DNA has been used as a substrate in studies of DNA repair utilizing base-excision repair enzymes such as DNA glycosylases. There is, however, no information available on the chemical identity of other OsO_4-induced base lesions in DNA. A complete knowledge of such DNA lesions may be of importance for repair studies. Using a methodology developed recently for characterization of oxidative base damage in DNA, we provide evidence for the formation of cytosine glycol and 5,6-dihydroxycytosine moieties, in addition to thymine glycol, in DNA on treatment with OsO_4. For this purpose, samples of OsO_4-treated DNA were hydrolysed with formic acid, then trimethylsilylated and analysed by capillary gas chromatography–mass spectrometry. In addition to thymine glycol, 5-hydroxyuracil (isobarbituric acid), 5-hydroxycytosine and 5,6-dihydroxyuracil (isodialuric acid or dialuric acid) were identified in OsO_4-treated DNA. It is suggested that 5-hydroxyuracil was formed by formic acid-induced deamination and dehydration of cytosine glycol, which was the actual oxidation product of the cytosine moiety in DNA. 5-Hydroxycytosine obviously resulted from dehydration of cytosine glycol, and 5,6-dihyroxyuracil from deamination of 5,6-dihydroxycytosine. This scheme was supported by the presence of 5-hydroxyuracil, uracil glycol and 5,6-dihydroxyuracil in OsO_4-treated cytosine. Treatment of OsO_4-treated cytosine with formic acid caused the complete conversion of uracil glycol into 5-hydroxyuracil. The implications of these findings relative to studies of DNA repair are discussed.

INTRODUCTION

Oxidative damage to DNA caused by reactive oxygen species, e.g. hydroxyl radicals, unless repaired by cellular repair processes, may have detrimental effects in living cells, such as mutagenesis, carcinogenesis and cell death (Painter, 1980; Ames, 1983; Friedberg, 1984; Cerutti, 1985). Oxidative damage can also be introduced into DNA by reagents such as OsO_4 and $KMnO_4$, which react readily with unsaturated organic compounds to give *cis*-glycols among other products (Hofmann, 1912; Criegee, 1936; Schröder, 1980). Investigations have shown that OsO_4 or $KMnO_4$ react with thymine in oligonucleotides and DNA to form *cis*-thymine glycol (Bayley & Jones, 1959; Burton & Riley, 1966; Beer *et al.*, 1966; Darby *et al.*, 1967; Iida & Hayatsu, 1971; Frenkel *et al.*, 1981). The reactivity of OsO_4 with DNA bases other than thymine has been reported to be minimal or absent (Beer *et al.*, 1966). However, under vigorous conditions, permanganate oxidation of DNA has been reported to lead to some ureido residues of thymine, cytosine and guanine (Bayley & Jones, 1959; Darby *et al.*, 1967). Formation of 5-hydroxy-5-methylbarbituric acid on oxidation of thymine with $KMnO_4$ has also been observed (Iida & Hayatsu, 1970, 1971). The reactions of Os(VIII) reagents with cytosine in the presence of some ligands have been reported to form oxo-Os(VI) esters of uracil (Chang *et al.*, 1981). However, no products from the reaction of OsO_4 with cytosine in DNA have yet been reported.

In the past, the production of altered bases in DNA was initiated in order to provide a suitable substrate for studies of DNA repair. OsO_4 has been used commonly as the chemical reagent of choice in studies of thymine glycol release from DNA by DNA glycosylases (Hariharan & Cerutti, 1974; Gates & Linn, 1977; Nes, 1980; Demple & Linn, 1980; Brent, 1983), on the basis of its selective conversion of thymine in DNA into thymine glycol. Typically, reaction mixtures included OsO_4-treated DNA and either cell extracts or partially purified enzymes. Those studies, however, have been conducted without any information on the possible OsO_4-induced products of DNA bases other than thymine. A complete knowledge of base alterations in OsO_4-treated DNA, in addition to thymine glycol, may be of great importance for the studies of DNA repair that use this reagent as well as other similarly acting oxidative agents in the synthesis of DNA substrates.

The present study was undertaken to elucidate other possible OsO_4-induced products in DNA. For this purpose we employed an assay that has been developed for characterization of oxidative DNA base damage (Dizdaroglu, 1984, 1985). Here we present evidence that cytosine glycol and 5,6-dihydroxycytosine moieties are formed in DNA on treatment with OsO_4.

* To whom correspondence should be addressed.

Abbreviations used: thymine glycol, 5,6-dihydroxy-5,6-dihydrothymine; uracil glycol, 5,6-dihydroxy-5,6-dihydrouracil; cytosine glycol, 5,6-dihydroxy-5,6-dihydrocytosine; g.c.–m.s., gas chromatography–mass spectrometry.

MATERIALS AND METHODS

Materials

Calf thymus DNA, 5-hydroxyuracil (isobarbituric acid), cytosine, 5-methylcytosine, thymine, uracil, bis-(trimethylsilyl)trifluoroacetamide and 5,6-dihydrothymine were purchased from Sigma Chemical Co. Acetonitrile was obtained from Pierce Chemical Co. OsO_4 was purchased from Aldrich Chemical Co. Dialysis membranes (Spectrapor; Arthur H. Thomas Co.) had a reported M_r cut-off of approx. 12000. Water purified through a Millipore system was used for all purposes. 5,6-Dihydroxyuracil (isodialuric acid) was synthesized by oxidation of isobarbituric acid with Br_2 (Behrend & Roosen, 1889). *cis*-Thymine glycol and *cis*-uracil glycol were isolated from OsO_4-treated thymine and uracil respectively by h.p.l.c.

Oxidation of DNA and bases with OsO_4

Numerous variations have been reported in the method for oxidizing DNA with OsO_4. DNA was denatured to react with OsO_4 by using heat (Beer *et al.*, 1966; Hariharan & Cerutti, 1974; Brent, 1983) or alkali (Gates & Linn, 1977; Nes, 1980). After the reaction of OsO_4 with DNA, unused OsO_4 was removed by either freeze-drying or diethyl ether extraction. The protocol employed in this work reflects a general attempt to duplicate the typical methods used for the synthesis of thymine glycol in DNA in several studies of DNA repair.

An aqueous solution of calf thymus DNA (0.4 mg/ml) was extensively dialysed against water and then treated with OsO_4 (2%) at 60 °C for 1 h. The solution, now coloured black, was cooled on ice and centrifuged to remove a precipitate. The supernatant was extracted three times with CCl_4 to remove excess OsO_4, dialysed against water and freeze-dried. For control purposes, a portion of the dialysed DNA solution was mixed with OsO_4, immediately extracted with CCl_4 and dialysed against water.

Thymine, cytosine and uracil were treated with OsO_4 as above, but without dialysis.

Hydrolysis with formic acid

To remove bases from the sugar–phosphate backbone of DNA, 1 mg of each sample was treated with 1 ml of concentrated formic acid (88%) in evacuated and sealed tubes at 150 °C for 30 min. After hydrolysis, samples were dried *in vacuo* in a desiccator before trimethylsilylation. For comparison, samples of OsO_4-treated cytosine were also treated with formic acid in the same manner.

Trimethylsilylation

Samples were trimethylsilylated in Teflon-capped Hypovials (Pierce Chemical Co.) with 0.2 ml of bis (trimethylsilyl)trifluoroacetamide/acetonitrile (1:1, v/v) mixture by heating for 15 min at 130 °C.

G.c.–m.s.

A Hewlett–Packard model 5880A microprocessor-controlled gas chromatograph interfaced to a Hewlett–Packard model 5970A Mass Selective Detector was used. The injection port and interface were both maintained at 250 °C. Separations were carried out by using a fused-silica capillary column (25 m × 0.2 mm internal diam.) coated with cross-linked SE-54 (5% phenylmethylsilicone; film thickness 0.11 μm) (Hewlett–Packard). Helium was used as the carrier gas with a linear velocity of 23.4 cm/s through the column. The split ratio was 10:1. Mass spectra were taken at 70 eV. The temperature of the ion source was approx. 200 °C.

H.p.l.c.

Separations were carried out with a Hewlett–Packard model 1090 microprocessor-controlled liquid chromatograph equipped with a model HP 1040A high-speed spectrophotometric detector and a 10 cm × 0.21 cm Hypersil ODS microbore reversed-phase column (particle size 5 μm; Hewlett–Packard). For semi-preparative separations, a Supelcosil LC-8-DB column (25 cm × 1 cm; particle size 5 μm; Supelco) was used.

RESULTS AND DISCUSSION

DNA samples were hydrolysed with formic acid and subsequently analysed by capillary g.c.–m.s. by using a method described previously (Dizdaroglu, 1985). Fig. 1 shows a total-ion chromatogram obtained from a trimethylsilylated formic acid hydrolysate of OsO_4-treated DNA. Peaks 1–4, 13 and 14 represent the trimethylsilyl derivatives of phosphoric acid, 2-deoxyribose, thymine, cytosine, adenine and guanine respectively. Peak 5 corresponds to the trimethylsilyl derivative of 5-methylcytosine, for which authentic material was available. Calf thymus DNA is known to have a 5-methylcytosine content of about 1.3% (Adams *et al.*, 1981). Peak 7 also represents cytosine but with an additional trimethylsilyl group attached to its amino group, as revealed both by comparison with authentic material and by its mass spectrum. Peaks marked with 'x' were also present in control samples. Peak 10, corresponding to the trimethylsilyl derivative of *cis*-thymine glycol, was verified by the use of authentic material and by comparison of its mass spectrum with previously published data (Dizdaroglu, 1984). *trans*-Thymine glycol was also observed (peak 12 in Fig. 1); however, its presence was due to the partial isomerization of *cis*-thymine glycol by acidic treatment (Iida & Hayatsu, 1970). The isomerization was confirmed in the present work by g.c.–m.s. analysis of formic acid-treated *cis*-thymine glycol. Peak 8 appeared to correspond to a sugar derivative; however, its origin could not be defined.

Peaks 6, 9 and 11 in Fig. 1 represent the trimethylsilyl derivatives of 5-hydroxyuracil (isobarbituric acid), 5-hydroxycytosine and 5,6-dihydroxyuracil (isodialuric acid or dialuric acid) respectively. Of these three, authentic materials were available for isobarbituric acid and isodialuric acid (for the mass spectra of their trimethylsilyl derivatives see Dizdaroglu, 1985). The trimethylsilyl derivative of dialuric acid is known to be identical with that of isodialuric acid as a consequence of enolization (Schuchmann & von Sonntag, 1983). 5-Hydroxycytosine was identified on the basis of the known mass spectrum and gas-chromatographic behaviour of its trimethylsilyl derivative (Dizdaroglu, 1984). The two uracil derivatives discussed above are believed to be derived from some OsO_4-induced products of the cytosine moiety of DNA by acid treatment. For example, it is well known that deamination and dehydration readily occur with the cytosine derivatives saturated at the C-5–C-6 double bond (Green & Cohen, 1957; Evans *et al.*, 1975; Taguchi *et al.*, 1977; Teoule & Cadet, 1978). It is therefore suggested that 5-hydroxyuracil was formed

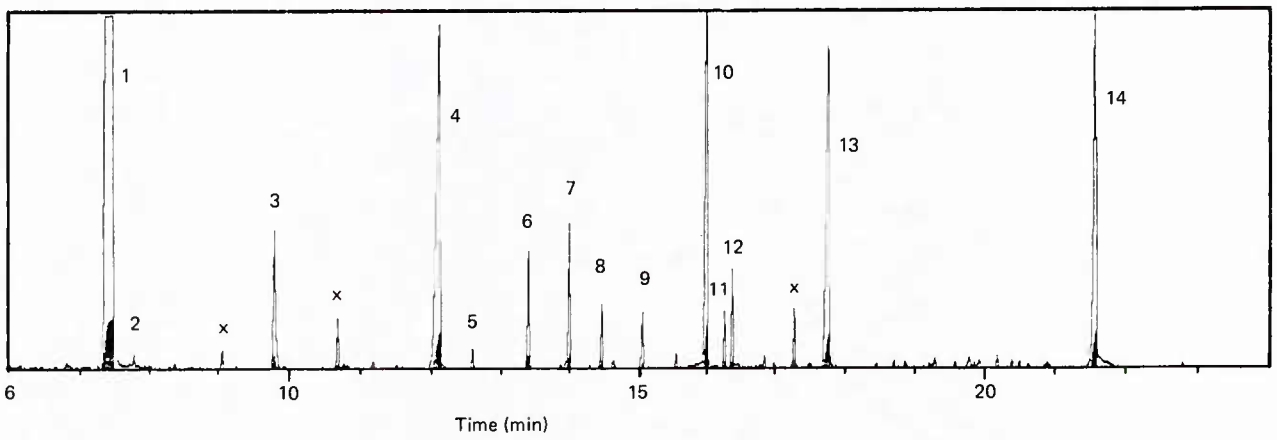

Fig. 1. Total-ion chromatogram obtained from a trimethylsilylated formic acid hydrolysate of OsO_4-treated calf thymus DNA

The column, a fused-silica capillary (25 m × 0.2 mm internal diam.) coated with cross-linked SE-54, was programmed after 3 min at 100 °C from 100 to 250 °C at 7 °C/min. For other details see the Materials and methods section.

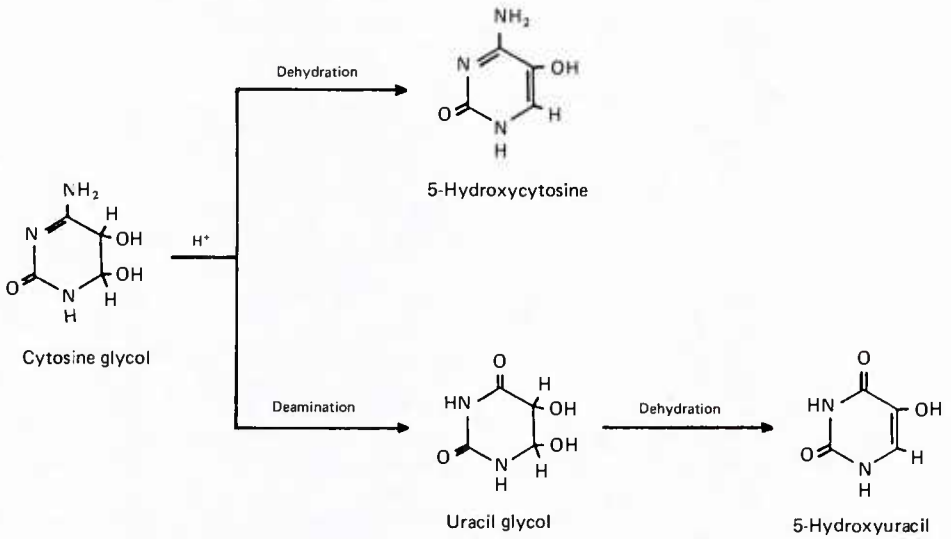

Scheme 1. Acid-induced formation of 5-hydroxycytosine and 5-hydroxyuracil from cytosine glycol

by formic acid-induced deamination and dehydration of cytosine glycol, which was the actual oxidation product of the cytosine moiety of DNA. 5-Hydroxycytosine was most probably the result of the dehydration of the same compound (Scheme 1).

The presence of 5,6-dihydroxyuracil (peak 11 in Fig. 1) can be explained analogously to the formation of 5-hydroxy-5-methylbarbituric acid from thymine on permanganate oxidation (Iida & Hayatsu, 1970, 1971) (Scheme 2). The actual oxidation products of cytosine, i.e. structures (I) and (II), were not observed in DNA. As the calf thymus DNA used in this work did not contain uracil, the uracil derivatives discussed above could not have been formed from uracil in DNA.

In order to support the suggestion that 5-hydroxyuracil and 5,6-dihydroxyuracil were derived from the cytosine moiety of DNA, cytosine was also treated with OsO_4, and analysed by g.c.–m.s. and h.p.l.c. before and after formic acid treatment. Fig. 2 shows a total-ion chromatogram obtained from a sample of OsO_4-treated cytosine after trimethylsilylation. Peaks 1 and 3 represent cytosine, and correspond to peaks 4 and 7 in Fig. 1. Peak 2 represents the trimethylsilyl derivative of 5-hydroxyuracil (as peak 6 in Fig. 1). A mass spectrum taken from peak 4 is illustrated in Fig. 3. A molecular ion ($M^{+\cdot}$) and a characteristic $M-CH_3$ ion were observed at m/z 434 and 419 respectively. This mass spectrum was assigned to the trimethylsilyl derivative of 5,6-dihydroxy-5,6-dihydrouracil (uracil glycol), which shows a fragmentation pattern similar to that of the trimethylsilyl derivative of thymine glycol (for a comparison of the mass spectra see Dizdaroglu, 1984). Authentic uracil glycol was also available, obtained from OsO_4 oxidation of uracil. Since cytosine used here did not contain uracil, the presence of uracil glycol in OsO_4-treated cytosine can only be explained by deamination of cytosine glycol, which was the actual oxidation product of cytosine. However, it is not known whether the deamination occurred spontaneously in aqueous solution or was induced by trimethylsilylation.

Peak 5 in Fig. 2 represents the trimethylsilyl derivative of 5,6-dihydroxyuracil, also observed in OsO_4-treated DNA, as explained above (peak 11 in Fig. 1). Although the g.c.–m.s. analysis of OsO_4-treated cytosine after

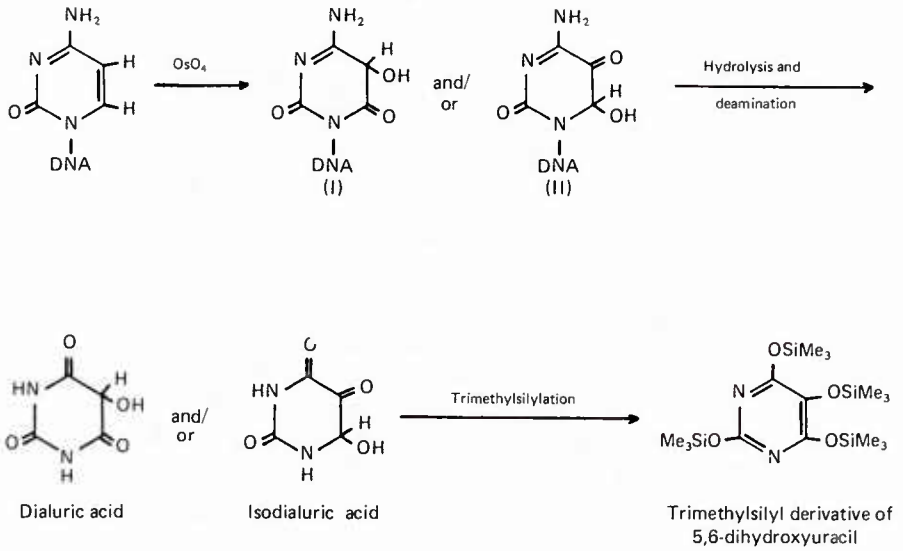

Scheme 2.

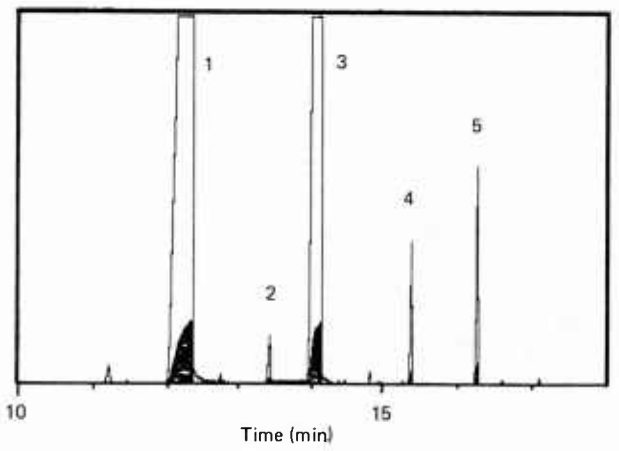

Fig. 2. Total-ion chromatogram obtained from a sample of OsO_4-treated cytosine after trimethylsilylation

Column details were as given in Fig. 1 legend.

formic acid treatment clearly showed the absence of uracil glycol (Fig. 4), 5-hydroxyuracil and 5,6-dihydroxyuracil were present (peaks 2 and 4 in Fig. 4 respectively). The increased amount of 5-hydroxyuracil (compare peaks 2 in Figs. 2 and 4) indicates its formation from uracil glycol by dehydration. In confirmation, formic acid treatment completely converted authentic uracil glycol into 5-hydroxyuracil.

OsO_4-treated cytosine was also analysed by reversed-phase h.p.l.c., as illustrated in Fig. 5. Cytosine gave a broad and tailing peak under these conditions (peak 5). Compounds represented by peaks 1–4 were collected by the use of a semi-preparative column and subsequently analysed by g.c.–m.s. Peaks 2 and 3 were found to correspond to uracil glycol and 5,6-dihydroxyuracil respectively. Fraction 2 also contained trace amounts of 5-hydroxyuracil. Fractions 1 and 4 contained no uracil or cytosine derivatives.

It is noteworthy that 5,6-dihydrothymine, which had been tentatively identified in OsO_4-treated DNA in

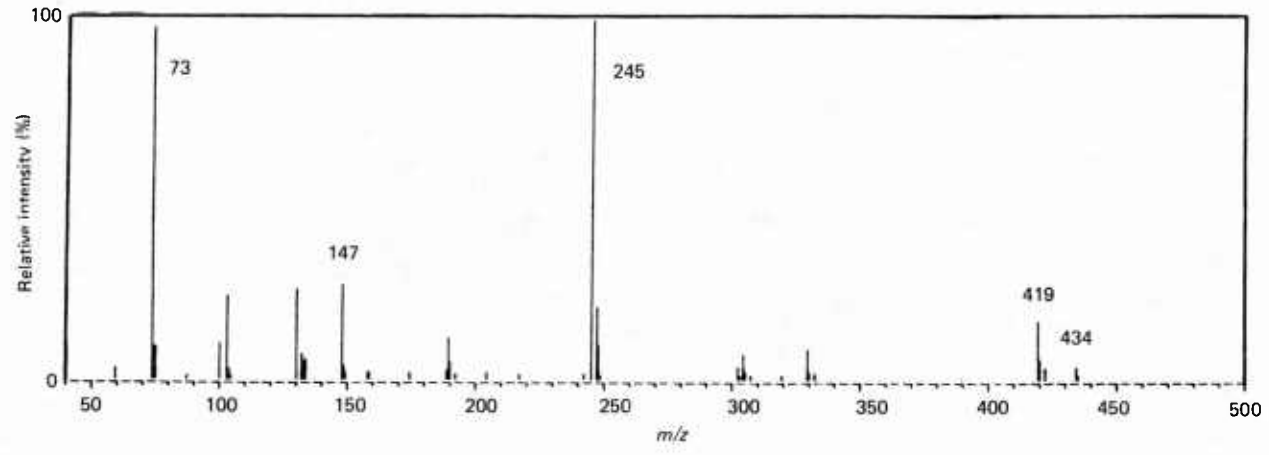

Fig. 3. Mass spectrum taken from peak 4 in Fig. 2

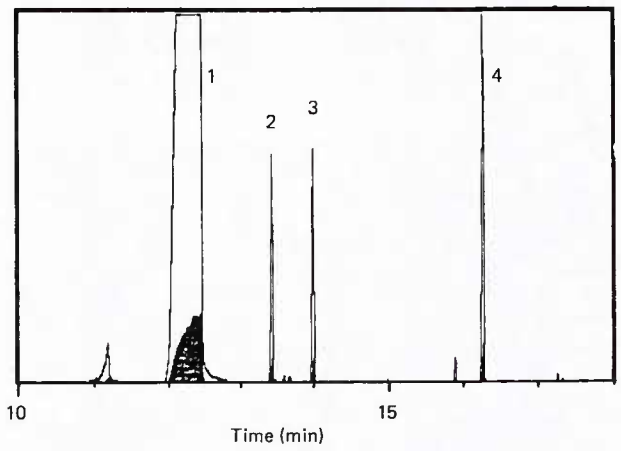

Fig. 4. Total-ion chromatogram obtained from a sample of OsO_4-treated cytosine after formic acid treatment and trimethylsilylation

Column details were as given in Fig. 1 legend.

previous work (Demple & Linn, 1980), was not observed in the present paper. This compound is easily detectable by g.c.–m.s. as demonstrated previously (Dizdaroglu, 1984, 1985), and authentic material was also available. The absence of 5,6-dihydrothymine from OsO_4-treated DNA confirms the assumption by Demple & Linn (1980) that this compound was most probably not formed in DNA by OsO_4 treatment.

The yields of conversion of thymine and cytosine into the products identified on OsO_4 treatment of DNA under the conditions described in the Materials and methods section were determined by g.c. with a flame ionization detector. Uracil was used as an internal standard and added to the samples before formic acid hydrolysis. The relative molar response factors versus uracil of thymine, thymine glycol, cytosine, 5-hydroxyuracil and 5,6-dihydroxyuracil were determined to be 0.95, 0.75, 1.1, 0.9 and 0.8 respectively. The relative molar response factor of 5,6-dihydroxycytosine versus uracil was assumed to be 1.0. The results showed that approx. 73% of thymine and 20% of cytosine were converted into products. The ratio of cytosine glycol (in terms of the sum of 5-hydroxyuracil and 5-hydroxycytosine) to 5,6-dihydroxycytosine (in terms of 5,6-dihydroxyuracil) was approx. 4:1.

CONCLUSIONS

The data presented here clearly suggest that, in addition to thymine glycol, cytosine glycol and 5,6-dihydroxycytosine are formed in DNA on OsO_4 treatment, and their subsequent deamination and dehydration give rise to formation of uracil glycol, 5-hydroxycytosine, 5-hydroxyuracil and 5,6-dihydroxyuracil. These results may be of importance to DNA repair studies that use OsO_4-treated DNA as a substrate for base-excision repair enzymes such as glycosylases.

This work was supported by the U.S. Armed Forces Radiobiology Research Institute, Defense Nuclear Agency, and Research Work Unit 00103. The views expressed in this paper are those of the authors and do not reflect the official policy or position of the Department of Defense or the U.S. Government. Also, although certain commercial equipment and materials are identified in this paper in order to specify the experimental procedure adequately, such identification does not imply recommendation or endorsement by the U.S. National Bureau of Standards, nor does it imply that the equipment and materials identified are necessarily the best available for the purpose.

REFERENCES

Adams, R. L. P., Burdon, R. H., Campbell, A. M., Leader, D. P. & Smellie, R. M. S. (1981) The Biochemistry of the Nucleic Acids, pp. 33–54, Chapman and Hall, London

Ames, B. N. (1983) Science **221**, 1256–1264

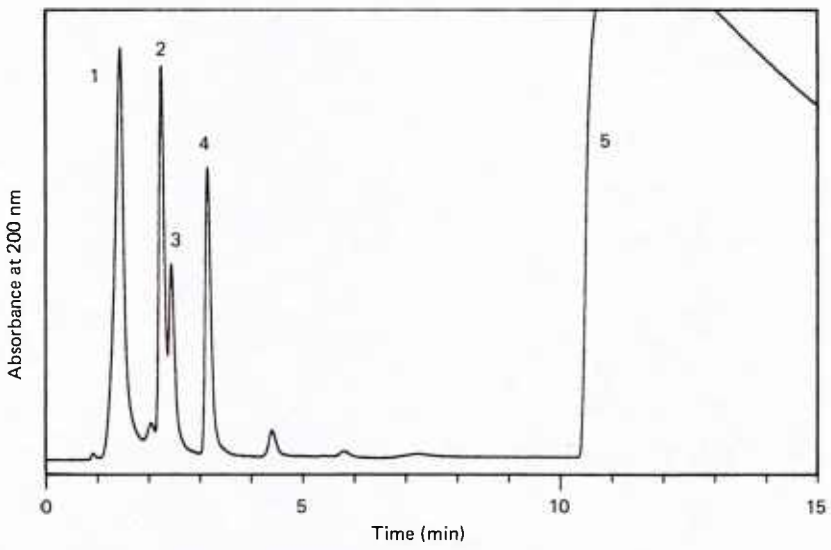

Fig. 5. H.p.l.c. profile obtained from a sample of OsO_4-treated cytosine

The column was microbore Hypersil ODS (10 cm × 0.21 cm; particle size 5 μm). The flow rate was 0.1 ml/min. The eluent was prepared from water (solvent A) and acetonitrile (solvent B); isocratic elution was with solvent A for 5 min, then gradient elution at 0.5% solvent B/min, at ambient temperature.

Bayley, C. R. & Jones, A. S. (1959) Trans. Faraday Soc. **55**, 492
Beer, M., Stern, S., Carmalt, D. & Mohlhenrich, K. H. (1966) Biochemistry **5**, 2283–2288
Behrend, R. & Roosen, O. (1889) Justus Liebigs Ann. Chem. **251**, 235–238
Brent, T. P. (1983) Biochemistry **22**, 4507–4512
Burton, K. & Riley, W. T. (1966) Biochem. J. **98**, 70–77
Cerutti, P. A. (1985) Science **227**, 375–381
Chang, C. H., Ford, H. & Behrman, E. J. (1981) Inorg. Chim. Acta **55**, 77–80
Criegee, R. (1936) Justus Liebigs Ann. Chem. **522**, 75–93
Darby, G. K., Jones, A. S., Tittensor, J. R. & Walker, R. T. (1967) Nature (London) **216**, 793–794
Demple, B. & Linn, S. (1980) Nature (London) **287**, 203–208
Dizdaroglu, M. (1984) J. Chromatogr. **295**, 103–121
Dizdaroglu, M. (1985) Anal. Biochem. **144**, 593–603
Evans, B. E., Mitchell, G. N. & Wolfenden, R. (1975) Biochemistry **14**, 621–624
Frenkel, K., Goldstein, M. S., Duker, N. J. & Teebor, G. W. (1981) Biochemistry **20**, 750–754
Friedberg, E. C. (1984) DNA Repair, pp. 1–77, Freeman and Co., New York
Gates, F. T. & Linn, S. (1977) J. Biol. Chem. **252**, 2802–2807
Green, M. & Cohen, S. S. (1957) J. Biol. Chem. **228**, 601–605
Hariharan, P. V. & Cerutti, P. A. (1974) Proc. Natl. Acad. Sci. U.S.A. **71**, 3532–3536
Hofmann, K. A. (1912) Ber. Dtsch. Chem. Ges. **45**, 3329–3336
Iida, S. & Hayatsu, H. (1970) Biochim. Biophys. Acta **213**, 1–13
Iida, S. & Hayatsu, H. (1971) Biochim. Biophys. Acta **240**, 370–375
Nes, I. F. (1980) Eur. J. Biochem. **112**, 161–168
Painter, R. B. (1980) in Radiation Biology in Cancer Research (Meyn, R. E. & Withers, H. R., eds.), pp. 59–68, Raven Press, New York
Schröder, M. (1980) Chem. Rev. **80**, 187–213
Schuchmann, M. N. & von Sonntag, C. (1983) J. Chem. Soc. Perkin Trans. 2, 1525–1531
Taguchi, H., Hahn, B. S. & Wang, S. Y. (1977) J. Org. Chem. **42**, 4127–4131
Teoule, R. & Cadet, J. (1978) in Effects of Ionizing Radiation on DNA (Hüttermann, J., Köhnlein, W. & Teoule, R., eds.), pp. 171–203, Springer-Verlag, Berlin

Received 4 October 1985; accepted 16 December 1985

MILITARY MEDICINE, 151, 9:487, 1986

Hepatobiliary Kinetics After Whole Body Irradiation

LTC Asaf Durakovic, MC USA

The purpose of this investigation was to study hepatobiliary kinetics after whole body gamma irradiation. Two groups of nine male beagle dogs were irradiated with a single whole body dose of 4 and 8 Gy Cobalt-60 photons. Each animal was injected with 2 mCi Tc-99m DISIDA and scintigraphic studies were obtained with gamma camera with parallel hole multipurpose collimator. The parameters studied included: [1]peak activity of the liver and gallbladder and [2]gallbladder and intestinal visualization from the time of Tc-99m DISIDA administration. Total and indirect bilirubin, LDH, SGOT, and SGPT determined as baseline studies before irradiation and at different time intervals after irradiation were not changed in irradiated animals. Results were expressed as baseline and postirradiation mean values with the standard error of the mean. Statistical significance was determined by the T-test.

Whole body Co-60 irradiation with 4 and 8 Gy produced no significant changes in the Tc-99m DISIDA visualization of the gallbladder or in the peak activity in the gallbladder or the liver 1 and 7 days after irradiation. No significant changes were observed in the 4 Gy Co-60 group. In contrast, intestinal visualization occurred significantly earlier in 8 Gy Co-60 irradiated animals on both day 1 (99.1 ± 15.8 minutes) and day 7 (78.2 ± 19.5 minutes) postirradiation, compared to baseline values where it was never observed before 195.0 minutes (195.0 ± 18.8, $p < 0.05$). Thus, gallbladder filling is not affected by Co-60 WB irradiation whereas, gallbladder emptying is significantly accelerated after 8 Gy but not after 4 Gy Co-60 gamma irradiation.

These observations suggest that gamma irradiation stimulates gallbladder contractility without modifying intrahepatic biliary kinetics.

Introduction

Hepatobiliary kinetics in acute radiation syndrome is of interest for understanding the mechanisms and pathophysiology of early transient incapacitation, particularly postirradiation nausea and vomiting involving entrogastric bile reflux. Modern diagnostic methods for the assessment of postirradiation changes in the biliary kinetics provide clinical insight in the quantitative parameters of the biliary pathways. Tc-99m DISIDA is a biliary homologue which is not adversely affected by even extreme hyperbilirubinemia. Its use in nuclear medicine diagnostic procedures offers a non-invasive method for quantitative assessment of intrahepatic cellular and ductal transit of biliary homologues and their concentration in the gallbladder and evacuation in the small intestine. Scintigraphic methods have proven advantageous over other biliary tract imaging modalities, including oral cholecystography, ultrasonography, intravenous cholecystography, transhepatic cholangiography, endoscopic pancreaticodudenography and computed tomographic studies.[1] Evaluation of hepatobiliary kinetics in acute radiation syndrome, in radiation casualties or radiation therapy is directly addressed by Tc-99m DISIDA cholescintigraphy, as the functional changes of hepatobiliary kinetics frequently precede morphologic alterations of the hepatobiliary system.[2]

From the Radiation Sciences Department, Nuclear Sciences Division, Armed Forces Radiobiology Research Institute, Defense Nuclear Agency, Bethesda, Maryland 20814-5145.

Materials and Methods

All experiments were performed on male adult beagle dogs, kept on standard dog feed and water ad libitum. Baseline values of liver and gallbladder visualization, gallbladder and liver peak activity and intestinal visualization of Tc-99m DISIDA were determined on each animal prior to irradiation. Each animal served as its own control. Serum determination of Total Bilirubin, Alkaline Phosphatase, LDH, SGOT, and SGPT were obtained prior to irradiation and daily from the day 1 to 6 after irradiation. All studies were performed in pentobarbital anesthesia (25 mg/kg i.v.). In each day of scintigraphic studies, each animal was injected with 2 mCi Tc-99m DISIDA and radionuclide imaging was obtained in the anterior view with gamma camera with a multipurpose collimator (peak ± 20%) interfaced with an A2 computer MDS-Medical Data System, Ann Arbor, Michigan. Imaging was obtained every minute for 60 minutes after administration of the radiopharmaceutical and every 15 minutes thereafter until visualization of the radiopharmaceutical in small intestine.

Experimental animals were exposed to total body irradiation using a Theratron-80 Cobalt-60 teletherapy unit. Radiation dose was 4 Gy in the first group (9 dogs) and 8 Gy in the second group (8 dogs), delivered at 50 cGy/min. Irradiated animals were studied 1 and 7 days after irradiation. All animals were sacrificed immediately after the last study using a lethal dose of nembutal (somlethol, 1.32 g/kg). Peak activity of the liver and gallbladder, as well as time of gallbladder and intestinal visualization of Tc-99m DISIDA, were determined using MDS computer. Results were expressed as a mean-time, in minutes, ± one standard error of the mean. Statistical significance was determined by the T-test.

Results

The hepatobiliary scan of the baseline Tc-99m DISIDA distribution demonstrated a rapid appearance of the radiopharmaceutical in the hepatocellular phase with subsequent transit to the biliary canaliculi and gallbladder (Fig. 1). Gallbladder visualization was demonstrated at the similar time intervals in 4 and 8 Gy groups of animals on the day 1 postirradiation compared to baseline. On day 7 after irradiation, gallbladder was visualized earlier in both 4 and 8 Gy irradiated animals, but the difference was not statistically significant compared to baseline (Range: 6.6–8.2 minutes vs. 11.3–12.9 minutes) (Table 1).

Gallbladder peak activity was seen in all experimental groups in the time interval of 29.4–42.3 minutes of injection, with no significant difference between baseline and both post-

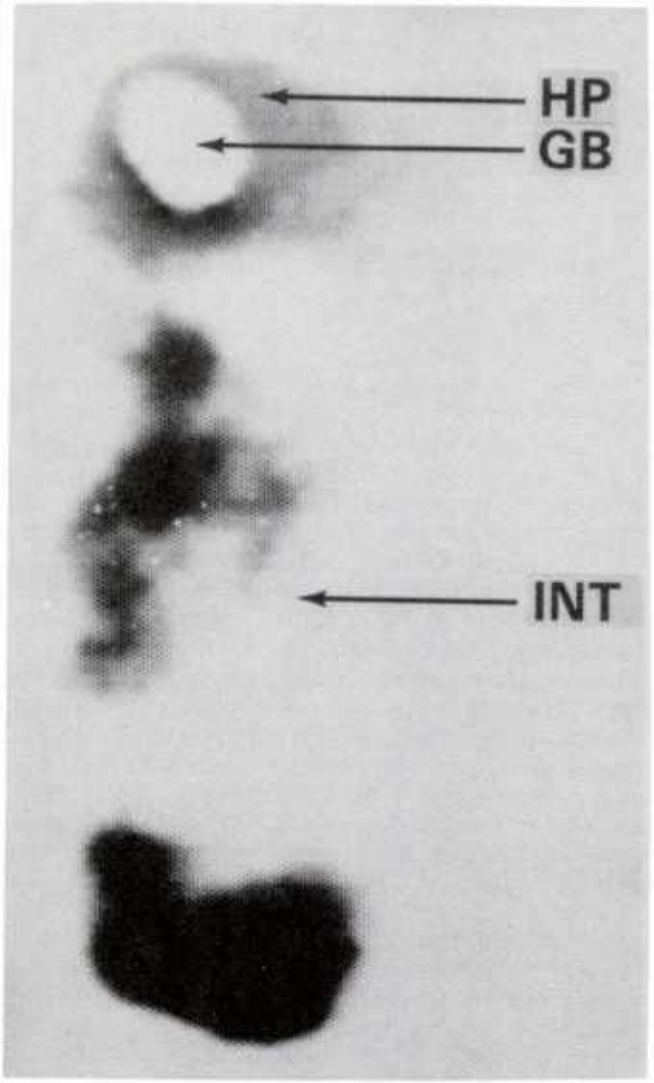

Fig. 1. DISIDA visualization in the Hepatocellular phase, gallbladder and intestine.

irradiation interval values in either 4 and 8 Gy irradiated animals (Table 1).

Liver peak activity was seen within 6.8–10.1 minutes injection with no statistical significance between baseline and postirradiation values in either 4 or 8 Gy irradiated dogs in either 1 or 7 days postirradiation intervals (Table 1).

In the 4 Gy irradiated animals, intestinal visualization of Tc-99m DISIDA was observed at a time which was not statistically different in either of the two postirradiation studies compared to baseline. In contrast, 8 Gy irradiated dogs had significantly shorter time to intestinal visualization ($p < 0.05$) on both day 1 and 7 after irradiation (Figure 2 and Table 1).

Four or eight Gy whole-body gamma irradiation did not modify significantly serum values of total Bilirubin, alkaline phosphatase, SGPT, and LDH. In contrast, SGOT was significantly decreased ($p < 0.05$) from day 1 through day 6 following both 4 and 8 Gy total-body irradiation.

Discussion

Radioresistance of the liver has been well documented.[3]

TABLE I

HEPATOBILIARY APPEARANCE TIME OF TC-99M DISIDA IN DOGS POSTIRRADIATION 4 GY CO-60

	Minutes After Injection (mean ± SE)		
	Baseline	1 Day	7 Days
Gallbladder Visualization	11.7 ± 2.0	11.3 ± 2.2	6.6 ± 0.8
Gallbladder Peak Activity	42.3 ± 4.5	31.8 ± 4.0	37.8 ± 7.4
Liver Peak Activity	10.1 ± 2.6	9.3 ± 1.9	7.6 ± 1.5
Intestinal Visualization	160.0 ± 20.6	121.2 ± 26.0	130.1 ± 15.3
		8 Gy Co-60	
Gallbladder Visualization	11.6 ± 2.7	12.9 ± 4.3	8.2 ± 1.2
Gallbladder Peak Activity	37.0 ± 4.4	29.4 ± 5.3	35.0 ± 6.1
Liver Peak Activity	9.3 ± 1.6	7.4 ± 1.1	6.8 ± 0.9
Intestinal Visualization	195.0 ± 18.8	99.1 ± 15.8	78.2 ± 19.5

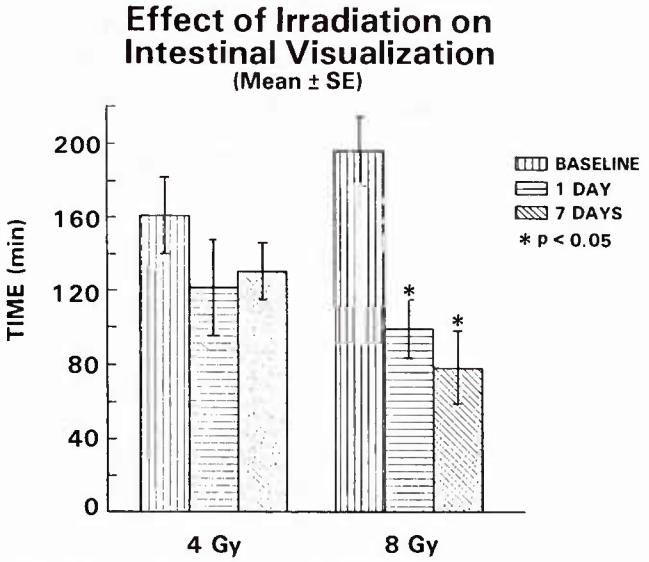

Fig. 2. Intestinal visualization of Tc-99m DISIDA before and after 4 and 8 Gy total body irradiation (mean ± SE).

Reversible radiation-induced hepatitis after the treatment of abdominal neoplasms with fractionated dose of 3000 rads has been described in the isolated number of patients.[4] Radiation-induced changes of the liver area is characterized by initial vascular endothelial damage eventually leading to congestive and degenerative parenchymal changes.[5,6] There is no documentation on the effect of radiation on the biliary system.

Our findings indicate that acute exposure to the total-body dose of 4 and 8 Gy of Co-60 does not produce any changes to the time to liver peak activity of Tc-99m DISIDA or the time to visualization and the time to peak activity of the gallbladder. Gallbladder filling was not affected by 4 Gy or 8 Gy whole body Co-60 irradiation; in contrast gallbladder emptying appeared

to be accelerated, as indicated by our observation that intestinal visualization of Tc-99m DISIDA was significantly accelerated after irradiation. Biochemical tests of hepatic function remained unchanged throughout the 7-day interval in both 4 and 8 Gy irradiated animals, with the exception of a decrease in SGOT after irradiation in both experimental groups.

In conclusion, our studies offer experimental evidence of altered response of the gallbladder to ionizing radiation. Our results are relevant to clinical management of acute radiation syndrome and radiation therapy, suggesting that further investigation of the different experimental and clinical modalities of radiation exposure on hepatobiliary kinetics are warranted. Furthermore, accelerated emptying of the gallbladder after radiation exposure offers an insight in the mechanisms and management of enterogastric reflux and vomiting in acute radiation syndrome.

References

1. Harvey E, Loberg M, Ryan T: Hepatic clearance mechanism of Tc-99m HIDA and its effect on quantitation of heptobiliary function. J Nucl Med 20:310, 1979
2. Rosly JJ, Den Besten L, Thompson JE: Roles of lithogenic bile and cystic duct occlusion in the pathogenesis of acute cholecystitis. Am J Surg 140:126, 1980
3. Shearman DJC, Finlayson NDC: Diseases of the gastrointestinal tract and liver. Churchill Livingston, 1982
4. Kim TH, Panahon AN, Friedman M, et al: Acute transient radiation hepatitis following whole abdominal irradiation. Clinical Radiology 27:449, 1976
5. Ingold JA, Reed GB, Kaplan HS, et al: Radiation Hepatitis. Am J Roentergenal 93:200, 1965
6. Wharton JT, Delclos L, Gallager S: Radiation hepatitis induced by abdominal irradiation with the Cobalt-60 moving strip technique. Am J Roentgenol 117:73, 1973

THE ROLE OF ENDOGENOUS PROSTAGLANDINS IN THE REGULATION OF GASTRIC SECRETION IN RHESUS MONKEYS

H. El-Bayar, L. Steel[1], E. Montcalm, E. Danquechin-Dorval, A. Dubois, T. Shea-Donohue[2].

Department of Medicine, Uniformed Services University of the Health Sciences, and [1]Department of Biochemistry, Armed Forces Radiobiological Research Institute, Bethesda, Maryland 20814

ABSTRACT

Prostaglandins (PG) are known to alter a variety of gastrointestinal functions, but the physiological role of endogenous PG remains unclear. This experiment was designed to evaluate changes in gastric secretion following both acute and chronic inhibition of PG synthesis with indomethacin (5 mg/kg s.c.). Gastric juice was collected by continuous aspiration in 8 conscious chair-adapted male rhesus monkeys following treatment with saline or indomethacin for one or four days. The gastric juice was analyzed for H^+, Na^+, K^+, and Cl^- concentrations. The amount of soluble mucus in the gastric juice was estimated using Alcian Blue dye binding of acidic glycoproteins and Periodic Acid Schiff reaction with neutral glycoproteins. PG levels were measured in the plasma and in biopsy samples of fundus, antrum and duodenum. Both one and four days of indomethacin significantly ($p < 0.05$) decreased tissue PG levels in the fundus, antrum and duodenum. Plasma levels of $PGF_{2\alpha}$ were significantly ($p < 0.05$)

[2] Correspondence.

decreased after both one and four days of indomethacin, while PGE_2 and 6-keto $PGF_{1\alpha}$ were significantly inhibited only after four days of indomethacin. Both acute and chronic inhibition of PG synthesis was accompanied by a decrease in the concentration of sodium and mucus in the gastric juice but by an increase in the output and concentration of hydrogen ion. These changes suggest a possible mechanism by which endogenous PC play a role in the regulation of gastric secretion and in the protection against gastrointestinal damage.

INTRODUCTION

PGE_2 and $PGF_{2\alpha}$ are the major end products of arachidonic acid metabolism in mucosal cells of the gastrointestinal (GI) tract. Other PG metabolites found in the GI tract are thromboxane A_2 (TXA_2) and prostacyclin (PGI_2), which are the major products of platelets, and vessel endothelial cells, respectively. PGE_2, PGI_2, and $PGF_{2\alpha}$ and their analogs as well as the analogs of the endoperoxides uniformly inhibit acid secretion in rats (1), dogs (2) and monkeys (3-5). In contrast to their inhibition of parietal secretion, several of the PG have a positive effect on non-parietal secretion. The 15(S), 15-methyl analogs of PGE_2 ($mePGE_2$) and $PGF_{2\alpha}$ ($mePGF_{2\alpha}$) enhance Na^+ output (4,6). In addition, PGE_2 and its analog also elevate bicarbonate and mucus secretion (6,7). Conversely, stimulated bicarbonate and mucus secretion are decreased by non-steroidal anti-inflammatory drugs (NSAID) (7,8) presumably as a result of their ability to inhibit PG synthesis.

Inhibition of endogenous PG synthesis has been associated with gastric mucosal damage (9-11). Moreover, exogenous administration of PG protects the gastric mucosa against toxic stimuli (12-13)

and accelerates the healing of gastric ulcers (14). The precise mechanism of these effects is unknown, but may be related to an inhibition of acid secretion, a stimulation of non-parietal secretion, an elevation of mucus secretion, a change in the quality of the mucus or some combination of the above. Studies in both animals and humans have demonstrated that acute (15,16) or chronic (9) oral administration of aspirin or indomethacin produces gastric mucosal lesions. Moreover, the severity of this damage is inversely correlated with mucosal PG levels (9,11). Eastwood et al, (17) however, observed that there was no evidence of inflammation or ulceration after four weeks of oral administration of aspirin to rats. Thus, there are discrepancies in the results following chronic administration of NSAID. Interpretation of these data is further complicated by the possibility of a direct contact effect of NSAID on the gastric mucosa (18). This study was designed, therefore, to examine the effect of both acute and chronic inhibition of endogenous PG production on gastric parietal, non-parietal and mucus secretion. Thus, the role of endogenous PG in the physiological regulation of gastric secretion and in the maintenance of gastric mucosal integrity can be further explored.

METHODS

Eight male, unanesthetized rhesus monkeys (Macaca mulatta) weighing 3-10 kg were placed in primate restraining chairs and housed in closed, lighted and ventilated booths between 9 a.m. and 12 a.m. The monkeys were trained to accept a French no. 12, double-lumen nasogastric Ventrol Levin tube (National Catheter

Company, Mallinkrodt, Argyle, NY; bore, 4 mm; wall thickness, 1 mm). The experiments were conducted after an overnight fast and at least 30 minutes after placement of the tube. Proper positioning of the tube in the most dependent part of the stomach was confirmed by demonstrating that, after injecting 15 ml of water into a previously emptied stomach, the total volume could be recovered. This procedure was performed twice a week for 1 month in order to habituate the monkeys before initiation of the studies. The subsequent studies were performed with the same frequency. Samples of gastric juice were collected using continuous aspiration (-2 mm Hg). The animals were studied for six 15 minute periods on 3 separate occasions: a control day (saline, 1-2 mls s.c. bolus), after 1 day of indomethacin (5 mg/kg s.c.) treatment (1DI) and after 4 days of indomethacin treatment (4DI). In 4 monkeys, after each of the three studies, blood was drawn and placed in tubes containing 2% EDTA (90 µl/ml blood) and 1.6% solution of indomethacin in $NaHCO_3$ buffer (5 µl/ml blood) for determination of plasma levels of 6-keto-$PGF_{1\alpha}$ (a stable breakdown product of PGI_2), PGE_2 and $PGF_{2\alpha}$ in the plasma.

The animals were then anesthetized with ketamine hydrochloride (Vetalar, Morris Plains, NJ, 5 mg/kg) and endoscoped using a GIF-P2 Olympus (Columbia, Maryland) fiberoptic pediatric endoscope (outside diameter = 8 mm). At this time, a visual examination was made to assess gastric damage in the fundus and antrum. Pinch biopsies (diameter = 1 mm) were then taken from the duodenum, antrum and fundus for measurement of tissue PG levels. On collection, the biopsies obtained from each area were immediately placed in an ice cold plastic vial put on dry ice and subsequently stored at -70°C. The time between the collection of the biopsy and freezing on dry ice was approximately 30 seconds. Mucosal biopsies

(wet weight approximately 2.6 mg) were individually sonicated in 1.5 ml Eppendorf tubes containing 200 µl of a saline solution at 4°C with 0.4% aspirin and 2% EDTA. Volume was brought to 1.5 ml and adjusted to pH 3.2 by the addition of 2M citric acid (4°C). Tubes were capped, vortexed and centrifuged 2 min at 10,000g (Brinkmann Eppendorf Microfuge) and supernatants were removed by aspiration. Pellets were resuspended in 1.5 ml of water adjusted to pH 3.2 by 2M citric acid (citric acid $-H_2O$); tubes were recentrifuged and supernatants were aspirated and combined with previous supernatants; 200 µl of 0.1 N NaOH was then added to each tissue pellet. Tubes were capped, vortexed, and left overnight on heat blocks maintained at 40°C. Protein concentration of the digests were determined by the method of Lowry et al. (19). Supernatants from the sonicated tissues were applied to individual C18 columns (Bond-Elut C18, 200 mg sorbent mass, Analytichem International, Harbor City, CA) which had been previously washed with methanol and equilibrated with citric acid $-H_2O$ solution. Each was sequentially washed with 2 ml citric acid-H_2O solution, 2 ml 12.5% methanol and 2 ml benzene. PG were eluted with ethyl acetate, dried under N_2 and subsequently reconstituted in assay buffer (phosphate-buffered saline at pH 6.8 containing 0.3% bovine gamma-globulin .005% Triton X-100 and 0.05% NaN_3). PGE_2 and 6-keto-$PGF_{1\alpha}$ levels were determined with ^{125}I-radioimmunoassay kits (New England Nuclear, Boston, MA). $PGF_{2\alpha}$ levels were determined employing ^{3}H-labeled $PGF_{2\alpha}$ tracer.

Plasma samples (1.0 ml) were acidified to pH 3.2 with approximately 100 µl of 2 M citric acid. Centrifugation did not result in a precipitable protein pellet. Acidified plasmas were applied to individual C18 columns (500 mg sorbent mass), sequentially washed and PG recovered from the column as described

above. N_2 evaporated extracts were reconstituted in 100 µl assay buffer and PG levels determined by radioimmunoassay as described above.

The gastric juice samples were centrifuged and the clear supernatant was analyzed for hydrogen (H^+), sodium (Na^+), potassium (K^+) and chloride (Cl^-) ion concentration. H^+ was determined by end-point titration to pH 7.4 with 0.02 NaOH (titration assembly, Radiometer, America, Westlake, OH). Na^+ and K^+ were measured using a flame photometer (IL Model 443, Lexington, MA) and Cl^- was determined using an amperometric titration method (Corning 920 M, Medfield, MA). In addition, concentrations of soluble mucus were estimated by two different assays, the Alcian blue (AB) dye binding method and the Periodic Acid Schiff (PAS) reaction as described elsewhere (20).

The statistical significance of differences observed for each gastric parameter was evaluated using a three-factor (treatment, time, and monkey) analysis of variance with repeated measures on the last two factors (time and monkey), the program LDU-040 (K.L. Dorn), and an IBM 370 computer (DCRT, National Institutes of Health) (3-5). Differences between PG levels in tissue and plasma were determined using a two-way analysis of variance.

RESULTS

Plasma concentrations of 6-keto-$PGF_{1\alpha}$ were reduced by 9%, PGE_2 by 27% following one day of indomethacin administration, but the difference was not significant. $PGF_{2\alpha}$, however, was significantly ($p<0.05$) inhibited by 39% (Fig 1). After 4DI plasma levels of

6-keto-$PGF_{1\alpha}$ were significantly ($p<0.05$) suppressed by 53%, PGE_2 by 77% and $PGF_{2\alpha}$ by 100%.

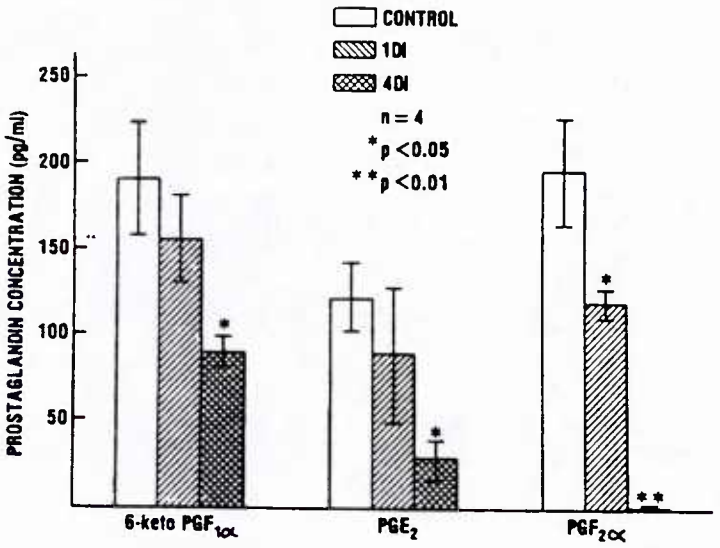

Fig. 1: Effect of 1 day (1DI) and 4 days (4DI) of indomethacin treatment (5mg/kg s.c.) on prostaglandin concentration (pg/ml) in plasma.

In the tissue biopsies, the levels of PG were significantly ($p<0.05$) inhibited during the entire course of indomethacin treatment for all PG measured (Fig 2). The percent inhibition of all PG for both 1DI and 4DI was greatest in the fundus (74-87%) and duodenum (73-87%), followed by the antrum (42-77%). Prior to treatment with indomethacin, there was no significant correlation between PG levels in the tissue and H^+ or mucus output or

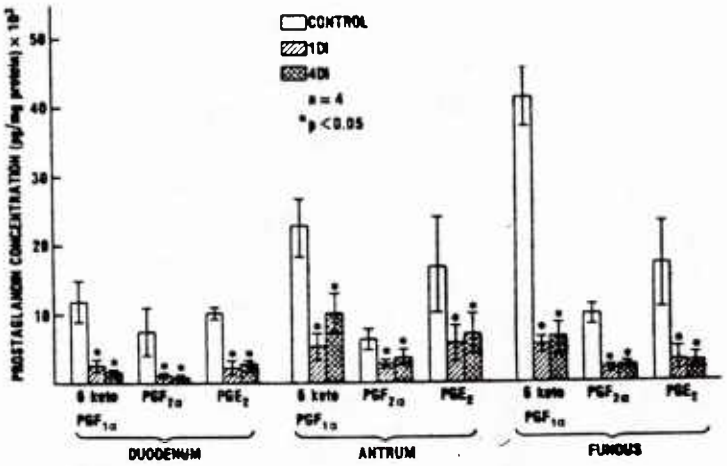

Fig. 2. Effect of 1 day (1DI) and 4 days (4DI) of indomethacin treatment (5 mg/kg s.c.) on tissue prostaglandin concentration (pg/mg protein X 10^3).

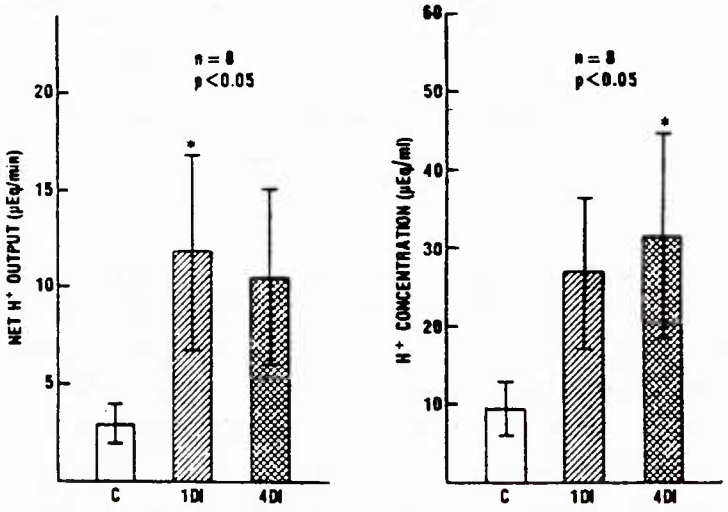

Fig. 3. Effect of 1 day (1DI) and 4 days (4DI) of indomethacin treatment (5 mg/kg s.c.) on H^+ output (μEq/min) and concentration (μEq/ml).

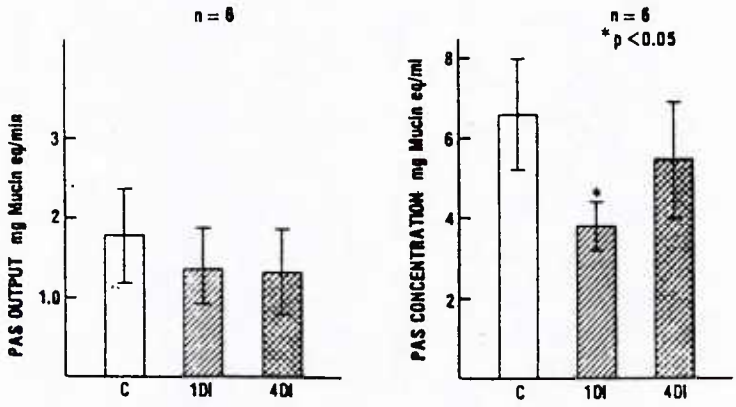

Fig. 4. Effect of 1 day (1DI) and 4 days (4DI) of indomethacin treatment (5 mg/kg s.c.) on neutral glycoprotein (PAS) output (mg Mucin eq/min) and concentration (mg Mucin eq/ml).

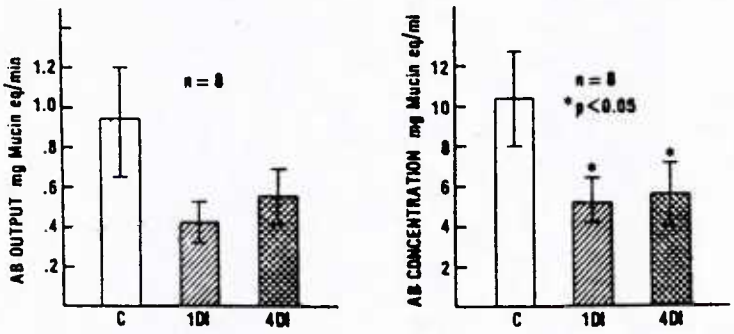

Fig. 5: Effect of 1 day (1DI) and 4 days (4DI) of indomethacin treatment (5 mg/kg s.c.) on acidic glycoprotein (AB) output (mg Mucin eq/min) and concentration (mg Mucin eq/ml).

Table 1. The Effect of Indomethacin on Fluid Output and Ion Output and Concentration

Treatment	Fluid Output ml/min	Na^+ Output µEq/min	Na Conc µEq/ml	K^+ Output µEq/min	K^+ Conc µEq/ml	Cl^- Output µEq/min	Cl Conc µEq/ml
CONTROL	0.27 ± 0.05	18.5 ± 3.0	79 ± 8	9.1 ± 2.6	28 ± 3	21.8 ± 6.5	85 ± 8
1DI	0.30 ± 0.07	17.1 ± 3.7	64 ± 6*	7.5 ± 1.6	29 ± 3	28.4 ± 8.5	104 ± 11
4DI	0.22 ± 0.07	12.0 ± 5.7	54 ± 6*	6.9 ± 2.2	27 ± 4	29.9 ± 9.8	99 ± 14

$p < 0.05$ vs. CONTROL Values are means ± SE of measurements of 8 monkeys.
Data were evaluated using a three-factor (treatments, time and monkey) analysis with repeated measures on the last two factors.

concentration.

Coincident with the reduction in both tissue and plasma PG levels, there was an increase in H^+ concentration and output over the course of indomethacin treatment (Fig 3). This was also accompanied by a decrease in Na^+ concentration over the same period (Table 1). However, fluid output, Na^+ output as well as K^+ and Cl^- concentrations and output were not significantly changed by PG inhibition (Table 1).

The concentration of soluble NG in the gastric juice was significantly inhibited after 1DI but was not significantly different from control after 4DI (Fig 4). NG output was not altered. The concentration of soluble AG in the gastric juice was significantly decreased following both 1DI and 4DI (Fig 5). AG output was also inhibited after 1DI and 4DI but the reduction was not significantly different from control.

The endoscopic appearance of the gastric and duodenal mucosa was not significantly altered on any day of study .

DISCUSSION

Exogenous PG have been previously shown to have an effect on gastric secretion and emptying. We have shown previously that me-PGE_2, me-$PGF_{2\alpha}$, PGI_2 as well as the endoperoxide analogue U-46619 uniformly inhibit parietal (H^+) secretion (3-5). In addition, me-PGE_2 and me-$PGF_{2\alpha}$, but not PGI_2 or U-46619 concurrently stimulated non-parietal (Na^+) secretion (4,5). However, a physiological role for endogenous PG in the regulation of gastric secretion has not been fully elucidated. This study

suggests that endogenous PG play a role in the physiological regulation of gastric secretion.

NSAID are used clinically for their analgesic, anti-inflammatory, and anti-pyretic properties, each agent having variable efficacy or potency depending on the therapeutic effect being measured. These effects have been attributed in part to their ability to inhibit PG production by blocking the cyclo-oxygenase pathway. One of their major side effects, however, has been the induction of varying degrees of gastric mucosal damage ranging from minor erosions to ulceration and bleeding (9,15,16). Our results demonstrate that in monkeys, the inhibition of endogenous PG production with indomethacin does not cause such damage while significantly increasing the H^+ output and concentration and decreasing the Na^+ concentration in the gastric juice. These results are in agreement with the demonstration that NSAID inhibit alkaline secretion (7). In contrast, Konturek et al (9) observed that indomethacin given orally over 7 days (25 mg, q.i.d.) had no effect on basal acid output. These differences may be due to the dose (1.47 mg/kg versus 5 mg/kg in the present study) or the route of administration (oral versus subcutaneous). In addition, 10 of the 18 subjects receiving indomethacin in Konturek's study reported moderate to severe side effects which necessitated their withdrawal from the study. Although the nature or cause of these symptoms was not reported, an increase in acid output could have been a contributing factor.

There is much evidence to suggest a positive correlation between gastric mucosal blood flow and acid secretion (21). However, PG have been shown to increase mucosal blood flow but to decrease acid secretion (22). Conversely, in dogs, indomethacin has been found to decrease basal mucosal blood flow (23) and to

reduce pentagastrin-stimulated mucosal blood flow while further increasing acid secretion (24). These results suggest that the increase in H^+ output observed in the present study is not secondary to changes in mucosal blood flow.

Our data also show that the inhibition of endogenous PG by indomethacin resulted in a decrease in soluble mucus in the gastric juice as represented by both acidic and neutral glycoproteins. This is supported by the observations of Menguy and Masters (8), who found that aspirin, another NSAID, significantly decreased the carbohydrate content of gastric mucus. Moreover, analogs of PGE_2 have been shown to produce a stimulation of soluble mucus secretion (6,25) and a reversal of NSAID effects (25). It has been shown recently that changes in soluble gastric mucus paralleled alterations in the adherent mucus gel (26) as determined by Alcian blue dye binding. Thus, the decrease in soluble mucus following indomethacin in the present study probably reflects a decrease in barrier mucus as well as soluble mucus.

Coincident with the rise in H^+ secretion and fall in Na^+ and mucus concentrations in the gastric juice, plasma and tissue levels of PGE_2, PGF_2 and PGI_2 were significantly decreased following indomethacin administration. It is of interest to note that the reduction in PG over time was less in plasma than in gastric mucosal tissue, although the reason for this difference is not readily apparent. PG concentration in the plasma probably reflect the net PG metabolism in various tissues and in blood. However, indomethacin and other NSAID given s.c. may not inhibit PG synthesis uniformly in all areas. Thus, the plasma concentration of PG may be higher than the concentration on a given tissue (e.g. gastric mucosa). Alternately, repeated administration may be necessary to attain a significant blood concentration of

indomethacin in order to specifically inhibit plasma PG.

While PGI_2, PGE_2 and $PGF_{2\alpha}$ uniformly suppress H^+ output, PGE_2 and $PGF_{2\alpha}$ also have a stimulating effect on Na^+ output (4). This suggests that the reduction of Na^+ following the inhibition of endogenous PG in the present study can be attributed primarily to decreases in tissue PGE_2 and $PGF_{2\alpha}$ rather than a reduction in PGI_2. Thus, PGE_2 and $PGF_{2\alpha}$ appear to have a greater role than PGI_2 in the physiological regulation of gastric non-parietal secretion. The largest decrease (% reduction) in tissue PG was found in biopsies of the fundus and duodenum followed by the antrum. Although the reason for this regional difference in sensitivity to PG inhibition is unclear, it is of interest to note that the major site for chronic ulceration is the antrum, the area exhibiting the smallest percent reduction in PG content. This suggests that the antral mucosa is more sensitive (i.e. more easily damaged) than either the duodenum or fundus to even slight reductions in tissue PG.

It has been proposed that PG have a "cytoprotective" effect which may be independent of their ability to inhibit acid secretion (13). There are many factors involved in the maintenance of the mucosal integrity. These factors may be divided into those which are damaging, and those which are protective. Pepsin and acid secretion (H^+) are two major damaging factors which are in turn opposed by alkaline (Na^+, HCO_3^-) and mucus secretion. The present study demonstrates that inhibition of endogenous PG in the gastric mucosa increases the output concentration of H^+ and decreases the concentration of Na^+ and soluble mucus glycoproteins in the gastric juice. The combination of these effects may be an important factor in the development of gastric mucosal damage observed following higher doses of indomethacin and other NSAID. Thus, these data

demonstrate that PG play an important physiological role in the regulation of gastric parietal, non-parietal and mucus secretion.

REFERENCES

1. Whittle B.J.R., N.K. Boughton-Smith, S. Moncada, J.R. Vane. Actions of prostacyclin (PGI_2) and its product 6-oxo-$PGF_{1\alpha}$ on the rat gastric mucosa in vivo and in vitro. Prostaglandins 15:955-967. 1978.

2. Kauffman, G.L., B.J.R. Whittle, D. Aures, J.R. Vane, M.I. Grossman. Effects of prostacyclin and a stable analogue, 6β-PGI_1, on gastric acid secretion, mucosal blood flow, and blood pressure in conscious dogs. Gastroenterology 77:1301-1306. 1979.

3. Nompleggi, D., L. Myers, D.O. Castell, A. Dubois. Effect of a prostaglandin E_2 analog on gastric emptying and secretion in rhesus monkeys. J. Pharmacol. Exp. Ther. 212:491-495. 1980.

4. Shea-Donohue, P.T., D. Nompleggi, L. Myers, A. Dubois. A comparison of the effects of prostacyclin and the 15(s), 15-methyl analogs of PGE_2 and $PGF_{2\alpha}$ on gastric parietal and nonparietal secretion. Dig. Dis. Sci. 27:17-22. 1982.

5. Shea-Donohue, P.T., D. Nompleggi, L. Myers, A. Dubois. A prostaglandin endoperoxide analog increases gastric emptying and suppresses gastric secretion in rhesus monkeys. J. Pharmcol. Exp. Ther. 222:379-383. 1982.

6. Bolton, J.P., D. Palmer, M. Cohen. Stimulation of mucus and non-parietal cell secretion by the E_2 prostaglandins. Dig. Dis. Sci. 2:359-364. 1978.

7. Garner, A., G. Flemstrom, J.R. Heylings. Effects of anti-inflammatory agents and prostaglandins on acid and bicarbonate secretions in the amphibian-isolated gastric mucosa. Gastroenterology 77:451-457. 1979.

8. Menguy, R. Y.F. Masters. Effects of aspirin on gastric mucous secretion. Surg. Gyn. Obst. 120:92-98. 1965.

9. Konturek, S.J., N. Kwiecien, W. Obtulowicz, A. Kiec-Dembinska, M. Polanski, B. Kopp, E. Sito, J. Olesky. Effect of carprofen and indomethacin on gastric function, mucosal integrity and generation of prostaglandins in men. Hepto-gastroenterol. 29:267-270. 1982.

10. Okabe, S., K. Tabata. Does indomethacin activate healed gastric ulcers in the dog? Digestion 21:179-183. 1981.

11. Rainsford, K.D., C. Willis. Relationship of gastric mucosal damage induced in pigs by antiinflammatory drugs to their effects on prostaglandin production. Dig. Dis. Sci. 27: 624-635. 1982.

12. Muller, P., N. Fischer, H. Kather, B. Simon. Prevention, through cytoprotection, of aspirin-induced drop in gastro mucosal potential difference in man by 16,16-dimethyl-prostaglandin E_2. Ital. J. Gastroenterol. 13:48-50. 1981.

13. Robert, A., J.E. Nezamis, C. Lancaster, A.J. Hanchar. Cytoprotection by prostaglandins in rats. Prevention of gastric necrosis produced by alcohol, HCl, NaOH, hypertonic NaCl, and thermal injury. Gastroenterology 77:433. 1979.

14. Rybicka, J., K. Gibinski: Methyl prostaglandin E_2 analogues for healing of gastroduodenal ulcers. Scand. J. Gastroenterol. 13:155-159. 1978.

15. Baskin, W.N., K.T. Ivey, W.J. Krause. Aspirin induced ultra-structural changes in human gastric mucosa. Correlation with potential difference. Ann. Intern. Med. 85:299-303. 1976.

16. Berstock, D.A., G.J. Frank, P.I. Stamford, A. Bennett. Decrease in aspirin-induced gastric mucosal damage in rats by oral administration of the cytotoxic drugs melphalan and methotrexate. J. Pharm. Pharmacol. 32:544-546. 1980.

17. Eastwood, G.L., G.F. Quimby. Effect of chronic aspirin ingestion in epithelial proliferation in rat fundus, antrum, and duodenum. Gastroenterology 82:852-856. 1982.

18. Ivey, K., D.B. Paone, W.H. Krause. Acute effect of systemic aspirin on gastric mucosa in man. Dig. Dis. Sci. 25:97-99. 1980.

19. Lowry, O.H., N. Rosenbrough, A. Fan, R. Randall R. Protein measurement with the folin phenol reagent. J. Biol. Chem. 1983:265-268. 1951.

20. Shea-Donohue, P.T., E. Dancquechin-Dorval, E. Montcalm, H. El-Bayer, A. Durakovic, J.J. Conklin, A. Dubois. Alterations in gastric mucus following exposure to ionizing radiation. Gastroenterology 88:685-690. 1985.

21. Jacobson, E.D. Comparison of prostaglandin E_1 and norepinephrine on the gastric mucosal circulation. Proc. Soc. Exp. Biol. Med. 133:516-519. 1970.

22. Main, I.H.M., B.J.R. Whittle. The effects of E and A prostaglandins on gastric mucosal blood flow and acid secretion in the rat. Br. J. Pharmacol. 49:428-436. 1973.

23. Kauffman, G.L., D. Aures, M.I. Grossman. Intravenous indomethacin and aspirin reduce basal gastric mucosal blood flow in dogs. Am. J. Physiol. 283:G131-G134. 1980.

24. Gerkens, J.F., D.G. Shand, C. Flexnor, A.S. Nies, J.A. Oates, J. L. Data. Effect of indomethacin and aspirin on gastric mucosal blood flow and acid secretion. J. Pharmacol. Exp. Ther. 203:646-652. 1972.

25. Shea-Donohue P.T., J. Arnold, A. Dubois. The role of endogenous prostaglandins in gastric secretion. Gastroenterology 82(5):1177A. 1982.

26. Lamont, J.T., A.S. Ventola, A.E. Maull, S. Szabo. Cysteamine and Prostaglandin $F_{2\alpha}$ stimulate rat gastric mucin release. Gastroenterology 84:306-13. 1983.

27. Whittle B.J.R. Relationship between the prevention of rat gastric erosions and the inhibition of acid secretion by prostaglandins. Eur. J. Pharmacol. 40:223-239. 1976.

Acknowledgements

We wish to thank William W. Wolfe for his technical assistance and Joy W. Barchers for her expert editorial assistance. We would also like to thank Merck, Sharp and Dohme, Rahway, New Jersey for the gift of indomethacin. This work was supported in part by DOD grant RO-8300 and CO-8343.

Editor: B.J. Whittle Received: 12-5-84 Accepted: 6-10-85

Chronobiology International, Vol. 3, No. 2, pp. 101–115, 1986
Printed in Great Britain

0742-0528/86 $3.00+0.00
Pergamon Journals Ltd.

CIRCADIAN RHYTHMS IN CATECHOLAMINE METABOLITES AND CYCLIC NUCLEOTIDE PRODUCTION

Marian S. Kafka*, Marco A. Benedito*, Robert H. Roth†, Linda K. Steele‡
William W. Wolfe,‡ and George N. Catravas‡

*Clinical Neuroscience Branch, National Institute of Mental Health, Bethesda, MD 20892, U.S.A.
†Departments of Pharmacology and Psychiatry, Yale University School of Medicine, New Haven, CT 06510, U.S.A.
‡Biochemistry Department, Armed Forces Radiobiology Research Institute, National Naval Medical Center, Bethesda, MD 20814-5145, U.S.A.

Abstract—Circadian rhythms in noradrenergic (NE) and dopaminergic (DA) metabolites and in cyclic nucleotide production were measured in discrete regions of rat brain. A circadian rhythm was found in the concentration of the NE metabolite, 3-methoxy-4-hydroxyphenylglycol (MHPG), in the hippocampus. No MHPG rhythm was found in frontal, cingulate, parietal, piriform, insular or temporal cortex, or in hypothalamus. Circadian rhythms in the concentration of the NE metabolite, 3,4-dihydroxyphenylglycol (DHPG), occurred in occipital and parietal cortex and hypothalamus, with no rhythm observable in temporal or insular cortex, hippocampus, pons–medulla or cerebellum. The 24-hr mean concentration of MHPG varied 3.5-fold, highest in cingulate and lowest in parietal, temporal and occipital cortex. The 24-hr mean concentration of DHPG varied 6-fold, highest in hypothalamus and lowest in parietal cortex. Circadian rhythms in the concentration of the DA metabolite, homovanillic acid (HVA), were found in olfactory tubercle, amygdala and caudate-putamen, but not in nucleus accumbens. A circadian rhythm in the concentration of the DA metabolite, 3,4-dihydroxyphenylacetic acid (DOPAC), occurred in nucleus accumbens, but not in olfactory tubercle or caudate-putamen. The mean 24-hr concentration of HVA was highest in caudate-putamen, intermediate in nucleus accumbens, and lowest in olfactory tubercle and amygdala. The mean 24-hr concentration of DOPAC was highest in nucleus accumbens and lower in olfactory tubercle and caudate-putamen. Circadian rhythms were found in the concentration of cyclic GMP (cGMP) in all regions measured except parietal cortex. The mean 24-hr concentration varied 128-fold, highest in nucleus accumbens, frontal poles, and hypothalamus and lowest in cingulate cortex. Circadian rhythms in cyclic AMP (cAMP) concentration were found in piriform, temporal, occipital, cingulate, and parietal cortex, amygdala and nucleus accumbens. No rhythms were found in frontal or insular cortex, hypothalamus, hippocampus, caudate-putamen or olfactory tubercle. The 24-hr mean cAMP concentration varied 4-fold, highest in parietal cortex and lowest in caudate-putamen and amygdala. Norepinephrine metabolites and dopamine metabolites were rhythmic in few regions. It is, therefore, unlikely that the rhythmicity measured in adrenergic receptors is, in general, a response to rhythmic changes in adrenergic transmitter release. The putative second messenger response systems, especially cGMP, were more often rhythmic. The rhythms in cGMP are parallel in form and region to those in the α_1-adrenergic receptor and may act as 2nd messenger for that receptor. In vivo, only the rhythm in cAMP in cingulate cortex parallels changes in the α_1-adrenergic receptor, even though rhythms in cAMP *in vitro* can reflect rhythms in cortical α_1- and β-receptor number. Cyclic AMP rhythms probably represent a summation of stimulatory and inhibitory transmitter receptor actions, perhaps modified by rhythms in the adenylate cyclase complex and its substrates.

Introduction

Circadian rhythms have been demonstrated in the number of α_1- and β-adrenergic, muscarinic cholinergic, dopamine, benzodiazepine and opiate receptors (1). Daily rhythms in the concentrations of rat brain biogenic amine have also been reported (2–5). Changes in neurotransmitter secretion or turnover have been shown to alter the levels of neurotransmitter receptors (6–8).

Daly *et al.* (9) found that in rat brain, agonist occupancy of the α_1-receptor and β-adrenergic receptors stimulated the production of cyclic AMP (cAMP). Daily rhythms in brain cAMP concentration have been reported (10, 11).

The preceding paper (12) described circadian

*Address all correspondence to: Marian S. Kafka, Clinical Neuroscience Branch, NIMH, Bldg. 10, Room 4N214, Bethesda, MD 20892, U.S.A.

Table 1. Statistics

Brain region	Anova *F*-value	*P*-value	Differences among means of time-points $P>0.05$ (hr)	$P>0.01$ (hr)
(a) MPG·SO_4 and DHPG·SO_4 concentration				
Frontal cortex	0.46 (5,39)	N.S.	—	—
Cingulate cortex	0.49 (5,31)	N.S.	—	—
Parietal cortex	2.38 (5,38)	N.S.	—	—
Piriform cortex	1.30 (5,38)	N.S.	—	—
Insular cortex	0.98 (5,15)	N.S.	—	—
Occipital cortex	4.60 (5,15)	<0.01*	10h > 14h = 18h	10h > 22h = 2h = 6h
Temporal cortex	0.22 (5.37)	N.S.	—	—
Hippocampu	3.02 (5,18)	N.S.	—	—
Hypothalamus	0.56 (5,36)	N.S.	—	—
Pons–Medulla	1.28 (5,41)	N.S.	—	—
Thalamus–septum	1.37 (5,39)	N.S.	—	—
Cerebellum	0.32 (5,42)	N.S.	—	—
DHPG·SO_4				
Insular	1.36 (4,14)	N.S.	—	—
Parietal	4.36 (5,37)	<0.01	14h > 18h	14h > 22h = 2h = 6h
Temporal	1.69 (5,31)	N.S.	—	—
Occipital	5.03 (5,16)	<0.01	10h > 6h	10h > 22h = 2h
Hippocampus	0.42 (5,18)	N.S.	—	—
Hypothalamus	2.95 (5,34)	<0.05	6h > 2h	—
Pons–Medulla	0.58 (5,41)	N.S.	—	—
Cerebellum	0.41 (5,42)	N.S.	—	—
(b) HVA and DOPAC concentrations				
HVA				
Olfactory tubercle	2.73 (5,36)	<0.05	2h > 22h	—
Amygdala	3.54 (5,15)	0.05	—	14h > 6h
Nucleus accumbens	1.14 (5,18)	<N.S.	—	—
Caudate-putamen	3.01 (5,40)	<0.05†	—	—
DOPAC				
Olfactory tubercle	1.30 (5,32)	N.S.	—	—
Nucleus accumbens	3.12 (5,18)	<0.05	10 > 6h	—
Caudate-putamen	0.80 (5,37)	N.S.	—	—
(c) cGMP concentration				
Olfactory tubercle	3.36 (5,37)	<0.05	14h > 22h = 2h	—
Frontal poles	12.50 (5,40)	<0.01	2h = 6h > 18h	22h = 2h = 6h > 10h = 14h
Frontal cortex	7.00 (5,42)	<0.01	14h > 22h	6h > 18h = 22h
Cingulate cortex	11.10 (5,42)	<0.01	—	6h > 10h = 14h = 18h = 22h = 2h
Insular cortex	10.60 (5,40)	<0.01	18h > 10h	22h = 2h = 6h > 10h 2h = 6h > 14h
Piriform cortex	2.50 (5,41)	<0.05	18h > 2h	—
Parietal cortex	1.85 (5,34)	N.S.	—	—
Temporal cortex	22.28 (5,41)	<0.01	—	14h > 10h = 18h = 22h = 2h = 6h
Occipital cortex	9.61 (5,37)	<0.01	2h > 14h = 22h	2h > 10h = 18h 6h > 10h = 14h = 18h = 22h
Rest of cortex	10.68 (5,41)	<0.05	6h = 10h > 22h	14h > 10h = 8h = 22h = 2h = 6h
Nucleus accumbens	14.90 (5,41)	<0.01	—	6h > 10h = 14h = 18h = 22h = 2h
Caudate-putamen	2.50 (5,37)	<0.05	18h > 10h = 14h = 2h 22h > 14h	—

(continued)

Table 1 *(continued)*

Brain region	Anova *F*-value	*P*-value	Differences among means of time-points $P<0.05$ (hr)	$P<0.01$ (hr)
Amygdala	5.80 (5,38)	<0.01	10h = 14h > 2h 18h = 22h > 6h	18h = 22h > 2h
Hypothalamus	3.08 (5,41)	<0.05	14h = 2h > 18h	—
Hippocampus	5.93 (5,39)	<0.01	6h > 14h = 18h	6h = 2h > 10h
(d) cAMP concentration				
Olfactory tubercle	0.33 (5,32)	N.S.	—	—
Frontal poles	0.48 (5,40)	N.S.	—	—
Frontal cortex	0.46 (5,42)	N.S.	—	—
Temporal cortex	4.62 (5,41)	<0.01	10h > 6h	14h > 6h
Occipital cortex	3.25 (5,40)	<0.05	14h > 2h	—
Cingulate cortex	5.11 (5,38)	<0.01	6h > 10h	—
Parietal cortex	10.8 (5,42)	<0.01	18h > 10h 14h > 6h 10h > 2h 22h > 6h	18h > 2h = 6h 14h > 2h 22h > 2h —
Insular cortex	2.26 (5,36)	<0.05	—	—
Piriform cortex	2.56 (5,38)	<0.05	22h > 2h	—
Hypothalamus	1.20 (5,37)	N.S.	—	—
Hippocampus	1.92 (5,38)	N.S.	—	—
Amygdala	2.01 (5,35)	<0.05	14h > 10h = 2h	—
Nucleus accumbens	3.90 (5,39)	<0.01	2h = 6h > 10h	22h > 10h
Caudate-putamen	1.74 (5,42)	N.S.	—	—

*$N=2$ at 1000hr in occipital MHPG·SO_4 making analysis of rhythm uncertain.
†ANOVA indicated a significant rhythm, but Tukey indicated no difference between time-points.

rhythms in α_1-, α_2- and β-adrenergic, cholinergic muscarinic and benzodiazepine receptors in discrete brain regions. In this paper, the occurrence of circadian rhythms in NE metabolites, HVA and DOPAC, as well as in putative second messengers, cGMP and cAMP, will be described. The relationships between these circadian rhythms in transmitter secretion and receptor responsiveness, and circadian rhythms in transmitter receptors, will be discussed.

Materials and Methods

Rats were cared for, enucleated, and sacrificed, the brains removed, dissected into regions, and frozen as described in the preceding paper (12). The study was carried out in two equal parts.

A region from four rats at each time-point was pooled on ice and kept frozen for metabolite assay. Frozen pooled regional samples were prepared and analyzed simultaneously for 3-methoxy-4-hydroxyphenylglycol (MHPG) and 3,4-dihydroxyphenylglycol (DHPG) by a gas chromatographic mass spectometric assay (13). Conjugated MHPG and DHPG (as sulfates) represent the majority of reduced NE metabolites present in rat brain (14).

Homovanillic acid (HVA) and 3,4-dihydroxyphenylacetic acid (DOPAC) were measured by a gas chromatographic mass spectrometric method measuring the free, unconjugated acidic dopamine metabolites (15). A significant portion of rodent DA acidic metabolites are in the free form.

Rats were housed and enucleated as described previously. Two–three days after enucleation, the rats were killed at 4-hr intervals over a 24-hr period, four rats at a time-point, by 5 sec of focused microwave irradiation to the head

(Litton Microwave Oven). The animals were guillotined, the brains quickly removed, put on ice and sliced (2-mm thick slices). The slices were transferred to microscope slides, frozen on dry ice and stored at −20°C. Later the slices were removed from the freezer, kept frozen on dry ice, and dissected, using a stereomicroscope, into the regions indicated (16, 17). They were then stored in a freezer (−70°C) until the measurement of the cGMP and cAMP concentration.

At the time of the cGMP and cAMP assays the brain regions (each analyzed separately) were sonicated in 1 ml of sodium acetate buffer (pH 6.2; 0.05 M) at 4°C. Sonicates were centrifuged at 30,000 *g* (Sorvall Superspeed, SS34 rotor) for 20 min at 4°C (Hunt and Dalton). The supernatents were transferred by aspiration to clean tubes. cGMP and cAMP were measured by radioimmunoassay (18) using cyclic nucleotide Kits (New England Nuclear). The pellets were hydrolyzed in 1 ml of 0.1 N NaOH overnight at 40°C and the protein measured (19), using bovine serum albumin as a standard.

The statistical significance of the rhythms in metabolites and nucleotides was measured by one-way analysis of variance (ANOVA), and the statistical significance of the difference between peaks and troughs, by Tukey's LSD test (Table 1). The data from the two parts of the experiment were not statistically different (2-way analysis of variance) for any of the variables; accordingly, all data from the same time-point in both parts were pooled.

Brain preparation

At each time-point (4-hr intervals over a 24-hr period) six groups of three rats were killed, their brains excised and immediately immersed in ice-cold Krebs–Ringer Bicarbonate Glucose buffer (KRG buffer) containing 122 mM NaCl, 3 mM KCl, 1.2 mM $MgSO_4$, 1.3 mM $CaCl_2$ 0.4 mM KH_2PO_4, 10 mM glucose and 25 mM $NaHCO_3$ and saturated with 95% O_2/5% CO_2. The three brains were dissected out at 4°C and the cerebral cortices (left and right separated) randomly processed. The five half-cortices were sliced (in a McIlwain tissue chopper, 260 × 260 μm) and utilized as will be described.

Tissue preparation for receptor measurements

One sliced half-cortex was incubated, shaking, in 15 ml of aerated KRG buffer at 37°C for 90 min. The buffer was filtered through polyester mesh which retained the slices. The slices were frozen on dry ice and stored at −20°C for measurement of binding to α_1- and β-receptors.

Tissue preparation and incubation for cAMP production

The four remaining cerebral half-cortices were pooled and incubated in 15 ml of aerated KRG buffer at 37°C. The slices, collected as before, were transferred to another 10 ml of aerated KRG buffer, containing 30 μM unlabelled adenine and 100 μl (10 μl/ml) of [2-^{3}H]adenine (S.A. 15 Ci/mmol, New England Nuclear), and incubated for 40 min at 37°C.

Slices labelled with [^{3}H]adenine were washed twice with KRG buffer, collected, and incubated again for 15 min in 15 ml of aerated, KRG buffer at 37°C. The tissue, was distributed in equal portions to beakers containing 10 ml of aerated KRG buffer at 37°C. The slices were incubated for 5 min with norepinephrine (NE 20 μM) to induce the accumulation of [^{3}H]cAMP, with and without phentolamine HCl or DL-propranolol (50 μM) to distinguish the [^{3}H]cAMP accumulation due to α_1- from that due to β-receptor stimulation. The slices were collected, and transferred to test tubes containing ice-cold trichloracetic acid (6%), homogenized with a Brinkmann Polytron and centrifuged for 15 min at 1700 *g*. The supernatant was stored at −20°C for the estimation of [^{3}H]cAMP.

Measurement of cAMP

For the measurement of [^{3}H]cAMP, 200 μl of unlabelled cAMP (1.25 mM) was added to each thawed, vortexed supernatant. Fifty microliters was counted for the estimation of total radioactivity. The [^{3}H]cAMP formed by the cortical slices was isolated from the supernatant by the double column method of Salomon *et al.* (38). The [^{3}H]cAMP accumulation is expressed as percentage conversion, i.e. the total radioactivity present as [^{3}H]cAMP divided by the baseline [^{3}H]cAMP measured. The method for measuring

[^{3}H]cAMP production was essentially the one described by Shimizu *et al.* (39).

α_1 and β-receptor measurement

Membrane preparations for α_1- and β-receptor binding assays were obtained by homogenizing tissue in ice-cold Tris buffer (pH 7.7., 0.05 M) at a concentration of 5% (W/V) wet weight of tissue. The homogenates were centrifuged at 27,200 *g* in a Beckman J-21C centrifuge (rotor JA 20) for 6 min, and the supernatant discarded. The pellet was washed, centrifuged, and resuspended in the same buffer (final concentration of 100 mg wet weight of brain/ml).

The number α_1-adrenergic receptors was measured by the specific binding of the α_1-antagonist [^{3}H]WB4101 (S.A. 24.7 Ci/mMol, New England Nuclear). Specific binding was defined as the difference between the total binding and the amount bound in presence of phentolamine (1×10^{-5}M). The tritiated ligand (0.42 nM) and cortical membranes, with and without phentolamine were incubated for 15 min at room temperature (24°C). In a similar manner, the number of β-adrenergic receptors was measured by the specific binding of the β-antagonist [^{3}H]dihydroalprenolol ([^{3}H]DHA) (S.A. 47.5 Ci/mMol, New England Nuclear), defined as the difference between the total binding of [^{3}H]DHA and the amount bound in the presence of the β-antagonist, DL-propranolol (2×10^{-6}M). The labelled ligand (0.76 nM) and cortical membranes were incubated in triplicate for 12 min at 37°C. For both α_1- and β-receptors, binding incubation was terminated by rapid filtration under vacuum through GF/B Whatman filters, followed by washing of the filters twice with 6 ml of ice-cold Tris buffer (pH 7.0, 0.05 M). Radioactivity was counted in a Beckman Scintillation Counter. Low concentrations of the ^{3}H-ligands were used so that a change in receptor affinity or number would appear as a change in binding, and the two could subsequently be distinguished by saturation experiments at appropriate time-points. Scatchard analyses of α_1- and β-adrenergic receptor binding were made from saturation curve data with [^{3}H]WB 4101 ranging in concentration from 0.6–12 nM, and [^{3}H]-DHA, from 0.5 to 14 nM. The affinity of the receptors was unchanged over the 24-hr day.

Results

A circadian rhythm in MHPG concentration, found in the hippocampus, peaked in the middle of subjective day (the period in the light : dark cycle [L : D] in which lights were on). No rhythms were found in frontal, cingulate, parietal, piriform, insular, or temporal cortex, pons–medulla, cerebellum, thalamus-septum or hypothalamus (Figure 1). A circadian rhythm with a peak at 1000 hr may exist in occipital cortex. The magnitude of the MHPG concentration at that time-point, however, may not be reliable, as there were only two samples.

The 24-hr mean MHPG concentration varied 3.5-fold, highest in cingulate and lowest in occipital cortex (Table 2).

Circadian rhythms in DHPG concentration were found in occipital and parietal cortex and hypothalamus. Peak DHPG concentrations in cortex were in early to middle subjective day and at subjective dawn, (period in L : D that immediately precedes turning on the light) in hypothalamus (Figure 1).

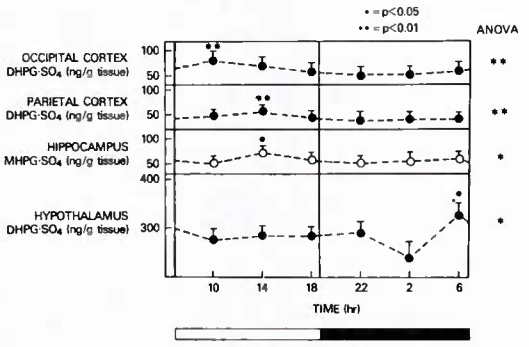

Figure 1. The concentration of MHPG·SO_4 and DHPG·SO_4 in rat brain regions. The concentration of MHPG and DHPG were measured at six time-points during the 24-hr day using a gas chromatography mass spectrometry method. Each point is the mean ± S.E.M. of metabolite measurements in four–eight rats, except for the 1000 hr point in insular and occipital cortex in which the measurement is in three rats. The black bar beneath the figure marks subjective night and the vertical lines through the figure, the timing of lights on and off during L : D. The significance of the rhythm was measured by one-way analysis of variance (ANOVA) and the significance of differences among time-points by Tukey's Test (HSD). Statistical data are given in Table 1.

Table 2. 24-hr mean metabolite, cGMP and cAMP concentrations

Brain region	MHPG·SO$_4$ (ng/g wet wt)		DHPG·SO$_4$		HVA (μg/g wet wt)		DOPAC (μg/g wet wt)		cGMP (pmol/mg protein)		cAMP (pmol/mg protein)	
Olfactory tubercle	—		—		465 ± 26	(42)	1379 ± 62	(38)	1.4 ± 0.07	(43)	9 ± 0.5	(38)
Frontal poles	—		—		—							
Frontal cortex	73 ± 1	(45)	—		—		—		0.52 ± 0.04	(48)	7 ± 0.2	(44)
Cingulate cortex	150 ± 2	(37)							0.03 ± 0.006	(40)	12 ± 0.5	(44)
Insular cortex	96 ± 3	(21)	118 ± 7	(19)	—		—		1.7 ± 0.11	(46)	6 ± 0.4	(42)
Piriform cortex	103 ± 4	(44)	—		—		—		1.4 ± 0.06	(42)	7 ± 0.4	(44)
Parietal cortex	50 ± 1	(44)	50 ± 2	(43)	—		—		0.37 ± 0.03	(44)	25 ± 2	(48)
Temporal cortex	48 ± 1	(43)	56 ± 1	(37)	—		—		3.0 ± 0.5	(47)	7 ± 0.4	(47)
Occipital cortex	42 ± 4	(21)	61 ± 5	(22)	—		—		0.12 ± 0.02	(43)	8 ± 0.5	(46)
Rest of cortex	—		—		—		—		0.46 ± 0.04	(47)	10 ± 0.5	(46)
Hypthalamus	84 ± 2	(42)	274 ± 11	(40)	—		—		2.0 ± 0.07	(47)	9 ± 0.3	(43)
Hippocampus	61 ± 3	(24)	91 ± 2	(24)	—		—		0.70 ± 0.04	(45)	8 ± 0.3	(44)
Amygdala	—		—		433 ± 97	(21)	—		1.5 ± 0.14	(44)	6 ± 0.3	(39)
Nucleus accumbens	—		—		684 ± 32	(24)	2087 ± 100	(24)	3.7 ± 0.25	(47)	9 ± 0.3	(45)
Caudate-putamen	—		—		846 ± 30	(46)	1590 ± 47	(43)	0.6 ± 0.006	(40)	6 ± 0.2	(48)
Thalamus-septum	102 ± 3	(45)	—		—		—		—		—	
Pons–Medulla	105 ± 4	(48)	156 ± 4	(47)	—		—		—		—	
Cerebellum	47 ± 1	(48)	58 ± 1	(48)	—		—		—		—	

M ± S.E.M.
( ) Number of measurements.

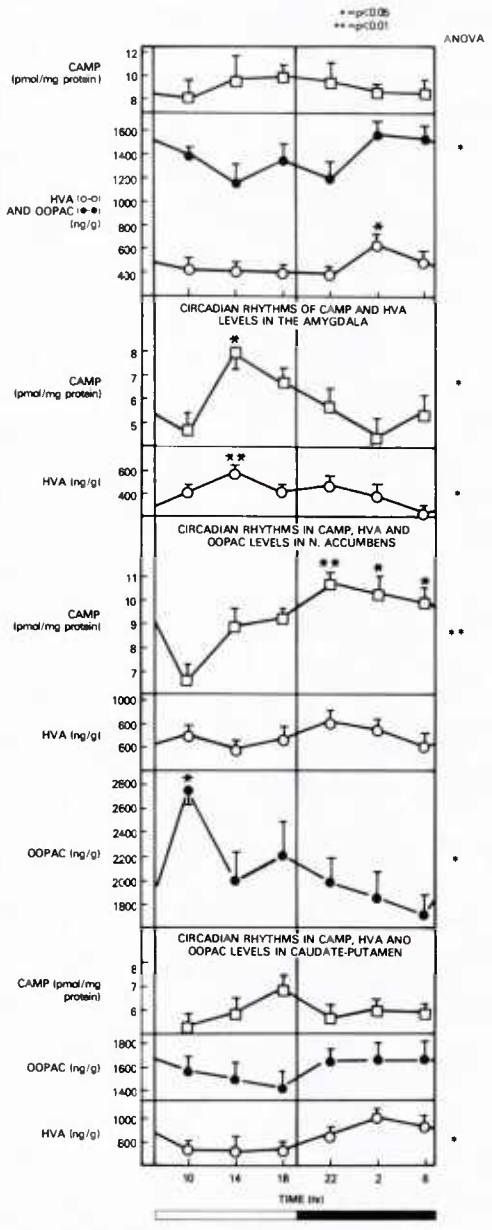

Figure 2. The concentration of HVA and DOPAC in rat brain regions. The concentration of HVA and DOPAC were measured at six time-points during the 24-hr period using a gas chromatography mass spectrometry method. Each point was the mean ± S.E.M. of metabolite measurements in four–eight rats, except for HVA in amygdala with three rats. The black bar beneath the figure delineates subjective night and the vertical, times of lights on and off during L : D. The significance of the rhythm was measured by one-way analysis of variance (ANOVA) and the significance of differences between time-points by Tukey's Test (HSD). Statistical data are in Table 1.

The 24-hr mean concentration of DHPG varied 5.5-fold, highest in hypothalamus and lowest in parietal cortex (Table 2).

Circadian rhythms in HVA concentration were observed in olfactory tubercle and amygdala. Peak concentration in olfactory tubercle was in the middle of subjective night (the period under L : D when lights were off) and, in amygdala, in the middle of subjective day (Figure 2). A significant rhythm in caudate-putamen was indicated by ANOVA, but the Tukey LSD test showed no significant difference between time-points. No rhythm was found in nucleus accumbens.

The 24-hr mean concentration of HVA varied 2-fold, highest in caudate-putamen and lowest in amygdala (Table 2).

A circadian rhythm in DOPAC concentration was found in nucleus accumbens, the peak concentration occurring early in subjective day. No rhythm was found in olfactory tubercle or caudate-putamen (Figure 2).

The 24-hr mean DOPAC concentration varied 1.5-fold, highest in nucleus accumbens and lowest in olfactory tubercle (Table 2).

Circadian rhythms in cGMP concentration were found in frontal poles, frontal, cingulate, insular, piriform, temporal and occipital cortex, olfactory tubercle, nucleus accumbens, caudate-putamen, amygdala, hypothalamus, and hippocampus. No rhythm was observed in parietal cortex (Figure 3).

The peak concentration of cGMP occurred in subjective night in frontal poles, frontal, cingulate, insular, and occipital cortex, nucleus accumbens, hypothalamus and hippocampus (Figure 3).

In contrast to regions with peaks in subjective night, regions with peak cGMP concentrations in subjective day included insular, piriform, and temporal cortex, olfactory tubercle, caudate-putamen and amygdala. In insular and piriform cortex and caudate-putamen the peak had begun at subjective dusk (the period in L : D just before lights were turned off). The concentration in insular cortex continued until subjective day and the concentration in the caudate-putamen fell in the middle of subjective night. The peak in cGMP in piriform cortex was at subjective dusk.

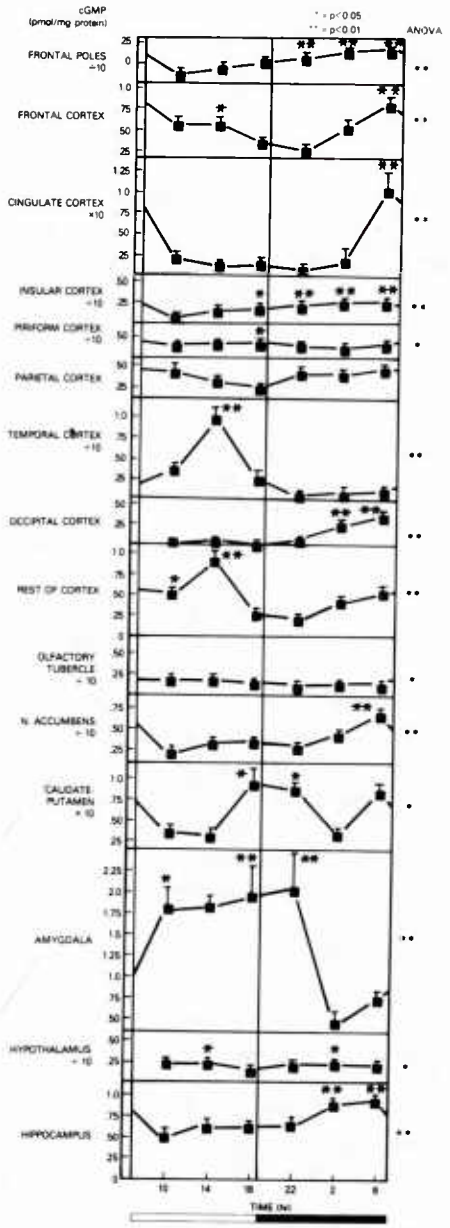

Figure 3. The concentrations of cGMP in rat brain regions. The cGMP concentration was measured at six time-points during the 24-hr day. Note that the range of amplitudes was so great that the ordinates of the figures for some regions are plotted at 1/10 or 10 times their true magnitudes to aid visualization. The black line beneath demarcates subjective night, and the vertical lines in the figures, times of lights on and off in L:D. Measurements were made using a radioimmune assay. Each point is the mean ± S.E.M. of cGMP measured in eight rats. The significance of the rhythm was measured by one-way analysis of variance (ANOVA) and the significance of differences among time-points by Tukey's Test (HSD). Statistical data are given in Table 1.

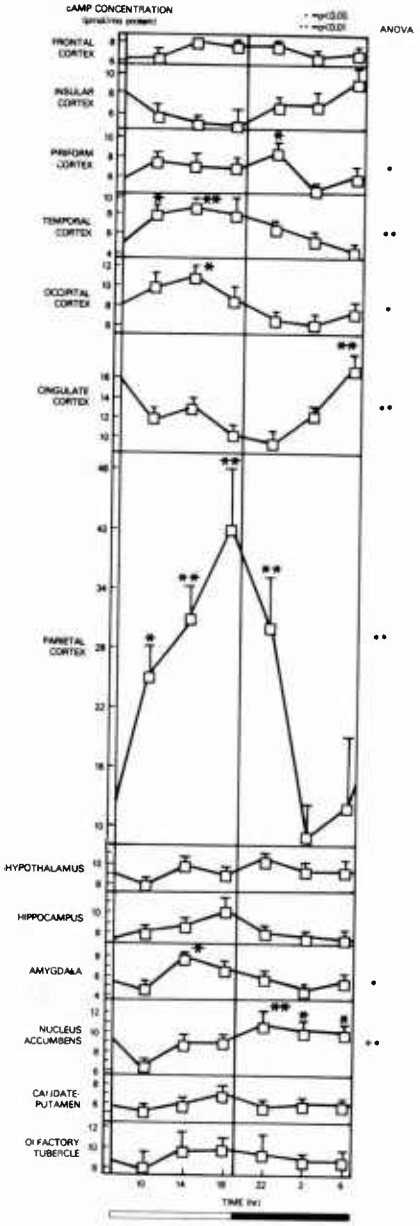

Figure 4. The concentration of cAMP in rat brain regions. The cAMP concentration was measured at six time-points during the 24-hr day. The black line beneath the figure delineates subjective night and the vertical lines, times of lights on and off during L:D. Measurements were made using a radioimmune assay. Each point is the mean ± S.E.M. of cAMP measured in eight rats. The significance of the rhythm was measured by one-way analysis of variance (ANOVA) and the significance of differences among time-points by Tukey's Test (HSD). Statistical data are given in Table 1.

In amygdala the peak had begun at subjective dawn, continued throughout subjective day, and fallen in the middle of subjective night. In hypothalamus, the trough was at subjective dusk with a higher concentration over the rest of the day.

The 24-hr mean cGMP concentration varied 123-fold (Table 2), highest in the nucleus accumbens and lowest in cingulate cortex.

Circadian rhythms in cAMP concentration were observed in piriform, temporal, occipital, cingulate and parietal cortex, and in amygdala and nucleus accumbens (Figure 4). No rhythms were found in frontal or insular cortex, hypothalamus, hippocampus, caudate-putamen or olfactory tubercle (Figure 4).

When the cAMP concentration was rhythmic in cortex, the rhythmic patterns differed with the cortical region. The temporal, occipital, and parietal rhythms peaked during subjective day, the peak in parietal cortex extending into subjective night. The cAMP concentration in piriform and cingulate cortex peaked in subjective night, the cingulate peak occurring at subjective dawn.

The patterns in cAMP concentration differed from one another in the nine limbic regions measured. Like the rhythms in cGMP concentration, the rhythms in cingulate cortex and the nucleus accumbens peaked in subjective night, and in amygdala, in subjective day. Unlike the cGMP concentration, the cAMP concentration was without circadian rhythm in frontal and insular cortex, hypothalamus, hippocampus, caudate-putamen and olfactory tubercle.

The 24-hr mean concentration of cAMP varied 4-fold, highest in parietal cortex and lowest in caudate-putamen and amygdala.

The wave-form of the circadian rhythms found in metabolites and cyclic nucleotides was unimodal.

Discussion

The wave-form of rhythms, not only in metabolites, cAMP, cGMP, but in all the receptors measured as well (12), was unimodal. Occurrence of peak and trough in the circadian rhythm is, consequently, clearer than that often encountered in such measurements under L : D conditions (1).

In rats entrained to an L : D cycle, it has been reported that cAMP levels in hypothalamus rose with the beginning of light, fell to a minimum in light, and remained low through the dark phase (11). In constant darkness, no rhythm in cAMP concentration was measured in hypothalamus in our rats. In another study (10), under an L : D regimen, rhythms in cAMP concentration were found in cerebellum and pons–medulla, the levels higher in the light than the dark. Even though those rats had been entrained to an L : D cycle when killed, no rhythms in cerebral cortex, midbrain, hippocampus, hypothalamus, or caudate were observed. It is possible that if hypothalamic nuclei were assayed, daily rhythms in cAMP might be present, as daily rhythms in adrenergic receptors (20, 21) have been reported.

The levels of cAMP measured in our study were similar to those measured by Valases *et al.* (11) and Choma *et al.* (10). In our study the level in parietal cortex is at least twice as high as the concentration in any other region, suggesting the presence of potent generators of cAMP in the parietal cortex.

Norepinephrine, secreted at presynaptic terminals in rat brain, is metabolized to DHPG and MHPG, the former, probably intraneuronally, and the latter, extraneuronally. In rat brain both MHPG and DHPG provide a measure of central NE metabolism and noradrenergic activity. The concentrations of total MHPG and DHPG are lower than those reported (13), as they have not been corrected for metabolite recovery. Confirming a previous report hypothalamic DHPG concentration is several-fold higher than MHPG, though the two are relatively similar in concentration in most regions (13, 14).

Circadian rhythms in NE metabolites were found in very few of the brain regions examined; for MHPG, only in hippocampus. The peak occurred early in subjective day in occipital and parietal cortex and hippocampus, at dawn in the hypothalamus. Though rhythms existing in very small regions may have been missed in measuring the regions selected in this study, the data suggest that presynaptic NE metabolism, including NE secretion, is not rhythmic in most

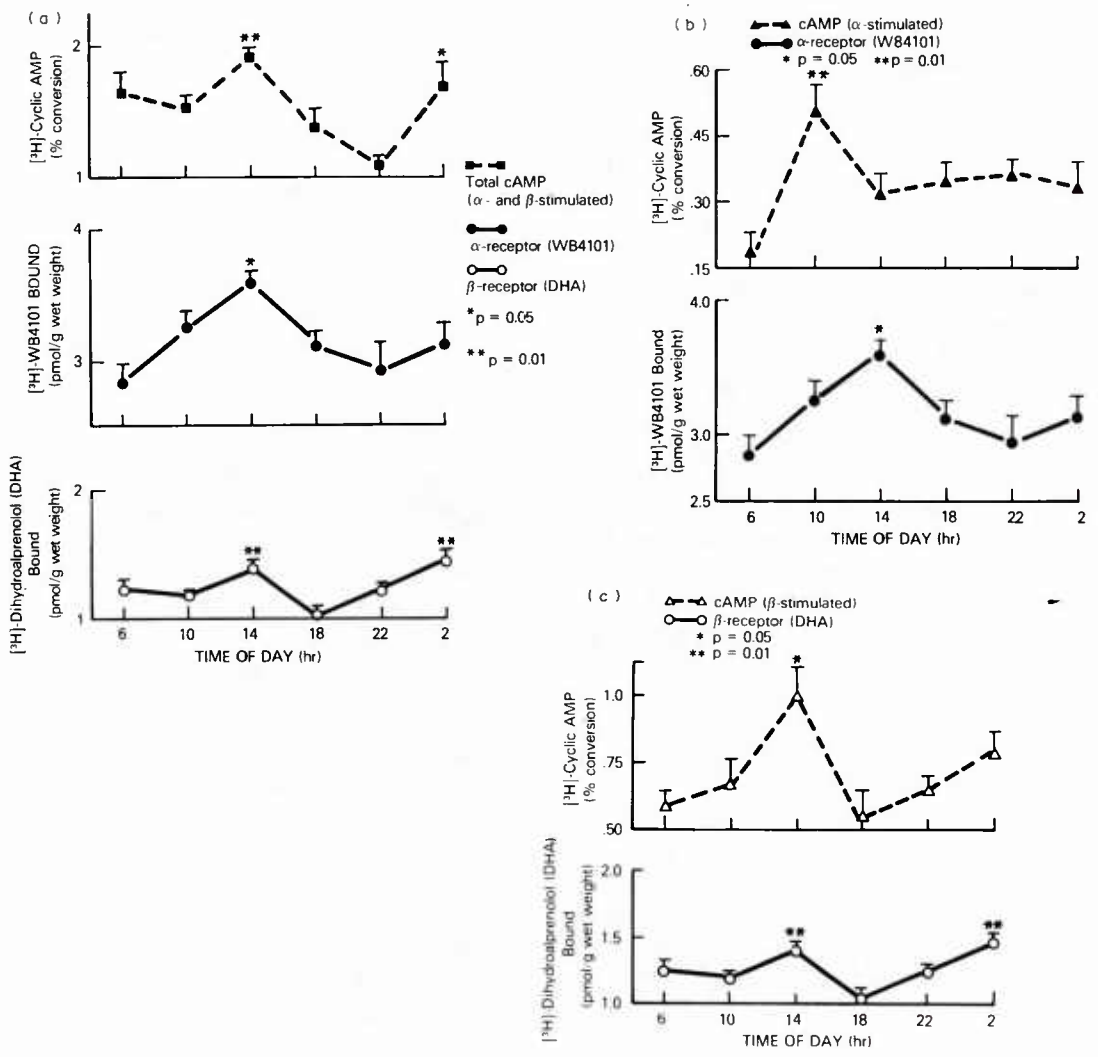

Figure 5. Alpha$_1$- and beta-adrenergic receptor-mediated cyclic AMP production and specific binding to α_1- and β-adrenergic receptors in cerebral cortical slices from male Sprague–Dawley rats maintained under L : D conditions for 18 days, then in constant darkness (D : D) for 2–3 days before death. (a) Alpha$_1$- and β-adrenergic receptor-mediated cAMP production, and specific binding to α_1- and β-adrenergic receptors in rat cerebral cortical slices measured at six points throughout the 24-hr day. Each point represents the mean ± S.E.M. of five–six sliced hemi-cortices measured in triplicate. One-way ANOVA for cAMP (closed squares): $F(5,30)=4.34$, $P<0.01$; for α_1-receptor (closed circles): $F(5,26)=2.63$, $P<0.05$; and for β-receptor (open circles): $F(5,29)=5.61$, $P<0.01$. Differences between time-points: for cAMP, 2200 hr= 0200 hr, for the α_1-receptor 1400 hr > 0600 hr, and for the β-receptor 1800 hr < 1400 hr = 0200 hr. (b) Alpha$_1$-adrenergic receptor-stimulated cAMP production and specific binding to α_1-adrenergic receptors in rat cerebral cortical slices measured at six points throughout the 24-hr day. Each point represents the mean ± S.E.M. of six pools of four sliced hemi-cortices (cAMP production), or of five–six sliced hemi-cortices measured in triplicate (binding). One-way ANOVA for α_1-stimulated cAMP production (closed triangles): $F(5,30)=2.9$ $P<0.05$, and the difference between time-points: 1000 hr > 0600 hr. One-way ANOVA, differences between time-points, and statistical data, for α_1-receptors (closed circles) are the same as in (a). (c) Beta-adrenergic receptor-stimulated cAMP production and specific binding to β-adrenergic receptors in rat cortical slices, measured at six points throughout the 24-hr day. Each point represents the mean ± S.E.M. of six pools of four sliced hemi-cortices (cAMP production), or of five–six sliced hemi-cortices measured in triplicate (binding). One-way ANOVA for β-stimulated cAMP production (open triangles): $F(5,30)=3.6$ ($P<0.05$) and the difference between time-points: 1400 hr > 1800 hr = 0600 hr. One-way ANOVA, differences between time-points, and statistical data for the β-receptor (open circles) are the same as in (a).

brain regions. For this reason, rhythms in NE secretion are, in general, unlikely to confer the rhythms measured in adrenergic receptors. As increased NE secretion has been shown to decrease the number of adrenergic receptors (6, 7), it is possible that, in hippocampus, increased NE secretion decreases the number of α_1-receptors during subjective day. The increase in α_2-receptors in parietal, and in α_1- and β-receptors in hypothalamus, paralleling increasing DHPG concentration, is, however, opposite in direction from that expected if increased transmitter down-regulates its homologous receptor numbers.

Rat brain DA metabolites provide a measure of dopaminergic cell activity, as their concentrations depend on the rates of DA turnover and release (15). Concentrations of DOPAC were similar to those reported previously (15) in olfactory tubercle and caudate-putamen, two regions accounting for about 90% of DA brain metabolites. Concentrations of HVA were lower. Variability in concentrations of DA metabolites is not unexpected, however, as differences in brain DA turnover can vary 2-fold within a rat species (22).

Circadian rhythms in HVA concentration were found in olfactory tubercle and amygdala; circadian rhythms in DOPAC concentration, only in nucleus accumbens. For the reasons mentioned above, rhythms may have been missed. The data suggest, however, that DA release often is not rhythmic.

The role of cGMP in neural tissue remains unclear. Changes in the concentration of cGMP could be a cause, or a result, of changes in neuronal activity. It is possible that cGMP acts, not as an activator of ion fluxes and neurotransmitter release, but as modulator of processes that restore neurons after periods of activity (23, 24). In contrast to the release of NE and DA, the concentration of cGMP displays rhythms of considerable amplitude in all regions measured except parietal cortex. (A rhythm similar to that in temporal cortex, was measured in the cortical tissue remaining after the indicated regions were removed).

Muscarinic cholinergic M_1-receptors and α_1-adrenergic receptors may stimulate phosphatidylinositol hydrolysis, and with it, generate cGMP (25, 26). The only region measured in the current study in which both cholinergic receptors and cGMP are rhythmic is caudate-putamen. Cyclic GMP is high at subjective dusk and during early subjective night, a rhythmic pattern contrasting with that in cholinergic receptor binding which has its trough at that time (12). The data suggest that the rhythm in cholinergic receptors (although M_1- and M_2-receptors were not measured separately) do not confer the caudate-putamen cGMP rhythm.

In contrast, cortical α_1-receptor rhythms and cGMP rhythms peak in subjective night except for piriform (α_1-receptor and cGMP rhythms) and temporal cortex (only cGMP rhythm). In caudate-putamen, hippocampus and hypothalamus the increase in α_1-receptor binding slightly precedes increasing cGMP concentration. It is possible, then, that α_1-receptor rhythms in frontal, cingulate, piriform and occipital cortex, caudate-putamen, hypothalamus and hippocampus may trigger an intraneuronal cascade conferring a rhythm in cGMP concentration. Though not measured in this study, α_1-receptor-mediated phosphatidylinositol hydrolysis itself might have circadian rhythmicity, and because it regulates many cell functions, may be a very important brain modulator of functions that vary across the day.

Circadian rhythmicity in cAMP concentration occurs more often in cortical than in non-cortical brain regions. The most rostral cortical regions, including the frontal poles (not shown), do not undergo circadian rhythms. As these regions are high in dopaminergic innervation, dopamine-stimulated cAMP production may not be rhythmic. Two other areas innervated by dopaminergic tracts were measured. The nucleus accumbens has a prolonged peak in cAMP concentration in subjective night (see below). No rhythm was measured in caudate-putamen cAMP concentration. Under entrained light: dark conditions, arrhythmia in the caudate has been observed before (10).

The relationships between circadian rhythms in cAMP and cGMP and the circadian rhythms in adrenergic receptors are complex. In regions in which both are rhythmic, the patterns in

cAMP and cGMP concentration are similar, except for parietal and occipital cortex in which they are opposite in phase, the cAMP peak occurring in subjective day, and cGMP, in subjective night.

In limbic regions the circadian rhythmic patterns in both cAMP and cGMP concentrations are of two kinds: cingulate cortex and nucleus accumbens peak in subjective night, and amygdala peaks in subjective day. In cortical slices, *in vitro*, increased cAMP production accompanies an increase in the densities of both α_1- and β-adrenergic receptors (Figure 5). In addition, both α_1- and β-receptors have been shown to stimulate cAMP production in the limbic forebrain, which includes the nucleus accumbens (9). In all regions in which a rhythm in cAMP concentration is found, there is a rhythm in α_1-receptors, and in some regions, in β-receptors as well (Ref. 12 : Figures 1 and 2). Adrenergic receptor binding was not measured in nucleus accumbens or amygdala, but like the cyclic nucleotide concentrations, binding to the α_1-receptor in the cingulate cortex peaks in subjective night.

In five cortical regions, there are circadian rhythms in cAMP concentration and in binding to at least one type of adrenergic receptor. The relationships between the rhythms in cAMP concentration and those in adrenergic receptor binding are of two different kinds. As mentioned above, in cingulate cortex, the peak cAMP concentration follows the binding to the α_1-adrenergic receptor. Stimulation of the adrenergic nerves to cingulate cortex may increase cAMP production via α_1-receptors. In contrast, in occipital, parietal and temporal cortices, the concentration of cAMP falls as the binding to adrenergic receptors rises in subjective night. This inverse relationship involves cAMP concentration and binding to α_1-receptors, in occipital cortex; cAMP concentration and binding to α_1- and α_2-receptors in temporal cortex; and cAMP and binding to α_1-, β- and α_2-receptors in parietal cortex.

Unlike the decreasés in cAMP concentration, the increases in cAMP concentration correlate in some ways with binding to adrenergic receptors. In parietal cortex, the peak in the α_2-receptor precedes and accompanies the rise in cAMP concentration. In temporal cortex the cAMP concentration rises before the peak in β-receptor binding. The contribution of α_2-receptors to cAMP production in the brain is unknown, but may be inhibitory as it is in neuroblastoma-glioma cells (27). The peak in α_2-receptors may not affect the peak in cAMP concentration in the parietal cortex, but it is possible that the peak in cAMP in temporal cortex may be sustained by the peak in β-receptor binding of NE, increased by stimulation of noradrenergic transmission to the temporal cortex.

The increased level of cAMP in subjective day, when the rat's activity is low, (in the temporal, occipital, parietal cortices and amygdala) could be analogous to the inhibitory effect of NE on cerebellar Purkinje cells (28).

In diurnal man, plasma cAMP, and in monkeys, CSF cAMP were high in the light and low in the dark (29, 30). In the nocturnal rat, cAMP concentrations in discrete brain regions were higher during waking than during sleep, except in the cerebellum (31). The increased cAMP level early in subjective night might play a role in wakefulness in these nocturnal animals.

Cyclic AMP concentration seems to be coupled with the rhythm in α_1-receptor binding in cingulate cortex. In other regions in which the cAMP concentration is rhythmic, its peak is in subjective day, when adrenergic peaks are in subjective night, and vice versa. Though the circadian rhythm in NE-stimulated CAMP production in cortical slices follows the rhythms in α_1- and β-receptor number (Figure 5), cAMP production *in vivo* does not appear to be so closely coupled to adrenergic receptor rhythms in most regions. In four of five regions in which cAMP is rhythmic, adrenergic receptor rhythms are not similar, whereas in one, the cingulate, they are. In five regions in which cAMP concentration is not rhythmic, adrenergic-receptor binding is rhythmic. Cyclic GMP rhythms are associated with α_1-rhythms, in many regions, but with β-rhythm in only one.

Regulation of cAMP concentration and the circadian rhythms in cAMP concentration seems to be complex. If adrenergic transmission alone is considered, the magnitude of the cAMP

concentration, its rhythmicity and the timing of its peaks (phase) in some regions, and its arrhythmicity in other regions could be affected by a number of parts of the system in addition to receptors.

The level of NE or epinephrine (E) in the synapse could change both the magnitude and the rhythm of the cAMP concentration. The only two regions measured in these rats in which cAMP and the NE-metabolite, DHPG, were both rhythmic, were occipital and parietal cortices. In occipital cortex, the peak DHPG concentration preceded the cAMP peak, and in parietal cortex, the maximum DHPG concentration occurred during the cAMP peak. In these two regions, it is possible that an increased NE secretion contributes to the cAMP peak. In other regions, no rhythm was found either in the concentration of cAMP or in the concentration of DHPG or MHPG. For this reason, no comparisons can be made. Though arrhythmic, the 24-hr mean level of cAMP is two-four times higher in parietal cortex than in other regions, whereas the levels of MHPG and DHPG are among their lowest in this region, suggesting that the increase in cAMP production may not be a result of increased NE secretion. The highest secretion of NE, as measured by MHPG, is in cingulate cortex, and by DHPG, is in hypothalamus. As in both of these regions cAMP concentrations are relatively high, perhaps elevated NE secretion accounts in part of the elevated cAMP levels.

Some enzymes, important in the synthesis and breakdown of adrenergic transmitters, and in the breakdown of cAMP, vary over the course of the day. Among them are dopamine-β-hydroxylase (32), NE-catabolizing monoamine oxidase (33), PNMT (4) and a phosphodiesterase (34). Variations in these enzymes could modulate the concentration of cAMP present at different times of day.

Transmitter systems other than the noradrenergic system stimulate or inhibit adenylate cyclase, and probably affect the concentration of cAMP at different times of day. Among transmitter systems altering cAMP production are the muscarinic cholinergic, dopaminergic, and opiate, all receptors which have been shown to undergo circadian rhythms (1) as do their transmitters. In amygdala, the peak in the dopamine metabolite, HVA, accompanies the peak in cAMP, suggesting DA may stimulate cAMP in this region. Many additional putative transmitters or modulators, in which circadian rhythms have not yet been investigated, e.g. adenosine and histamine, alter cyclase activity.

A large number of peptides stimulate or inhibit adenylate cyclase. Daily or circadian rhythms in the concentrations of α-MSH (35) and arginine vasopressin (36) have been reported.

Just as brain regions differ in their functions, they differ in which of their neurochemical parameters show circadian rhythmicity. The concentration of cAMP in cells has been shown to regulate protein phosphorylation and activation (37). Understanding the significance of the presence or absence of a regional circadian rhythm in cAMP concentration depends upon a more profound understanding than is currently available of the functional interactions between the transmitter systems which innervate that region.

Both the presence and the absence of regional rhythms in cAMP and cGMP concentration may be the result of rhythmic changes in the adrenergic system or complex, even rhythmic, interactions between a multiplicity of transmitter systems. The presence of regional circadian rhythms in cAMP and cGMP concentrations may be important in regulating the biochemical reactions, physiological processes, and behaviors which permit animals to adapt to daily events in the environment. The absence of regional circadian rhythms in these cyclic nucleotide concentrations may, on the other hand, help to maintain a constant internal milieu, despite changes in the external environment throughout the day.

References

1. Kafka M. S., Wirz-Justice A., Naber D., Moore R. Y. and Benedito M. A. Circadian rhythms in rat brain neurotransmitter receptors. *Fed Proc* **42**, 2796–2801, 1983.
2. Scheving L. E., Harrison W. H., Gordon P. and Pauly J. E. Daily fluctuations in biogenic amines of the rat brain. *Am J Physiol* **214**, 166–173, 1968.
3. Simon M. L. and George R. Diurnal variations in plasma corticosterone and growth hormone as correlated with regional variations in norepinephrine, dopamine, and serotonin content of rat brain. *Neuroendocrinolology* **17**, 125–138, 1975.
4. Turner B. B., Wilens T. E., Schroeder K. A., Katz R. J. and Carrol B. J. Comparison of brainstem and adrenal circadian patterns of epinephrine synthesis. *Neuroendocrinology* **32**, 257–261, 1981.
5. Hillier J. G., Martin P. R. and Redfern P. H. A possible interaction between 24H rhythms in catecholamine and 5-hydroxytryptamine concentration in the rat brain. *J Pharm Pharmacol* (Suppl) **27** 1–40, 1975.
6. Byland D. B. and U'Prichard D. C. Characterization of α_1- and α_2-adrenergic receptors. *Int Rev Neurobiol* **24**, 343–431, 1983.
7. Reisine T. Adaptive changes in catecholamine receptors in the central nervous system. *Neuroscience* **6**, 1471–1502, 1981.
8. Creese I. and Snyder S. H. Nigrostriatal lesions enhance striatal [^{3}H]-apomorphine and [^{3}H]-spiroperiodol binding. *Eur J Pharmacol* **56**, 277–281, 1979.
9. Daly J. W., Padgett W., Creveling C. R., Cantacuzene D. and Kir K. L. Cyclic AMP-generating systems: regional differences inactivation by adrenergic receptors in rat brain. *J Neurosci* **1**, 49–59, 1981.
10. Choma P. P., Puri A. K. and Volicer L. Circadian rhythm of cyclic nucleotide and GABA levels in the rat brain. *Pharmacology* **19**, 307–314, 1979.
11. Valases C., Wright S. J., Jr. and Catravas G. N. Diurnal changes in cyclic nucleotide levels in the hypothalamus of the rat. *Exp Brain Res* **40**, 261–264, 1980.
12. Kafka M. S., Benedito M. A., Blendy J. A. and Tokola N. S. Circadian rhythms in neurotransmitter receptors in discrete rat brain areas. *Chronobiol Int* **3**, 91–100, 1986.
13. Ellsworth J. D., Roth R. H. and Redmond D. E., Jr. Relative importance of 3-methoxy-4-hydroxyphenylglycol and 3,4-dihydroxyphenylglycol as norepinephrine metabolites in rat, monkey and humans. *J Neurochem* **41**, 786–793, 1983.
14. Ellsworth J. D., Redmond D. E., Jr. and Roth R. H. Plasma and cerebrospinal fluid 3-methoxy-4-hydroxyphenylethylene glycol (MHPG) as indices of brain norepinephrine metabolism in primates. *Brain Res* **235**, 115–124, 1982.
15. Bacopoulos N. G., Hattox S. E. and Roth R. H. 3,4-dihydroxyphenylacetic acid and homovanillic acid in rat plasma: possible indicators of central dopaminergic activity. *Eur J Pharmacol* **56**, 225–236, 1979.
16. Krieg W. J. S. Connections of the cerebral cortex—I. The albino rat—A. Topography of cortical areas. *J Comp Neurol* **84**, 222–275, 1947.
17. Konig J. F. R. and Klippel J. *The Rat Brain.* Krieger, New York, 1963.
18. Steiner A. L., Pagliara A. S., Chase L. R. and Kipnis D. M. Radioimmunoassay for cyclic nucleotides.—II. Adenosine 3′, 5′-monophosphate and guanosine 3′,5′-monophosphate in mammalian tissues and bodily fluids. *J Biol Chem* **247**, 1114–1120, 1972.
19. Lowry O. H., Rosebrough N. J., Farr A. L. and Randall R. J. Protein measurement with the Folin phenol reagent. *J Biol Chem* **193**, 265–275, 1951.
20. Leibowitz S. F., Jhanwar-Uniyal M. and Roland C. R. Circadian rhythms of circulating corticosterone and α_2-noradrenergic receptors in discrete hypothalamic and extrahypothalamic areas of rat brain. *Soc Neurosci Abstracts* **10**, 294, 1984.
21. Kraüchi K., Wirz-Justice A., Morimasa T., Willener R. and Feer H. Hypothalamic α_2- and β-adrenoceptor rhythms are correlated with circadian feeding: evidence from chronic methamphetamine treatment and withdrawal. *Brain Res* **321**, 83–90, 1984.
22. Brodie B. B., Costa E., Dlabac A., Neff N. H. and Smookler H. H. Application of steady state kinetics to the estimation of synthesis rate and turnover time of tissue catecholamines. *J Pharmacol Exp Ther* **154**, 493–498, 1966.
23. Symposium: Cyclic GMP in the nervous system. *Fed Proc* **42**, 3098–3113, 1983.
24. Goldberg N. D. and Haddox M. K. Cyclic GMP metabolism and involvement in biological regulation. *Annu Rev Biochem* **46**, 823–896, 1977.
25. Berridge M. J., Downes C. P. and Hanley M. R. Lithium amplifies agonist-dependent phosphatidylinositol responses in brain and salivary glands. *Biochem J* **206**, 587–595, 1982.
26. Berridge M. J. and Irvine R. F. Inositol trisphosphate, a novel second messenger in cellular signal transduction. *Nature* **312** 315–321, 1984.
27. Sabol S. L. and Nirenberg M. Regulation of adenylate cyclase of neurblastomax glioma hybrid cells by α-adrenergic receptors. *J Biol Chem* **254**, 1913–1920, 1979.
28. Bloom F. E., Hoffer B. J. and Siggins G. R. Norepinephrine mediated cerebellar synpases. A model system for neuropsychopharmacology *Bio Psychiat* **4**, 157–177, 1972.
29. Markianos M. and Lykouras L. Circadian rhythms of dopamine-β-hydroxylase and cAMP in plasma of controls and patients with affective disorders. *J Neural Transm* **50**, 149–155, 1981.
30. Perlow M. J., Festoff B., Gordon E. K., Ebert M. H., Johnson D. K. and Chase T. N. Daily fluctuation in the concentration of cAMP in the concious primate brain. *Brain Res* **126**, 391–396, 1977.
31. Ogasahara S., Taguchi Y. and Wada H. Changes in the levels of cyclic nucleotides in rat brain during the sleep–

wakefulness cycle. *Brain Brs.* **213**, 163–170.
32. Daiguji M., Mi Kuin M., Okada F. and Yamashita I. The diurnal variation of dopamine-β-hydroxylase activity in the hypothalamus and locus coeruleus of the rat. *Brain Res* **155**, 409–412, 1978.
33. Chevillard C., Barden N. and Saavedra J. M. Twenty-four hour rhythm in monamine oxidase activity in specific areas of the rat brainstem. *Brain Res* **223**, 205–209, 1981.
34. Minneman K. P. and Iversen L. I. Diurnal rhythms in rat pineal cyclic nucleotide phosphodresterase activity. *Nature* **260**, 59–61, 1976.
35. O'Donohue T. L., Wirz-Justice A., Kafka M. S., Naber D., Campbell I. C. and Wehr T. A. Effects of chronic lithium, clorgyline, imipramine, fluphenazine and constant darkness on the α-melanotropin content and circadian rhythm in rat brain. *Eur J Pharmacol* **85**, 1–7, 1982.
36. Kafka M. S., Benedito M. A., Steele L. K., Gibson M. J., Zerbe R. L., Jacobowitz D. M., Roth R. H. and Zander K., Relationships between behavioral rhythms, plasma corticosterones and hypothalamic circadian rhythms. *Chronobiol Int* **3**, 117–122, 1985.
37. Greengard P. Phosphorylated proteins as physiological effectors. *Science* **199**, 146–152, 1978.
38. Salomon Y., Londos C. and Rodbell M. A highly sensitive adenylate cyclase assay. *Anal Biochem* **58**, 541–548, 1974.
39. Shimizu H., Daly J. W. and Creveling C. R. A radioisotope method for measuring the formation of 3',5'-cyclic monophosphate in incubated brain slices *J Neurochem* **16**, 1609–1619, 1969.

Chronobiology International, Vol. 3, No. 2, pp. 117–122, 1986
Printed in Great Britain

0742-0528/86 $3.00+0.00
Pergamon Journals Ltd.

RELATIONSHIPS BETWEEN BEHAVIORAL RHYTHMS, PLASMA CORTICOSTERONE AND HYPOTHALAMIC CIRCADIAN RHYTHMS

Marian S. Kafka*, Marco A. Benedito*, Linda K. Steele†, Marie J. Gibson‡, Robert L. Zerbe§, David M. Jacobowitz‖, Robert H. Roth¶ and Karl Zander**

*Clinical Neuroscience Branch, National Institute of Mental Health, Bethesda, MD 20892, U.S.A.
†Biochemistry Department, Armed Forces Radiobiology Research Institute, National Naval Medical Center, Bethesda, MD 20814, U.S.A.
‡Department of Endocrinology, Mt. Sinai School of Medicine, New York, 10029, U.S.A.
§Lilly Research Laboratories, Indianapolis, IN 46285, U.S.A.
‖Laboratory of Clinical Science, National Institute of Mental Health, Bethesda, MD 20892, U.S.A.
¶Departments of Pharmacology and Psychiatry, Yale University School of Medicine, New Haven, CT 06510, U.S.A.
**Biological Psychiatry Branch, National Institute of Mental Health, Bethesda, MD 20892, U.S.A.

Abstract—Circadian rhythms in physiological processes and behaviors were compared with hypothalamic circadian rhythms in norepinephrine (NE) metabolites, adrenergic transmitter receptors, cAMP, cGMP and suprachiasmatic nucleus (SCN) arginine vasopressin (AVP) in a single population of rats under D : D conditions. Eating, drinking and locomotor activity were high during the subjective night (the time when lights were out in L : D) and low during the subjective day (the time when lights were on in L : D). Plasma corticosterone concentration rose at subjective dusk and remained high until subjective dawn. Binding to hypothalamic α_1- and β-adrenergic receptors also peaked during the subjective night. Cyclic cGMP concentration was elevated throughout the 24-hr period except for a trough at dusk, whereas DHPG concentration peaked at dawn. Arginine vasopressin levels in the suprachiasmatic nucleus peaked in the middle of the day. No rhythm was found either in binding to the α_2-adrenergic receptor, or in MHPG or cAMP concentration. Behavioral and corticosterone rhythms, therefore, are parallel to rhythms in hypothalamic α_1- and β-receptor binding and NE-release. Cyclic GMP falls only at dusk, suggesting the possibility that cGMP inhibits activity much of the day and that at dusk the inhibition of nocturnal activity is removed. SCN AVP, on the other hand, peaking at 1400 hr, may play a role in the pacemaking function of the SCN that drives these other rhythms.

Keywords—Circadian rhythms, behavioural, hypothalamic, arginine vasopressin, SCN.

Introduction

The hypothalamus (and, in particular, the SCN) plays a central role in the generation of circadian rhythms, including regulation of feeding, drinking, locomotor activity and corticosterone secretion (1). The well-established circadian rhythms in these physiological processes and behaviors were compared with circadian rhythms in the hypothalamic noradrenergic system, cAMP, cGMP and SCN arginine vasopressin.

Materials and Methods

Three days after enucleation, food and water consumption was measured over six 4-hr intervals in twenty rats in individual cages. Food and water loss, monitered by absorbent paper beneath each cage, was negligible.

Locomotor activity was measured in nine rats 2–5 days after enucleation (2). Rats were put in Plexiglass cages (24 × 24 × 15 cm), and the cages set on top of 40 infrared photoelectric cells (Motron motility meter) for measurement of horizontal locomotion. Five photoelectric cells, at a height of 12 cm, measured vertical locomotor activity. Total activity counts for each rat during six 4-hr intervals over the 24-hr day were recorded.

For plasma corticosterone and ACTH measurements, rats were decapitated and trunk blood collected through ice-cold heparinized funnels into ice-cold tubes. Tubes were centrifuged at 1500 *g* for 10 min; 2 ml plasma was transferred to another tube and 25 μl/ml of *n*-

Table 1. Statistics

Variable	ANOVA		Differences between Means of time-points	
	F-value	*P*-value	$P < 0.05$	$P < 0.01$
Plasma corticosterone	5.30 (5,47)	<0.01	—	2h > 10h = 14h = 6h
Eating	14.8 (5,95)	<0.001	22h > 18h	10h = 2h = 6h > 14h = 18h
Drinking	6.9 (5, 95)	<0.001	2h > 14h	2h = 6h > 14h = 18h = 22h
Horizontal locomotion	11.74 (5, 18)	<0.001	22h = 2h = 6h > 10h = 14h = 18h	—
Vertical locomotion	6.85 (5,18)	<0.001	22h = 2h = 6h > 10h = 14h = 18h	—
Arginine vasopressin	3.39 (5,48)	<0.05	14h < 6h = 10h = 18h = 2h	14h > 22h

Statistics for binding are given in Table 1, ref. (7).
Statistics for MHPG, DHPG, cGMP, and cAMP are given in Table 2, ref. (8).

ethylmaleimide (Sigma Chem. Co.) was added. Samples were frozen until assay.

Plasma corticosterone concentrations were measured by a competitive protein-binding radioassay (the CBG method) (3). ACTH was measured by radioimmunoassay (4) in extracted plasma using an antibody (provided by NIAMDDK) that cross-reacts equally with ACTH (1–39) and ACTH (1–24) but not α- or β-MSH, or ACTH (1–10 or 25–39). Samples were evaluated in a single assay (with an intra-assay coefficient of variation of 3.9%).

For the measurement of arginine vasopressin (AVP) in the suprachiasmatic nucleus (SCN) at six 4-hr intervals over the 24-hr day, groups of five rats, 3 days after enucleation, were decapitated and the brains quickly removed sliced (5), and the slice containing hypothalamus, frozen. At a later time, SCN were punched out and analyzed for arginine vasopressin content by radioimmunoassay (6), utilising a rabbit anti-vasopressin antibody.

Conditions for housing the rats, enucleation, decapitation, brain dissection, and storage are given in (7), as are methods for measuring specific binding to the α_1-, α_2- and β-adrenergic receptors. MHPG, DHPG, cGMP and cAMP assay methods are given in (8).

The statistical significance of rhythms was assessed by 1-way analysis of variance (ANOVA), and of differences between maxima and minima, by Tukey's LSD test (Table 1). The experiment was carried out in two identical parts, separated by 4 days. As rhythms in each variable measured in the two parts of the experiment were not statistically different (2-way analysis of variance), all data from the same time-point in the two parts of the experiment were combined.

Results

Under the conditions of constant darkness (D : D) in which these rats were maintained, eating, drinking and locomotor activity followed the well-known circadian patterns of nocturnal behavior (Figure 1), and indicated that the animals were at similar phases even after some days of free-run. Plasma corticosterone followed the characteristic pattern in rats of a rise at dusk and a minimum at dawn. High values well into the dark-phase may have been due to a slight stress response. No rhythm was found in ACTH concentration (data not shown).

Both specific binding of [^{3}H]dihydroalprenolol ([^{3}H]DHA) to β-, and of [^{3}H]prazosin

Table 2. 24-hr Means for plasma corticosterone, eating, drinking, locomotion and arginine vasopressin

Variable	
Plasma corticosterone (μg %)	20 ± 11 (53)
Eating (g)	28.5 ± 1 (120)
Drinking (ml)	21.6 ± 2 (120)
Horizontal locomotion (counts)	1213 ± 201 (54)
Vertical locomotion (counts)	156 ± 29 (54)
Arginine vasopressin (pg/mg protein)	26.8 ± 1.5 (54)

Mean ± S.E.M. (Number of measurements).
24-hr means for binding are given in Table 2, ref. (7).
24-hr means for MHPG, DHPG, cGMP and cAMP are given in Table 2, ref. (8).

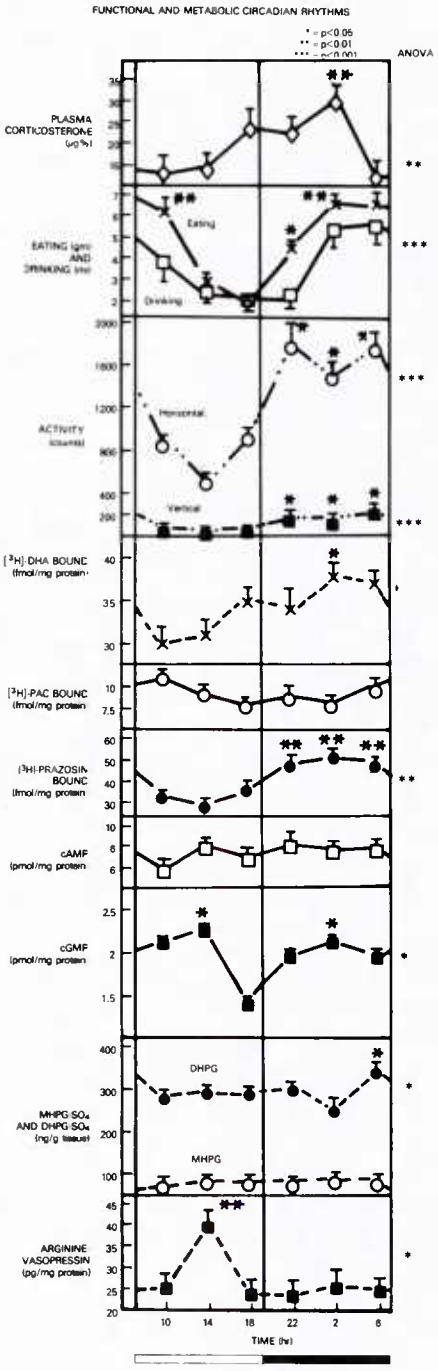

Figure 1. Circadian rhythms in plasma corticosterone concentration eating, drinking, locomotion and arginine vasopressin (AVP) concentration in the suprachiasmatic nucleus (SCN), and some variables in whole hypothalamus. Statistics are given in Table 2. Measurements were made at six 4-hr intervals over the 24-hr day. Details are in the text. (1) Plasma corticosterone was measured by a competitive protein-binding assay. Each point is the mean ± S.E.M. of measurements in eight–nine rats. (2) Eating and drinking were measured by weighing the food pellets and measuring the volume of water consumed by a rat in each 4-hr interval. Each point is the mean ± S.E.M. of 20 rats. (3) Locomotor activity was measured in an activity monitor with photoelectric cells. Counts registered over 4-hr intervals were calculated. Each point represents mean ± S.E.M. of nine rats. Both horizontal and vertical locomotor activity were significantly higher during subjective night than during subjective day (mean horizontal locomotor activity 1683 ± 83 [M ± S.E.M.] cf. 745 ± 99 counts/4 hr, $P < 0.001$; and mean vertical locomotor activity, 222 ± 19 cf. 90 ± 9 counts/4 hr, $P < 0.001$). (4) [^{3}H]Dihydroalprenolol specific binding to hypothalamic β-adrenergic receptors [see legend to Figure 3, ref. (7)]. (5) [^{3}H]*para*-Aminoclonidine specific binding to hypothalamic α_2-adrenergic receptors [see legend to Figure 2, ref. (7)]. (6) [^{3}H]Prazosin specific binding to hypothalamic α_1-adrenergic receptors [see legend to Figure 1, ref. (7)]. (7) Cyclic AMP concentration in hypothalamus [see legend to Figure 4, ref. (8)]. (8) Cyclic GMP concentration in hypothalamus [see legend to Figure 3, ref. (8)]. (9) MHPG and DHPG concentrations in hypothalamus [see legend to Figure 1, ref. (8)]. (10) Arginine vasopressin (AVP) concentration in SCN of anterior hypothalamus. Rats were decapitated, brains removed, sliced, and SCN punched as described in text. AVP was measured by an RIA. Each point is the mean ± S.E.M. of AVP concentration in SCN of nine rats.

to α_1-adrenergic receptors in the hypothalamus peaked in subjective night, with a trough at the beginning of subjective day. [Figure 1, Figures 1 and 3 and Table 1A and C in (7)]. No rhythm was found in [^{3}H]*para*-aminoclonidine ([^{3}H]PAC) specific binding to α_2-adrenergic receptors [Figure 1; Figure 2 in (7)].

The concentration of hypothalamic cGMP was the same at all times except for a fall at dusk [Figure 1; Figure 3 and Table 1C in (8)]. No rhythm was found in hypothalamic cAMP concentration (Figure 1).

The concentration of DHPG was similar all day except for a peak at dawn [Figure 1; Figure 1 and Table 1A (8)]. No significant changes occurred in hypothalamic MHPG concentration (Figure 1).

The concentration of arginine vasopressin (AVP) in the SCN peaked sharply at 1400 hr and remained low at all other time-points (Figure 1).

Discussion

An important methodological point is the reproducibility of the circadian rhythm measured in each variable in this study (7, 8, current paper). There were no significant differences between the two identical parts of the study which were run 4 days apart. Receptor rhythms, which can vary with brain region and rat strain, do replicate when conditions are maintained constant. For this reason, modifications of these rhythms, e.g. with psychoactive drugs (9), are probably significant and not due to experimental variability.

The hypothalamus is a region of great importance in the control of circadian rhythms (1, 10). The SCN of the anterior hypothalamus are thought to be the rat circadian pacemaker (11) that, via efferents to other hypothalamic nuclei, drive rhythms in pituitary hormones, and through them, hormones of pituitary target endocrine glands, such as the adrenal cortex. The noradrenergic system in the hypothalamic paraventricular nuclei regulates feeding and corticosterone rhythms; and medial and lateral hypothalamic control of ingestive behaviors are correlated with α_2- and β-adrenergic receptor rhythms, respectively (12).

Feeding, drinking and locomotor activity and corticosterone levels all were high in the subjective night, and, in general, low in the subjective day, following established patterns. The rhythms were not disturbed, then, by enucleation, and remained of large amplitude. Corticosterone values were somewhat higher than normal, suggesting that the animals were slightly stressed.

Specific binding to hypothalamic α_1- and β-adrenergic receptors, indicative probably of the number of receptors, is also greater in subjective night, suggesting that α_1- and β-receptors may mediate adrenergic transmission during rats' active-phase. No rhythm was found in α_2-receptor binding. In smaller hypothalamic regions, however, in α_2-receptors, circadian rhythms in the medial hypothalamus have been found (12). In addition, circadian rhythms in α_2-receptor binding in the hypothalamic paraventricular, suprachiasmatic, and supraoptic nuclei, but not in other hypothalamic areas, has been reported (13). In both studies, binding to α_2-receptors in the paraventricular nucleus of the medial hypothalamus increased when feeding increased (12, 13). The α_2-adrenergic agonist, clonidine, can stimulate feeding at dusk, when α_2-receptor binding is high, but not at dawn, when binding is low, suggesting that the α_2-receptor circadian rhythm may underlie the difference in clonidine's stimulatory action (14). As it is likely that a receptor rhythm measured in whole hypothalamus represents a composite of rhythms, present or lacking, in discrete nuclei (or even smaller units), the parallel patterns in increased nocturnal behaviors and α_1- and β-receptor binding can only be acknowledged, but not interpreted. A detailed understanding of the role of receptors in consumption and satiation necessitates studies, e.g. (13), in which receptor rhythms in nuclei or parts of nuclei are related to the eating and drinking behaviors of the whole animal.

By phosphorylating neuronal proteins, cyclic AMP appears to act as second messenger for a number of neurotransmitters and hormones, including α_1- and β-receptors in the hypothalamus (15). The role of cGMP is less clear. Neurotransmitters and hormones, through the

hydrolysis of phosphoinositides, initiate a cascade of cellular metabolic events, among which is an increase in cGMP concentration. (8). Of the receptors measured in the current study the α_1-adrenergic receptor stimulates both of these systems, the M_2-muscarinic acetylcholine receptor, the former, and the M_1-, the latter. The β-adrenergic receptor stimulates, and the α_2-adrenergic receptor inhibits, cAMP production.

Cyclic GMP concentration in hypothalamus was level throughout the 24-hr day, except for one low point at dusk. If cGMP is acting as a second messenger, perhaps it mediates inhibition of the onset of locomotor and ingestive behaviors, and a fall in its concentration permits them to begin. Cyclic AMP concentration, which showed no rhythm in the hypothalamus, is probably controlled by a large number of factors in addition to the number of α_1- and β-receptors which themselves were rhythmic.

In hypothalamus, the peak in DHPG concentration as well as α_1- and β-receptor binding, at subjective dawn, suggests, that at that timepoint, hypothalamic noradrenergic transmission is increased. As the rest phase of the activity cycle begins then, such increased transmission might inhibit activity.

Arginine vasopressin (AVP) is a putative peptide neurotransmitter intrinsic to the SCN (11). The AVP concentration has a discrete peak at 1400 hr in the SCN. At all other times it is low. The peak AVP concentration occurs just after the midpoint of the increases in SCN circadian rhythms in deoxyglucose uptake (16) and neuronal firing (17–19). These processes of energy utilization and electrical activity are related to the pacemaking activities of the SCN (17). The function of AVP, however, is not known, as it does not seem to play an essential role in the SCN's rhythm-generating function.

Diurnal rhythms in AVP concentration in rat SCN, paraventricular, and supraoptic nuclei (20) and rat cerebrospinal fluid (CSF) (21) were reported while this work was in progress. Under L : D conditions, the peak AVP concentration occurred at dusk and dawn in the SCN (20). In enucleated rats, peaks in CSF occurred about the middle of subjective day (21) as in our study.

Comparing variables in the hypothalamus has pointed up the need to compare circadian rhythms in behaviors with circadian rhythms in even smaller brain regions than those examined in this study (e.g. hypothalamic nuclei). By this means, biochemical and physiological processes involved in the rhythmic features of a behavior may be discriminated from processes necessary simply for the manifestation of the behavior.

It is clear, however, that by studying a number of relatively discrete brain areas, different rhythms manifest themselves, and the complexity of receptor rhythms is shown. In addition, the parallel measurement of receptor rhythms and rhythms in a second messenger(s), suggests that there are regional differences in feedback mechanisms, as manifested by positive, negative, and no correlations. Only by linking functional measures, biochemical and behavioral, to changes in receptor number and transmitter secretion, can we understand the significance of the changes measured over the 24-hr day.

Acknowledgement—The authors thank Ms. Jean Seeback for typing these manuscripts.

References

1. Aschoff J. Chapter 6. In Aschoff J., ed. *Handbook of Behavioral Neurobiology* Vol. 4, *Biological Rhythms,* Plenum, New York, pp. 81–93, 1981.
2. Post R. M. and Rose H. Increasing effects of repetitive cocaine administration in the rat. *Nature* **260**, 731–732, 1976.
3. Murphy B. E. P. Some studies of the protein-binding of steroids and their application to routine micro- and ultramicro-measurement of various steroids in body fluids by completitive protein-binding radioassay. *J Clin Endocrinol Metab* 27, 973–990, 1967.
4. Rees L. H., Cook D. M., Kendall J. W., Allan C. F., Kramer R. M., Ratcliffe J. G. and Knight R. A. A radioimmunoassay for rat plasma ACTH. *Endocrinology* **89**, 254–261, 1971.
5. Jacobowitz D. M. Removal of discrete fresh regions of the rat brain. *Brain Res* **80**, 111–115, 1974.
6. Feuerstein G., Zerbe R. L., Drori B-I, Kopin I. J and Jacowitz D. M. Catecholamines and resopressin in p = forebrain nuclei of hypertension prone and resistant rats. *Brain Res Bull* 7, 671–676, 1981.

7. Kafka M. S., Benedito M. A., Blendy J. A. and Tokola N. S. Circadian rhythms in neurotransmitter receptors in discrete rat brain regions. *Chronobiol Int* 3, 91–100, 1986.
8. Kafka M. S., Benedito M. A., Roth R. H., Steele L. K., Wolfe W. W. and Catravas G. N. Circadian rhythms in catecholomine metabolites and cyclic nucleotide production. *Chronobiol Int* 3, 101–115, 1986.
9. Kafka M. S., Wirz-Justice A., Naber D., Moore R. Y. and Benedito M. A. Circadian rhythms in rat brain neurotransmitter receptors. *Fed Proc* **42**, 2796–2801, 1983.
10. Symposium: Central nervous system control of mammalian circadian rhythms. *Fed Proc* **42**, 2782–2814.
11. Moore R. Y. Organization and function of a central nervous system circadian oscillator: the suprachiasmatic hypothalamic nucleus. *Fed Proc.* **42**, 2783–2789, 1983.
12. Kraüchi K., Wirz-Justice A., Morimasa T., Willener R. and Feer H. Hypothalamic α_2- and β-adrenoceptor rhythms are correlated with circadian feeding: evidence from chronic methamphetamine treatment and withdrawal. *Brain Res* **321**, 83–90, 1984.
13. Leibowitz S. F., Jhanwar-Uniyal M. and Roland C. R. Circadian rhythms of circulating corticosterone and α_2-noradrenergic receptors in discrete hypothalamic and extrahypothalamic areas of rat brain. *Soc Neurosci Abstracts* **10**, 294, 1984.
14. Kraüchi K., Wirz-Justice A., Suetterlin-Willener R. and Feer H. Clonidine stimulation of food intake is circadian phase dependent. *IRCS Med Sci* **13**, 561, 1985.
15. Daly J. W., Padgett W., Creveling C. R., Cantacuzene D., and Kirk K. L. Cyclic AMP-generating systems: regional differences in activation by adrenergic receptors in rat brain. *J Neurosci* **1**, 49–59, 1981.
16. Schwartz W. J., Davidsen L. C. and Smith C. B. In-vivo metabolic activity of a putative circadian oscillator, the rat suprachiasmatic nucleus. *J Comp Neurol* **189**, 157–167, 1980.
17. Inouye S. T. and Kawamura H. Characteristics of a circadian pacemaker in the suprachiasmatic nucleus. *J Comp Physiol* **146**, 153–160, 1982.
18. Green D. J. and Gillette R. Circadian rhythm of firing rate recorded from single cells in the rat suprachiasmatic brain slice. *Brain Res* **245**, 198–200, 1982.
19. Groos G. and Hendriks J. Circadian rhythms in electrical discharge of rat suprachiasmatic neurones recorded *in vitro*. *Neurosci Lett* **34**, 283–288, 1982.
20. Noto T., Hasimoto H., Doi Y., Nakajima T. and Kato N. Biorhythm of arginine-vasopressin in the paraventricular, supraoptic, and suprachiasmatic nuclei of rats. *Peptides* **4**, 875–878, 1983.
21. Schwartz W. J., Coleman R. J. and Reppert S. M. A daily vasopressin rhythm in rat cerebrospinal fluid. *Brain Res* **263**, 105–112, 1983.

Int. J. Radiation Oncology Biol. Phys., Vol. 12, pp. 1463–1467
Printed in the U.S.A.

0360-3016/86 $3.00 + .00

● *Session VII*

A NOVEL INTERACTION OF DIETHYLDITHIOCARBAMATE WITH THE GLUTATHIONE/GLUTATHIONE PEROXIDASE SYSTEM

K. SREE KUMAR, PH.D, ANNA M. SANCHO, B.S. AND JOSEPH F. WEISS, PH.D.

Biochemistry Department, Armed Forces Radiobiology Research Institute, Bethesda, MD 20814-5145

Diethyldithiocarbamate (DDC) exhibits a variety of pharmacologic activities, including both radioprotective and sensitizing properties. Since the glutathione/glutathione peroxidase system may be a significant factor in determining radiation sensitivity, the potential mechanisms of action of DDC in relation to this system were examined *in vitro*. The interaction of DDC with reduced glutathione (GSH) was tested using a simple system based on the reduction of cytochrome c. When DDC (0.005 mM) was incubated with GSH (0.5 mM), the reduction of cytochrome c was eightfold greater than that expected from an additive effect of DDC and GSH. GSH could be replaced by oxidized glutathione and glutathione reductase. Cytochrome c reduced by DDC was oxidized by mitochondria. The interaction of DDC with both the hexosemonophosphate shunt pathway and the mitochondrial respiratory chain suggests the possibility of linking these two pathways through DDC. Oxidation of DDC by peroxide and reversal by GSH indicated that the drug can engage in a cyclic reaction with peroxide and GSH. This was confirmed when DDC was used in the assay system for glutathione peroxidase (GSHPx) without GSHPx. DDC at a concentration of 0.25 mM was more active than 0.01 unit of pure GSHPx in eliminating peroxide, and much more active than the other sulfhydryl compounds tested. These studies indicate that DDC can supplement GSHPx activity or substitute for it in detoxifying peroxides, and suggests a unique role in the chemical modification of radiation sensitivity.

Diethyldithiocarbamate, Glutathione peroxidase, Glutathione, Sulfhydryl radioprotectors.

INTRODUCTION

Diethyldithiocarbamate (DDC) exhibits a variety of pharmacologic activities resulting in diverse therapeutic effects: radioprotection,[1,2,8,16,23] radiosensitization,[7,13,24] immunostimulation,[18] and protection against the toxicity of cancer chemotherapeutic agents and other chemicals.[5,15,20] The most studied biochemical effect of DDC has been its inhibition of superoxide dismutase (SOD) because of Cu^{2+} chelation,[10] an effect probably contributing to its radiosensitizing property. The mechanism(s) of immunomodulation by DDC (which can occur *in vivo* at much lower concentrations than those required for the inhibition of SOD) are not clear and may indirectly involve the induction of factors that act on immune cells.[18] The sulfhydryl moieties of DDC may be responsible for the chelating properties of the drug, as well as, being active in counteracting (by direct intervention or indirect processes) the reactive oxygen species induced by ionizing radiation and some chemicals. During the course of investigations on mechanisms of modification of radiation sensitivity by DDC, we observed that DDC could reduce cytochrome c at a rate greater than reduced glutathione (GSH). We report here experiments indicating that (a) DDC exhibits 'glutathione-peroxidase' like activity, and (b) it may act as a link between the hexosemonophosphate shunt pathway and the respiratory chain of mitochondria.

METHODS AND MATERIALS

All chemicals and enzymes were purchased.* WR-1065, 2-(3-aminopropylamino)ethanethiol dihydrochloride, was obtained from the Drug Synthesis and Chemistry Branch, Division of Cancer Treatment, National Cancer Institute, Bethesda, MD. Mice (CD2F1 male) weighing 25–30 g were killed by cervical dislocation and livers were removed and homogenized in 0.25 M sucrose. Homogenates were centrifuged at 1000 × g for 10 min. Supernatants were centrifuged at 25,000 × g for 20 min and the sedimented mitochondria were suspended in sucrose and centrifuged again. The pellet obtained was used as the mitochondrial preparation.

Presented at the Chemical Modifiers of Cancer Treatment Conference, Clearwater, Florida, 20–24 October 1985.

Reprint requests to: Dr. Joseph F. Weiss, Biochemistry Department, Armed Forces Radiobiology Research Institute, Bethesda, MD 20814-5145.

Acknowledgements:—Dr. Kumar was a National Research Council-AFRRI Research Associate. This research was supported by Armed Forces Radiobiology Research Institute, Defense Nuclear Agency, under Research Work Unit MJ 00026. The views presented in this paper are those of the authors; no endorsement by the Defense Nuclear Agency has been given or should be inferred.

Accepted for publication 25 February 1986.

* Sigma Chemical Co., St. Louis, MO.

Table 1. Reduction of cytochrome c by DDC in presence or absence of GSH

Concn. of DDC (mM)	Concn. of GSH (mM)	Cytochrome c reduced (ΔA 550 nm/min)
0.0025	—	0.005 ± 0.000
0.005	—	0.017 ± 0.005
0.010	—	0.095 ± 0.004
0.020	—	0.191 ± 0.012
0.050	—	0.342 ± 0.022
—	0.500	0.002 ± 0.001
0.0025	0.500	0.053 ± 0.003
0.0025	0.250	0.040 ± 0.003
0.0025	0.100	0.032 ± 0.002
0.0025	0.050	0.019 ± 0.001
0.005	0.500	0.160 ± 0.027
0.025	0.500	0.260 ± 0.060
0.050	0.500	0.370 ± 0.040
*0.020	0.500	0.065 ± 0.000

* Disulfiram.
Each value represents the mean of at least five determinations ± SD.

Cytochrome c reduction was measured at 25°C by the increase in absorption at 550 nm using a spectrophotometer.† The medium in a final volume of 1.0 ml contained 0.01 mM ferricytochrome c, 0.1 mM EDTA, and 50 mM potassium phosphate buffer (pH 7.0). The oxidation of DDC by peroxide was monitored spectrophotometrically by scanning the absorption from 320–400 nm. Peroxide was generated *in situ* by xanthine oxidase (0.002 unit) and hypoxanthine (0.1 mM) in 50 mM phosphate buffer at pH 7.0. The glutathione peroxidase assay was a modification of the method of Lawrence and Burk.[12] The final concentrations of the components of the assay system in 1.0 ml were NADPH 0.16 mM, GSH 1.0 mM, and glutathione reductase 0.5 units. The reaction was started by the addition of 0.25 mM H_2O_2 and the oxidation of NADPH was monitored spectrophotometrically at 340 nm. Other components were added as mentioned under appropriate figures and tables.

RESULTS

DDC reduced cytochrome c at a very high rate (Table 1). There was an increase in the formation of reduced cytochrome c as the concentration of DDC was increased. Glutathione added at a concentration of 0.5 mM (tenfold higher than the highest concentration of DDC tested) did not reduce cytochrome c significantly (Table 1). When DDC (0.0025 or 0.005 mM) was added to cytochrome c, either before or after GSH (0.5 mM), reduction was eightfold higher than would be expected from the additive reduction of cytochrome c by DDC and GSH (Table 1, Fig. 1). This effect was best noted at lower concentrations of

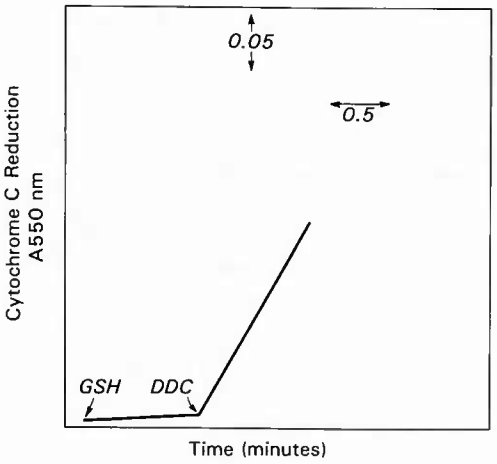

Fig. 1. Reduction of cytochrome c by DDC (0.005 mM) in the presence of 0.5 mM reduced glutathione (GSH).

DDC and higher concentrations of GSH. When the concentration of GSH was decreased to 0.05 mM, the potentiating effect was only 2.5-fold. Cytochrome c was also reduced by the disulfide of DDC, disulfiram (0.02 mM as a sonicated suspension), in the presence of 0.5 mM GSH. Disulfiram had no effect on cytochrome c reduction.

GSH in the cytochrome c reduction assay could be replaced by a system capable of generating it, such as, the hexose monophosphate shunt pathway. The NADPH formed in this pathway can be used by glutathone reductase to reduce GSSG (oxidized glutathione). Thus, the reducing equivalents formed in the pentose phosphate pathway can sustain the reduction of cytochrome c (Fig. 2). The addition of freshly prepared mitochondria to cytochrome c, reduced by GSH and DDC, resulted in the immediate oxidation of cytochrome c. The inhibition of this oxidation by potassium cyanide (KCN) illustrates that it is catalyzed by cytochrome oxidase (Fig. 3). In the absence of mitochondria, KCN had only a very small effect.

DDC could be oxidized by peroxide generated from xanthine oxidase and hypoxanthine, which resulted in an increase in absorption over a broad range of 320–400 nm. After the addition of GSH, a decrease was seen in the absorption, indicating the reduction of the oxidized product (Fig. 4). There was no change in the absorption spectrum of DDC *per se*. The ability of DDC to be oxidized and the reduction of the oxidized product was also tested in a glutathione peroxidase assay system. When the enzyme in this assay was replaced by DDC, a concentration-dependent 'enzyme-like' activity was seen (Fig. 5). Other commonly used sulfhydryl compounds did not have the same properties. Only WR-1065, the dephosphorylated free-thiol formed from WR-2721, had some activity, but it was not as effective as DDC. On an equimolar basis (1.0 mM), DDC was 2.5-fold more effective than WR-1065 (ΔO.D at 340 nm/min of 0.190 vs 0.075). The following compounds at 1.0 mM showed no activity with

† Cary 219, Varian Associates, Palo Alto, CA.

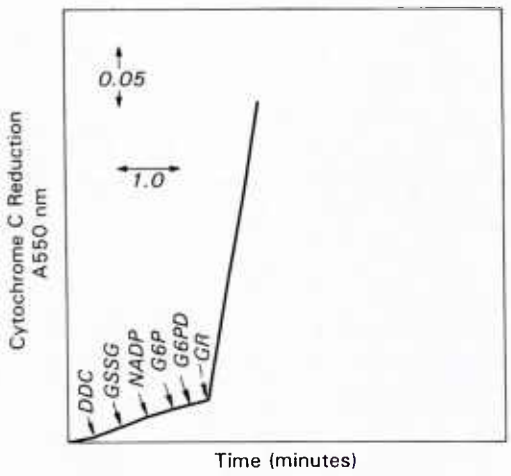

Fig. 2. Reduction of cytochrome c by DDC in the presence of components of the hexosemonophosphate shunt pathway. GSH and NADPH were formed by the addition of oxidized glutathione (GSSG), glutathione reductase (GR), and glucose-6-phosphate (G6P), NADP, and glucose-6-phosphate dehydrogenase (G6PD). Concentrations of components in a final volume of 1.0 ml were cytochrome c, 0.01 mM; GSSG, 0.5 mM; GR and G6PD, 0.5 unit each; NADP, 0.15 mM; G-6-P, 1.0 mM; and DDC, 0.005 mM.

respect to the blank ΔO.D of 0.013: 2-mercaptoethanesulfonic acid; cysteamine; S-(2-aminoethyl)isothiouronium Br-HBr; and N-(2-mercaptopropionyl) glycine. Dithiothreitol showed slight activity (ΔO.D of 0.033).

DISCUSSION

The mechanism of action of DDC is complex, and is reflected in its many pharmacologic properties. The effects of DDC cannot be explained solely by its inhibition of SOD, although this may partly explain its radiosensitizing

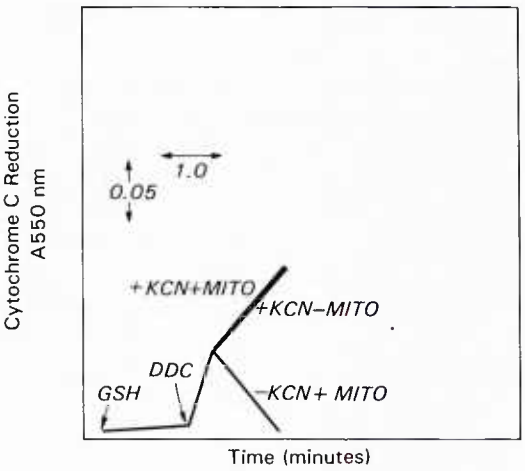

Fig. 3. Mitochondrial oxidation of cytochrome c reduced by DDC and its inhibition by cyanide. Two mg of freshly prepared mouse liver mitochondria (mito) were added to cytochrome c reduced by DDC (0.005 mM) and GSH (0.5 mM) in the presence or in the absence of 0.1 mM potassium cyanide (KCN).

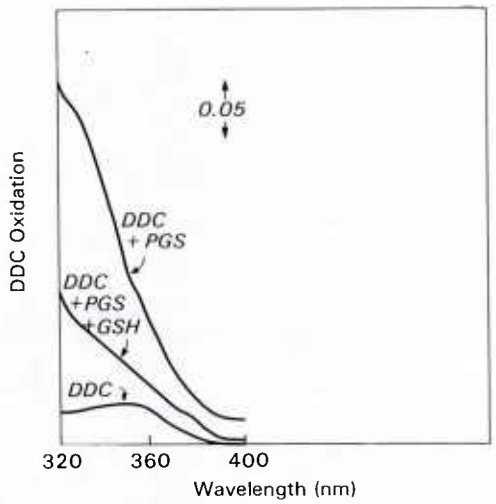

Fig. 4. Oxidation of DDC by peroxide and its reversal by GSH. DDC (0.02 mM) oxidized by a peroxide-generating system (PGS) in the presence or absence of GSH (0.5 mM).

effects and potentiation of toxicities of drugs where superoxide radical is involved, for example, toxicity of bleomycin,[14] paraquat,[9] and 1-methyl-4-phenyl-1,2,3,6-tetrahydropyridine (Corsini, G. U., Pintus, S., Chiueh, C. C., Weiss, J. F., Kopin, I. J. unpublished data, June, 1985). Whether the inhibition of SOD is an overriding effect may be very dependent on the cellular concentration of the drug and the biochemical differences in cell types, especially enzyme levels. SOD levels vary with tissue type[17] and cell lines, as well as, with the cell-cycle stage.[4] The inhibition of SOD is probably not a major factor in the many reported immunological effects of DDC,[18] since DDC is immunologically active at much lower doses than are required for SOD inhibition. The possibility that sulfhydryl immunomodulators might have biphasic effects, because of prooxidant effects at low concentrations and antioxidant effects at higher concentrations,[11] must be evaluated. The pharmacology of DDC, however, is

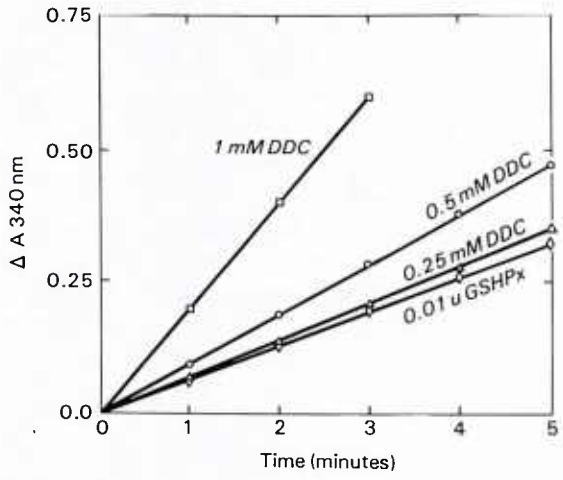

Fig. 5. Substitution of glutathione peroxidase (GSHPx) by DDC in the GSHPx assay system.

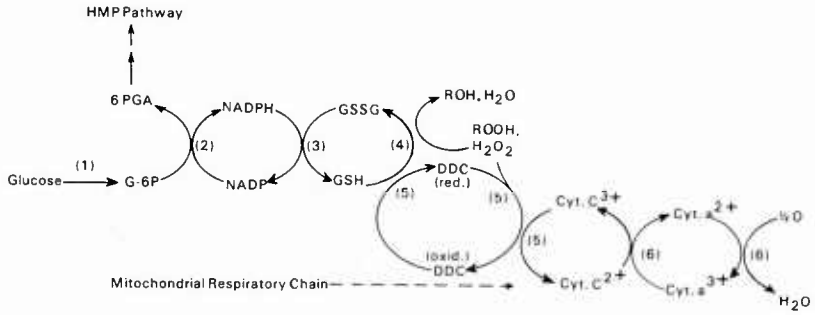

Fig. 6. DDC-mediated linkage of hexosemonophosphate shunt pathway and respiratory chain. G-6P, glucose-6 phosphate; 6-PGA, 6-phosphogluconic acid; HMP, hexosemonophosphate; GSH, reduced glutathione; GSSG, oxidized glutathione; DDC, diethyldithiocarbamate (oxid: oxidized; red: reduced); (1) hexokinase; (2) glucose-6 phosphate dehydrogenase; (3) glutathione reductase; (4) glutathione peroxidase; (5) nonenzymatic; (6) cytochrome oxidase. In the nonenzymatic reactions (5), DDC (red.) can be oxidized either by peroxides (ROOH, H_2O_2) or Cyt. c^{3+}.

more complex than other sulfhydryl immunomodulators, because of its chelating properties, for example, the inhibition of SOD appears to contribute to the biphasic toxicity and radiosensitization toward lymphocytes.[19] In the context of radiation exposure, much higher doses of DDC (10–100 times) are needed for immunohematopoietic protection in mice.[12,23]

The mechanisms of radioprotection and chemoprotection by DDC may have elements in common with other sulfhydryl radioprotectors,[7,16] but the structure of DDC appears to provide some unique properties. The present *in vitro* study emphasizes the antioxidant properties of DDC, which are quantitatively different from other sulfhydryl compounds. This is exemplified by the ability of DDC to reduce cytochrome c synergistically in conjunction with GSH. Cytochrome c can also be reduced synergistically by disulfiram. GSH in this reaction may reduce disulfiram to DDC, which in turn may reduce cytochrome c. This may also indicate that disulfiram is an intermediate in the process. Alternatively, the structure of DDC might allow the formation of an internal disulfide, which could be reduced by GSH. These reactions (shown in Fig. 6) may also explain the role of the hexosemonophosphate shunt pathway in sustaining the reduction of cytochrome c. GSSG formed in this reaction can be reduced to GSH by glutathione reductase and NADPH formed in this pathway. The cyanide-sensitive mitochondrial oxidation of reduced cytochrome c, formed in these reactions, suggests that the hexosemonophosphate shunt pathway and respiratory electron transport chain can be linked through DDC (Fig. 6). According to this scheme, it may be possible, in instances where the energy production by mitochondria is hampered by inhibition or dysfunction at points before cytochrome c, for the partial restoration of energy production to be achieved by shuttling electrons from NADPH to cytochrome c via DDC. Whether this interaction of DDC with the respiratory system has any role in the oxygen-dependent radioprotective effects of the drug[7] remains to be evaluated.

Another important property of DDC is its ability to detoxify peroxides in a cyclic manner in conjunction with GSH. The removal of peroxides was also demonstrated using the glutathione peroxidase assay system in which DDC replaces GSHPx. DDC exhibited "GSHPx activity" to a much greater extent than the other sulfhydryl compounds tested, including WR-1065, the dephosphorylated form of WR-2721. The decreased release of H_2O_2, reported earlier from macrophages activated *in vivo*,[21] may be because of the reduction of peroxide by DDC. Some of the radioprotective and chemoprotective properties of the drug might involve the elimination of lipid hydroperoxides, which are formed by the action of reactive oxygen intermediates and may also cause DNA damage.[3] We found that DDC (400 mg/kg) injection in mice resulted in an increase in liver glutathione peroxidase (cumene hydroperoxide as substrate) after 2 hr.[22] It is not clear whether the increased activity is because of drug activity *per se*, or induction. In contrast to our study, decreased glutathione peroxidase activity was found in lung and liver after a very high dose of DDC (1.2 g/kg).[9] Another study showed that DDC-induced resistance to hyperoxia in mice appeared to be associated with increased GSHPx activity.[6] The degree to which DDC might contribute to the reactions proposed (Fig. 6) and provide protection versus sensitization would probably depend on oxygen tension, glutathione status, SOD content of the particular cell, as well as, the reactive oxygen intermediates involved in the insult. In this context, it might not be too surprising to find both radioprotection and radiosensitization by DDC within the same animal.[7]

REFERENCES

1. Alexander, P., Bacq, Z.M., Cousens, S.F., Fox, M., Herve, A., Lazar, J.: Mode of action of some substances which protect against the lethal effects of X-rays. *Radiat. Res.* **2:** 392–415, 1955.
2. Allalunis-Turner, M.J., Chapman, J.D.: Evaluation of diethyldithiocarbamate as a radioprotector of bone marrow. *Int. J. Radiat. Oncol. Biol. Phys.* **10:** 1569–1573, 1984.
3. Ames, B.N.: Dietary carcinogens and anticarcinogens: Ox-

ygen radicals and degenerative diseases. *Science* **221:** 1256–1264, 1983.

4. Blakely, W.F., Kumar, K.S., Holahan, E.V., Hagan, M.P., Weiss, J.F., Jacocks, H.M. III: Intrinsic cellular mechanism(s) of resistance to oxidative damage: Age response (Abstr.). *Abstracts of Papers for the 33rd Annual Meeting of the Radiation Research Society,* Los Angeles. 1985, p. 115.
5. Borch, R.F., Pleasants, M.E.: Inhibition of *cis*-platinum nephrotoxicity by diethyldithiocarbamate rescue in a rat model. *Proc. Natl. Acad. Sci.* (U.S.A.) **76:** 6611–6614, 1979.
6. Deneke, S.M., Fanburg, B.L.: Involvement of glutathione enzymes in O_2 tolerance development by diethyldithiocarbamate. *Biochem. Pharmacol.* **29:** 1367–1373, 1980.
7. Evans, R.G.: Tumor radiosensitization with concomitant bone marrow radioprotection: A study in mice using diethyldithiocarbamate (DDC) under oxygenated and hypoxic conditions. *Int. J. Radiat. Oncol. Biol. Phys.* **11:** 1163–1169, 1985.
8. Evans, R.G., Engel, C.R., Wheatley, C.L., Nielsen, J.R., Ciborowski, L.J.: An *in vivo* study of the radioprotective effect of diethyldithiocarbamate (DDC). *Int. J. Radiat. Oncol. Biol. Phys.* **9:** 1635–1640, 1983.
9. Goldstein, B.D., Rozen, M.G., Quintavalla, J.C., Amoruso, M.A.: Decrease in mouse lung and liver glutathione peroxidase activity and potentiation of the lethal effects of ozone and paraquat by the superoxide dismutase inhibitor diethyldithiocarbamate. *Biochem. Pharmacol.* **28:** 27–30, 1979.
10. Heikkila, R.E., Cabbat, F.S., Cohen, G.: *In vivo* inhibition of superoxide dismutase in mice by diethyldithiocarbamate. *J. Biol. Chem.* **251:** 2182–2185, 1976.
11. Kumar, K.S., Dobbs, C.R., Weiss, J.F., Chirigos, M.A.: Levamisole inhibition of microsomal lipid peroxidation as related to its sulfhydryl metabolite DL-2-oxo-3-(2-mercaptoethyl)-5-phenylimidazolidine. *J. Immunopharmacol.* **2:** 73–83, 1980.
12. Lawrence, R.A., Burk, R.F.: Glutathione peroxidase activity in selenium-deficient rat liver. *Biochem. Biophys. Res. Commun.* **71:** 952–958, 1976.
13. Lin, P.S., Kwock, L., Butterfield, C.E.: Diethyldithiocarbamate enhancement of radiation and hyperthermia effects on Chinese hamster cells *in vitro*. *Radiat. Res.* **77:** 501–511, 1979.
14. Lin, P.S., Kwock, L., Goodchild, N.T.: Copper chelator enhancement of bleomycin cytotoxicity. *Cancer* **46:** 2360–2364, 1980.
15. Masuda, Y., Nakayama, N.: Protective effect of diethyldithiocarbamate and carbon disulfide against liver injury induced by various hepatotoxic agents. *Biochem. Pharmacol.* **31:** 2713–2725, 1982.
16. Milas, L., Hunter, N., Ito, H., Peters, L.J.: *In vivo* radioprotective activities of diethyldithiocarbamate (DDC). *Int. J. Radiat. Oncol. Biol. Phys.* **10:** 2335–2343, 1984.
17. Oberley, L.W., Buettner, G.R.: Role of superoxide dismutase in cancer: A review. *Cancer Res.* **39:** 1141–1149, 1979.
18. Renoux, G., Renoux, M.: DTC. A summary of the current status. In *Current Concepts in Human Immunology and Cancer Immunomodulation,* B. Serrou, C. Rosenfeld, J.C. Daniels, J.P. Saunders (Eds.). Amsterdam, Elsevier Biomedical. 1982, pp. 575–584.
19. Rigas, D.A., Eginitis-Rigas, C., Bigley, R.H., Stankova, L., Head, C.: Biphasic radiosensitization of human lymphocytes by diethyldithiocarbamate: possible involvement of superoxide dismutase. *Int. J. Radiat. Biol.* **38:** 257–266, 1980.
20. Sossai, M., Pozza, F., Cima, L., Calzavara, F., Tóth, C.E.: Action of diethyl-dithiocarbamate (DEDTC) against the toxicity of mechlorethamine (HN_2) in selective radiomimetic pulmonary perfusion. *Progr. Biochem. Pharmacol.* **1:** 720–724, 1965.
21. Tsunawaki, S., Nathan, C.F.: Enzymatic basis of macrophage activation. Kinetic analysis of superoxide production in lysates of resident and activated mouse peritoneal macrophages and granulocytes. *J. Biol. Chem.* **259:** 4305–4312, 1984.
22. Weiss, J.F., Jacobs, A.J., Kumar, K.S.: Some immunological and biochemical effects of radioprotectant sulfhydryl compounds (Abstr.). *Int. J. Immunopharmacol.* **7:** 338, 1985.
23. Weiss, J.F., Jacobs, A.J., Rankin, W.A.: Effects of diethyldithiocarbamate and WR-2721 on delayed-type hypersensitivity and survival of irradiated mice (Abstr.). *Proceedings of the Seventh International Congress of Radiation Research,* Broerse, J.J., Barendsen, G.W., Kal, H.B., van der Kogel, A.J. (Eds.). The Netherlands, Martinus Nijhoff. 1983, pp. C1–37.
24. Westman, G., Marklund, S.L.: Diethyldithiocarbamate, a superoxide dismutase inhibitor, decreases the radioresistance of Chinese hamster cells. *Radiat. Res.* **83:** 303–311, 1980.

Biochemical Pharmacology, Vol. 35, No. 18, pp. 3143–3146, 1986.
Printed in Great Britain.

0006-2952/86 $3.00 + 0.00
Pergamon Journals Ltd.

INHIBITION OF GLUTATHIONE PEROXIDASE AND GLUTATHIONE TRANSFERASE IN MOUSE LIVER BY MISONIDAZOLE

K. SREE KUMAR* and JOSEPH F. WEISS

Biochemistry Department, Armed Forces Radiobiology Research Institute, Bethesda, MD 20814-5145, U.S.A.

(*Received* 22 *July* 1985; *accepted* 6 *February* 1986)

Abstract—The mechanisms of toxicity and sensitization by the radiosensitizer misonidazole [1-(2-nitro-1-imidazolyl)-3-methoxy-2-propanol] are not well understood. We report here on the inhibition of total glutathione peroxidase (GSHPx), selenium-dependent glutathione peroxidase (selenium-GSHPx) and glutathione transferase (GSHTx) activities by misonidazole. Mouse liver cytosol GSHPx and selenium-GSHPx were inhibited *in vitro* with 0.5 mM misonidazole. On administration of the drug intraperitoneally (800 mg/kg) to mice, it was found that GSHPx, selenium-GSHPx, and GSHTx were inhibited in homogenate, cytosol, and microsomal fractions of mouse liver. GSHPx was depressed in all fractions up to 60–70% of control values, with maximum depression occurring in the cytosol and homogenate fractions in less than 2 hr. Recovery of activity was slower in the microsomes. In general, the pattern of depression of selenium-GSHPx was parallel to that of GSHPx except in microsomes, where GSHPx is minimal. Quantitatively, selenium-GSHPx was least affected. GSHTx was inhibited 70–80% of control values in cytosol and homogenate with recovery by 24 hr, whereas a second period of depression occurred at 24 hr in the microsomes. The inhibition of peroxide-metabolizing enzymes may lead to elevation of intracellular peroxide levels, contributing to the radiosensitizing effect and/or toxicity of misonidazole.

Misonidazole [1-(2-nitro-1-imidazolyl)-3-methoxy-2-propanol] is an imidazole derivative under investigation as a radiosensitizer of hypoxic tumor cells [1]. The use of this drug in radiation therapy of cancer is limited by its toxicity [2], manifested mainly as neuropathies [3, 4].

The mechanisms of radiosensitization and toxicity of misonidazole are relatively unknown. The metabolism of misonidazole depends on the oxygen content of tissues, and the metabolites formed result in sensitizing or toxic effects [5]. In hypoxic cells, reductive metabolites are formed, which can interact with critical biomolecules, such as DNA [6], and under aerobic conditions reactive oxygen species can be generated [5]. Misonidazole metabolites formed under anaerobic conditions (or by chemical reduction) can conjugate with glutathione (GSH) [5, 7], decreasing the effective concentration of this intracellular thiol vital for the detoxification of peroxides. We have examined the effects of misonidazole on the enzymes that generally act on GSH, namely, glutathione peroxidase (EC 1.11.1.9, total and selenium-dependent) and glutathione transferase (EC 2.5.1.18), and the results are presented in this paper.

MATERIALS AND METHODS

Misonidazole was dissolved in warm, neutral saline and administered (800 mg/kg body wt) intraperitoneally to male CD2F1 mice. At various times after drug injection, each animal was anesthetized with nembutal and its liver was perfused *in situ* with saline. Liver homogenates (10%) were prepared in 0.25 M sucrose, and the combined mitochondrial-nuclear fraction was sedimented at 10,000 *g* for 20 min. Cytosol and microsomal fractions were obtained by centrifuging the postmitochondrial supernatant fraction at 105,000 *g* for 1 hr. These fractions were diluted, and the assay system for glutathione peroxidase contained 0.0250, 0.0700 and 0.0080 mg protein of homogenate, microsomes and cytosol respectively. For the glutathione transferase assay, the respective amounts of the fractions used were 0.0042, 0.0170 and 0.0013 mg protein.

For *in vitro* studies, the 105,000 *g* liver cytosol fraction from control mice was used as the source of glutathione peroxidase. Misonidazole was added to the assay system to test any direct effect of the drug on glutathione peroxidase (GSHPx) activity in mouse liver. The direct effect of the drug on mouse liver glutathione transferase (GSHTx) activity was not tested.

GSHPx was assayed according to the method of Lawrence and Burk [8] with modifications. The assay system in 0.9 ml contained 0.5 ml of 0.2 M potassium phosphate buffer (pH 7.0), 0.5 units glutathione reductase, 1 mM GSH, 0.16 μmoles NADPH, 1.0 mM sodium azide, tissue extract, and water. The reaction was initiated by the addition of 0.1 ml of 15 mM cumene hydroperoxide, and the absorbance change was recorded every minute at 340 nm using a Cary–Varian spectrophotometer. The use of cumene hydroperoxide as a substrate provides for the determination of total glutathione peroxidase activity, which includes selenium-dependent glutathione peroxidase. The selenium-dependent glutathione peroxidase (selenium-GSHPx) activity was assayed sep-

* Author to whom all correspondence should be addressed.

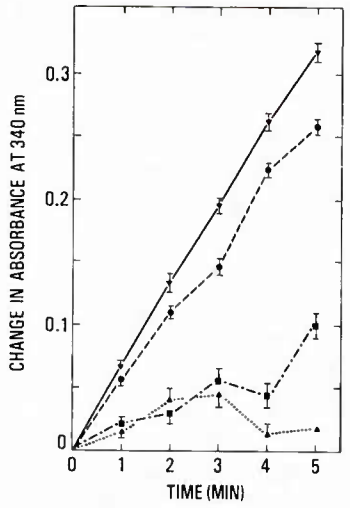

Fig. 1. Inhibition of mouse liver cytosol total glutathione peroxidase *in vitro* by misonidazole. Mouse liver cytosol fraction was incubated with misonidazole at various concentrations for 2 min and assayed with cumene hydroperoxide. Values given are means of five separate determinations ± S.E.M. Key: (▼——▼) control; misonidazole concentrations: (●——●) 0.2 mM; (■—·—■) 0.4 mM; and (▲----▲) 0.5 mM.

arately using 0.1 ml of 2.5 mM hydrogen peroxide (H_2O_2) instead of cumene hydroperoxide [8]. Glutathione transferase activity was assayed by the method of Habig *et al.* [9] by the nucleophilic attack of glutathione anion on 1-chloro-2,4-nitrobenzene measured at 340 nm. The amount of GSH added was in excess so that any direct effect of misonidazole on GSH could not be a factor in the glutathione peroxidase measurement. The amount of glutathione reductase was also in excess so that any decrease in this enzyme would not be interpreted as a depression in glutathione peroxidase. This was determined in a separate study of the effects of misonidazole on pure glutathione reductase (conversion of GSSG to GSH). Misonidazole did not have any effect on the absorption of NADPH used in the assay system.

Misonidazole was supplied by the Drug Synthesis and Chemistry Branch, Division of Cancer Treatment, National Cancer Institute, Bethesda, MD. All other reagents were purchased from the Sigma Chemical Co., St. Louis, MO.

RESULTS

When misonidazole was tested *in vitro* for its effect on glutathione peroxidase at a concentration of 0.2 mM, a significant ($P < 0.05$) inhibition of total GSHPx was seen from 2 min onward, compared to control activity. Almost total inhibition of the activity was seen at 0.4 and 0.5 mM (Fig. 1). Higher concentrations of the drug could not be tested due to its absorbance at 340 nm. The effect of misonidazole on selenium-GSHPx was not significant at 0.2 mM (Fig. 2). At 0.5 mM it was inhibited significantly, but even at this concentration the inhibition was less than that observed for GSHPx with 0.4 mM misonidazole. Increasing the GSH concentration from 1 to 5 mM, 10-fold more than the highest concentration of misonidazole used (0.5 mM), did not relieve the inhibition.

The data for GSHPx, selenium-GSHPx, and GSHTx in the homogenate, microsomes, and cytosol fractions of liver from control mice (saline administered) and from mice killed at different periods after the administration of misonidazole are given in Tables 1, 2, and 3 respectively. In general, total GSHPx activity (Table 1) decreased significantly at 0.5 hr after the drug administration, and the decrease persisted up to 12 hr after the drug was given. Significant inhibition of selenium-dependent GSH-Px activity (Table 2) was seen in cytosol and homogenate at 1 hr and inhibition at some later periods. The inhibition, compared to control, was less than that observed with GSHPx. Selenium-GSHPx in the microsomes was insufficient to assay.

GSHTx was also inhibited, with the greatest inhibition observed in the cytosol fraction, although recovery was seen at 12 hr. In microsomes, GSHTx was inhibited at 3 hr and a second period of depression occurred at 24 hr.

Table 1. Total glutathione peroxidase activity in mouse liver fractions at various periods after administration of misonidazole (800 mg/kg body wt)

Period after treatment (hr)	Enzyme activity (units/mg protein) in:					
	Homogenate		Microsomes		Cytosol	
	Saline	Misonidazole	Saline	Misonidazole	Saline	Misonidazole
0.5	0.58 ± 0.01	0.48 ± 0.02*	0.22 ± 0.01	0.15 ± 0.01*	1.46 ± 0.04	1.15 ± 0.01†
1.0	ND	0.36 ± 0.01†§	0.19 ± 0.01	0.10 ± 0.01‡	ND	0.75 ± 0.04†§
2.0	0.62 ± 0.02	0.39 ± 0.06‡	0.21 ± 0.02	0.15 ± 0.01‡	1.50 ± 0.09	1.08 ± 0.02*
3.0	0.55 ± 0.05	0.49 ± 0.02	ND	ND	1.45 ± 0.06	1.05 ± 0.04†
4.0	ND	0.41 ± 0.02§	0.29 ± 0.02	0.14 ± 0.01†	1.34 ± 0.12	0.98 ± 0.05‡
6.0	0.61 ± 0.01	0.49 ± 0.04‡	0.17 ± 0.01	0.08 ± 0.02*	1.39 ± 0.03	1.22 ± 0.04*
12.0	0.56 ± 0.02	0.39 ± 0.01†	0.29 ± 0.04	0.21 ± 0.03	1.28 ± 0.06	0.99 ± 0.03*
24.0	0.62 ± 0.03	0.54 ± 0.03	0.24 ± 0.02	0.15 ± 0.01*	1.27 ± 0.05	1.15 ± 0.04

Values are expressed as mean of activities from four to six animals ± S.E.M. ND = not determined.
*–‡ Significantly different compared with saline value: *$P < 0.01$, †$P < 0.001$, and ‡$P < 0.05$.
§ These values were compared with mean of all saline (control) values of respective fractions.

Table 2. Selenium-dependent glutathione peroxidase activity in mouse liver fractions at various periods after administration of misonidazole (800 mg/kg body wt)

Period after treatment (hr)	Enzyme activity (units/mg protein) in: Homogenate		Cytosol	
	Saline	Misonidazole	Saline	Misonidazole
0.5	0.36 ± 0.02	0.39 ± 0.02	0.86 ± 0.05	0.74 ± 0.07
1.0	0.42 ± 0.02	0.29 ± 0.01*	0.86 ± 0.05	0.59 ± 0.08†
2.0	0.43 ± 0.02	0.42 ± 0.05	0.89 ± 0.02	0.75 ± 0.03‡
3.0	0.44 ± 0.03	0.44 ± 0.03	1.02 ± 0.08	0.76 ± 0.06†
4.0	0.35 ± 0.02	0.38 ± 0.02	1.00 ± 0.06	1.00 ± 0.03
6.0	0.49 ± 0.01	0.35 ± 0.04†	1.12 ± 0.06	0.99 ± 0.08
12.0	0.42 ± 0.03	0.41 ± 0.02	0.93 ± 0.04	0.93 ± 0.07
24.0	0.44 ± 0.01	0.40 ± 0.03	1.25 ± 0.09	1.15 ± 0.03

Values are expressed as mean of activities from four to six animals ± S.E.M.
*–‡ Significantly different compared with saline value: *$P < 0.001$, †$P < 0.05$, and ‡$P < 0.01$.

DISCUSSION

Glutathione peroxidase is a selenoenzyme that can detoxify hydrogen peroxide or organic hydroperoxides [10]. When enzyme activity is assayed with organic hydroperoxides like cumene hydroperoxide, the activity obtained includes a non-selenium-dependent component that was later shown to be associated with glutathione transferase [11]. In the present study, GSHPx (assayed with cumene hydroperoxide) was more sensitive to misonidazole *in vitro* and *in vivo* than selenium-GSHPx (assayed with H_2O_2). GSHTx was also inhibited by misonidazole *in vivo*. The pattern of inhibition of GSHPx was somewhat similar to GSHTx in the liver fractions, but the quantitative results suggest that the GSHTx component of GSHPx is more affected than the selenium-GSHPx.

The aerobic and anaerobic metabolism of misonidazole appear to result in different end products [5], probably explaining its sensitizing and toxic effects. Hypoxic reduction of misonidazole by microsomes is known to produce a radical anion [12], which may be responsible for the formation of adducts with glutathione or DNA [6, 7]. Aerobic metabolism of heterocyclic nitrocompounds produces superoxide, which may undergo interconversions to other reactive oxygen species [13]. The *in vitro* inhibition of glutathione peroxidase and *in vivo* inhibition of glutathione peroxidase and glutathione transferase may be due to the direct reaction of protein thiols of these enzymes with misonidazole. However, this reaction would be more likely under anaerobic conditions where both protein and nonprotein thiols react with misonidazole [5]. Under the conditions of the present experiments, it is unlikely that depression of GSH concentration contributed to the decrease in enzyme activity. The inhibition (*in vivo*) may also be related to the cyclic reduction–oxidation of the nitro-radical anion [14, 15] of misonidazole. The probable generation of superoxide from this cyclic reaction may result in the inhibition of the enzyme although it is reported that misonidazole is not as good a promoter of superoxide formation [12] or of oxygen consumption as other heterocyclic nitro compounds [5]. The greater inhibition of the microsomal glutathione peroxidase and transferase may be due to the activation of misonidazole in the microsomes [12] and its

Table 3. Glutathione transferase activity in mouse liver fractions at various periods after administration of misonidazole (800 mg/kg body wt)

Period after treatment (hr)	Enzyme activity (units/mg protein) in: Homogenate		Microsomes		Cytosol	
	Saline	Misonidazole	Saline	Misonidazole	Saline	Misonidazole
0.5	1.92 ± 0.06	1.80 ± 0.05	0.25 ± 0.01	0.27 ± 0.01	5.50 ± 0.07	5.70 ± 0.14
1.0	1.92 ± 0.06	1.92 ± 0.09	0.21 ± 0.01	0.18 ± 0.04	6.41 ± 0.14	5.03 ± 0.14*
2.0	ND	1.50 ± 0.19‡	0.22 ± 0.01	0.22 ± 0.01	5.80 ± 0.13	4.97 ± 0.07*
3.0	1.90 ± 0.12	1.70 ± 0.08	ND	0.12 ± 0.01*‡	5.99 ± 0.11	4.09 ± 0.08*
4.0	ND	1.40 ± 0.04‡	0.22 ± 0.01	0.21 ± 0.01	ND	4.46 ± 0.08*‡
6.0	2.20 ± 0.04	1.80 ± 0.09†	0.21 ± 0.01	0.19 ± 0.01	6.30 ± 0.19	4.17 ± 0.06*
12.0	1.94 ± 0.03	1.82 ± 0.06	0.21 ± 0.01	0.19 ± 0.01	6.09 ± 0.15	5.90 ± 0.17
24.0	1.97 ± 0.07	1.94 ± 0.06	0.24 ± 0.01	0.13 ± 0.01*	6.15 ± 0.08	6.26 ± 0.12

Values are expressed as mean of activities from four to six animals ± S.E.M. ND = not determined.
*,† Significantly different compared with saline value: *$P < 0.001$, and †$P < 0.01$.
‡ These values were compared with mean of all saline (control) values of respective fractions.

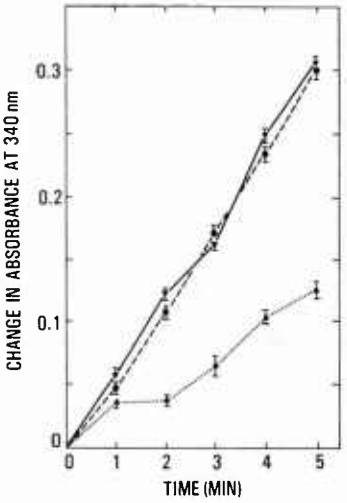

Fig. 2. Inhibition of mouse liver cytosol selenium-dependent glutathione peroxidase *in vitro* by misonidazole. Mouse liver cytosol fraction was incubated with misonidazole at various concentrations for 2 min and assayed with hydrogen peroxide. Values given are means of five separate determinations ± S.E.M. Key: (▼——▼) control; misonidazole concentrations: (●——●) 0.2 mM; and (▲----▲) 0.5 mM.

subsequent binding to these enzymes. Alternatively, the enzyme may be irreversibly bound at the active site with glutathione–misonidazole conjugate.

The inhibition of these two enzymes may be one of the causes of the elevation of hydrogen peroxide levels reported in the presence of misonidazole [5]. The present investigation may provide more insight into toxicity resulting from misonidazole treatment than on sensitization, which is limited more likely to hypoxic cells. Small increases in lysosomal enzyme activity [16] in the nerve region and the increase in lysosomal membrane permeability [17] in the presence of misonidazole may be due to an increase in lipid peroxidation resulting from elevated peroxide level. Thus, one of the probable mechanisms of action of misonidazole may be the susceptibility of tissue to lipid peroxidation due to the inhibition of glutathione peroxidase and glutathione transferase. The inhibition of these enzymes and the lipophilicity of the drug could contribute to the neuropathies observed in the use of misonidazole. Further studies on neural tissue after treatment with misonidazole are needed to obtain direct evidence for this view.

Acknowledgements—We are grateful to William E. Jackson III for performing statistical analyses. Dr. Kumar is a National Research Council-AFRRI Research Associate. This research was supported by the Armed Forces Radiobiology Research Institute, Defense Nuclear Agency, under Work Unit MJ00026. The views presented in this paper are those of the authors; no endorsement by the Defense Nuclear Agency has been given or should be inferred. Research was conducted according to the principles enunciated in the *Guide for the Care and Use of Laboratory Animals* prepared by the Institute of Laboratory Animal Resources, National Research Council.

REFERENCES

1. T. H. Wasserman, T. L. Phillips, R. J. Johnson, C. J. Gomer, G. A. Lawrence, W. Sadee, R. A. Marques, V. A. Levin and G. Vanaralte, *Int. J. Radiat. Oncol. Biol. Phys.* **5**, 775 (1979).
2. M. D. Walker and T. A. Strike, *Cancer clin. Trials* **3**, 105 (1980).
3. M. I. Sanders, S. Dische, P. Anderson and I. R. Flockhart, *Br. J. Cancer* **37** (Suppl. III), 268 (1978).
4. R. C. Urtasun, P. Band J. D. Chapman, A. F. Wilson, B. Marynowski and E. Starreveld, *New Engl. J. Med.* **295**, 901 (1976).
5. J. E. Biaglow, M. E. Varnes, M. Astor, J. Mitchell and A. Russo, in *Radioprotectors and Anticarcinogens* (Eds. O. F. Nygaard and M. G. Simic), p. 203. Academic Press, New York (1983).
6. A. J. Varghese and G. F. Whitmore, *Cancer Res.* **40**, 2165 (1980).
7. A. J. Varghese, *Biochem. biophys. Res. Commun.* **112**, 1013 (1983).
8. R. A. Lawrence and R. F. Burk, *Biochem. biophys. Res. Commun.* **71**, 952 (1976).
9. W. H. Habig, M. J. Pabst and W. B. Jakoby, *J. biol. Chem.* **249**, 7130 (1974).
10. L. Flohe, in *Free Radicals in Biology* (Ed. W. A. Pryor), p. 223. Academic Press, New York (1982).
11. R. A. Lawrence, L. K. Parkhill and R. F. Burk, *J. Nutr.* **108**, 981 (1978).
12. M. E. McManus, M. A. Lang, K. Stuart and J. Strong, *Biochem. Pharmac.* **31**, 547 (1982).
13. M. Dubin, S. G. Goijman and A. O. M. Stoppani, *Biochem. Pharmac.* **33**, 3419 (1984).
14. R. P. Mason and J. L. Holtzman, *Biochemistry* **14**, 1626 (1975).
15. F. J. Peterson, R. P. Mason, J. Hosepian and J. L. Holtzman, *J. biol. Chem.* **254**, 4009 (1979).
16. G. P. Rose, A. J. Dewar and B. J. Moffett, *Clin. Toxic.* **18**, 1411 (1981).
17. G. M. Barratt and E. D. Wills, *Eur. J. Cancer* **17**, 21 (1981).

0022-3565/86/2383-0839$02.00/0
THE JOURNAL OF PHARMACOLOGY AND EXPERIMENTAL THERAPEUTICS

Vol. 238, No. 3
Printed in U.S.A.

Organophosphate-Induced Histamine Release from Mast Cells[1]

HAROLD H. NEWBALL, MILDRED A. DONLON, LAWRENCE R. PROCELL, ELEANORA A. HELGESON and DAVID R. FRANZ

U.S. Army Medical Research Institute of Chemical Defense, Physiology Division, Edgewood Area, Aberdeen Proving Ground, Maryland (L.R.P., D.R.F.), Armed Forces Radiobiological Research Institute, Bethesda, Maryland (M.A.D., E.A.H.) and Physiology Division, Uniformed Services University of The Health Sciences, Bethesda, Maryland (H.H.N.)

Accepted for publication May 23, 1986

ABSTRACT

To examine the hypothesis that soman intoxication leads to degranulation of mast cells with the release of histamine, we studied the effects of soman on rat peritoneal mast cells (RPMC) *in vitro* and *in vivo*. *In vitro* studies were performed with RPMC harvested from Edgewood rats, and challenged with soman (10^{-8}–3×10^{-3} M) in Tyrode's buffer. The RPMC exhibited a dose-dependent release of histamine, with maximal release of 50% at 3 to 6×10^{-4} M. The release process is an active, secretory, noncytotoxic event, which is calcium and temperature dependent, requires metabolic energy and is influenced by intracellular levels of cyclic AMP. We next studied the *in vivo* effects of disodium cromoglycate (DSCG, 10^{-4} M) on soman and Compound 48/80-induced histamine release. *In vivo* studies were performed by the i.p. injection of 5 ml of Tyrode's buffer containing soman (0–1 LD_{50}), or Compound 48/80 as a positive control, with or without DSCG. The fluid recovered after approximately 10 min in the pentoneal cavity was examined for percentage of histamine release. *In vivo*, Compound 48/80 induced 49 ± 1% histamine release, with no inhibition by DSCG (Compound 48/80 plus DSCG induced 49 ± 0.4% histamine release). On the other hand, soman (1 LD_{50}) induced 17 ± 5% extracellular histamine release, with complete inhibition by DSCG (soman plus DSCG induced 3 ± 1% histamine release). The data indicate that soman induced a dose-dependent release of histamine from RPMC, and provide evidence that histamine is a potentially important mediator of the pathophysiological response to organophosphate intoxication. The data also indicate that *in vivo* soman-induced histamine release can be inhibited by DSCG, suggesting that the *in vivo*, like the *in vitro* release process, is a calcium-dependent event.

Organophosphate intoxication with insecticides has become a major concern due to the increasing number of accidental agricultural exposures and suicidal attempts (Du Toit *et al.*, 1981; AMA Report, 1950). Organophosphate intoxication with nerve agents such as soman (O-1,2,2-trimethylpropylmethylphosphonofluoridate) has also become a major concern in view of the large number of reported casualties resulting from nerve agent exposure of Afghanistan soldiers during the invasion of their country (Isby, 1983).

Preliminary data suggest that the s.c. administration of soman to rats results in extensive and widespread degranulation of mast cells (Doebler *et al.*, 1982). Furthermore, intoxication with organophosphates such as soman may produce an anaphylactoid syndrome suggesting the systemic release of histamine (Nikolayevich/Stroykov, 1978). It is of interest that benactazine, a drug with antihistaminic properties, has been included in the therapy of organophosphate intoxication (Nikolayevich/Stroykov, 1978). Thus, there is suggestive evidence that soman intoxication may be associated with mast cell degranulation followed by elevation of plasma histamine levels.

We examined the hypothesis that soman intoxication leads to degranulation of mast cells. To test this hypothesis, we studied the *in vivo* and *in vitro* effects of soman on RPMC. Soman induced a dose-dependent release of histamine from RPMC, both *in vivo* and *in vitro*. This release process is an active, secretory, noncytotoxic event, which is calcium and temperature dependent, requires metabolic energy and is influenced by the intracellular levels of cAMP. The soman-induced release process is thus similar to the release of histamine and other mediators from human lung mast cells and basophils (Newball *et al.*, 1979; Newball *et al.*, 1980; Peters *et al.*, 1982; Newball and Lichtenstein, 1983). The *in vivo* data indicate that soman-induced release of histamine is inhibited by DSCG, which inhibits mediator release through the inhibition of calcium uptake (Mazurek *et al.*, 1983), suggesting that the *in vivo* release of histamine is also a calcium-dependent event.

Received for publication April 17, 1985.

[1] The opinions or assertions contained herein are the private views of the authors and are not to be construed as official or as reflecting the views of the U.S. Army or the Department of Defense. In conducting the research described in this report, the investigators adhered to the "Guide for the Care and Use of Laboratory Animals of the Institute of Laboratory Animal Research Council."

Materials and Methods

The following were purchased: theophylline, histamine, bovine serum albumin (BSA), EDTA, magnesium chloride, sodium chloride, sodium phosphate, DFP (Sigma Chemical Co., St. Louis, MO); dextrose, cal-

ABBREVIATIONS: RPMC, rat pentoneal mast cells; cAMP, cyclic AMP; DSCG, disodium cromoglycate; BSA, bovine serum albumin; DFP, diisopropyl fluorophosphate.

cium chloride, sodium bicarbonate (Fisher Scientific Co., Fairlawn, NJ); potassium chloride (Allied Chemical Corp., Morristown, NJ); heparin (Elkins-Sinn, Inc., Cherry Hill, NJ); antimycin A (Calbiochem, San Diego, CA); soman (99.1% purity) was synthesized by the Chemical Research and Development Center (Aberdeen Proving Ground, Aberdeen, MD); and DSCG was kindly provided by Fisons Corp. (Bedford, MA).

Buffers. Tyrode's buffer contains (grams per liter): NaCl, 8.0; KCl, 0.2; NaH_2PO_4, 0.05; $CaCl_2$-$2H_2O$, 0.26; $MgCl_2$-$6H_2O$, 0.25; and glucose, 1.0; the pH was titrated to 7.4 by the addition of sodium bicarbonate.

Mast cells. Mast cells were harvested from the peritoneal cavity of Edgewood Albino rats [AMRI:(SDXWI)BR]. Tyrode's buffer (without calcium or magnesium) containing BSA (100 mg/l) and heparin (10 U/ml) was used to lavage the peritoneal cavity. Rats were sacrificed by CO_2 inhalation, after which 20 ml of Tyrode's buffer was instilled in the peritoneal cavity with an 18-gauge hypodermic needle. After gentle massage for 90 sec, the instillate was recovered through an abdominal incision, and centrifuged at 500 × *g*, 5°C for 5 min. The mast cells (5–8% of total cellular content) were resuspended in Tyrode's buffer and aliquoted to plastic tubes in which they were challenged.

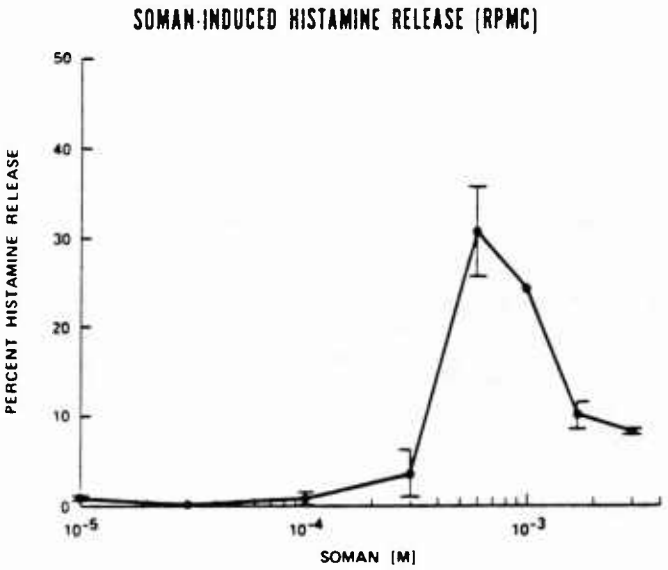

Fig. 1. Soman-induced histamine release from RPMC. There is a bell-shaped dose-response curve with maximal release at a concentration of 6×10^{-4} M. Vertical bars are ±1 SE.

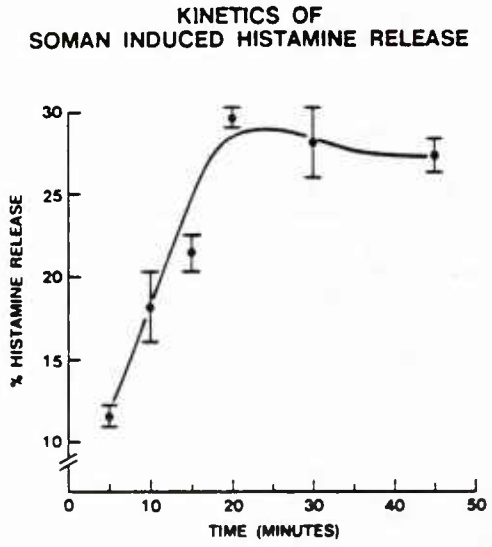

Fig. 2. Kinetics of soman-induced histamine release. Maximal release occurred in approximately 20 min.

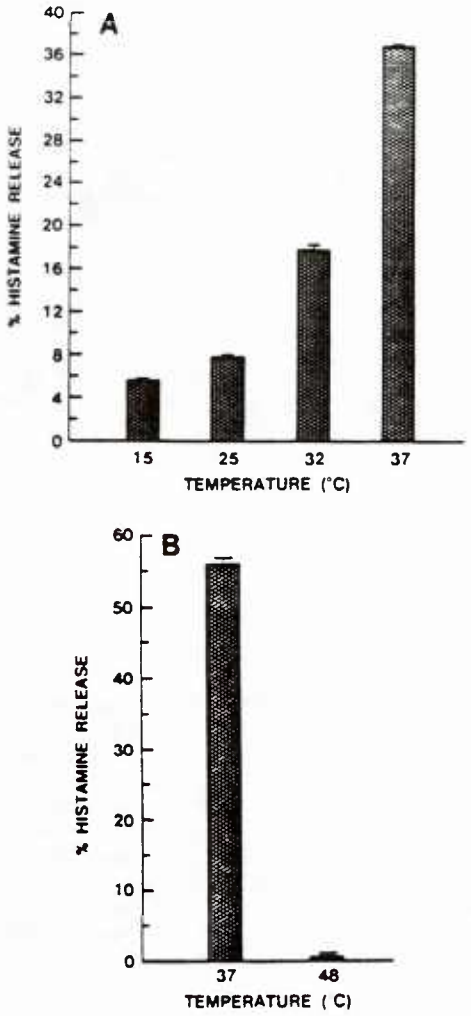

Fig. 3. Effect of temperature on soman-induced histamine release. Maximal release occurred at 37° (A) with no significant release at 48° (B).

Histamine release. For dose response and pharmacological studies, aliquots of RPMC were challenged in Tyrode's buffer in triplicate. Challenges were performed with either buffer alone (control), or with various concentrations of soman in a final volume of 0.5 ml at 37°C for 20 min. In pharmacological studies, compounds prepared in aqueous buffer were added in a range of concentrations 5 min before soman challenge. At the completion of the experiments, samples were centrifuged at 500 × *g* for 5 min and supernatants assayed for histamine with the automated fluorometric method of Siraganian (1976), or the radioenzymatic assay for histamine (Verburg *et al.*, 1983) (purified histamine N-methyltransferase was kindly provided by Dr. D. P. Henry, Eli Lilly and Co., Indianapolis, IN). The percentage of histamine release was calculated from the ratio of supernatant histamine to the sum of supernatant histamine plus the remaining cellular histamine.

The data were analyzed by the student's *t* test, and changes with P values of 0.05 or less were considered significant (Snedecor and Cochran, 1967).

Results

In Vitro Studies

Soman dose-response, kinetics and temperature studies. The agonist effect of soman on RPMC was studied using

final concentrations of 10^{-6} to 3×10^{-1} M. Figure 1 shows a bell-shaped dose-response curve, with maximal release occurring at a concentration of 6×10^{-4} M. Optimal concentrations of soman for maximal release vary between 3 and 6×10^{-4} M. Mast cells exhibited a release of histamine that was dependent on the molar concentration of soman to which they were exposed, with maximal release of approximately 50% of the cellular histamine. Kinetic studies of soman-induced histamine release from mast cells show maximal release in 20 to 45 min, depending on the concentration of soman to which the cells are exposed (fig. 2). In the kinetic studies, a suspension of RPMC was challenged with soman (6×10^{-4} M), then aliquots of cells were removed at increasing time points and the percentage of histamine released determined, as previously described (Newball *et al.*, 1979). Further studies show that there is a temperature dependence of soman-induced histamine release. Challenged cells showed no release at 4°C; little, albeit increasing, release at 15, 25 and 32°C; maximal release at 37°C; and no significant release at 48°C (fig. 3, A and B) as described previously (Newball *et al.*, 1979; Chhatwal *et al.*, 1982).

Calcium dependence of soman-induced histamine release. RPMC were harvested and washed with calcium-free Tyrode's buffer. To determine whether soman-induced histamine release was calcium dependent, we performed studies as illustrated in figure 4. Control triplicate tubes contained cells that were exposed to EDTA (5×10^{-3} M), calcium (10^{-3} M) or EDTA (5×10^{-3} M) plus soman (6×10^{-4} M). Experimental tubes contained cells that were exposed to calcium (10^{-3} M) plus soman (6×10^{-4} M). It is clear from figure 4 that calcium (10^{-3} M) enhanced soman-induced histamine release. Further studies with increasing concentrations of calcium (3×10^{-5}–3×10^{-3} M) showed that soman-induced histamine release is a calcium-dependent process (fig. 5).

Energy requirement for soman-induced histamine release. Mediator release is an active process, with an absolute requirement for metabolic energy, and if glycolytic processes are impaired, histamine release ceases (Newball *et al.*, 1979). We studied the effects of antimycin A (Johansen, 1983), a metabolic inhibitor that inhibits the release of histamine from RPMC. As shown in figure 6, the histamine release process is energy dependent (it is inhibited by antimycin A). The molar concentration of antimycin A required for 50% inhibition of release is approximately 5×10^{-7} M.

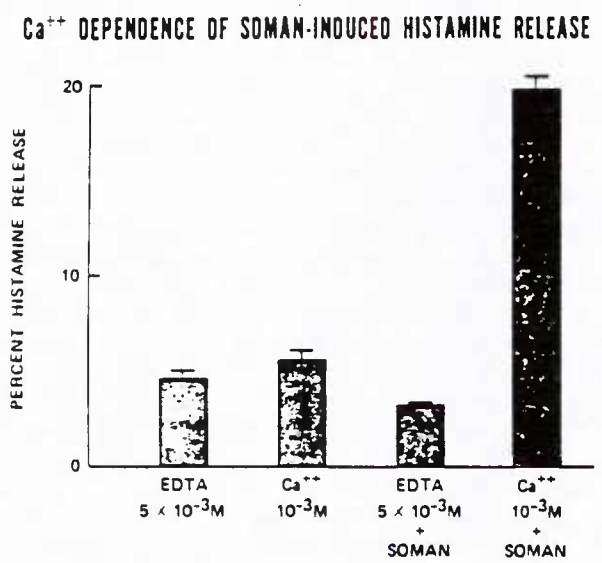

Fig. 4. Calcium dependence of soman-induced histamine release. There is an absolute requirement for divalent cations (calcium) during the release process.

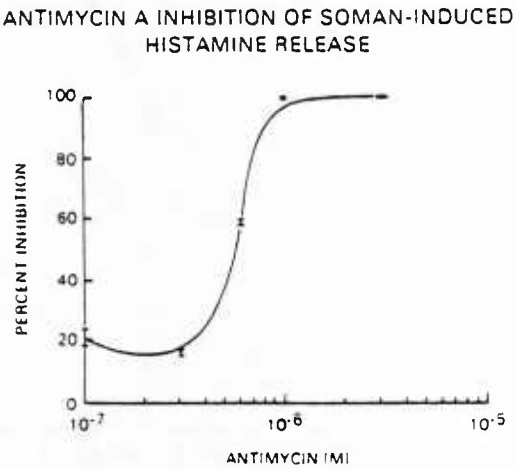

Fig. 6. Energy requirement for soman-induced histamine release. The histamine release process is energy dependent; it is inhibited by antimycin A $IC_{50} \approx 5 \times 10^{-7}$ M).

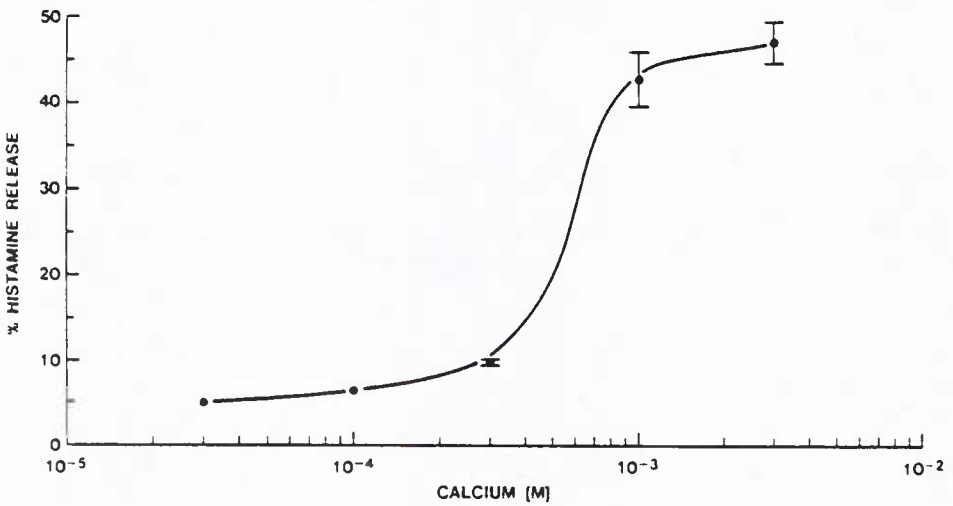

Fig. 5. Calcium dependence of soman-induced histamine release.

Modulation of soman-induced histamine release. Earlier studies have shown that cAMP and agents that increase the cAMP level of cells inhibit the release of histamine (Newball and Lichtenstein, 1981). In the following experiments, we studied the modulating effects of theophylline, a cAMP-active drug, on the release of histamine. The pharmacological effects of theophylline were determined by adding aliquots of RPMC suspensions to a series of test tubes containing a constant concentration of soman (6×10^{-4} M), and variable concentrations of theophylline. The test tubes were incubated at 37°C for 20 min, and the percentage of histamine released into the supernatant determined. The percentage of inhibition of release resulting from theophylline was determined from the equation: Percent inhibition = $[(C - E)/C] \times 100$, where C and E represent the net percentage of histamine release in the control (C) and experimental (E) tubes, respectively. Figure 7 shows the influence of theophylline on soman-induced release of histamine. The molar concentration of theophylline required for 50% inhibition of histamine release is approximately 4×10^{-4} M, which is comparable to the concentration reported for inhibition of histamine release from human basophils and mast cells (Newball *et al.*, 1979; Newball *et al.*, 1980; Peters *et al.*, 1982).

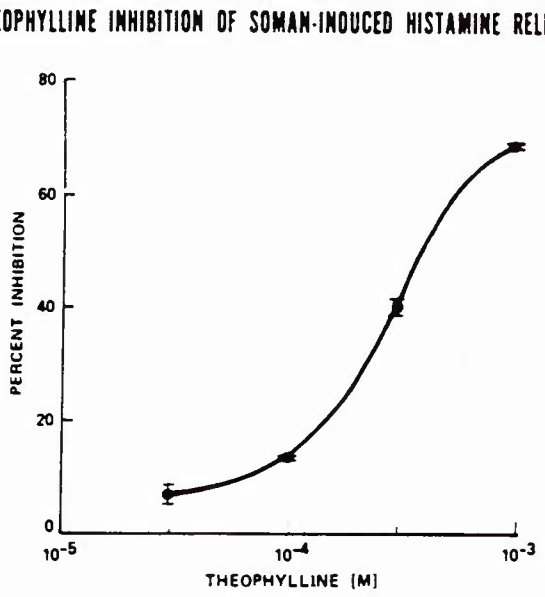

Fig. 7. Theophylline inhibition of soman-induced histamine release. Theophylline, which increases intracellular levels of cAMP inhibits histamine release.

Effect of soman and DFP on Compound 48/80-induced histamine release. Compound 48/80 has secretagogue effects on RPMC. To determine the influence of soman and DFP on Compound 48/80-induced histamine release, we first determined the dose-response relationships of Compound 48/80 for RPMC. Figure 8 shows a dose response study in which a maximal histamine release of 95% was achieved with a concentration of Compound 48/80 of approximately 3 μg/ml. For our studies on the influence of soman and DFP on Compound 48/80-induced histamine release, we used a concentration that would induce the release of 40 to 50% of the histamine content.

We next determined the pharmacological effects of soman on Compound 48/80-induced histamine release by adding aliquots of RPMC suspensions to a series of test tubes containing a constant concentration of Compound 48/80 (0.3 μg/ml), and variable concentrations of soman (10^{-5}–3×10^{-3} M). Compound 48/80 (0.3 μg/ml) induced 43% histamine release, which was inhibited by soman (3×10^{-3} M). Even though soman induced histamine release from RPMC in a parallel study (figure 9), soman did not enhance Compound 48/80-induced histamine release even at a concentration (6×10^{-4} M) where it induced maximal histamine release. Soman did inhibit Compound 48/80-induced histamine release, but did not do so until a concentration (1.5×10^{-3} M) was achieved where soman itself exhibited an inhibitory effect on its own release process.

Similar dose response studies were carried out with DFP to determine its secretagogue effects on RPMC. DFP likewise induced histamine release from RPMC with maximal release at a concentration of 6×10^{-3} M (figure 10). Like soman, the dose response pattern of DFP included excess inhibition at a concentration of 10^{-2} M. Even though DFP induced histamine release from RPMC, like soman, it did not enhance Compound 48/80-induced histamine release even at a concentration (6×10^{-3} M) where it induced maximal histamine release. DFP did inhibit Compound 48/80-induced histamine release, but not

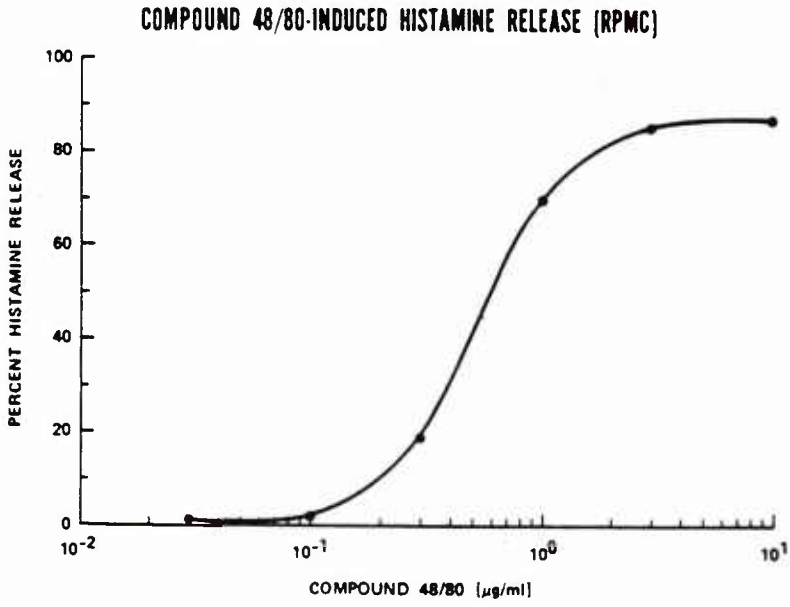

Fig. 8. Dose-response curve for Compound 48/80-induced histamine release.

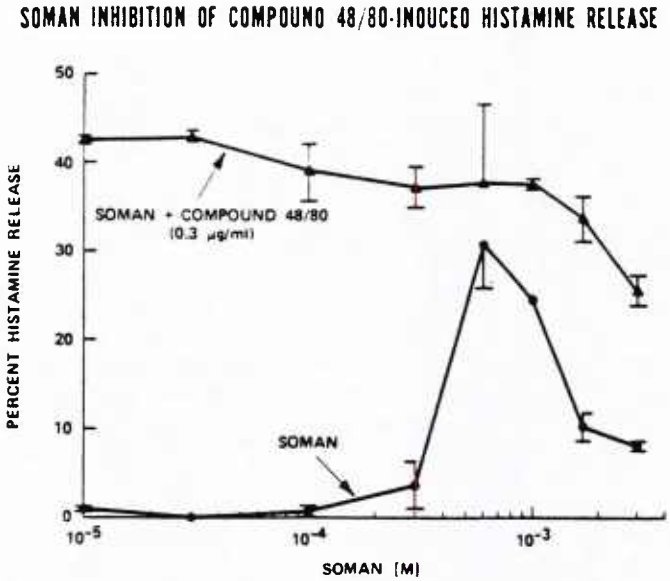

Fig. 9. Soman inhibition of Compound 48/80-induced histamine release. Soman did not enhance Compound 48/80-induced histamine release, and only inhibited Compound 48/80-induced histamine release at a concentration where soman itself exhibited an inhibitory effect on its own release process.

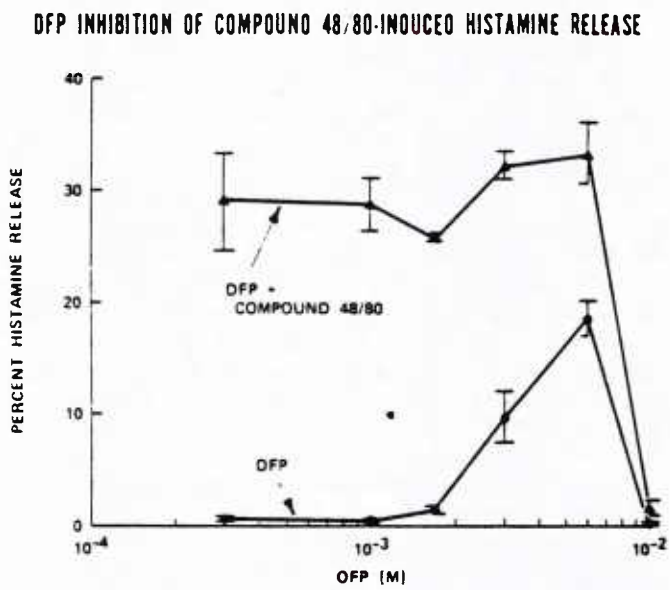

Fig. 10. DFP inhibition of Compound 48/80-induced histamine release. DFP did not enhance Compound 48/80-induced histamine release, and only inhibited Compound 48/80-induced histamine release at a concentration where DFP itself exhibited an inhibitory effect on its own release process.

until a concentration (10^{-2} M) was achieved where DFP itself exhibited an inhibitory effect on its own release process.

In Vivo Studies

In vivo challenges were performed by the i.p. injection of 5 ml of Tyrode's buffer (control), or 5 ml of Tyrode's buffer containing soman (1 LD_{50}, 120 μg/kg), or 5 ml of Tyrode's buffer containing Compound 48/80 (0.5 μg/g rat) as a positive control. The rats were sacrificed by CO_2 inhalation and then the fluid, recovered after approximately 10 min in the peritoneal cavity, was examined for percentage of histamine release,

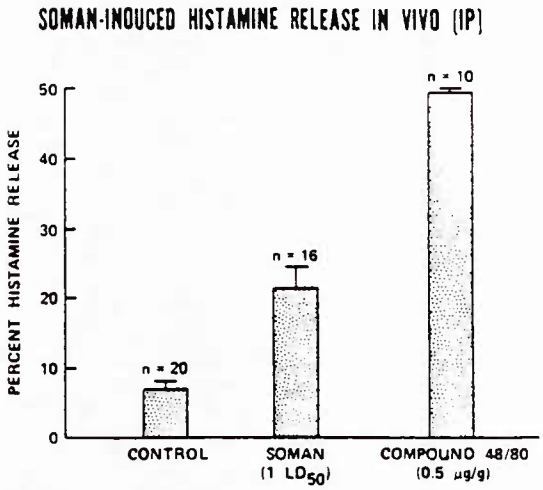

Fig. 11. Soman-induced histamine release *in vivo*. 1 LD_{50} (120 μg/kg) given i.p. induced histamine release within 10 min.

expressed as the ratio of supernatant histamine to the sum of supernatant histamine plus the remaining cellular histamine. *In vivo*, Compound 48/80 (0.5 μg/g) induced a release of 50 ± 1%, whereas soman (1 LD_{50}) induced a release of 21 ± 3% of the free histamine content (figure 11).

DSCG inhibition of *in vivo* soman-induced histamine release. We determined whether DSCG could inhibit the *in vivo* soman and Compound 48/80-induced histamine release. DSCG (10^{-4} M) was injected simultaneously with soman (1 LD_{50}) or Compound 48/80 (0.25 or 0.5 μg/g of rat) i.p. in 5 ml of Tyrode's buffer and the extent of histamine release determined. Table 1 illustrates the effects of DSCG on soman-induced histamine release *in vivo*. In Table 1, data reported under "first wash" represent the fluid that was injected i.p. while the rats were alive, and which was recovered after sacrifice by CO_2 inhalation. The "second wash" represents the fluid that was collected from a 5-ml wash of the peritoneal cavity after the animal had been sacrificed, and completion of the first wash. All fluid was recovered through an abdominal incision. In Study I (first wash) the control buffer induced 4 ± 3% histamine release. Compound 48/80 (0.5 μg/g of rat) induced 49 ± 1% histamine release, with no inhibition by DSCG (Compound 48/80 plus DSCG induced 49 ± 0.4% histamine release). On the other hand, soman (1 LD_{50}) induced 17 ± 5% histamine release, with complete inhibition by DSCG (soman plus DSCG induced 3 ± 1% histamine release). The second wash (Table 1) showed a similar pattern that was consistent in additional studies (Study II) where the dosage of Compound 48/80 was 0.25 μg/g of rat.

Discussion

Organophosphates are known to induce a number of pathophysiological effects during intoxication of animals and man (Grob, 1956; Nikolayevich/Stroykov, 1978; Sidell, 1974). These pathophysiological effects include bronchoconstriction, hypotension and cardiac arrhythmias, all of which may result, to variable extents, from an elevation of plasma histamine levels (Douglas, 1980). We examined the hypothesis that soman intoxication leads to degranulation of mast cells by studying the *in vivo* and *in vitro* effects of soman on RPMC. We reasoned that mast cell degranulation within the peritoneal cavity might lead to elevated plasma histamine levels, which may be respon-

TABLE 1

Effect of DSCG on soman-induced histamine release *in vivo* (*rats, i.p.*)

Groups 1 and 2 are significantly different ($P < .01$), as are Groups 4 and 5 ($P < .05$)

Group	Study I Percentage of Histamine Release		Study II Percentage of Histamine Release		N
	First wash	Second wash	First wash	Second wash	
1. Control (Tyrode s Buffer)	4 ± 3	9 ± 5	6 ± 4	9 ± 5	2
2. Compound 48/80	49 ± 1	49 ± 0.3	51 ± 0.2	52 ± 0.5	2
3. Compound 48/80 + DSCG	49 ± 0.4	48 ± 1	52 ± 0.1	55 ± 4	2
4. Soman (1 LD_{50})	17 ± 5	25 ± 5	16 ± 6	18 ± 5	6
5. Soman (1 LD_{50}) + DSCG	3 ± 1	7 ± 3	2 ± 0.5	4 ± 0.2	6

sible partially for the bronchoconstriction, hypotension and cardiac arrhythmias reported in soman intoxication.

The data indicate that *in vitro*, soman induces a dose-dependent release of histamine from rat peritoneal mast cells (fig. 1). This release process is an active, secretory, noncytotoxic event, which is divalent cation (calcium) (figs. 4–5) and temperature dependent (fig. 3), requires metabolic energy (fig. 6) and is influenced by intracellular levels of cAMP (fig. 7), as has been described for the release of histamine and other mediators from human lung mast cells and basophils (Newball *et al.*, 1979; Newball *et al.*, 1980). Thus, in many respects, the release process is similar to the active secretion of histamine from human mast cells and basophils.

The release process is dependent on calcium throughout its course; the removal of extracellular divalent cations by EDTA promptly stops the release process, as described earlier for histamine release (Newball *et al.*, 1979). The release process is also temperature dependent, with no release at 4°C, minimal release at temperatures of or below 25°C, maximal release at 37°C and no significant release at 48°C (fig. 3). Not only is the initiation of the release process temperature sensitive, but decreasing the reaction temperature at any point during the release process to 4°C promptly stops the reaction (data not shown), as described earlier for histamine release from human basophils (Newball *et al.*, 1979). Finally, the release process requires metabolic energy as indicated by its inhibition in the presence of antimycin A, an inhibitor of glycolysis (Johansen, 1983). All of the above characteristics indicate that soman-induced histamine release from RPMC is an active, secretory event, and not the result of a cytotoxic process.

Soman and DFP have secretagogue effects on RPMC (figs. 9–11) as does Compound 48/80 (Morrison *et al.*, 1975; Newball *et al.*, 1984) (fig. 8). One of our objectives was to determine whether or not soman and DFP would enhance Compound 48/80-induced histamine release. As shown in figures 9 and 10, neither soman nor DFP enhanced Compound 48/80-induced histamine release at a concentration of Compound 48/80 that induced submaximal release (43%, fig. 8). Rather, both soman (1.5×10^{-3} M) and DFP (10^{-2} M) inhibited the secretion of histamine from RPMC. Curiously, this inhibition of Compound 48/80-induced histamine release only occurred at concentrations of soman and DFP which also caused inhibition of soman and DFP-induced histamine release, respectively. In other words, the soman and DFP dose-response curves exhibited what appeared to be "concentration excess inhibition." Inhibition of Compound 48/80-induced histamine release only occurred at concentrations of soman and DFP that exhibit excess inhibition. Earlier investigations have suggested that DFP inhibits the release of histamine from mast cells through the inhibition of a DFP-sensitive esterase (Kaliner *et al.*, 1973; Kazimierczak *et al.*, 1984). The mechanism through which DFP and soman inhibit the secretion of histamine is unknown.

Soman induces the release of histamine from RPMC not only *in vitro*, but also *in vivo* (fig. 11). RPMC exposed to soman (1 LD_{50}) secreted 21 ± 3% of their cellular histamine content. DSCG inhibits the soman-induced release of histamine *in vivo* (table 1). The observation that DSCG inhibits soman-induced histamine release *in vivo* suggests that the *in vivo*, like the *in vitro*, release is a calcium-dependent process. DSCG is thought to inhibit histamine secretion by the regulation of phosphorylation, a calcium-dependent process (Mazurek *et al.*, 1983; Theoharides *et al.*, 1980). It is thus not surprising that DSCG did not inhibit Compound 48/80-induced histamine release, inasmuch as Compound 48/80-induced histamine release is not calcium dependent (Kruger, 1976).

Our data provide *in vitro* and *in vivo* evidence that establishes histamine as a potentially important mediator of the pathophysiological response to organophosphate intoxication. The concentration of soman required for maximal release of histamine *in vitro* is relatively high (6×10^{-4} M). However, lower concentrations provided by doses of 0.3 (data not shown) and 1 LD_{50} given *in vivo* also induce substantial release of histamine. Also, the kinetics of the *in vitro* release process show maximal release in approximately 20 to 45 min, which is slightly slower than the kinetics of antigen-induced histamine release from basophils or mast cells (Newball *et al.*, 1979; Schulman *et al.*, 1982). However, the *in vivo* studies show substantial release of histamine within 5 to 10 min of challenge. The above differences between the *in vitro* and the *in vivo* release processes suggest an *in vivo* cofactor that enhances the release process. Finally, *in vivo*, soman-induced histamine release can be inhibited by DSCG, suggesting that the *in vivo* like the *in vitro* process is a calcium-dependent event.

References

Chhatwal, G. S., Ahnert-Hilger, G., Beress, L. and Habermann, E.: Palytoxin both induces and inhibits the release of histamine from rat mast cells. Intern. Arch. Allergy Appl. Immunol. **68:** 97–100, 1982.

Doebler, J., Anthony, A., Bocan, T. and Shih, T. M.: Mast cell degranulation in rats during acute soman toxication. Proceedings of Society of Neuroscience Annual Meeting **8:** 1010, 1982.

Douglas, W. W.: Histamine and 5-hydroxytryptamine and their antagonists. *In* Pharmacological Basis of Therapeutics, ed. by A. G. Gilman, L. S. Goodman and A. Gilman, 6th ed., pp. 611–613, The Macmillan Company, New York, 1980.

Du Toit, P. W., Muller, F. O., Van Tonder, W. M. and Ungerer, M. J.: Experience with the intensive care management of organophosphate insecticide poisoning. S. Afr. Med. J. **60:** 227–229, 1981.

Grob, D.: The manifestations and treatment of poisoning due to nerve gas and other organic phosphate anticholinesterase compounds. A.M.A. Arch. Internal Med. **98:** 221–239, 1956.

Isby, D. C.: Red rain—Anybody ready for communist chemicals? Soldier of Fortune, pp. 58–74, January 1983.

Johansen, T.: Estimation of the rate of energy production of rat mast cells *in vitro*. Acta Pharmacol. Toxicol. **53:** 413–416, 1983.

Kaliner, M., Austen, K. F. and Rapp, H. J.: A sequence of biochemical events

in the antigen-induced release of chemical mediators from sensitized human lung tissues. J. Exp. Med. **138:** 1077, 1973.

KAZIMIERCZAK, W., MEIER, H. L., MACGLASHAN, D. W., JR. AND LICHTENSTEIN, L. M.: An antigen-activated DFP-inhibitable enzyme controls basophil desensitization. J. Immunol. **132:** 399–405, 1984.

KRÜGER, T. G.: Histamine release process and concomitant structural changes in rat peritoneal mast cells. *In vitro* study on effects of compound 48/80 and the dependence of the process on cell preparation, temperature and calcium. Intern. Arch. Allergy Appl. Immunol. **51:** 608–626, 1976.

MAZUREK, N., BASHKIN, P., LOYTER, A. AND PECHT, I.: Restoration of Ca^{2+} influx and degranulation capacity of variant RBL-2H3 cells upon implantation of isolated cromolyn binding protein. Proc. Natl. Acad. Sci. U.S.A. **80:** 6014–6018, 1983.

MORRISON, D. C., ROSER, J. F., COCHRANE, C. G. AND HENSON, P. M.: Two distinct mechanisms for the initiation of mast cell degranulation. Intern. Arch. Allergy Appl. Immunol. **49:** 172–178, 1975.

NEWBALL, H. H., DONLON, M. A., PROCELL, L. R., HELGESON, E. A. AND FRANZ, D. R.: Inhibition of nerve-agent induced hiatamine release from mast cells (U). Army Science Conference Proceedings, vol. II, pp. 269–282, 1984.

NEWBALL, H. H. AND LICHTENSTEIN, L. M.: Mast cells and basophils: Effector cell of inflammatory disorders of the lung. Thorax **36:** 721–725, 1981.

NEWBALL, H. H. AND LICHTENSTEIN, L. M.: Pharmacologic modulation of the immune release of mediators from mast cells and basophils. *In* Immunopharmacology of the Lung, ed. by H. H. Newball, pp. 1–23, Marcel Dekker, New York, 1983.

NEWBALL, H. H., MEIER, H. L. AND LICHTENSTEIN, L. M.: Basophil mediators and their release with emphasis on BK-A. J. Invest. Dermatol. **74:** 344–348, 1980.

NEWBALL, H. H., TALAMO, R. C. AND LICHTENSTEIN, L. M.: Anaphylactic release of a basophil kallikrein-like activity. II. A mediator of immediate hypersensitivity reactions. J. Clin. Invest. **64:** 466–475, 1979.

NIKOLAYEVICH/STROYKOV, Y.: Clinical, diagnostic and therapeutical procedures for toxic chemical agent casualties. Klinika, Diagnostika i Lechenive Porazhenly Otravlyayusi Chimi Veshchestvami. Moscow, p. 178, 1978.

PETERS, S. P., SCHULMAN, E. S., SCHLEIMER, R. P., MACGLASHAN, D. W., JR., NEWBALL, H. H. AND LICHTENSTEIN, L. M.: Dispersed human lung mast cells: Pharmacological aspects and comparison with human lung tissue fragments. Am. Rev. Respir. Dis. **126:** 1034–1039, 1982.

PHARMACOLOGY AND TOXICOLOGY OF CERTAIN ORGANIC PHOSPHORUS INSECTICIDES. Report to the Council on Pharmacy and Chemistry of the American Medical Association. J. Am. Med. Assoc. **144:** 104–108, 1950.

SCHULMAN, E. S., ADKINSON, N. F., JR. AND NEWBALL, H. H.: Cyclooxygenase metabolites in human lung anaphylaxis: Airway vs. parenchyma. J. Appl. Physiol. **53:** 589–595, 1982.

SIDELL, F. R.: Soman and sarin: Clinical manifestations and treatment of accidental poisoning by organophosphates. Clin. Toxicol. **7:** 1–17, 1974.

SIRAGANIAN, R. P.: Histamine release and assay methods for the study of human allergy. *In* Manual of Clinical Immunology, ed. by N. R. Rose and H. Friedman, p. 603, American Society for Microbiology, Washington, 1976.

SNEDECOR, G. W. AND COCHRAN, W. G.: Statistical Methods. Iowa State University Press, 6th ed., pp. 91–119, 1967.

THEOHARIDES, T. C., SIEGHART, W., GREENGARD, P. AND DOUGLAS, W.: Antiallergic drug cromolyn may inhibit histamine secretion by regulating phosphorylation of a mast cell protein. Sci. Am. **207:** 80–82, 1980.

VERBURG, K. M., BOWSHER, R. R. AND HENRY, D. P.: A new radioenzymatic assay for histamine using purified histamine N-methyltransferase. Life Sci. **32:** 2855–2867, 1983.

Send reprint requests to: Harold H. Newball, M.D., Physiology Division, U.S. Army Medical Research Institute of Chemical Defense, Aberdeen Proving Ground, MD 21010-5425.

JOURNAL OF IMMUNOPHARMACOLOGY, 8(3), 407-425 (1986)

HEMOPOIETIC EFFECTS OF INTRAVENOUS SOLUBLE GLUCAN ADMINISTRATION

M. L. PATCHEN*
T. J. MACVITTIE

Department of Experimental Hematology
Armed Forces Radiobiology Research Institute
Bethesda, Maryland 20814-5145

ABSTRACT

A soluble form of the reticuloendothelial- and immune modulating agent glucan (glucan-F) has been evaluated for its effects on hemopoiesis. A single 5.0 mg intravenous injection of glucan-F into C3H/HeN mice increased peripheral white blood cellularity, bone marrow and splenic cellularity, bone marrow and splenic granulocyte-macrophage progenitor cell numbers (GM-CFC), and splenic pluripotent stem cell (CFU-s) and erythroid progenitor cell (CFU-e) numbers. Serum levels of granulocyte-macrophage colony stimulating activity (CSA) were also elevated following glucan-F administration. These hemopoietic responses correlate well with those previously shown to be induced by intravenous administration of particulate glucan (glucan-P). In contrast to glucan-P, however, intravenous glucan-F administration has been shown not to induce granuloma formation and severe hepatosplenomegaly, thus the potential clinical use of glucan-F as a hemopoietic stimulant is more likely than that of glucan-P.

INTRODUCTION

Bone marrow suppression is a common effect in patients undergoing radiotherapy and/or chemotherapy (1,2). Such patients usually develop anemia, lymphocytopenia, thrombocytopenia and

 0163-0571/86/0803-0407$3.50/0

granulocytopenia, the latter of which in particular predisposes them to the risks of a variety of serious and potentially lethal infections (3,4). Because of the many adverse problems and questionable effectiveness associated with granulocyte transfusions, other means of hemopoietic enhancement have been sought.

In the past several years, a variety of immunomodulating agents have been shown to be capable of stimulating hemopoiesis at the stem and committed progenitor cell levels. Bacillus Calmette Guerin (BCG) and Corynebacterium parvum (CP), in particular, have repeatedly been shown to be capable of modulating hemopoiesis (5,6,7,8,9). However, adverse side effects have been associated with these agents due to their potentially infectious capabilities, antigenic properties, and undefined chemical composition (10,11,12). Fortunately, other immunomodulators with fewer side effects have also been shown to alter hemopoiesis. In particular, our studies have concentrated on investigating the hemopoietic effects of glucan, a B, 1-3 polyglycan. Unlike BCG and CP, glucan is not potentially infectious, is not antigenic, and has a known molecular structure (for review see 13). Glucan has been shown to be an extremely potent reticuloendothelial stimulant and immune modulator. Non specific modification of a variety of bacterial, viral, fungal and parasitic infections, as well as, neoplastic diseases has been reported following glucan adminsitration (for review see 13).

Glucan has also been shown to significantly modulate hemopoieisis (for review see 14). In normal mice glucan has been shown to alter a variety of hemopoietic responses ranging from peripheral blood cell counts to the production of bone marow and splenic pluripotent hemopoietic stem cells (CFU-s), and granulocyte-macrophage (GM-CFC), pure macrophage (M-CFC), and erythroid (CFU-e, BFU-e) hemopoietic progenitor cells

(15,16,17,18,19,20,21). Likewise, in irradiated mice, glucan has been shown to enhance the recovery of hemopoietic stem and progenitor cells when administered either before or after a hemopoietically damaging dose (e.g. 6.5 Gy) of Cobalt-60 irradiation (14,22,23,24,25). When administered before an otherwise lethal dose (e.g. 9.0 Gy) of Cobalt-60 irradiation, glucan has even been shown to significantly increase survival (14,23,26). The exact mechanisms through which glucan mediates its effects on hemopoiesis are still largely unknown, however, both macrophages and T-lymphocytes have been shown to be involved (17, 20, 27).

Although when compared to other immunomodulators, glucan has negligable side effects, the glucan preparations available until recently have been shown to produce clinically undesirable severe hepatosplenomegaly and granuloma formation (13,21). The glucan preparations producing these side effects were all particulate in nature (1-3 u particles in saline or dextrose suspensions) and have sometimes recently been referred to as glucan-P preparations in order to distinguish them from newly produced soluble glucan preparations (13,25,28,29). Glucan-F is one such recently produced soluble glucan which is of particular interest because it appears to maintain the reticuloendothelial activating and immunostimulating characteristics of glucan-P without producing hepatosplenomegaly and granuloma formation. Even at extremely high intravenous doses, glucan-F has failed to produce detrimental side effects in mice or dogs and it is currently undergoing Phase I drug evaluation in humans. The purpose of this study was to evaluate the hemopoietic effects of glucan-F in normal mice and in irradiated mice following bone marrow transplantation. These effects are discussed in comparison to the hemopoietic effects previously shown to be produced by glucan-P.

MATERIALS AND METHODS

Mice

In all experiments 10 to 12-week-old female C_3H/HeN mice (Charles River Laboratories, Wilmington, MA) were used. Animals were maintained on a 6:00 am to 6:00 pm light-dark cycle. Wayne Lab Blox and hyperchlorinated water were available ad libitum. All mice were quarantined and acclimated to laboratory conditions for at least 2 weeks before experimentation. During this time, the mice were examined and found to be free of lesions of murine pneumonia complex and oropharyngeal Pseudomonas sp.

Glucan

Soluble endotoxin-free glucan (glucan-F) was obtained from Dr. N. R. DiLuzio (Tulane University School of Medicine, New Orleans, LA) and was prepared as described by DiLuzio et al. (28). Glucan-F was diluted in sterile saline and 5.0 mg in a 0.5 ml volume was intravenously injected into experimental mice via the lateral tail veins. Where indicated, normal control mice (not irradiated and not glucan-F-treated) and radiaton control mice (irradiated but not glucan-F-treated) were injected with an equivalent volume of sterile saline.

Cell Suspensions

Each cell suspension represented the pool of tissues from three mice. Cells were flushed from femurs with 3 ml of Hank's Balanced Salt Solution (HBSS) containing 10% heat-inactivated fetal bovine serum (HIFBS). Spleens were pressed through a stainless-steel mesh screen, and the cells were washed from the screen with 6 ml of HBSS plus 10% HIFBS. The total number of nucleated cells in each suspension was determined by counting the cells on a hemocytometer.

Irradiation

Bilateral total-body irradiation adminsistered from the AFRRI ^{60}Co source at a dose rate of 0.4 Gy per minute was used in all radiation experiments.

Peripheral Blood White Cell Counts, Hematocrit Determinations and Serum Collection

Mice were ether anesthetized and bled from the retroorbital sinus. White blood cell counts were performed by collecting 20 ul of blood into a calibrated capillary tube, dispensing it into 1.98 ml of 3% acetic acid (Unopettes by Becton-Dickenson, Rutherford, NJ), and counting the cells on a hemocytometer. Hematocrits were used as an indicator of red blood cellularity. The remaining blood from each mouse was allowed to clot, was centrifuged at 400 X g for 10 min and the serum was then collected and stored at -70^{o}C until used.

Spleen Colony-Forming Unit Assay

Exogenous spleen colony-forming units (CFU-s) were evaluated by the method of Till and McCulloch (30). Recipient mice were exposed to 9.0 Gy of total body irradiation in order to eradicate endogenous hemopoietic stem cells. Three to five hours later, 5 x 10^4 bone marrow or 5 x 10^5 spleen cells from normal or glucan-F-treated mice were intravenously injected into the irradiated recipients. Twelve days after transplantation, the recipients were euthanized by cervical dislocation and their spleens removed. The spleens were fixed in Bouin's solution, and the number of grossly visible spleen colonies were counted. In some experiments, the irradiated recipient mice were injected with graduated numbers of normal bone marrow cells (5 x 10^2 - 5 x 10^4/mouse) and then 1 hour later were also intravenously injected with either 5.0 mg of glucan-F or an equivalent volume of sterile saline. Twelve days later these mice were also euthanized by

cervical dislocation their spleens removed, fixed in Bouin's solution and the number of spleen colonies counted.

Granulocyte-Macrophage Colony-Forming Cell Assay.

Committed granulocyte-macrophage hemopoietic progenitor cells (GM-CFC) were assayed by a modification (8) of the semi-solid agar technique originally described by Bradley and Metcalf (31) and Pluznik and Sachs (32). The upper agar-medium mixture for cell suspensions consisted of equal volumes of 0.66% agar and double-strength supplemented CMRL #1066 medium. The CMRL #1066 was supplemented with final concentrations of 10% HIFBS, 5% trypticase soy broth, 5% heat-inactivated horse serum, antibiotics, and L-asparagine (30 ug/ml). The agar-medium mixture for the lower feeder layer consisted of equal volumes of 1.0% agar and supplemented double-strength CMRL #1066. Both pregnant mouse uterine extract (PMUE) (2.5% v/v) and mouse L-cell-conditioned medium (LCM) (13% v/v) were added to each 1-ml feeder layer as sources of colony-stimulating actiity (CSA). Colonies (>50 cells) were counted after 10 days of incubation in a 37^{o}C humidified environment containing 7.5% Co_2.

Granulocyte-Macrophage Colony Stimulating Activity Assay.

Serum levels of granulocyte-macrophage colony stimulating activity (CSA) in normal and in glucan-F-treated mice were determined by incorporating 0.1 ml of 1:2 or 1:4 diluted serum instead of PMUE and LCM into the lower agar feeder layers in the GM-CFC assay. Normal mouse bone marrow cells were then plated in the upper agar layer. Cultures were incubated and GM-CFC colonies were scored as described above.

Erythroid Colony-Forming-Unit Assay

Bone marrow and splenic erythroid colony forming units (CFU-e) were assayed by a modification of the original plasma

clot technique described by Stephenson et al. (33). Each ingredient was either reconstituted or diluted with supplemented alpha medium (SAM) (34). Briefly, to make 1 ml of the plasma clot suspension, the following were mixed: 0.1 ml cells (5×10^5 nucleated cells), 0.3 ml HIFBS, 0.1 ml 25% beef embryo extract, 0.1 ml 10% bovine serum albumin, 0.1 ml (0.02 mg) L-asparagine, 0.1 ml 10^{-3} M 2-mercaptoethanol, 0.1 ml erythropoietin (Ep), and 0.1 ml of 37°C bovine citrated plasma. Immediately, 0.1 of the mixture was pipetted into each of six microtiter wells. Step III anemic sheep plasma (Connaught Labs, Inc., Swiftwater, PA) was used as the source of Ep. Bone marrow and splenic CFU-e clot suspensions contained 0.25 and 0.5 units of Ep per ml, respectively. Control clots contained SAM in place of Ep. After incubation at 37°C in a humidified atmosphere containing 5% CO_2 in air for 2 days, plasma clots were harvested, fixed with 5% gluteraldehyde, and stained with benzidine and giemsa (35). A CFU-e was defined as an individual aggregate of eight or more benzidine-positive cells.

Statistics

For each data point, results are reported as the arithmetic mean $\pm$ 1 standard error of data pooled from multiple individual experiments (see figure legends). The student's t-test was used to calculate p values. Values of $p \leq .05$ were considered significant and are indicated by asterisks in the figures.

RESULTS

Effects of Glucan-F on Peripheral Blood Cellularity

Mice were injected with either glucan-F or sterile saline and 3 hours, 1, 5, 11, 15, 21 and 28 days later peripheral white blood cellularity and hematocrit values determined (Figure 1). The white cell count in glucan-F-treated mice decreased as early

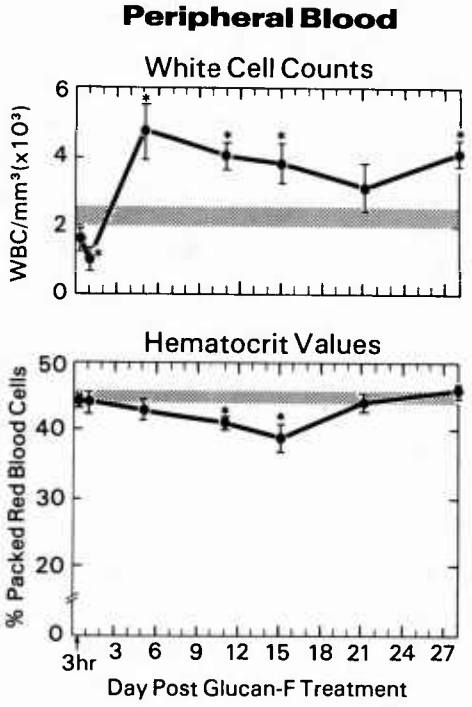

FIGURE 1

Temporal effects of glucan-F on peripheral blood white cell counts and hematocrit values. Each glucan-F value represents the mean $\pm$ SE from values obtained from nine individual mice. Since normal control values did not significantly differ over the 28 day period examined, all normal values were pooled and are represented by the shaded areas on the graphs. Asterisks indicate $p \leq 0.05$.

as 3 hours post injection and continued to decrease to approximately one half that of normal control mice by one day post injection. This decrease was followed by a significant increase in white cell numbers which peaked at 214% of normal control values on day 5 post injection then gradually returned to near normal control values by 21 days post injection. However, a

second increase in white cell numbers occurred at day 28 post injection (186% of normal control values). In contrast to white blood cellularity, red blood cellularity in glucan-F treated mice (as measured by hematocrit values) never rose above that of normal control mice. In fact on days 11 and 15 post glucan-F-treatment a significant decrease in hematocrit values was observed.

Effects of Glucan-F on Bone Marrow and Splenic Cellularity

Changes in bone marrow and splenic cellularity at 1,5,11,15 and 21 days after glucan-F injection are illustrated in Figure 2. Bone marrow cellularity decreased slightly on day 1 post glucan-F injection, then gradually increased and was significantly greater than control values by day 21 post injection. Splenic cellularity also gradually increased throughout the 21 day observation period post glucan-F injection.

Effects of Glucan-F on Pluripotent Hemopoietic Stem Cells (CFU-s)

Bone marrow and splenic content of pluripotent stem cells was also measured at 1,5,11,15 and 21 days after glucan-F administration (Figure 3). Although a slight increase in bone marrow CFU-s numbers was observed 11 days post glucan-F treatment, this increase was not statistically elevated above normal control values. By contrast, splenic CFU-s numbers were significantly increased above normal control values from days 5-21 post glucan-F administration.

Effects of Glucan-F on Granulocyte-Macrophage Progenitor Cells GM-CFC)

Bone marrow GM-CFC numbers dropped significantly one day post glucan-F injection, then increased and significantly exceeded normal control values by 21 days post treatment (131% of normal control values) (Figure 4). Splenic GM-CFC numbers were

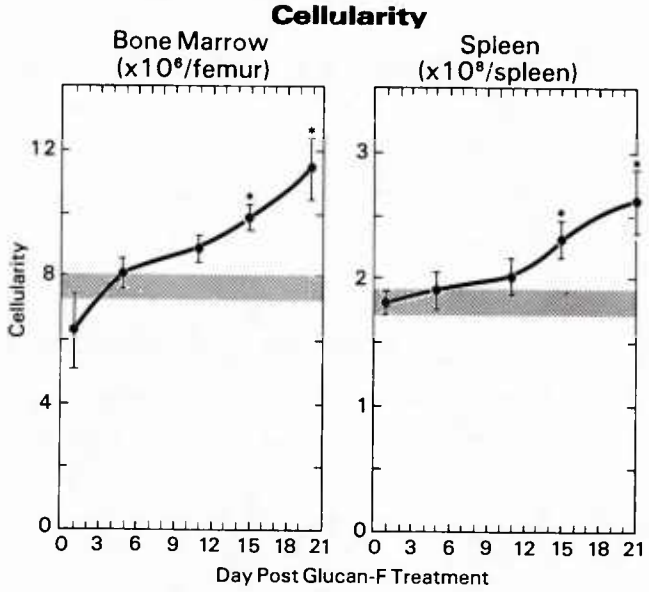

FIGURES 2,3,4, & 6

Temporal effects of glucan-F on bone marrow and splenic cellularity (2), CFU-S (3), GM-CFC(4) and CFU-e (6). Each glucan-F value represents the mean ± SE from values obtained form six individual experiments. Since normal control values did not significantly differ over the 21 day period examined, these values were pooled and are represented by the shaded areas in the graphs. Asterisks indicate $p \leq 0.05$.

not altered on day 1 post glucan-F injection, however, were significantly increased above control values on days 5,11,15 and 21 post treatment (respectively, 414%, 466%, 451% and 392% of normal control values).

Effects of Glucan-F on Granulocyte-Macrophage Colony Stimulating Activity (CSA)

Serum levels of CSA were most elevated 3 hours after

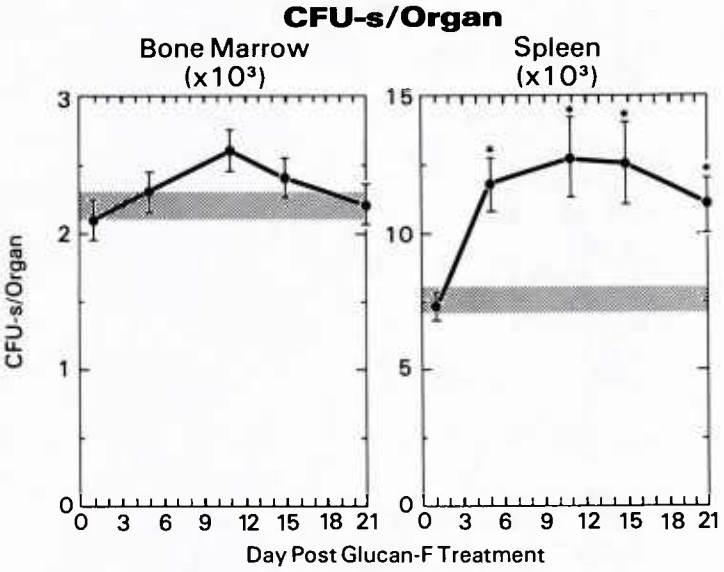

FIGURE 3

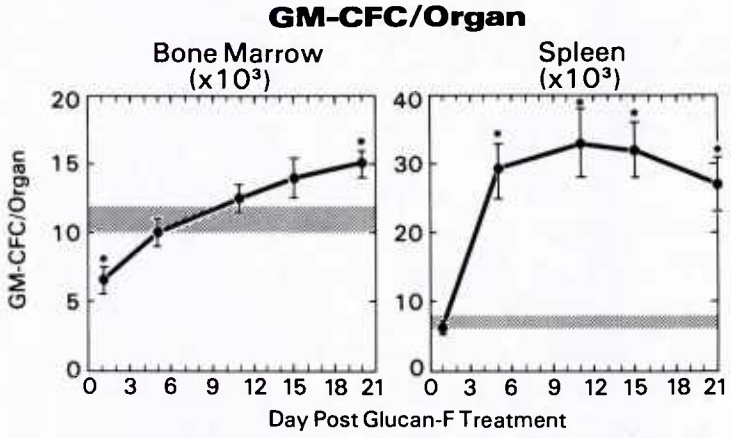

FIGURE 4

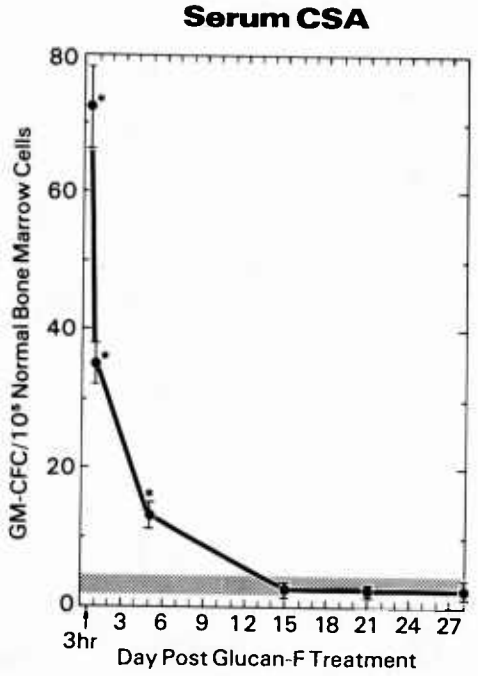

FIGURE 5

Temporal effects of glucan-F on serum CSA levels. Each glucan-F value represents the mean $\pm$ SE of values obtained from 3 individual experiments. Since normal control values did not significantly differ of the 28 day period examined, these values were pooled and are represented by the shaded area in the graph. Asterisks indicate $p \leq 0.05$.

glucan-F administration (Figure 5). At this time, approximately a 2000% increase over normal mouse serum CSA levels was observed. Within 24 hours post glucan-F treatment, serum CSA levels decreased to 1100% of normal control CSA values. This decline continued and by day 15 post injection, serum CSA in glucan-F-treated mice did not differ from that in normal control mice.

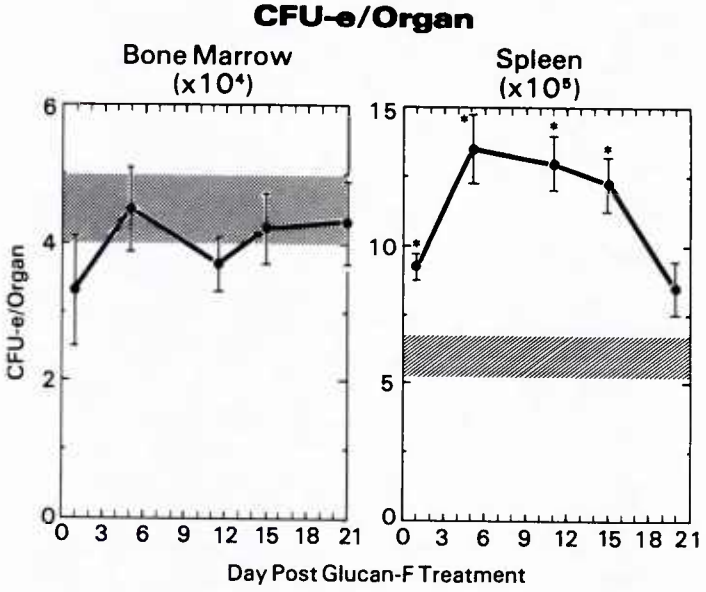

FIGURE 6

Effects of Glucan-F on Erythropoiesis (CFU-e)

Bone marrow CFU-e numbers decreased slightly 1 day after glucan-F administration then rose and fluctuated within the normal CFU-e control range throughout the duration of these experiments (Figure 6). By contrast, on days 1,5,11, and 15 post glucan-F injection splenic CFU-e numbers were significantly elevated above normal control values.

Effects of Glucan-F on Pluripotent Stem Cell Proliferation when Administered after Bone Marrow Transplantation

Figure 7 illustrates that at each cell dose examined, post-transplantation glucan-F-treatment significantly increased CFU-s numbers.

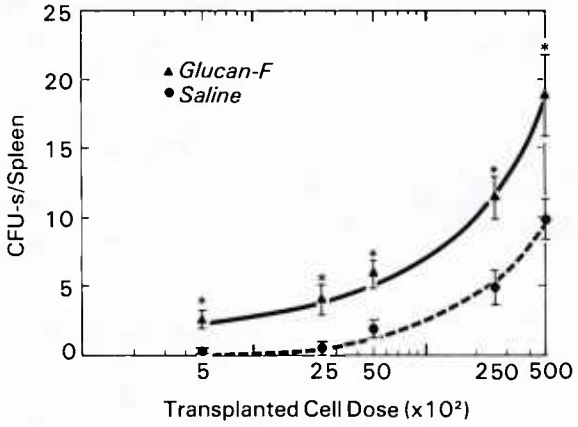

FIGURE 7

Effects of glucan-F on CFU-s numbers when administered one hour after bone marrow transplantation. Each data point represents the mean ± SE of values obtained from 15 individual mice. Asterisks indicate $p \leq 0.05$.

DISCUSSION

These results clearly indicate that glucan-F is capable of modulating hemopoiesis in normal mice. Bone marrow and splenic cellularity and GM-CFC content, as well as splenic CFU-s and CFU-e content, all significantly increased following glucan-F administration. In general, splenic responses were significantly greater and of longer duration than bone marrow responses. These results are consistent with those observed after the administration of particulate glucan preparations (i.e., glucan-P) (16,18,27). However, a "potency" difference does exist between glucan-F and glucan-P. A 5.0 mg dose of glucan-F is needed to produce hemopoietic effects similar to those produced by only a 1.5 mg dose of glucan-P. In addition, the time of onset and duration of the responses induced by 5.0 mg of glucan-F

slightly differ from those induced by 1.5 mg of glucan-P in that they occur slightly later and are of longer duration. The exact reason for the differences observed between glucan-F and glucan-P dosages are not known at this time. However, since glucan-F is soluble, and has a smaller molecular weight than glucan-P, it is possible that glucan-F may simply be more rapidly cleared and excreted from the body and thus a larger dose is required to produce hemopoietic effects.

In spite of these minor differences, in normal mice hemopoietic stimulation can be induced by either glucan-P or glucan-F. In irradiated mice, however, glucan-F produced effects quite different from those produced by glucan-P. Our current studies clearly indicated that when administered after bone marrow transplantation, glucan-F could significantly enhance CFU-s numbers and that this phenomenon was evident at every cell dose tested. We have previously conducted similar studies with glucan-P. In marked contrast, when glucan-P was administered post bone marrow transplantation, it caused the recipient mice to die earlier than the radiation control mice (i.e. mice which were simply irradiated and not transplanted with bone marrow cells). The differences produced by glucan-P and glucan-F when injected after bone marrow transplantation are probably not due to a difference in the hemopoietic effects induced by the two glucan preparations, but rather due to reactions triggered when these substances are injected into lethally irradiated mice. This is suggested by the fact that even when animals are simply given 9.0 Gy of ^{60}Co, (i.e. are <u>not</u> transplanted with bone marrow cells) and are subsequently injected with glucan-F or glucan-P one hour after irradiation, glucan-F treated mice survive at least as long as radiation controls, while glucan-P treated mice die significantly earlier than radiation controls (36). The exact mechanisms by which glucan-F and glucan-P produce these results when administered post irradiation are currently being pursued in

our laboratories. However, the fact that glucan-F can very effectively enhance CFU-s proliferation when administered post bone marrow transplantation suggests that glucan-F may be useful for enhancing engraftment of autologous bone marrow transplants - especially when only low numbers of cells are available for transplantation.

Although our studies have primarily been concerned with glucan's hemopoietic effects, glucan is probably better known for its ability to non specifically modify an extensive array of bacterial viral, fungal, and parasitic infections as well as neoplastic states (for review see 13). Glucan-F maintains the reticuloendothelial, immunologic and hemopoietic enhancing capabilities of glucan-P and in addition, does not produce undesirable side effects, such as sever hepatosplenomegaly and granuloma formation (37). In particular glucan-F appears to be an intriguing immunopharmacological agent which may be capable of not only enhancing hemopoietic recovery, but also capable of combating septicemia which is often associated with chemotherapy, radiotherapy, and bone marrow transplantation.

ACKNOWLEDGEMENTS

The authors would like to acknowledge the excellent technical assistance of Brenda Watkins-Bell, James Atkinson and Brian Solberg. The excellent editorial and typing skills of Junith Van Deusen and Gloria Contreras also greatly contributed to the completion of this manuscript.

Supported by Armed Forces Radiobiology Research Institute, Defense Nuclear Agency, under Research Work Unit MJ 00132. The views presented in this paper are those of the authors; no endorsement by the Defense Nuclear Agency has been given or should be inferred.

REFERENCES

1. Williams, W.; Beutler, E.; Erslev, A.; Rundles, W., Hematology, McGraw-Hill Book Co, New York, 1972.

2. Robbins, S.; Angell, M., Basic Pathology W. B. Saunders Co, Philadelphia, 1976.

3. Benacerraf, B., Influence of irradiation and resistance to infection, Bact. Rev., 24:35-40, 1960.

4. Talmage, D.W., Effect of Ionizing Radiation or resistance and infection, Ann. Rev. Microbiol., 9:335-346, 1955.

5. Fisher, B.; Taylor, S.; Levine, M.; Saffer, E.; Fisher, E., Effect of Mycobacterium bovis (Strain Bacillus Calmette Guerin) on macrophage production by the bone marrow of tumor bearing mice, Cancer Res., 34:1668-1670, 1974.

6. Dimitrov, N.; Andre, S.; Eliopoulos, Y.; Halpern, B., Effect of Corynebacterium parvum on bone marrow cell cultures, Pro. Soc. Exp. Biol. Med., 148:440-442, 1975.

7. Foster, R.; MacPherson, B.; Brodie, D., Effect of Corynebacterium parvum on colony-stimulating factor and granulocyte-macrophage colony formation, Cancer Res., 37:1349-1355, 1977.

8. MacVittie, T.J. Alternations induced in macrophage and granulocyte-macrophage colony forming cells by a single injection of mice with Corynebacterium parvum, J. Reticuloendothel. Soc., 26:479-490, 1979.

9. MacVittie, T.J., in Experimental Hematology Today, edited by S. J. Baum and G.D. Ledney, p. 3, Karger, New York, 1979.

10. Mansell, P.; Klementz, E., Reaction to BCG, J. Am. Med. Assoc., 226:1570-1571, 1973.

11. Scott, M., Corynebacterium parvum as a therapeutic antitumor agent in mice. I. Systemic effects of intravenous injection, J. Natl. Cancer Inst. 53:855-860, 1974.

12. Sparks, F.; Silverstein, M.; Hunt, J.; Haskell, C.; Pilch, Y.; Morton, D., Complications of BCG immunotherapy in patients with cancer, New Eng. J. Med. 289:827-830, 1973.

13. DiLuzio, N.R., Immunopharmacology of glucan. A broad spectrum enhancer of host defense mechanisms, Trends in Pharmaceutical Sci., 4:344-347, 1983.

14. Patchen, M.L., Immunomodulators and Hemopoiesis, Surv. Immunol. Res., 2:237-242, 1983.

15. Patchen, M.L.; Lotzova, E., Modulation of Murine Hemopoiesis by glucan, Exp. Hematol., 8:409-422, 1980.

16. Patchen, M.L.; MacVittie, T.J., Dose-dependent responses of murine pluripotent stem cells and myeloid and erythroid progenitor cells following administration of the immunomodulating agent glucan, Immunopharmacol., 5:303-313, 1983.

17. Burgaleta, C.; Golde, D.W., Increased granulopoiesis and macrophage genesis in mice, Cancer Res., 37:1739-1742, 1979.

18. Patchen, M.L.; MacVittie, T.J., Temporal response of murine pluripotent stem cells and myeloid and erythroid progenitor cells to low-dose glucan treatment, Acta. Haemol., 70:281-288, 1983.

19. Liu, P.; Poon, K.; Liu, S., In vitro effect of glucan on mouse hemopoietic committed progenitor cells, Life Sci., 29:1027-1032, 1981.

20. Niskanen, E.; Burgaleta, C.; Cline, M.; Golde, D., Effect of glucan, a macrophage activator on murine hemopoietic cell proliferation in diffusion chambers, Cancer Res., 38:1406-1409, 1978.

21. Deimann, W.; Fahimi, H., Induction of focal hemopoiesis in adult rat liver by glucan, a macrophage activator, Lab. Invest., 42:217-224, 1980.

22. Patchen, M.L.; MacVittie, T.J., Use of glucan to enhance hemopoietic recovery after exposure to cobalt-60 irradiation, Adv. Exp. Med. Biol., 155:267-272, 1982.

23. Popisil, M.; Jary, J.; Netikova, J.; Marek, M., Glucan-induced enhancement of hemopoietic recovery in gamma-irradiated mice, Experientia, 38:1232-1234, 1982.

24. Patchen, M.L.; MacVittie, T.J;; Wathen, L.K., Effects of pre- and post irradiation glucan treatment on pluripotent stem cells, granulocyte, macrophage and erythroid progenitor cells and hemopoietic stromal cells, Experientia, 40:1240-1244, 1984.

25. Patchen, M.L.; DiLuzio, N.R.; Jacques, P.; MacVittie, T.J., Soluble polyglycans enhance recovery from cobalt-60 induced hemopoietic injury, J. Biological Response Modifiers, 3:627-633, 1984.

26. Patchen, M.L.; MacVittie, T.J., Stimulated hemopoieses and enhanced survival following glucan treatment in sublethally and lethally irradiated mice, Int. J. Immunopharmacol., in press.

27. Patchen, M.L.; Lotzova, E., The role of macrophages and T-lymphocytes in glucan-mediated alteration of murine hemopoieses, Biomed., 34:71-77, 1981.

28. DiLuzio, N.R.; Williams, D.L.; McNamee, R.B.; Edwards, B.F.; Kilahama, A., Comparative tumor-inhibitory and antibacterial activity of a soluble and particulate glucan, Int. J. Cancer, 24:773-779, 1979.

29. DiLuzio, N.R.; Chihara, G., in Advances in Immunopharmacology, edited by J.W. Hadden, L. Chedid, P. Dukor, F. Spreafico, and D. Willoughby, p. 799, Pergamon Press, New York, 1983.

30. Till, J.E.; McCulloch, E.A., A direct measurement of radiation sensitivity of normal bone marrow cells, Radiat. Res., 14:213-222, 1961.

31. Bradley, T.R.; Metcalf, D., The growth of mouse bone marrow cells in vitro, Aust. J. Exp. Med. Sci., 448:287-300, 1966.

32. Pluznik, D.H.; Sachs, L., The cloning of normal "mast" cells in tissue culture, J. Cell Physiol., 66:219-324, 1965.

33. Stephenson, J.R.; Axelrad, A.A.; McLeod, D.L.; Shreeve, M.M., Induction of colonies of hemoglobin-synthesizing cells by erythropoietin in vitro, Proc. Natl. Acad. Sci. USA, 68:1542-1546, 1971.

34. Weinberg, S.R.; McCarthy, E.G.; MacVittie, T.J.; Baum, S.J., Effect of Low dose irradiation on pregnant mouse hemopoiesis, Br. J. Haematol., 48:127-132, 1981.

35. McLeod, D.L.; Shreeve, M.M.; Axelrad, A.N., in In Vitro Aspects of Erythropoiesis, edited by M.J. Murphy, p. 31, Spring-Verlag, New York, 1979.

36. Patchen, M.L.; MacVittie, T.J., Comparative effects of soluble and particulate glucans on survival in irradiated mice, J. Biol. Resp. Modifiers, in press.

37. DiLuzio, N.R.; Jacques, P., Glucans as immunomodulators Adv. in Immunopharmacol., in press.

Electrophysiological Techniques in Pharmacology, pages 91–102
Published 1986 by Alan R. Liss, Inc.

Single-Electrode Voltage Clamp in Mammalian Electrophysiology

TERRY PELLMAR

INTRODUCTION

Voltage clamping is a very important technique in neurophysiology. It provides a direct method of studying both intrinsic membrane currents and transmitter- or drug-induced currents. Until recently, many cells were unavailable for voltage clamping because their small size prevented inpalement with two electrodes. A single-electrode circuit (SEC) was developed by W.A. Wilson [Wilson and Goldner, 1975] to provide a means of voltage clamping with only one electrode. Dunn and Wilson [1977] demonstrated that the SEC could be used to voltage clamp cat spinal motononeurons in vivo. With the advent of a commercially available SEC (Dagan 8100, Axoclamp 2), a number of laboratories have applied this technique to their preparations [Brown and Griffith, 1983a,b; Constanti and Galvan, 1983; Gallin, 1981; Gustafsson et al., 1982; Halliwell and Adams, 1982; Johnston et al., 1980; Pellmar, 1986]. Two methods are currently popular for voltage clamping small cells. The patch-clamp technique [Barros et al; this volume] has proved especially suitable for cells in tissue culture, where the cell membrane is directly accessible to the electrode tip. The method I describe is suitable for all cells that can be impaled, either in vivo or in vitro.

Much information can be obtained about the electrophysiological and pharmacological properties of neurons simply by recording changes in membrane potential. The voltage clamp provides the added ability to control voltage and to monitor membrane current. The real power of the voltage clamp lies in the study of voltage-dependent and time-dependent conductances. When voltage is free to vary, the opening of voltage-dependent channels will cause current to flow across the membrane, resulting in a change in membrane potential. The potential change can result in further opening, or perhaps closing, of the channels involved. The voltage measurement, therefore, reflects a complex combination of events. In

From the Physiology Department, Armed Forces Radiobiology Research Institute, Bethesda, Maryland 20814.

contrast, eliciting a voltage-dependent conductance under voltage clamp conditions, where membrane potential is not allowed to change, the current flowing across the membrane can be directly measured. The time course and the potential-dependence of the current can be easily evaluated. This simplifies analysis of pharmacological agents on the various membrane currents.

THE VOLTAGE CLAMP

A voltage clamp uses a feedback circuit to compare the actual potential of the cell to a commanded holding potential. Current is injected to compensate for any offset, including spontaneous events that would otherwise shift membrane potential. The injected current, equal and opposite to that flowing across the cell membrane, is monitored. From holding potential, voltage commands to other membrane potentials can be applied. The currents required to produce and sustain the voltage step are recorded; they reflect the various currents present in the cell.

Space Clamp Considerations

Because of the complex microanatomy of most neurons in the central nervous system, electrophysiological recordings reflect primarily electrically local events. Electrical signals gradually decay with distance from the site of initiation. Whether one attempts to voltage clamp or just to record membrane potential, synaptic responses originating on a distant dendritic spine will be attenuated at the cell body. When current is being injected to depolarize or hyperpolarize membrane potential, the cell will not be isopotential; the shift in membrane voltage will decline with distance from the electrode. These problems are present with or without voltage clamping and with both one- and two-electrode clamp systems.

With voltage clamping, it is important to keep in mind that remote sites will not see the full extent of a voltage command and cannot be adequately clamped to prevent spontaneous fluctuations in potential. Events initiating in the remote regions will not be under good voltage control and will not be accurately represented by recordings in the soma. For a further discussion of the consequences of inadequate space clamp, the reader is referred to Johnston and Brown [1983].

Switching Circuit

The single-electrode circuit requires that one electrode both record potential and pass current. This is accomplished through a switching circuit that alternates between a current-injecting mode and a voltage-recording mode. The percentage of time spent injecting current is called the "duty cycle." Near the end of the

current-injecting period, the "sample and hold" circuit samples the current. This value is provided to the continuous current output until the next sample is taken. Similarly, the voltage is sampled at the end of each voltage-recording period.

The rate at which the clamp alternates between the two modes is called the "switching frequency." The clamp relies on the RC time constant of the cell (membrane resistance, R × membrane capacitance, C) to smooth out the injected square waves of current and to provide essentially a steady DC current across the cell membrane. If the switching frequency is much slower than the time constant of the cell membrane, the injected current will have a substantial AC component. To minimize the AC component, the switching cycle should be as fast as possible. Faster switching frequencies also improve the time resolution of recordings. Electrophysiological events with high-frequency components can be faithfully reproduced only if the switching frequency is substantially higher. For example if the switching frequency is set at 5 kHz, voltage is sampled only once every 0.2 ms. Ten sample points will be taken during a 2-ms event. An event faster than this will not be accurately represented.

If the headstage output and the unsampled current are directly monitored, one can observe the consequences of switching. In Figure 1, the top trace is the unsampled current. For 50% of the time, no current is injected through the electrode; the rest of the time, hyperpolarizing current flows. The lower trace is the headstage output. When no current is passed, the electrode records zero

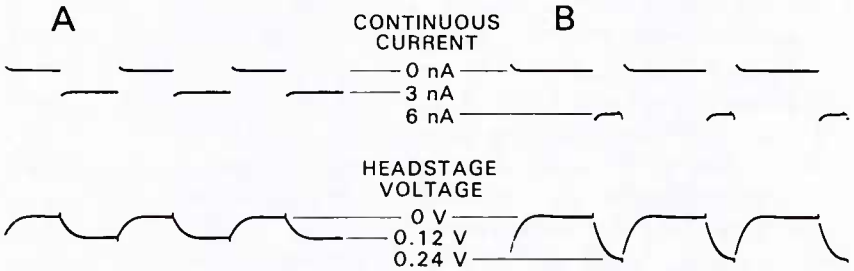

Fig. 1. Effect of duty cycle on continuous current and headstage output of single-electrode voltage clamp. Top traces are oscilloscope tracings (sweep speed 0.1 ms/div) of continuous current. Bottom traces are unsampled headstage output. (A) Using 50% duty cycle, 3 nA are injected through the electrode to pass an average of 1.5 nA of current. A voltage deflection across the electrode resistance results in a square wave on the headstage output. The ratio of the voltage change to the current injected provides a measure of the electrode resistance, in this case 40 Mohms. (B) Using a 25% duty cycle, 6 nA must be passed to provide an average current of 1.5 nA. Similarly, the deflection of headstage voltage is increased due to the electrode resistance. A 25% duty cycle provides a longer voltage recording period, allowing more time for voltage to reach a steady state level before a sample is taken. Switching frequency is 3 kHz.

voltage; when current is injected, a voltage drop occurs across the electrode resistance. In Figure 1B, the duty cycle was changed to 25%. To inject the same amount of net current, the electrode must carry twice as much current for half the time.

Notice that the voltage does not return to baseline level instantaneously. A capacitance is associated with the electrode that requires charging and discharging. The voltage must return to baseline levels before the beginning of the next current injection, or incorrect voltage levels will be sampled. A 25% duty cycle allows 75% of the switching period for voltage levels to return.

Under some experimental conditions, the time constant associated with the electrode and wiring is large enough to prevent complete decay of the electrode voltage. Efforts should be made to minimize capacitance of the recording system. Although the capacitance feedback control of the amplifier can compensate for some capacitance of the system, it has limitations. Microelectrodes are frequently associated with several time constants, some of which can be slow and unresponsive to capacitance compensation. In addition, increasing capacitance feedback can accentuate high-frequency noise. It is preferable to minimize capacitance rather than compensate for it.

Once the duty cycle and switching frequency are set, the capacitance feedback should be adjusted to compensate for system capacitance. This procedure should cause the headstage output waveform to become more square. As shown in Figure 2, if the capacitance feedback is set too low, the voltage may never reach a plateau during the voltage-recording mode (trace 3). If it is set too high, oscillations can occur (trace 4). In either case, the voltage reading at the end of the voltage-recording period is erroneous. Again, it is important to set the capacitance compensation to a level that allows the voltage (which developed across the electrode while passing current) to decay completely.

Most commonly the cause of incomplete return of voltage during the duty cycle is the large time constant associated with the high resistance electrodes that are often necessary for impalement of small cells. In this situation, voltage clamping may be possible only if the switching frequency is low, to allow more time for the voltage to return to its steady-state level. But it is necessary to remember that switching frequency must be much faster than the time constant of the cell and that a reduced frequency limits the time response of the clamp, allowing only slower events to be accurately controlled.

Using the SEC

An electrode used with the single-electrode circuit must be tested for its ability to pass current. With the electrode in the extracellular solution, the offset voltage should be adjusted to ground level. Under these conditions, injecting current

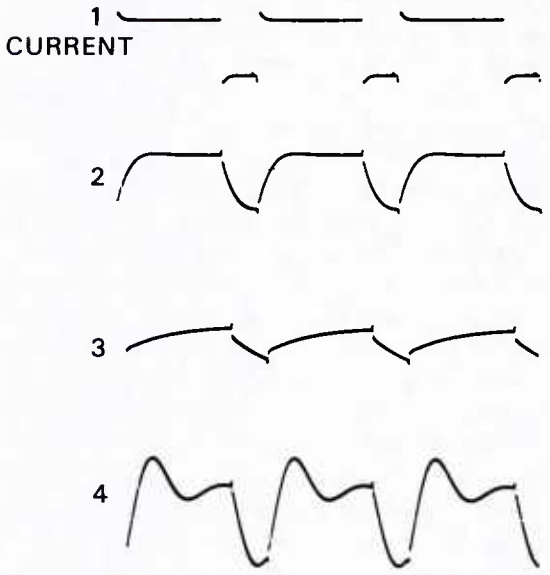

Fig. 2. Effect of adjusting capacitance feedback. Appearance of the headstage output provides important information on the electrode. All traces are from same electrode. Trace 1, continuous current record. Trace 2, headstage voltage with capacitance feedback properly adjusted. Trace 3, headstage voltage with undercompensation of capacitance. Trace 4, headstage voltage with overcompensation of capacitance. Only in trace 2 does the voltage reach a steady-state level during the voltage-recording period. Switching frequency is 3 hKz.

should not alter the sampled voltage. An electrode must be tested with at least as much current (both hyperpolarizing and depolarizing) for at least as long a duration as will be required during the course of an experiment. Ideally the sampled voltage will not change at all. Practically though, there usually is at least a small deviation from recorded ground, especially with larger currents. This reflects rectification of the electrode. Electrodes filled with KCl appear to work best. It should be noted that rectification problems can occur in the ground return of the system. Rectification problems can often be corrected by replacing the electrode or the KCl/agar bridge used to reference the bathing solution to ground potential. Ensuring well-chlorided silver wires in the electrode and the ground return also can improve current-passing capabilities. Experimental requirements determine the tolerance limits for rectification.

During the course of an experiment, the electrode may change some of its characteristics. These changes are revealed in the headstage output and continuous current traces. For this reason, it is quite useful to keep an eye on these

traces throughout an experiment. Usually after impaling a cell, the electrode increases in both resistance and capacitance. Capacitance feedback again requires adjustment to allow the headstage potential to reach a steady state during the voltage-recording period. The process of adjustment is continuous. Capacitance can change with varying fluid levels, for example, and may require readjustment to allow continued accurate monitoring of membrane voltage.

When the voltage clamp is turned on, the injected current begins to fluctuate, and the headstage output begins to look somewhat unstable (Fig. 3). The higher the gain of the clamp, the more accurately the membrane voltage will follow a voltage command. It should be noted that changing the gain on the voltage clamp can alter quantitative data. At lower clamp gains, membrane potential will not follow exactly the voltage command. A voltage command to a particular membrane potential may not agree with the voltage actually realized. For example, a hyperpolarizing command of 40 mV may actually elicit a hyperpolarization of only 37 mV. For this reason it is important to monitor the actual membrane potential and not just the command potential. In addition, a voltage command that evokes large transient currents may not result in constant membrane potential throughout the step. If a transient outward current is evoked, for instance, the potential realized early in a depolarizing step may be less positive than that realized later in the step.

ANALYSIS OF CURRENTS IN MAMMALIAN NEURONS

Voltage clamp techniques can provide information on how pharmacological agents alter membrane currents. This approach requires a knowledge of the

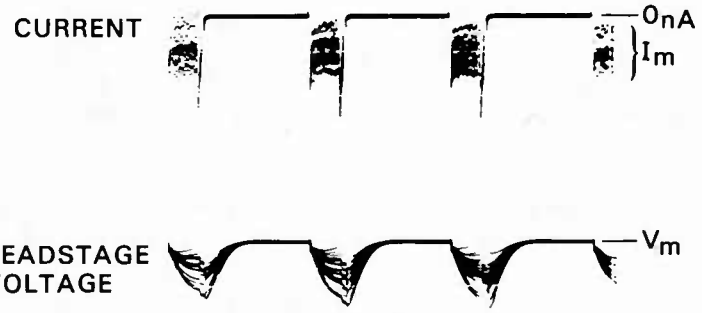

Fig. 3. Continuous current and headstage voltage while voltage clamping. The variability of the continuous records during the current-passing phase increases with increasing the clamp gain. The current injected is sampled and provides the membrane current trace. At the end of the voltage-recording period the headstage voltage will be the membrane potential. Switching frequency is 3 kHz.

intrinsic membrane currents in the neurons of interest. As an example of the kinds of currents that can be encountered in mammalian cells and the kinds of manipulations used to study them, hippocampal pyramidal cells and the actions of histamine will be discussed [Pellmar, 1986]. A brain slice preparation is ideal for these studies, since it allows control of the extracellular environmemt. Drugs can be applied at known concentrations, and the ionic composition of the bathing solution can be manipulated. Because the switching circuitry of the single-electrode voltage clamp is not fast enough to resolve the currents underlying the action potential, tetrodotoxin (TTX) is usually present in these experiments to eliminate contamination of current records by unclamped spikes.

Potassium Currents

The most dominant outward current in hippocampal pyramidal cells is the calcium-mediated potassium current (C-current) [Brown and Griffith, 1983a]. In the hippocampal pyramidal cell illustrated in Figure 4, membrane potential was voltage clamped to a holding potential of −40 mV, and 500 ms voltage commands to various membrane potentials were applied. The current required to produce the voltage steps was plotted against the membrane potential attained to construct a current–voltage (I–V) curve. Because of the presence of C-current, the I–V curve is not linear; there is rectification in the outward direction at depolarized potentials. If calcium is removed from the bathing solution, or the calcium channel blocker manganese is added to the solution, much of this outward rectification is eliminated. C-current turns on slowly, reaching a maximum about 2 seconds after the depolarizing step [Brown and Griffith, 1983a]. When the voltage step is terminated, the current does not immediately return to its previous level. There is a slowly decaying outward current that reflects the turning off of the potassium channels opened during the depolarization. This residual outward current is called a tail current. Analysis of the amplitude and kinetics of the tail currents can provide further information about the channel involved [for example, see Brown and Griffith, 1983a]. As can be seen in Figure 4, application of histamine reduced the outward current in the region of the I–V curve where C-current predominates. A pharmacological agent affecting this region of the I–V curve might be acting on C-current or perhaps one of the other outward currents such as the delayed rectifier (not described here).

Hippocampal pyramidal cells also show a transient outward current called the A-current [Gustafsson et al, 1982]. The A-current is very sensitive to holding potential. At potentials more positive than −55 mV, the A-current is completely inactivated; hyperpolarizing the cell increases the amplitude of this transient outward current. In Figure 5A, the A-currents at two different holding potentials are compared. Stepping to −40 mV from −80 mV produced a large A-current.

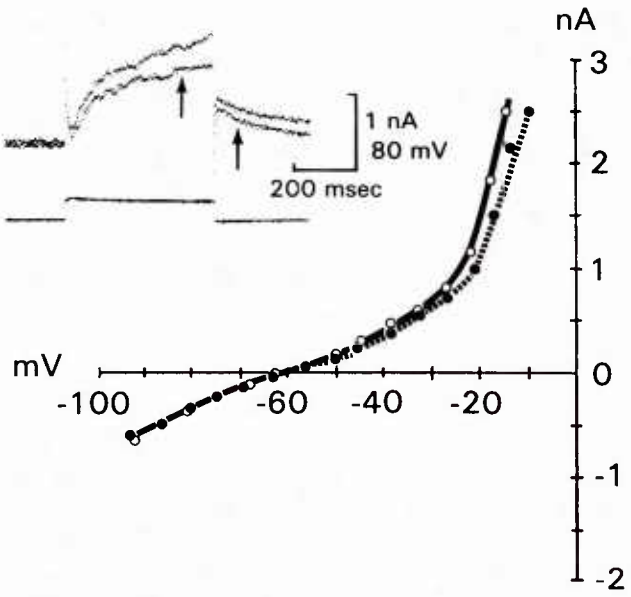

Fig. 4. Current-voltage relationship for hippocampal pyramidal cell. Membrane potential was held at −38 mV. Voltage was stepped for 500 ms to a variety of potentials. Current at the end of the step is plotted against potential. Histamine (1 μM) (filled circles) decreases the outward current at potentials positive to −50 mV. The inset shows a sample step from −38 mV to −17 mV. The outward current developed slowly during the step. An outward tail current was present after the voltage was returned to original holding potential. After 1 μM histamine (trace marked with arrows), the outward current was reduced. TTX (0.3 μM) was present to prevent sodium spikes.

As can be seen in Figure 5B, the amplitude of the A-current depends also on the size of the depolarizing step. With a holding potential of −76 mV, A-current begins to activate with steps to −60 mV and increases in amplitude with further depolarization. A-current is very sensitive to the blocking agent 4-aminopyridine (4-AP). Histamine, on the other hand, had no effect on A-current (Fig. 5B).

Another voltage-dependent potassium current observed in hippocampal pyramidal cells is M-current [Halliwell and Adams, 1982]. M-current is turned on at potentials positive to −45 mV. Small hyperpolarizing steps from a holding potential near −40 mV reveal a slow inward current resulting from the inactivation of this current at the more negative potential. The M-current is blocked by muscarinic agonists but not affected by histamine (Fig. 6).

Calcium Current

In the presence of blockers of the outward currents, a slow inward current is revealed in hippocampal pyramidal cells [Johnston et al, 1980; Brown and

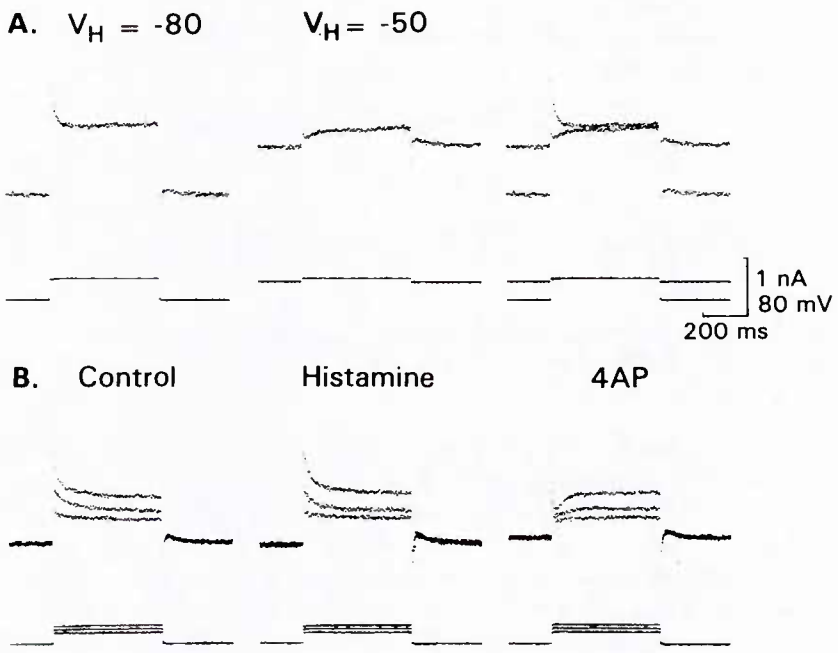

Fig. 5. A-current in hippocampal pyramidal cell. A) Fast transient outward current was present with holding potential of −80 mV, but it was inactivated with holding potential of −50 mV. B) Voltage steps of increasing amplitude show activation of A-current. Holding potential was −76 mV. Voltage steps go to −58 mV, −52 mV, and −46 mV. Histamine (10 μM) had no effect on A-current. 4-AP selectively blocked A-current. Calibration same as in A. Traces in A and B are from same cell. Experiment was done in manganese to eliminate C-current and calcium current. TTX (0.3 μM) was also present.

Griffith, 1983b]. A number of methods have been used to block potassium currents: high concentrations of tetraethylammonium (TEA), injections of cesium, and replacement of calcium with barium. Under these conditions, holding the membrane potential at −40 mV and stepping to depolarized potentials produces an inward current that is sustained for the duration of a 500 ms step (Fig. 7). The I–V curve constructed from these steps reveals a region with a negative slope. The negative slope region of the I–V curve and the inward currents are blocked by calcium blockers such as cadmium and manganese (Fig. 7).

CONCLUSIONS

The single-electrode voltage clamp has made voltage clamp techniques applicable to small central neurons. When applying this technique to neurons with a

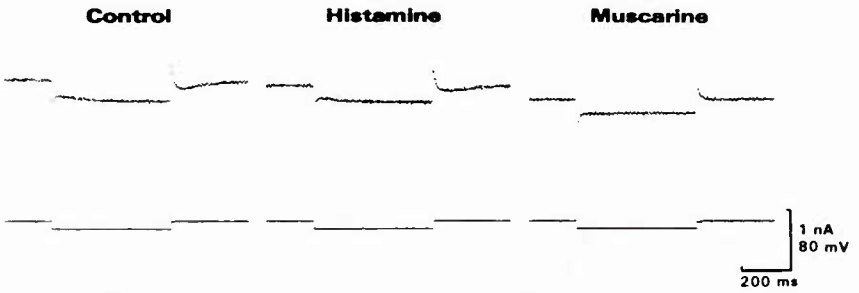

Fig. 6. M-current in hippocampal pyramidal cell elicited with 500 ms voltage step from −38 mV to −48 mV. TTX (0.3 μM) was present. Histamine (10 μM) had no effect on M-current, but muscarine (20 μM) blocked the current.

complex microanatomy, it is important to keep in mind that the cell will probably not be isopotential. Electrical events initiated at points remote from the recording site will not be well clamped. Active currents such as those underlying the sodium and calcium action potentials can invade the clamped region of the cell and appear in the current records. If an event of interest occurs in an electrically remote part of the cell, a true representation of the currents is not obtained.

With the SEC, good electrodes are crucial. They must be capable of passing adequate current without much rectification. The electrode capacitance must be sufficiently low to allow complete discharge during the voltage-recording period at the chosen switching frequency. The switching circuitry limits the time resolution of the SEC; it is much slower than a two-electrode system in following a voltage command. While a two-electrode system continually compares actual membrane voltage to the command voltage, the SEC can compare the two values only when a sample of potential is obtained, that is, once each cycle. Therefore, very fast currents are difficult, if not impossible, to follow. A faster switching frequency can improve clamp speed, but it requires electrodes with a very low time constant. Poor electrodes can sometimes be used at a slower switching frequency, but more high frequency response is lost.

Despite its limitations, the SEC is a powerful tool. The technique allows direct examination of membrane currents and characterization of their voltage-dependence and time dependence. With a knowledge of the currents present in the cells of interest, the actions of pharmacological agents and transmitter substances can be defined.

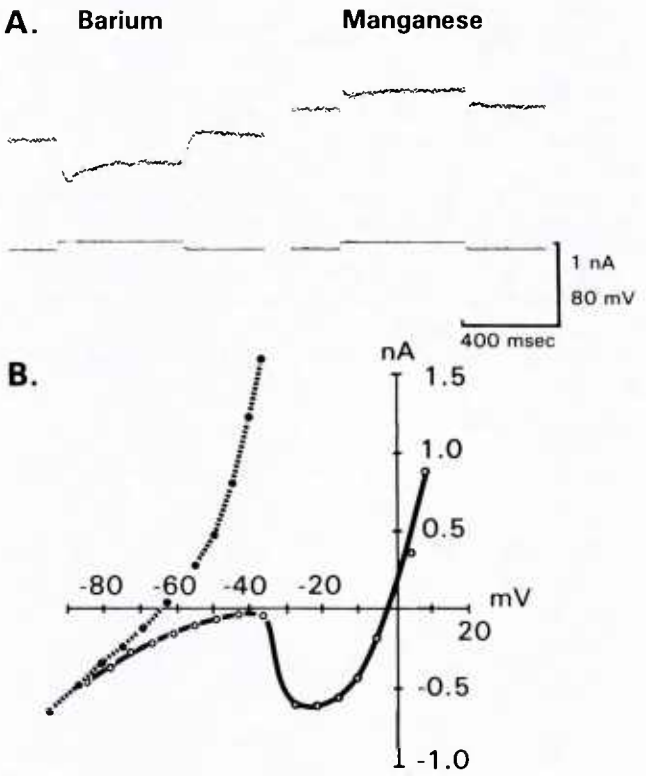

Fig. 7. Calcium inward current in hippocampal pyramidal cell. A) In the presence of barium (replacing calcium), a voltage step from −37 mV to −24 mV elicits an inward current sustained throughout the 500 ms command. When manganese replaced the divalent cation, the inward current was blocked. B) In barium, the I-V curve (open circles) shows a negative slope region due to the inward calcium current (same cell as A). In manganese, the negative slope region is absent (filled circles) (different cell than A). TTX (0.3 μM) was present in bathing solution.

REFERENCES

Brown DA, Griffith WH (1983a): Calcium-activated outward current in voltage-clamped hippocampal neurones of the guinea-pig. J Physiol (Lond) 337:287–301.

Brown DA, Griffith WH (1983b): Persistent slow inward calcium current in voltage-clamped hippocampal neurones of the guinea pig. J Physiol (Lond) 337:303–320.

Constanti A, Galvan M (1983): Fast inward rectifying current accounts for anomalous rectification in olfactory cortex neurones. J Physiol (Lond) 385:153–178.

Dunn PF, Wilson WA (1977): Development of the single microelectrode current and voltage clamp for central nervous system neurons. Electroenceph Clin Neurophysiol 43:752–756.

Gallin E (1981): Voltage clamp studies in macrophages from mouse spleen cultures. Science 214:458–460.

Gustafsson B, Galvan M, Grafe P, Wigstrom H (1982): A transient outward current in a mammalian central neurone blocked by 4-aminopyridine. Nature 229:252–254.

Halliwell JV, Adams PR (1982): Voltage-clamp analysis of muscarinic excitation in hippocampal neurons. Brain Res 250:71–92.

Johnston D, Brown TH (1982): Interpretation of voltage-clamp measurements in hippocampal neurons. J Neurophysiol 50:464–486.

Johnston D, Hablitz J, Wilson WA (1980): Voltage clamp discloses slow inward current in hippocampal burst firing neurones. Nature 286:391–393.

Pellmar TC (1986): Histamine decreases calcium-mediated potassium current in guinea pig hippocampal CA1 pyramidal cells. J Neurophysiol 55:727–738.

Wilson WA, Goldner MM (1975): Voltage clamping with a single microelectrode. J Neurobiol 6:411–422.

CELLULAR IMMUNOLOGY 98, 300–310 (1986)

II. Prostaglandin-Mediated Suppression of Delayed-Type Hypersensitivity to Infected Erythrocytes during *Babesia microti* Infection in Mice[1]

MARY J. RUEBUSH,* LINDA K. STEEL,† AND DEBBIE A. KENNEDY*

*Division of Tropical Public Health, Department of Preventive Medicine and Biometrics, Uniformed Services University of the Health Sciences, 4301 Jones Bridge Road, Bethesda, Maryland 20814-4799, and †Department of Biochemistry, Armed Forces Radiobiology Research Institute, Bethesda, Maryland 20814

Received May 24, 1985; accepted October 31, 1985

The mechanism of suppression of delayed-type hypersensitivity (DTH) to intraerythrocytic *Babesia microti* which occurs during infection in mice was examined. The suppression was not specific for anti-parasite DTH; infected mice immunized and challenged with sheep red blood cells had a similar depression of anti-sheep red blood cell DTH. Sublethal or lethal irradiation did not significantly alter the suppression of the DTH response, and cyclophosphamide pretreatment of infected mice also had no effect on suppression. Multiple passive transfer experiments using serum or regional lymph node cells from immunized or infected and immunized (suppressed) donor animals failed to demonstrate any ability to transfer suppression of DTH. Adherent cells from the spleens or peritoneal exudates of suppressed mice, however, did significantly depress the ability of immunized mice to express a DTH response. The cells responsible for this suppression were Thy 1^- and nonspecific esterase$^+$. Treatment of suppressive cell populations with 10 μg/ml indomethacin for 24 hr *in vitro* abrogated their suppressive ability, and *in vivo* administration of indomethacin to suppressed mice also restored DTH to normal levels. By examining levels of prostaglandin E_2 (PGE_2) in supernates of cultured peritoneal exudate cells from immune or suppressed mice, it was shown that infected mice had peritoneal exudate cells which produced significantly more PGE_2 than similar cells from immune mice. These data suggest that *B. microti* infection elicits synthesis of PGE_2 by macrophage-like cells which results in suppression of DTH to parasite as well as heterologous antigens.

INTRODUCTION

The response of mice to *Babesia microti* of human origin is strongly T-cell dependent both during the primary and the anamnestic immune responses (1, 2); however, the mechanism(s) by which T cells exert their positive influence on recovery are not known. It has previously been shown that intraerythrocytic *B. microti* parasites (IEP)[2] are an

[1] This work was supported by National Institutes of Health Grant AI19336. The opinions or assertions contained herein are the private ones of the authors and are not to be construed as official or reflecting the views of the Uniformed Services University of the Health Sciences, the Armed Forces Radiobiology Research Institute, or the Department of Defense, at large.

[2] Abbreviations used: DTH, delayed-type hypersensitivity; IEP, intraerythrocytic parasites; sc, subcutaneous; PGE_2, prostaglandin E_2; ip, intraperitoneal; SRBC, sheep red blood cells; PBS, phosphate-buffered saline; CY, cyclophosphamide; ELISA, enzyme-linked immunosorbent assay; SC, spleen cells; PEC, peritoneal

0008-8749/86 $3.00

effective antigen for elicitation of the T-cell-dependent delayed-type hypersensitivity (DTH) response (3). Positive footpad swelling is easily elicited in mice after subcutaneous (sc) inoculation of 10^8 IEP, followed 6–14 days later by challenge sc in the ipsilateral footpad with 10^8 IEP. Mice infected intraperitoneally (ip) with *B. microti* before immunization, however, showed greatly reduced ability to mount a normal DTH response. This infection-induced suppression was both rapid in onset and long in duration.

The DTH response is known to be dependent on Ly 1^+ T lymphocytes (4) and modulated by complex interactions with other T lymphocyte subsets, B lymphocytes, and macrophages (5). Defects in any one or all of these cell types could be responsible for the observed suppression. In addition, various chemicals and hormones can modulate the activities of lymphocytes and macrophages involved in the DTH response. Adrenal corticosteroids (6), cAMP (7), endotoxin (8), C-reactive protein (9), interferons (10), and prostaglandins (11, 12) have all been shown to modulate expression of these responses. We present evidence here that infection induces synthesis of prostaglandin E_2 (PGE_2) by macrophage-like cells in the spleen and peritoneal cavity which acts in turn to depress the DTH response to homologous and heterologous antigens.

MATERIALS AND METHODS

Mice. BALB/c mice were raised in our breeder colony from stock originally obtained from Jackson Laboratories (Bar Harbor, Maine). Mice were used at 6 to 8 weeks of age, in groups of 5 to 10 animals each.

Parasite. The Peabody strain of *B. microti* was originally isolated in 1979 from a clinical case of babesiosis and was subsequently adapted to mice as previously described (13). Donor animals were infected ip with 2 to 3×10^8 IEP. At the time of expected peak parasitemia these mice were exsanguinated by cardiac puncture into sodium heparin. The number of parasites per milliliter of blood was determined by means of Giemsa-stained thin blood smears and hemacytometer counts. Experimental mice were infected ip with 0.1 ml of blood containing 10^8 IEP.

Immunization and Suppression of DTH. Mice were immunized to express DTH (immunized mice) by sc injection into the right flank of 10^8 sheep red blood cells (SRBC) or IEP. Mice with suppressed DTH responses (suppressed mice) were treated identically except that they were infected ip with 10^8 IEP 2 days before immunization.

Elicitation of DTH. Seven days after immunization, experimental mice were challenged with 10^8 SRBC or IEP. All mice were given 50 μl of the appropriate antigen sc in the right footpad, and an equivalent amount of phosphate-buffered saline (PBS) in the left footpad. These conditions for immunization and challenge of mice for DTH expression have previously been shown to elicit maximal responsiveness (3).

Measurement of footpad swelling. Measurements of right and left footpad thickness were obtained using a dial micrometer 24 hr after administration of the challenge

---

exudate cells; LNC, lymph node cells; RPMI–BSA, RPMI 1640 + 0.03% bovine serum albumin; AdSC, adherent spleen cells; RIA, radioimmunoassay; ILNC, immune lymph node cells; NLNC, normal lymph node cells; SLNC, suppressed lymph node cells; IS, immune serum; SS, suppressed serum; NS, normal serum; SAdSC, suppressed adherent spleen cells; NAdSC, normal adherent spleen cells; IAdSC, immune adherent spleen cells; SPEC, suppressed peritoneal exudate cells; IPEC, immune peritoneal exudate cells; NPEC, normal peritoneal exudate cells.

antigen. Data were tabulated as the increase in footpad thickness of the right (antigen-stimulated) over the left (PBS-injected) footpad.

Treatment with cyclophosphamide. Cyclophosphamide (CY; Cytoxan, Meade Johnson Labs, Evansville, Ind.) was given ip at a dose of 200–600 mg/kg body wt 1 to 2 days before infection.

Treatment with indomethacin. Indomethacin (Sigma Chemical Co., St. Louis, Mo.) was administered to mice ip in daily doses of 100 μg from the day of infection to the day of DTH challenge. It was initially dissolved in absolute ethanol and then adjusted to the appropriate concentration in PBS. Control animals received similar concentrations of ethanol in PBS.

Irradiation. Lethal (700 R) γ irradiation was delivered at 7890 R/hr from a 137 cesium source (AECL Gammacell 40, Atomic Energy of Canada, Ltd., Ottawa, Canada).

Enzyme-linked immunoadsorbent assay (ELISA). Assays of total specific immunoglobulin levels in sera from immunized, suppressed, and normal mice were performed by ELISA. For this purpose, *B. microti* antigen was prepared from IEP suspended to a concentration of 10^9/ml. Infected blood was layered over Isolymph (Gallard-Schlesinger Chemical Manufacturing Corp., Carle Place, N.Y.) and left for 1 hr at 20–25°C to remove white blood cells. The red blood cells which were obtained were washed twice in PBS at pH 8.0 containing 0.01 *M* Na_2HPO_4, 0.15 *M* NaCl, and 0.02% Tween 20. The red cell pellet obtained after the final centrifugation was resuspended in three volumes of PBS and frozen at −70°C for at least 8 hr. The material was then thawed at room temperature, centrifuged at 4000*g*, and the hemoglobin-containing supernate was removed and discarded. The pellet was resuspended in three volumes of PBS, mixed, and allowed to stand at room temperature for 30 min. The suspension was then centrifuged at 20,000*g* for 30 min and the protein content in the supernate was determined by the Bradford technique (Bio-Rad Laboratories, Richmond, Calif.). Working antigen was prepared by adjusting the concentration to 10 μg/ml in PBS coating buffer (PBS without Tween 20). Polystyrene plates were sensitized overnight at room temperature by addition of 100 μl of working antigen (10 μg/ml) to half of the wells of a 96-well microplate. Whole sera and fractions were added at a dilution of 1:20 to antigen-coated wells and blank wells to detect background levels for individual sera. Peroxidase-conjugated affinity-purified anti-mouse IgG and IgM (Kirkegaard and Perry Labs, Gaithersburg, Md.) were added at a dilution of 1:1000 and final reactions were read at 414 nm using a Titertek Multiskan plate reader (Flow Laboratories, McLean, Va.).

Passive transfer. Donors of cells and serum for passive transfer experiments were immunized, suppressed, or untreated. Six days after immunization they were exsanguinated. Sera were collected and pooled, and spleen cells (SC), peritoneal exudate cells (PEC), or cells from popliteal and inguinal lymph nodes (LNC) were dispersed into RPMI 1640 medium containing 0.03% L-glutamine, gentamicin (Flow Laboratories), and 0.03% bovine serum albumin (RPMI–BSA). The number of viable cells per milliliter was determined using a hemacytometer and trypan blue dye exclusion. Spleen cells and PEC were suspended to 10^6/ml in RPMI–BSA and placed in petri dishes in a humidified 37°C incubator with 6% CO_2 in air. After 2 hr incubation, monolayers were washed extensively with PBS, adherent SC (AdSC) and PEC were dislodged from the dishes with a rubber policeman, and suspensions were recounted with hemacytometers and trypan blue dye. Recipient mice were given 5×10^6 viable

LNC, AdSC, or PEC or 25 μl of serum from immunized, suppressed, or untreated donors sc mixed 1:1 with 10^8 IEP in the right footpad. Left footpads were inoculated with 50 μl of PBS, and DTH reactions were read as before.

Nonspecific esterase detection. Suspensions of PEC (10^6/ml) were placed in Leighton tubes and allowed to adhere for 2 hr at 37°C. The coverslip was then removed, fixed in citrate-acetone-methanol fixative, and stained for detection of α-naphthyl acetate esterase using a staining kit from Sigma Chemical Company. In some cases, coverslips were double stained for detection of naphthol AS-D chloroacetate esterase in granulocytes.

Inhibition of synthesis of PG in vitro. Cultures of adherent PEC were treated with indomethacin (10 μg/ml) in RPMI–BSA for 24 hr before cell transfer.

Radioimmunoassay (RIA) for PG. Supernates from PEC cultures were stored at −20°C and assayed for PGE_2 content within 5 days by RIA (14). Culture supernates (100 μl) or known standards (2.5–1000 pg) were incubated with 50 μl of rabbit PGE_2 antiserum (Clinical Assays, Boston, Mass.) for 2 hr at 22°C. The specificity of this antiserum has been previously described (14). Tritiated PGE_2 (50 μl; 8000 cpm; New England Nuclear Corp., Boston, Mass.) was then added and the incubation was continued at 4°C for 12–16 hr (final volume, 200 μl). The bound [^{3}H]PGE_2 was separated from the uncomplexed tracer after the addition of 250 μl of iced Trizma–NaCl–gelatin (1.0%) by adding 500 μl iced charcoal (0.5%)–dextran (0.05%) in Trizma–NaCl and incubating at 4°C for 20 min. Following centrifugation (200*g*, 12 min, 4°C), the supernate was decanted into scintillation vials. Ultrafluor scintillation cocktail (10 ml; National Diagnostics, Somerville, N.J.) was added and the radioactivity was determined in a Mark III scintillation counter (Beckman Corp., Fullerton, Calif.) All RIA were performed in duplicate. The level of sensitivity was 2.5 pg per assay.

Analysis of data. Data were analyzed for statistical significance using analyses of variance with significance at $P \leq 0.05$.

RESULTS

Specificity of suppression of the DTH response. Although immunization of normal mice with either SRBC or IEP elicited a positive DTH response only when mice were challenged with the homologous antigen (3), infected mice exhibited a depressed ability to respond to either IEP or SRBC regardless of whether challenge was made with the homologous or heterologous antigen (Table 1).

Effect of irradiation on the DTH response. Lethal (700 R) irradiation did not significantly affect the suppression of the DTH response by infection (Fig. 1). When irradiation was given 2 days before immunization, the DTH response was significantly reduced in uninfected mice ($P \leq 0.05$) below levels seen in similarly immunized, unirradiated mice (Fig. 1A). There was no significant difference using this protocol, however, whether or not suppressed mice were irradiated. When mice were immunized 7 days before they were irradiated (Fig. 1B), there was no significant difference between the response of irradiated or unirradiated suppressed or immunized mice.

Effect of CY on DTH suppression. A single dose of 200 mg/kg CY 2 days before infection did not cause any significant change in the DTH response of suppressed mice on any of the days tested (Fig. 2). In addition, other experiments (not shown) which varied the time of CY administration and the dosage given failed to demonstrate any significant effect of CY on suppression of the response except at levels which were fatal to treated mice.

TABLE 1

Specificity of Suppression of the DTH Response[a]

Mouse	Immunization	Challenge	$\bar{X} \pm SD^b$
Infected	IEP	IEP	0.40 ± 0.24
	IEP	SRBC	0.06 ± 0.09
	SRBC	IEP	0.32 ± 0.16
	SRBC	SRBC	0.24 ± 0.23
Uninfected	IEP	IEP	0.96 ± 0.15
	IEP	SRBC	0.22 ± 0.22
	SRBC	IEP	0.34 ± 0.09
	SRBC	SRBC	0.95 ± 0.13

[a] Groups of mice were either infected with 10^8 IEP ip on Day −2 or left untreated. On Day 0, groups of mice were given 10^8 SRBC or IEP sc in the right flank. Challenge with 10^8 SRBC or IEP was given sc in the right footpad 7 days after immunization.

[b] Mean increase in footpad thickness (mm) for each group ± 1 standard deviation, as measured 24 hr after challenge.

Effect of passive transfer of LNC on the DTH response. Transfer of LNC from immunized (ILNC), normal (NLNC), or suppressed (SLNC) mice into immunized (Fig. 3A) or suppressed (Fig. 3B) recipients was attempted in five similar experiments of which one is shown (Fig. 3). Both ILNC and SLNC elicited similar responses in immunized recipients regardless of whether recipient mice were lethally irradiated before cell transfer. Immunized recipients of NLNC had DTH responses which were significantly lower than their irradiated or nonirradiated counterparts which received ILNC or SLNC ($P \leq 0.05$). When these cell types were given to suppressed mice, none of the cell types was significantly different in its effect in irradiated or nonirradiated recipients.

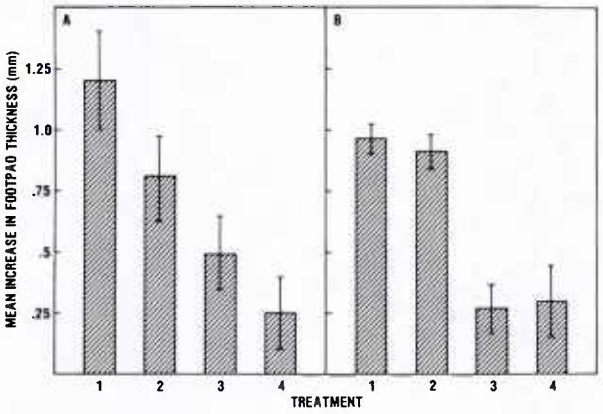

FIG. 1. Effect of irradiation on the DTH response. Groups of mice were lethally irradiated (700 R) on Day −2 (Fig. 1A) or Day 7 (Fig. 1B) as follows: (1) immunized (10^8 parasites sc right flank, Day 0) alone; (2) irradiated and immunized; (3) suppressed (10^8 parasites ip Day −2; 10^8 parasites sc Day 0) alone; or (4) irradiated and suppressed. Challenge was administered to all groups on Day 7 and DTH responses were read 24 hr later.

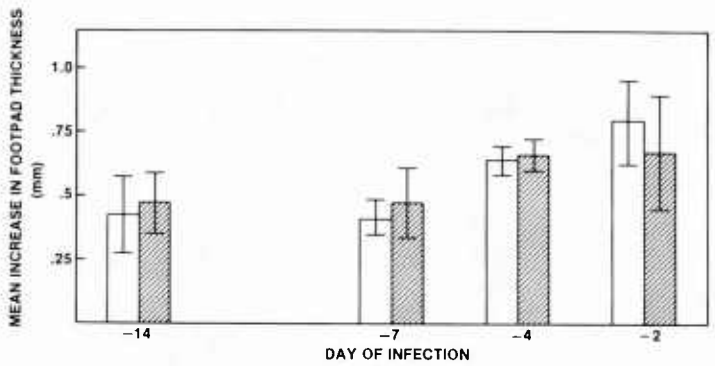

FIG. 2. Effect of CY on DTH suppression. Groups of mice were infected with 10^8 IEP ip 14, 7, 4, or 2 days before immunization with 10^8 IEP sc in the right flank. Challenge was given 7 days after immunization and DTH responses were read as before. One-half of the infected mice for each day shown were given CY (200 mg/kg) in a single dose ip 2 days before infection (open bars) and the remaining mice were given an equivalent volume of PBS ip (shaded bars).

Effect of passive transfer of serum on the DTH response. When serum from immunized (IS), suppressed (SS), or normal (NS) mice was inoculated into immunized or suppressed recipients 1 day before challenge, the DTH response was not significantly altered (Fig. 4). The levels of specific antibody in these sera were relatively low when tested by IgM or IgG ELISA using freed *B. microti* as an antigen. Sera from suppressed mice had titers of 1:40 for IgM and 1:80 for IgG, while the sera from immunized mice had titers of 1:160 for IgM and 1:40 for IgG.

Effect of transfer of adherent spleen cells on the DTH response. The transfer of 5×10^6 AdSC from suppressed (SAdSC) mice into immunized recipient mice significantly depressed the DTH response below levels seen in recipients of immune (IAdSC) cells (Fig. 5). There was no significant difference in responses of recipients of SAdSC and normal cells (NAdSC). When these cells were given to suppressed recipients (Fig. 5B) there was no significant difference in the response observed in recipients of IAdSC, SAdSC, or NAdSC. Since similar results were obtained after transfer of PEC (data not

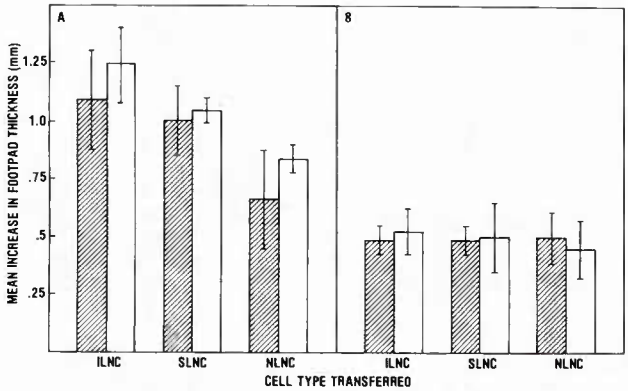

FIG. 3. Effect of LNC transfer on the DTH response. Immunized (A) or suppressed (B) recipient mice were lethally irradiated (700 R; shaded bars) or left unirradiated (open bars) immediately before inoculation of 10^7 ILNC, SLNC, or NLNC mixed with 10^8 IEP sc into the right footpad on Day 7 postimmunization.

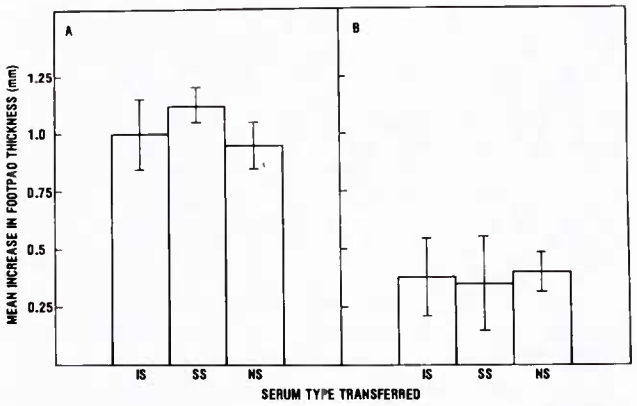

FIG. 4. Effect of serum transfer on the DTH response. (A) Immunized recipient mice were given 25 μl IS, SS, or NS mixed with 10^8 IEP sc in the right footpad. Mean increase in footpad thickness was determined as before. (B) Suppressed recipient mice were treated similarly.

shown) all further experiments were conducted using PEC because of the greater ease with which these cells could be obtained.

Characteristics of the suppressive cell. In order to characterize which cells in the PEC from suppressed mice were capable of suppressing the DTH response, populations of PEC from suppressed (SPEC) or immunized (IPEC) mice were treated with anti-Thy 1 plus C before transfer into immunized recipients (Table 2). The suppressive cells appeared to be theta antigen-negative, since this treatment had no significant effect on the ability of SPEC to suppress the DTH response. The θ antigen-negative suppressive cells which remained following treatment were strongly positive for non-specific esterases and thus appeared to satisfy the criteria for definition of cells of monocyte lineage.

Effect of indomethacin on suppression. In order to determine whether prostaglandin synthesis by PEC might be responsible for the DTH suppression observed, groups of

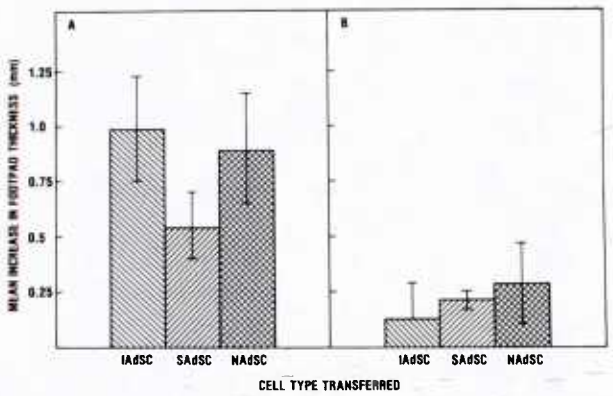

FIG. 5. Effect of transfer of AdSC on the DTH response. (A) Immunized recipient mice were given 5 $\times$ 10^6 IAdSC, SAdSC, or NAdSC mixed with 10^8 IEP sc in the right footpad. (B) Suppressed recipients were treated similarly.

TABLE 2

Characteristics of the Suppressive Cells

Cell type[a]	Treatment[b]	%NSE[c]	±1 SD[d]
IPEC	C	85	1.78 ± 0.18
IPEC	Anti-Thy 1 + C	95	1.65 ± 0.06
SPEC	C	87	1.08 ± 0.17
SPEC	Anti-Thy 1 + C	95	0.21 ± 0.17

[a] Peritoneal exudate cells were removed on Day 6 from mice which had been infected with 10^8 IEP ip on Day 0 and immunized with 10^8 IEP sc in the right flank on Day 2 (SPEC) or immunized with 10^8 IEP sc in the right flank on Day 2 (IPEC). Cells were suspended to 10^6/ml and allowed to adhere to plastic dishes for 2 hr at 37°C. Monolayers were then washed in PBS and adherent cells were removed with a rubber policeman.

[b] Washed adherent PEC were treated with Thy 1 plus C or C alone (Cedarlane Laboratories, Ontario, Canada) according to package instructions.

[c] A suspension of treated PEC was placed in a Leighton tube, allowed to adhere for 2 hr at 37°C, and the coverslip was fixed and stained for detection of nonspecific esterase (NSE; α-naphthyl acetate esterase; Sigma Chemical Co., St. Louis, Mo.) The percentage of cells showing black granulation was determined microscopically.

[d] Treated PEC were washed twice in PBS, suspended to 2×10^8/ml, mixed 1:1 with a suspension of 4×10^9 IEP/ml, and inoculated into the right footpad of mice immunized with 10^8 IEP sc in the right flank 6 days earlier. The increased thickness (mm) of the right (cells + antigen) over the left (PBS) footpad was measured after 24 hr.

immunized or suppressed mice were given 100 μg indomethacin ip daily for 7 days or left untreated. Mean increase in footpad thickness was determined 24 hr after challenge of all groups. Suppressed mice treated with indomethacin had responses which were significantly higher than those of untreated, suppressed mice but not significantly different from those of indomethacin-treated immunized mice (Table 3). Indomethacin did not significantly affect the ability of immunized mice to mount a DTH response.

When SPEC, IPEC, or PEC from untreated mice (NPEC) were treated for 24 hr *in vitro* with 10 μg/ml indomethacin before transfer into suppressed or immunized mice,

TABLE 3

Effect of Indomethacin *in Vivo* on DTH Suppression

	Treatment (Day no.)			
Group	Infection[a]	Immunization[b]	Indomethacin[c]	$\bar{X} \pm$ SD[d]
1	0	2	0–7	1.15 ± 0.17
2	0	2	—	0.54 ± 0.11
3	—	2	0–7	0.94 ± 0.22
4	—	2	—	1.20 ± 0.10

[a] Mice were infected with 10^8 IEP ip or left uninfected.

[b] Mice were immunized with 10^8 IEP sc in the right flank and challenged with 10^8 IEP sc in the right footpad on Day 7.

[c] Mice were given 100 μg of indomethacin daily ip or left untreated.

[d] Mean increase in footpad thickness (mm) ± 1 standard deviation.

similar results were obtained (Fig. 6). Indomethacin treatment abrogated the suppressive effect of SPEC transferred into immunized mice, but did not significantly affect the results of transfer of IPEC or NPEC into these mice. It is not likely that these findings were a result of transfer of indomethacin along with PEC since in control cultures incubated with tritiated indomethacin (Amersham, Arlington Heights, Ill.) PEC retained only 0.15% of the total counts after one wash. Control measurements of PGE_2 content in the supernates from cultured cells demonstrated that PGE_2 synthesis was eliminated by indomethacin treatment. In addition, PGE_2 synthesis by untreated SPEC was significantly higher than that of NPEC or IPEC. None of the cell types tested had any ability to transfer DTH responsiveness to suppressed mice whether they were pretreated with indomethacin and regardless of the amounts of PGE_2 being produced.

DISCUSSION

We have shown previously that mice infected with *B. microti* exhibit a profound depression of ability to respond to immunization for expression of DTH (3). The kinetics of this immunosuppression taken together with the known appearance of anti-*Babesia* antibodies (unpublished observations) suggested that the lack of DTH responsiveness in infected mice is not modulated by the standard antibody feedback which has been described in other systems (15). Antibodies and other soluble substances found in the serum must also be ruled out as mechanisms of suppression since serum from suppressed mice did not abrogate responsiveness in immunized animals.

In other systems, suppression of DTH has been found to be associated with suppressor T cells (4, 16). In *Leishmania tropica* infections, for example, abrogation of these cells by irradiation causes restoration of a strong anti-parasite DTH response which develops in parallel with resistance to disease (17). These workers found that suppressor cells of the Thy-1^+, Lyt 1^+2^-, and I-J^- phenotype were capable of inhibiting the induction and expression of DTH as well as reversing the healing of lesions (18). Irradiation did not restore the responsiveness of *B. microti*-infected mice, however.

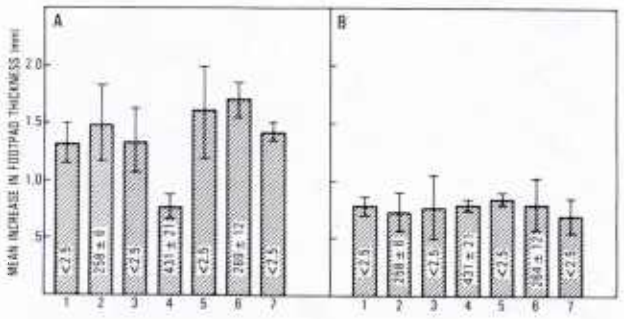

FIG. 6. Effect of inhibition of PEC prostaglandin synthesis on transfer of suppression. IPEC, SPEC, and NPEC were cultured for 24 hr in the presence of 10 μg/ml indomethacin in RPMI–BSA or in RPMI–BSA alone. Cells were scraped from plates, washed twice in PBS, suspended to 2×10^8 cells/ml, and inoculated into the right footpads of immunized (Fig. 1A) or suppressed (Fig. 1B) recipients in a 1:1 mixture with 4×10^9 IEP/ml. Mean increase in footpad thickness was measured after 24 hr and is shown ±1 standard deviation. Immunized and suppressed recipients were given: (1) RPMI–BSA + IEP, (2) IPEC + IEP, (3) indomethacin-cultured IPEC + IEP, (4) SPEC + IEP, (5) indomethacin-cultured SPEC + IEP, (6) NPEC + IEP, or (7) indomethacin-cultured NPEC + IEP. The numbers inside the bars represent the PGE_2 levels in supernates from the cultured PEC ±1 standard deviation. The level of sensitivity was 2.5 pg/assay.

Similarly, CY is an alkylating agent classically used for elimination of suppressor T cells (19) and proliferating B cells (20), but even in large doses it did not restore DTH in *B. microti*-infected mice.

During murine malaria infections, the macrophage has been implicated in suppression of the DTH-like response of schistosome granuloma formation (21), and Liew (22) has suggested that suppressor cell generation during *L. tropica* infection is secondary to a primary defect in macrophages. Our results using *B. microti* support an important role for the macrophage in suppression of the anti-parasite DTH response. The suppression was nonspecific and could not be transferred with SLNC. It was transferred by adherent, θ antigen-negative, nonspecific esterase-positive cells from the peritoneal cavities of suppressed mice.

At least one specific mechanism by which the macrophage affects this suppression in our model system appears to be through release of PGE_2. Production of PGE_2 by PEC is significantly increased following infection, and inhibition of prostaglandin synthesis with indomethacin eliminates the suppressive effects of SPEC. These findings are in keeping with the observation that mice infected with rodent-derived *B. microti* have increased macrophage phagocytic activity as measured by clearance of colloidal carbon (23). Prostaglandins are produced at an accelerated rate in activated macrophages such as these (24), and have been shown to inhibit the responses of T and B lymphocytes to antigenic and mitogenic stimulation (25).

Prostaglandins are a family of chemically related fatty acid derivatives which are important mediators of inflammation (26). They may function by influencing intracellular levels of cyclic nucleotides in other cell types and thus affecting their proliferation or differentiation (25). A wide variety of possible biochemical changes during *Babesia* infections could explain the increased production of PGE_2 we have observed. *Plasmodium berghei*-infected erythrocytes have been shown to produce more cAMP than their uninfected counterparts (27), and if the same is found to hold true for *Babesia,* a direct modulating effect on prostaglandin synthesis could be expected. Endotoxins, which have been suggested as a cause of disease as well as parasite death in malaria and *Babesia* infections (8), can also stimulate production of prostaglandins (28). Finally, complement levels can finely modulate prostaglandin synthesis, and since *B. rodhaini* has been shown to require complement for penetration of human erythrocytes (29), *B. microti* might easily be expected to have an effect on complement levels which could in turn influence prostaglandin synthesis.

Once elicited, E-type prostaglandins have been implicated as major regulators of the immune response. Mediated by increased levels of cAMP, culture of T cells with PGE_2 causes release of suppressors of T-cell activation and lymphokine secretion (30), and B-cell activation, antibody production, and natural killer cell function are also modulated by PGE_2 *in vitro* (31). A direct effect of PGE_2 on the macrophage membrane appears to be responsible for inhibition of phagocytosis (29). Thromboxane A_2 and prostacyclin may be involved in modulating cell-mediated immunity (32), and this prospect has led some workers to propose that positive–negative feedback of macrophage–lymphocyte cooperation may be kept in balance by endogenous metabolites of arachidonic acid (31).

It is not clear at this time whether this prostaglandin production and DTH suppression are important in the outcome of infection with *B. microti.* Although mice which have been immunized to express a strong DTH response are resistant to subsequent infection (3), it may not be the DTH response itself which is protective. In *L. tropica*

infections, for example, although DTH usually develops in parallel with resistance to disease, immunity was found to be attributable to a population of Lyt-1^+2^- T cells distinct from those expressing classical DTH activity (33). Whether protective immunity to *B. microti* infections is found to reside in DTH cells, the PGE_2 production which occurs during infection will probably be found to suppress more than DTH alone.

ACKNOWLEDGMENTS

The authors gratefully acknowledge the secretarial assistance of Ellen Klein and Joy Holland in the preparation of this manuscript.

REFERENCES

1. Ruebush, M. J., and Hanson, W. L., *Amer. J. Trop. Med. Hyg.* **29,** 507, 1980.
2. Ruebush, M. J., and Hanson, W. L., *Cell. Immunol.* **252,** 255, 1980.
3. Ruebush, M. J., Troutman, E. H., and Kennedy, D. A., *Cell. Immunol.* **98,** 289, 1986.
4. Ramshaw, I. A., Woodsworth, M., Wright, K., and McKenzie I. F. C., *J. Immunol.* **125,** 197, 1980.
5. Turk, J. L., and Parker, D., *Immunology* **24,** 751, 1973.
6. Terry, R. J., *Inst. Santé Rech. Med.* [*Colloq*] **72,** 161, 1977.
7. Droller, M. J., and Remington, J. S., *Cell. Immunol.* **19,** 349, 1975.
8. Clark, I. A., *Lancet* **1978,** 75, 1978.
9. Cooperband, S. R., and Badger, A. M., *In* "Naturally Occurring Biological Immunosuppressive Factors and Their Relationship to Disease" (R. H. Neubauer, Ed.), p. 115. CRC Press, Boca Raton, Fla., 1978.
10. DeMaeyer, E., *J. Infect. Dis.* **133,** A63, 1976.
11. Kendall, R. A., and Targan, S., *J. Immunol.* **125,** 2770, 1980.
12. Mavligit, G. M., Raphael, L. S., Calvo, D. B., III, and Wong, W. L., *J. Natl. Cancer Inst.* **65,** 317, 1980.
13. Ruebush, M. J., and Hanson, W. L., *J. Parasitol.* **65,** 430, 1979.
14. Steel, L. K., and Catravas, G. N., *Int. J. Radiat. Biol.* **42,** 517, 1982.
15. McDonald, V., and Sherman, I. W., *Clin. Exp. Immunol.* **42,** 421, 1980.
16. Lelchuk, R., Sprott, V. M. A., and Playfair, J. H. L., *Clin. Exp. Immunol.* **45,** 433, 1981.
17. Howard, J. G., Hale, C., and Liew, F. Y., *J. Exp. Med.* **153,** 557, 1981.
18. Liew, F. Y., Hale, C., and Howard, J. G., *J. Immunol.* **128,** 1917, 1982.
19. Laux, D. C., and Parker, B. M., *Immunol. Commun.* **9,** 559, 1980.
20. Finerty, J. F., and Krehl, E. P., *Infect. Immun.* **14,** 1103, 1976.
21. Abdel-Wahab, M. F., Powers, K. G., Mahmoud, S. S., and Good, W. C., *Amer. J. Trop. Med. Hyg.* **23,** 915, 1974.
22. Liew, F. Y., *Nature (London)* **305,** 630, 1983.
23. Purvis, A. C., *Parasitology* **75,** 197, 1977.
24. Gordon, D., Bray, M. A., and Morley, J., *Nature (London)* **262,** 401, 1976.
25. Chisari, F. V., and Edgington, T. S., *J. Exp. Med.* **140,** 1122, 1974.
26. Allison, A. C., *Int. Rev. Exp. Pathol.* **18,** 303, 1978.
27. Hertelendy, F., Toth, M., and Fitch, C. D., *Life Sci.* **25,** 451, 1979.
28. Rampart, M., Bult, H. and Herman, A. G., *Arch. Int. Pharmacodyn.* **249,** 328, 1981.
29. Chapman, W. E., and Ward, P. A., *Science (Washington, D.C.)* **196,** 67, 1977.
30. Rogers, T. J., DeHaven, J. I., Connelly, R. P., and Lamb, B., *Cell. Immunol.* **87,** 703, 1984.
31. Bonta, I. L., and Poarnhgam, M. J., *Int. J. Immunopharmacol.* **4,** 103, 1982.
32. Leung, K. H., and Mihich, E., *Nature (London)* **288,** 597, 1980.
33. Howard, J. G., and Liew, F. Y., *Philos. Trans. R. Soc. Lond. B* **307,** 87, 1984.

GASTROENTEROLOGY 1986;91:660–6

Gastric Protection by Sucralfate
Role of Mucus and Prostaglandins

T. SHEA-DONOHUE, L. STEEL, E. MONTCALM, and A. DUBOIS
Department of Medicine, Uniformed Services University of the Health Sciences, and Radiation Sciences Department, Armed Forces Radiobiological Research Institute, Bethesda, Maryland

Sucralfate promotes the healing of peptic ulcers and, in large doses, increases gastric mucosal prostaglandins. The present study was designed to further elucidate the protective effect of sucralfate and to evaluate the role of prostaglandins in this action. Eight chair-adapted rhesus monkeys received a subcutaneous injection of either 150 mg/kg of aspirin or vehicle in combination with either a therapeutic oral dose of sucralfate (50 mg/kg · day) or water. Gastric soluble mucus concentration was determined in samples of gastric juice by Alcian blue dye binding of acidic glycoproteins, and mucus output was determined using a technetium 99m–diethylenetriaminepentaacetic acid dilution technique. Monkeys underwent endoscopy to assess gastric mucosal damage, which was ranked blindly on a scale of 0–5, and to obtain biopsy specimens for determination of mucosal prostaglandin E_2, prostaglandin $F_{2\alpha}$, and 6-keto-prostaglandin $F_{1\alpha}$. Aspirin did not alter soluble mucus but did significantly increase gastric mucosal damage and suppress tissue levels of all prostaglandins. Sucralfate significantly increased the output of soluble mucus, even after aspirin treatment, and protected against aspirin-induced damage, although it did not modify aspirin-induced suppression of prostaglandins. These results suggest that the gastric protection afforded by sucralfate is related to a prostaglandin-independent increase in mucus production.

Sucralfate, a basic aluminum salt of sucrose sulfate, promotes the healing of gastric and duodenal ulcers (1,2) and reduces their recurrence (3,4). Sucralfate binds to denuded mucosa, inhibits peptic activity, binds bile salts, and has a small buffering capacity. In addition, sucralfate has been shown to prevent gastric damage induced by ethanol in rats (5). The mechanism by which sucralfate produces its therapeutic effect, however, is unclear. As large doses of sucralfate have been shown to increase prostaglandin (PG) release into gastric juice in rats (6), it has been suggested that this protective effect may be mediated via a release of PG. The present study was designed, therefore, to further examine the mechanism of the protective effect of sucralfate on the gastric mucosa and to determine the role of PG in this action.

Materials and Methods

Eight unanesthetized rhesus monkeys (*Macaca mulatta*) weighing 3–4 kg were adapted to primate restraining chairs and housed in closed, ventilated, lighted booths between 9 AM and 12 noon. The monkeys were trained to accept a 12F double-lumen, nasogastric Ventrol Levin tube (National Catheter, Mallinckrodt, Argyle, N.Y.). The experiments were conducted after an overnight fast and were started 45 min after the tube had been placed. Proper positioning of the tube in the most dependent part of the stomach was verified by demonstrating that, after injecting 15 ml of water into a previously emptied stomach, the total volume could be recovered. Thirty minutes

Received September 24, 1985. Accepted March 11, 1986.

Address requests for reprints to: Terez Shea-Donohue, Ph.D., Department of Medicine, Uniformed Services University of the Health Sciences, 4301 Jones Bridge Road, Bethesda, Maryland 20814-4799.

This work was supported in part by the Uniformed Services University of the Health Sciences Protocol No. CO-8343.

The opinions and assertions contained herein are the private ones of the authors and are not to be construed as official policy or as reflecting the views of the Department of Defense.

The experiments reported herein were conducted according to the principles set forth in the "Guide for the Care and Use of Laboratory Animals," Institute of Animal Resources, National Research Council, DHEW Publication No. (NIH) 78-23.

The authors thank William W. Wolfe and Nelson Fleming for their technical assistance and Joy W. Barchers for her expert editorial assistance.

Abbreviations used in this paper: AG, acidic glycoprotein; AS, aspirin (s.c.) + sucralfate (oral); AW, aspirin (s.c.) + water (oral); CS, control ($NaHCO_3$, s.c.) + sucralfate (oral); CW, control ($NaHCO_3$, s.c.) + water (oral); NG, neutral glycoprotein; PG, prostaglandin.

Table 1. Scale of Evaluation of Gastric Injury

Grade	Description
0	No injury
1	Reddening or 1 discrete submucosal hemorrhage
2	2 or more submucosal hemorrhages
3	1 erosion, ≤1 mm in diameter
4	2–5 erosions, 1 mm in diameter
5	>5 erosions, or ≥1 linear erosion

This table has been modified from that of Lanza et al. (13).

after the administration of either vehicle or drug, gastric emptying and gastric fluid, ion, and soluble mucus output were determined using a technique previously described and validated in monkeys and humans (7–9) that is based on the marker dilution principle (7–11).

The concentrations and outputs of neutral glycoproteins (NGs) and acidic glycoproteins (AGs) were determined separately. The concentration of soluble mucus in each sample was estimated using two previously described methods (9). The Alcian blue dye binding method was used to determine AGs and the periodic acid–Schiff method was used to estimate NGs. Porcine gastric mucin was used as a standard in both assays.

The calculations were performed using a locally developed program and a PDP-10 computer (Division of Computer Research and Technology, National Institutes of Health, Bethesda, Md.). The assumptions involved have been described and discussed elsewhere (7) and are based on the original contribution of Hildes and Dunlop (11).

In this study, each monkey randomly received one of four different treatments on separate days ~4–5 wk apart. A subcutaneous (s.c.) injection of $NaHCO_3$ (75 mg/kg) as a control (C) or aspirin (A, 150 mg/kg) was given in combination with an oral administration of water (CW, AW) or sucralfate (CS, AS). Aspirin was dissolved in $NaHCO_3$ and warmed gently to 37°C immediately before injection. Aspirin or $NaHCO_3$ was given 16 h and 30–45 min before the start of the study. Sucralfate was suspended in 3 ml of water and given 20 h, 16 h, and 30–45 min before the study. The total dose of sucralfate was 50 mg/kg · day, which is similar to the recommended dose for humans of 1 g, q.i.d.

Values for gastric secretory parameters obtained during the first four 10-min intervals were averaged for each study to obtain one fasting value per animal, and the mean (±SE) was calculated for each treatment. Values obtained during the seven 5–10-min intervals after the 80-ml water load (postload) were also averaged for each study to determine one postload value per animal, and the mean (±SE) postload value was then calculated for each treatment. The statistical significance of differences observed for each measurement of gastric function (i.e., mucus output) was evaluated using a three-factor (treatment, time, and monkey) analysis of variance with repeated measures on the last two factors (12), the program LDU-040 (K.L. Dorn), and an IBM 370 computer (Division of Computer Research and Technology, National Institutes of Health).

A sample of gastric juice was taken 30 min after intubation and was immediately placed in a cold vial on dry ice with 5 μl of 1.6% indomethacin solution per milliliter of juice. The samples were then stored at −70°C for subsequent determination of PGE_2, $PGF_{2\alpha}$, and 6-keto-$PGF_{1\alpha}$. When the marker dilution study was completed, the nasogastric tube was removed. One hour later, the monkeys were anesthetized using 5–10 mg/kg ketamine hydrochloride (Vetalar, Morris Plains, N.J.) and underwent endoscopy using an Olympus GIF-P2 pediatric fiberscope (Olympus Corporation of America, New Hyde Park, N.Y.). At this time, a visual examination was made to determine the status of the gastric mucosa in both the antrum and fundus. A record was made of the overall appearance of the mucosa as well as the size and number of lesions observed. The recorded visual descriptions of the gastric mucosa were later scored by two investigators who were blinded to the treatment that the monkeys had received. The degree of gastric damage was assessed using a modification of the method described by Lanza et al. (13). This grading system allows not only the evaluation of the severity and density of individual lesions, but also an evaluation of the area of the stomach involved. Findings were graded on a scale of 0–5 as described in Table 1. Differences in the damage scores among the various treatments were determined using a two-way analysis of variance.

After the stomach had been visually evaluated, two pinch biopsy specimens were obtained, each from the antrum and fundus, for determination of PGE_2, $PGF_{2\alpha}$, and 6-keto-$PGF_{1\alpha}$. Upon collection, the biopsy specimens obtained from each area were immediately placed in an ice-cold plastic vial, put on dry ice, and subsequently stored at −70°C. The time between the collection of the biopsy specimen and the freezing on dry ice was ~30 s. Levels of PGE_2, $PGF_{2\alpha}$, and 6-keto-$PGF_{1\alpha}$ were measured in the mucosal biopsy specimens using a previously described method (14).

Briefly, the specimens were sonicated in saline containing 0.4% aspirin and 2% ethylenediaminetetraacetic acid and acidified (pH 3.2) by the addition of citric acid. Protein concentrations were determined by the method of Lowry et al. (15). Supernatants from the sonicated tissues were applied to individual C18 solid-phase extraction columns (Bond-Elut C18, Analytichem International, Harbor City, Calif.) and sequentially washed with citric acid, 12.5% methanol, and benzene. Prostaglandins were eluted off the C18 column with ethyl acetate. Samples of gastric juice were diluted 1:1 with water and adjusted to pH 3.2 with 2 M citric acid and vortexed. Acidified gastric juice samples were applied to extraction columns, the columns were sequentially washed, and the PG was recovered from the columns as described above. After N_2 evaporation of the ethyl acetate, extracts of tissue or juice were reconstituted in 100 μl of assay buffer, and levels of PGE_2 and 6-keto-$PGF_{1\alpha}$ were determined with ^{125}I-radioimmunoassay kits (New England Nuclear, Boston, Mass.). Prostaglandin $F_{2\alpha}$ levels were determined using ^{3}H-labeled PGF_2 tracer (New England Nuclear). Differences among PG levels in tissue and gastric juice were determined using a two-way analysis of variance.

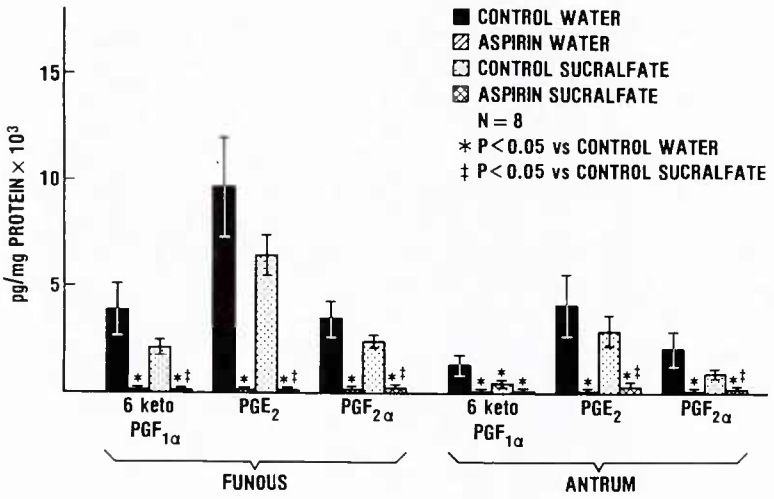

Figure 1. Effect of aspirin, sucralfate, and aspirin given with sucralfate on mucosal prostaglandin levels. Each bar represents the mean ± SE of values obtained in 8 monkeys.

Results

When compared to controls given water orally (CW), aspirin (s.c.) given along with water orally (AW) significantly suppressed the mucosal content of PGE_2, $PGF_{2\alpha}$, and 6-keto-$PGF_{1\alpha}$ in both the antrum and fundus (Figure 1). This inhibitory effect of aspirin on PG levels was not modified by the administration of sucralfate (AS). Similarly, aspirin significantly reduced the levels of PGE_2 and $PGF_{2\alpha}$ in the gastric juice (Figure 2). When compared with controls (CW), sucralfate alone (CS) did not alter the gastric juice level of PGE_2 but significantly decreased the content of $PGF_{2\alpha}$. Furthermore, sucralfate did not significantly modify the aspirin-induced inhibition of either PGE_2 or $PGF_{2\alpha}$ (AS). The level of 6-keto-$PGF_{1\alpha}$ in the gastric juice was not modified by any treatment.

Coincident with the inhibition of PG in the gastric tissue and gastric juice, aspirin produced an increase in endoscopic mucosal damage in the antrum, but not in the fundus, when compared with controls (Table 2). Although the difference was not significant, sucralfate (CS) tended to improve the endoscopic appearance of the mucosa when compared with controls and completely prevented ($p < 0.05$) the aspirin-induced damage (AS).

Control fasting fluid (0.13 ± 0.05 ml/min), as well as H^+ (3.7 ± 2.3 μEq/min), Na^+ (14.3 ± 2.3 μEq/min), K^+ (4.3 ± 1.3 μEq/min), and Cl^- (24.2 ± 5.3 μEq/

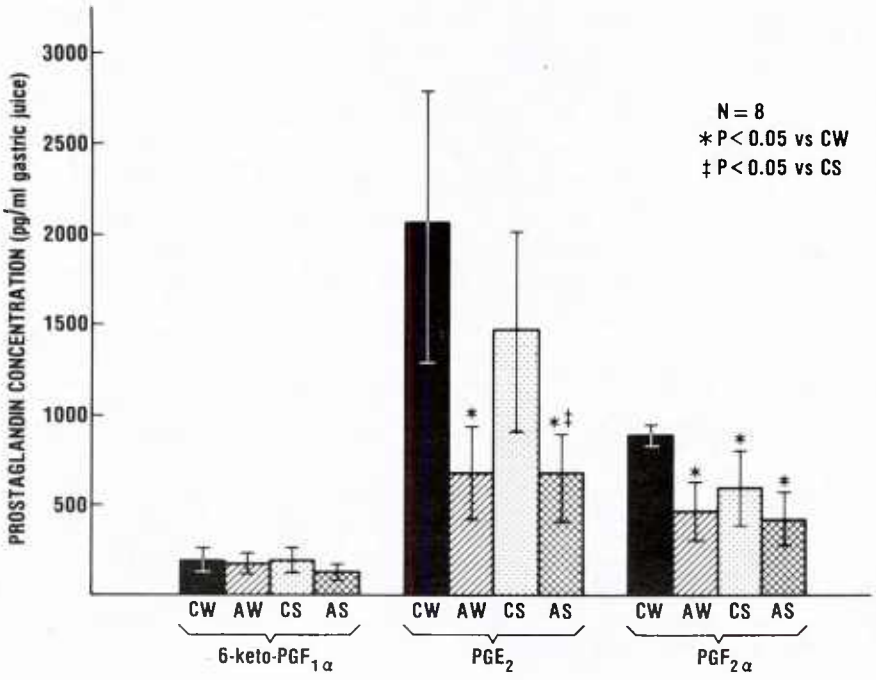

Figure 2. Effect of aspirin, sucralfate, and aspirin given with sucralfate on prostaglandin levels in the gastric juice. Each bar represents the mean ± SE of values obtained in 8 monkeys. AS, aspirin (s.c.) + sucralfate (oral); AW, aspirin (s.c.) + water (oral); CS, $NaHCO_3$ (s.c.) + sucralfate (oral); CW, $NaHCO_3$, (s.c.) + water (oral).

Table 2. Effect of Subcutaneous Aspirin, Oral Sucralfate, and Subcutaneous Aspirin Given With Oral Sucralfate on Gastric Mucosal Damage

Agent			
Subcutaneous	Oral	Symbol	Score
$NaHCO_3$	Water	CW	0.8 ± 0.5
Aspirin	Water	AW	2.5 ± 0.8[a]
$NaHCO_3$	Sucralfate	CS	0.0 ± 0.0
Aspirin	Sucralfate	AS	0.3 ± 0.1[b]

Values are mean ± SE of measurements in 8 monkeys. [a] $p < 0.05$ vs. CW and [b] $p < 0.05$ vs. AW using a two-way analysis of variance.

min) outputs were not significantly altered by any treatment. After the water load, however, fluid, Na^+, and K^+ outputs were significantly decreased by aspirin (Table 3). Sucralfate did not alter the aspirin-induced reduction of Na^+ output, but it did attenuate the effect of aspirin on fluid and K^+ output. Postload H^+ and Cl^- outputs were not significantly altered by any treatment.

Neutral glycoprotein output was not significantly altered by any treatment, during either the fasting (0.28 ± 0.05 mg mucin eq/min) or postload (Table 3) periods. In contrast, sucralfate significantly ($p < 0.05$) increased fasting AG output, and aspirin did not modify this sucralfate stimulation of AG output (AS; Figure 3). Postload AG output was not significantly altered by any treatment (CW, 1.7 ± 0.4; AW, 0.6 ± 0.7; CS, 1.1 ± 0.7; AS, 1.1 ± 0.7 mg mucin eq/min).

Discussion

Aspirin can cause gastric mucosal damage both when given intragastrically (16,17) and parenterally (18–20), a phenomenon that is assumed to be mediated by a suppression of endogenous PG production (21,22). In the present study, parenteral aspirin induced a significant decrease in the PG content of the gastric mucosa and gastric juice. Prostaglandins in the gastric juice are thought to reflect release of PGs by the gastric mucosa, whereas mucosal PGs are an index of synthetic ability (17). Moreover, the concentration of PG secreted into the lumen has been considered to accurately reflect local endogenous PG production (22). It is of interest to note that, in the current study, aspirin was more effective in lowering the concentration of PG in the mucosa than in the gastric juice. McCready et al. (23) also observed this difference in humans, raising the possibility of an additional source of PG that contributes to PG present in the lumen.

The decrease in PG in both gastric mucosa and gastric juice in the current study was associated with an increase in gastric mucosal damage. Sucralfate completely prevented the gastric damage, but not the suppression of PG. Previous studies on the ability of sucralfate to protect against aspirin-induced damage are conflicting. Sucralfate has been shown to reduce (24,25) or to have no effect (26) on gastric damage induced by intragastric aspirin. The discrepancy among these observations may be due to differences in the time-course of drug administration, in the method of administration (i.e., tablet or suspension), as well as in the dose of sucralfate given. In humans, tablets of sucralfate (1 g, q.i.d.) protected against aspirin damage when given orally 30 min before oral administration of aspirin tablets (900 mg, q.i.d.) (25) but not when given *simultaneously* with aspirin (650 mg, q.i.d.) (26). In contrast, higher doses (300 mg/kg) of sucralfate given in solution concurrently with a solution of aspirin (150 mg/kg) reduced gastric damage in rats (24).

The mechanism by which sucralfate exerts its gastroprotective effect is unclear. In rats, high doses (28–56 g for a man weighing 70 kg) of sucralfate have been shown to increase the content of PGE_2 in the gastric juice (6,27) and to enhance the ability of the tissue to synthesize PGE_2 (28). It has been proposed, therefore, that the protective effect of this drug is mediated via PGs. However, the ability of sucralfate to completely prevent aspirin-induced injury in the present study suggests that, in primates, the protective action of sucralfate is independent of endogenous PG production. Moreover, sucralfate did not significantly alter PGE_2, $PGF_{2\alpha}$, or 6-keto-$PGF_{1\alpha}$ lev-

Table 3. Postload Fluid, Ion, and Neutral Glycoprotein Output

	Fluid output (ml/min)	H^+ output (μEq/min)	Na^+ output (μEq/min)	K^+ output (μEq/min)	Cl^- output (μEq/min)	NG output (mg mucin eq/min)
CW	0.29 ± 0.03	10.9 ± 4.4	20.0 ± 4.7	4.8 ± 1.0	32.8 ± 4.8	0.55 ± 0.15
AW	0.18 ± 0.11	2.9 ± 1.5	11.9 ± 1.7[a]	2.9 ± 1.0[b]	32.0 ± 10.9	0.31 ± 0.13
CS	0.29 ± 0.03	17.4 ± 8.3	16.5 ± 2.6	5.1 ± 1.5	42.8 ± 12.2	0.29 ± 0.12
AS	0.29 ± 0.05	7.9 ± 6.4	12.6 ± 1.7[a]	3.7 ± 1.1	25.4 ± 7.9	0.39 ± 0.12

AS, aspirin (s.c.) + sucralfate (oral); AW, aspirin (s.c.) + water (oral); CS, $NaHCO_3$ (s.c.) + sucralfate (oral); CW, $NaHCO_3$, (s.c.) + water (oral); NG, neutral glycoprotein. Values are mean ± SE of measurements in 8 monkeys. [a] $p < 0.05$ and [b] $p < 0.01$ when compared to CW using a three-factor analysis of variance (treatment, time, and monkey) with repeated measures on the last two factors.

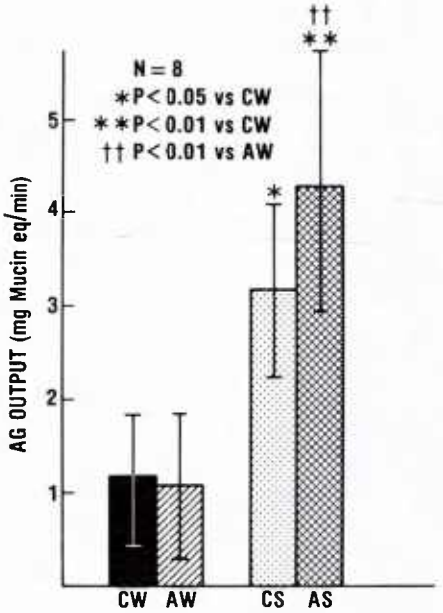

Figure 3. Fasting acidic glycoprotein (AG) output after aspirin, sucralfate, and aspirin given with sucralfate. Each *bar* represents the mean ± SE of values obtained in 8 monkeys. AS, aspirin (s.c.) + sucralfate (oral); AW, aspirin (s.c.) + water (oral); CS, $NaHCO_3$ (s.c.) + sucralfate (oral); CW, $NaHCO_3$ (s.c.) + water (oral).

els in either the mucosal biopsy specimens or in the gastric juice. In fact, after sucralfate, all values tended to be slightly lower than controls, with a significant decrease in the content of 6-keto-$PGF_{1\alpha}$ in the antrum and of $PGF_{2\alpha}$ in the gastric juice. In addition, sucralfate did not alter the aspirin-induced inhibition of PG. The discrepancy between the effect of sucralfate on PG in the present study and in previous studies may be due to the dose of sucralfate given. The dose of sucralfate in the present study was 25 mg/kg twice daily suspended in 3 ml of water, which is based on the recommended therapeutic dose for humans of 1 g, q.i.d. In contrast, the dose was considerably greater (~500–1000 mg/kg) in studies showing an increase in PGE_2 after sucralfate (7,27,28). Therefore, we conclude that the protective effect of sucralfate appears to be independent of endogenous PG production in primates.

Our studies suggest that protection by sucralfate may be related to a PG-independent enhancement of mucus secretion. Sucralfate significantly increased AG output during the fasting period, an effect that was not diminished by aspirin. Neutral glycoprotein output also tended to be enhanced by sucralfate but the change was not significant. This difference in the effect of sucralfate on AG and NG output may be attributed to a selective effect of sucralfate on individual populations of mucus-secreting cells. The gastric mucosa has several histologically distinct cell types, which secrete biochemically distinct mucins. Mucus cells located on the gastric surface and in gastric pits contain a highly sulfated mucus that is stained by Alcian blue, as well as NGs that stain with periodic acid–Schiff (29). In contrast, the mucus neck cells contain predominantly NGs (29). Thus, sucralfate, acting from the luminal side, might be expected to influence mucus-containing cells on or near the surface rather than those lying deeper in the gastric pits. Changes in AG, but not NG, output were also observed after γ-irradiation (9). Two days after irradiation, AG secretion was significantly suppressed, whereas NG output was normal. Concurrent with these changes in mucus output, scanning electron microscopy of mucosal biopsy specimens revealed an absence of surface mucosal cells and exposure of lamina propria in certain areas (30). In addition, there was a persistence of ulceration at the sites of biopsy specimens obtained on the day of irradiation. Thus, it appears that after three very different treatments (sucralfate, aspirin, and irradiation), an increase in AG secretion was coincident with mucosal protection, or a decrease in AG output was associated with mucosal damage.

Decreases in the quantity and quality of mucus glycoproteins have been associated with gastric mucosal injury after oral administration of aspirin (16,31,32). This damage may reflect changes in the integrity of the surface epithelial cells producing the mucus gel layer or in the ability of the cells to synthesize and release mucus. Correlations between the thickness of the mucus gel layer (insoluble mucus) and the concentration of soluble mucus in the gastric juice are controversial. McQueen et al. (33) observed that changes in insoluble mucus did not correlate with changes in the NG concentration in the gastric juice. Recent studies, however, have demonstrated that increases in AG concentrations of soluble mucus were positively correlated with changes in the AG concentration of the adherent mucus gel (34), and paralleled morphologic observations of hypertrophy of mucus-containing epithelial cells (9,30). Thus, changes in soluble AG may reflect similar alterations in surface AG under certain conditions.

Aspirin inhibited both Na^+ and K^+ output but did not have a significant effect on either fluid or Cl^- output. This finding is consistent with data demonstrating an increase in Na^+ output after PGE_2 (35) and a decrease in Na^+ output after indomethacin (14). H^+ output also tended to be slightly lower after aspirin but the change was not significant. This decrease may be due to a back diffusion of H^+ associated with gastric mucosal injury, to a reduction in gastric mucosal blood flow, or to a direct action of aspirin on parietal cells. In support of this,

aspirin has been postulated to inhibit adenosine triphosphate production by uncoupling of oxidative phosphorylation or to antagonize the action of acetylcholine on parietal cells (36). This inhibitory effect, however, appears to be specific for aspirin, as other nonsteroidal antiinflammatory drugs, such as indomethacin, have been found to increase H^+ output (14). Sucralfate alone had no effect on fluid or ion output. Moreover, sucralfate did not alter the inhibitory effect of aspirin on Na^+ output, but attenuated the inhibitory effect of aspirin on K^+ output. Small changes in ion output have been associated with protection after PG, or disruption of the gastric mucosa after aspirin, and are thought to reflect the functional state of the mucosa. Thus, the lack of an effect of sucralfate on aspirin-induced alteration in Na^+ output indicates that sucralfate does not modify the functional changes produced by aspirin, although it does protect the gastric mucosa. Moreover, these findings suggest that the protective action of sucralfate is independent of changes in acid or alkaline secretion.

In conclusion, sucralfate prevents the gastric mucosal damage produced by parenteral aspirin by a mechanism that appears to be independent of PG. This conclusion is further supported by the fact that sucralfate did not elevate PG in either the gastric mucosa or the gastric juice. In addition, sucralfate increased the output of soluble mucus in the gastric juice both in the presence and absence of aspirin. Thus, the present study indicates that the protective action of sucralfate may be attributed to a PG-independent increase in gastric mucus secretion.

References

1. Lam SK, Lau WY, Cai CL, et al. Efficacy of sucralfate in corpus, prepyloric, and duodenal ulcer—associated gastric ulcers: a double-blind, placebo-controlled study. Am J Med 1985;79:24–31.
2. Hollander D. Efficacy of sucralfate for duodenal ulcers: a multicenter, double-blind trial. J Clin Gastroenterol 1981; 3:153–7.
3. Marks IN, Wright JP, Girdwood AH, Gilinsky NH, Lucke W. Maintenance therapy with sucralfate reduces rate of gastric ulcer recurrence. Am J Med 1985;79:32–5.
4. Moshal MG, Spitaels JM, Manion GL. Double-blind placebo-controlled evaluation of one year therapy with sucralfate in healed duodenal ulcer. Scand J Gastroenterol 1982;18(Suppl. 83):57–9.
5. Hollander D, Tarnawski A, Krause WJ, Gergely H. Protective effect of sucralfate against alcohol-induced gastric mucosal injury in the rat. Macroscopic, histologic, ultrastructural, and functional time sequence analysis. Gastroenterology 1985; 88:366–74.
6. Hollander D, Tarnawski A, Gergely H, Zipser RD. Sucralfate protection of gastric mucosa against alcohol induced necrosis: a prostaglandin mediated process. Scand J Gastroenterol 1984;19(Suppl. 101):97–102.
7. Dubois A, Van Erdewegh P, Gardner J. Gastric emptying and secretion in Zollinger–Ellison syndrome. J Clin Invest 1977;59:255–63.
8. Danquechin-Dorval E, Mueller GP, Eng RR, Durakovic A, Conklin JJ, Dubois A. Effect of ionizing radiation on gastric secretion and gastric motility in monkeys. Gastroenterology 1985;89:374–80.
9. Shea-Donohue PT, Danquechin-Dorval E, Montcalm E, et al. Alterations in gastric mucus secretion in rhesus monkeys after exposure to ionizing radiation. Gastroenterology 1985; 88:685–90.
10. George J. New clinical method for measuring the rate of gastric emptying: the double sampling test meal. Gut 1968;9:237–42.
11. Hildes HA, Dunlop KL. A method for estimating the ratio of gastric secretion and emptying. Can J Med Sci 1951;29:83–9.
12. Kirk RE. Procedures for the behavioral sciences. In: Experimental design. Monterey, Calif.: Brooks/Cole, 1968;110–2.
13. Lanza FL, Royer GL, Nelson RS. Endoscopic evaluation of the effects of aspirin, buffered aspirin, and enteric-coated aspirin on gastric and duodenal mucosa. N Engl J Med 1980; 303:136–8.
14. El-Bayer H, Steel L, Montcalm E, Danquechin-Dorval E, Dubois A, Shea-Donohue T. The role of endogenous prostaglandins in the regulation of gastric secretion in rhesus monkeys. Prostaglandins 1985;30:401–19.
15. Lowry OH, Rosenbrough NJ, Farr AL, et al. Protein measurement with Folin phenol reagent. J Biol Chem 1951;193: 265–75.
16. Lev R, Siegal HI, Glass GBJ. Effects of salicylates on the canine stomach: a morphological and histochemical study. Gastroenterology 1972;62:970–80.
17. Cohen MM, MacDonald WC. Mechanisms of aspirin injury to human gastro-duodenal mucosa. Prostaglandins Leukotrienes Med 1982;9:241–5.
18. Bugat R, Thompson MR, Aures D, Grossman MI. Gastric mucosal lesions produced by intravenous infusion of aspirin in cats. Gastroenterology 1976;71:754–9.
19. Kauffman G, Grossman MI. Prostaglandin and cimetidine inhibit the formation of ulcers produced by parenteral salicylates. Gastroenterology 1978;75:1099–102.
20. Hansen D, Aures D, Grossman MI. Comparison of intravenous and intragastric aspirin in production of antral gastric ulcers in cats. Proc Soc Exp Biol Med 1980;164:589–92.
21. Konturek SJ, Obtulowicz W, Sito E, Oleksy J, Wilkon S, Kiec-Dembinska A. Distribution of prostaglandin in gastric and duodenal mucosa of healthy subjects and duodenal ulcer patients: effects of aspirin and paracetamol. Gut 1981; 22:283–9.
22. Johansson C, Bergstrom S. Prostaglandins and protection of the gastroduodenal mucosa. Scand J Gastroenterol 1982; 18(Suppl. 77):21–46.
23. McCready DR, Wallace JL, Cohen MM. Prostaglandin biosynthesis by gastric mucosa. II. Studies in man. Clin Biochem 1984;17:183–7.
24. Danesh BJZ, Duncan A, Mitchell G, Russell RI. Effect of sucralfate on the occurrence of mucosal damage induced in rats, by acetylsalicylic acid (ASA) alone and when combined with taurodeoxycholic acid (TDCA), at different pH values (abstr). Gastroenterology 1985;88:1359.
25. Tesler MA, Lim ES. Protection of the gastric mucosa by sucralfate from aspirin-induced erosions. J Clin Gastroenterol 1981;3:175–9.
26. Wu WC, Castell DO. Does sucralfate protect against aspirin-induced mucosal lesions? Yes and no (abstr)! Gastroenterology 1984;86:1303.
27. Quadros E, Ramsamooj E, Wilson DE. Relationship between

sucralfate, gastric cytoprotection and prostaglandin and mucus synthesis and secretion (abstr). Gastroenterology 1985; 88:1548.
28. Ligumsky M, Karmeli F, Rachmilewitz D. Sucralfate stimulation of gastric PGE_2 synthesis—possible mechanism to explain its effective cytoprotective properties (abstr). Gastroenterology 1984;86:1164.
29. Zalewsky CA, Moody EF. Mechanisms of mucus release in exposed canine gastric mucosa. Gastroenterology 1979; 77:719–29.
30. Dubois A, Danquechin-Dorval E, Wood L, et al. Effect of γ-irradiation on the healing of gastric biopsy sites in monkeys. An experimental model for peptic ulcer disease and gastric protection. Gastroenterology 1985;88:375–81.
31. Saroseik J, Slomiany BL, Swierczek J, Slomiany A, Jozwiak Z, Konturek SJ. Effect of acetylsalicylic acid on the constituents of the gastric mucosal barrier. Scand J Gastroenterol 1984; 19:150–3.
32. Menguy R, Masters YF. Effects of aspirin on gastric mucous secretions. Surg Gynecol Obstet 1965;120:92–8.
33. McQueen S, Hutton D, Allen A, Garner A. Gastric and duodenal surface mucus gel thickness in rat: effects of prostaglandins and damaging agents. Am J Physiol 1983;8: G388–93.
34. Lamont JT, Ventola AS, Maull EA, Szabo S. Cysteamine and prostaglandin $F_{2\beta}$ stimulate rat gastric mucin release. Gastroenterology 1983;84:306–13.
35. Shea-Donohue PT, Nompleggi D, Myers L, Dubois A. A comparison of the effects of prostacyclin and the 15(S) 15-methyl analogs of PGE_2 and $PGF_{2\alpha}$ on gastric parietal and non-parietal secretion. Dig Dis Sci 1982;27:17–22.
36. Rainsford KD. Gastrointestinal and other side-effects from the use of aspirin and related drugs; biochemical studies on the mechanisms of gastrotoxicity. In: Rainsford KD, Brune K, Whitehouse MM, eds. Proceedings of the symposium on aspirin and related drugs: their actions and uses. Stuttgart: Bukhauser Verlag, Basel, 1977:59–70.

INT. J. RADIAT. BIOL., 1986, VOL. 50, NO. 4, 695–715

Urinary excretion of cyclic nucleotides, creatinine prostaglandin E_2 and thromboxane B_2 from mice exposed to whole-body irradiation from an enhanced neutron field

L. K. STEEL, M. A. RAFFERTY, W. W. WOLFE, J. E. EGAN, D. A. KENNEDY, G. N. CATRAVAS, W. E. JACKSON, III and M. A. DOOLEY

Biochemistry, Computer and Radiological Sciences Departments, Armed Forces Radiobiology Research Institute, Bethesda, Maryland 20814-5145, U.S.A.

(*Received 8 August 1985; final revision received 6 February 1986; accepted 18 February 1986*)

Urine volume and excretion of cyclic AMP, cyclic GMP, prostaglandin E_2 (PGE_2), thromboxane B_2 (TxB_2) and creatinine were evaluated as potential indicators of radiation damage in mice given 2–5 Gy to the whole body from an enhanced neutron field. In general, urinary cyclic AMP, cyclic GMP, creatinine and urine volumes were positively correlated across time postexposure, for each radiation dose. TxB_2 levels positively correlated with urine volume and cyclic AMP excretion only in animals given 2·0 Gy. None of these parameters suggests their use as a prognostic indicator of the extent of radiation damage. Urinary excretion of PGE_2 was negatively correlated with other urinary parameters. Biphasic increases in urinary PGE_2 were also observed. The initial transient elevation 2–3 days postexposure was not correlated with the dose (2–5 Gy). The second elevation of PGE_2 excretion occurred at 6–10 days. The magnitude of the latter increase suggests that urinary PGE_2 excretion may be a useful indicator of whole-body or kidney exposure to neutron fields.

Indexing terms: prostaglandin E_2, thromboxane B_2, cyclic AMP, cyclic GMP, creatinine, neutrons.

1. Introduction

It is now documented that exposure of animals to ionizing radiation affects the synthesis and/or release of a variety of biochemicals. Many of these substances are eliminated from the body in the urine and several of these show increasing levels with increasing dose of radiation (Donlon *et al.* 1983, 1985, Schneidkraut *et al.* 1983). Most such studies have been performed with rats; however, several reports of altered metabolite excretion have been described in the guinea pig (Steel *et al.* 1984), mouse, dog, monkey, radiotherapy patients, and radiation accident victims (for review see Gerber and Altman (1970)).

The elegant experiments of Williams and Denekamp (1983, 1984) and Stewart *et al.* (1978, 1984) have demonstrated that urination frequency and isotope clearance can be used as noninvasive indicators of late renal damage following localized, fractionated, bilateral kidney irradiation in the mouse. Our interest in whole-body radiation effects has been directed toward determining whether urinary metabolites are feasible for quantitative correlation of biochemical changes and pathophysiological effects with radiation dose and quality. Changes in tissue mediators and

intracellular messengers with potent pharmacological actions may play an important role in tissue response and development of radiation sickness.

Previous studies have shown that ionizing radiation increases *in vivo* and *in vitro* synthesis of cyclo-oxygenase products of arachidonate (Steel and Catravas 1982, Donlon *et al.* 1983, 1985, Schneidkraut *et al.* 1983, 1984). The ubiquitous production of the arachidonate metabolites, prostaglandin E_2 (PGE_2) and thromboxane A_2 (TxA_2), coupled with their roles in the development and modulation of immune processes and inflammation, have been established (for reviews see Goodwin and Webb (1980), Kunkel *et al.* (1984), Dunn and Hood (1977), Trang (1980)). The antagonistic activities of prostaglandins in several symptoms of radiation damage such as increased intestinal motility (Borowska *et al.* 1979), diarrhoea, flatulence, abdominal pain (Mennie *et al.* 1975), esophagitis (Northway *et al.* 1982) and mucositis (Tanner *et al.* 1981) have also been demonstrated. Conversely, exogenous prostaglandins, particularly of the E type, have been shown to improve survival of irradiated mammalian cells in culture (Prasad 1972) and gastrointestinal crypt cells *in vivo* (Hanson and Thomas 1983, Uribe *et al.* 1984, Thomas de-la Vega *et al.* 1984). In view of the antagonistic as well as cytoprotective properties of these mediators, their contributions to the biochemical and pathological events associated with radiation injury require clarification.

The actions of many mediators, as well as a number of peptide hormones, are largely expressed by their regulation of intracellular levels of cyclic AMP (cAMP) and cyclic GMP (cGMP) (for reviews see Sutherland *et al.* (1967), Sutherland (1970)). The clinical diagnostic use of urinary cyclic nucleotides (Murad 1973, Pak 1980) has been reported in several endocrine and metabolic disorders. Therefore, the present studies examined these urinary metabolites as potential indicators of radiation damage in the mouse. Urine output and creatinine levels were measured to qualitatively evaluate glomerular filtration and metabolic state of the animals. The excretion patterns of the cyclo-oxygenase products, PGE_2 and TxB_2 (the stable metabolite of TxA_2) were also determined. Radiation doses ranging from nonlethal to those resulting in 100 per cent mortality were studied in order to ascertain dose-response information.

2. Materials and methods

2.1. *Protocol and assays*

Experiments were performed in the following calendar months and years: 2·0 Gy, December 1984–March 1985; 3·0 Gy, February–May 1984; 3·5 Gy, March–June and April–July 1984; 3·67 Gy, June–September 1984; 3·85 Gy, July–October 1984, 4·0 Gy, August–November 1984; 4·25 Gy, July–August 1983; 5·0 Gy, April and December 1983. B6D2F1 (C57BL/6JxDBA/2J) female mice were obtained from Jackson Labs (Bar Harbor, ME). Animals were housed in groups of 9 for two weeks in a quarantine facility. Those determined to be free of histological lesions or common murine diseases (random sampling) and whose sterile water bottle cultures were negative for *Pseudomonas* species were used. Mice weighing 22–24 g (14–16 wks old) were randomly selected and housed in Lucite metabolic cages (Robertson Instrument Co., Seabrook, MD), three animals per cage, for a period of 7 days in order to acclimatize them to their new environment and before initiating urine collection. The mice were kept on a 7 a.m. (light) to 7 p.m. (dark) cycle and transferred to clean cages at 10 a.m. daily. Standard rodent diet (Wayne Lab Blox,

Continental Grain Co., Chicago, IL) and double distilled water were provided *ad libitum*. Seven days prior to irradiation and up to 30 days postexposure, urine was collected from each 3-animal cage at 24 h intervals. A funnel and diverter successfully separated urine samples from contaminating faecal or food material. Vaporization-resistant collection vessels were used to minimize losses due to evaporation. No preservatives were added to the collection vessels or urine samples. The volume of each urine collection was measured to an accuracy of 0·01 ml and aliquots sampled for subsequent analyses. All daily urine collections and aliquots thereof were frozen at −70°C. Subsequent analyses were performed on 'first thaw' material.

Prepacked silica gel columns (500 mg sorbent mass) were purchased from Analytichem International (Harbor City, CA). ^{125}I-PGE_2, ^{125}I-cAMP and ^{125}I-cGMP radioimmunoassay kits and ^{3}H-TxB_2 (120 Ci/mmol) were obtained from New England Nuclear (Boston, MA). Thromboxane B_2 was the generous gift of Dr. John Pike (Upjohn Co., Kalamazoo, MI). Creatinine reagents and standards were purchased from Gilford Diagnostics (Cleveland, OH). Chemicals and solvents were A.C.S. grade.

Urine samples were diluted 1 : 10 with 0·05 M sodium acetate buffer (pH 6·2) containing 0·1 per cent sodium azide, and 10 μl of the diluted sample was used for radioimmunoassay determination of urinary cAMP and cGMP concentrations (Steiner *et al.* 1972). Analyses were performed in duplicate using ^{125}I-cAMP and ^{125}I-cGMP radioimmunoassay kits. The sensitivity of the radioimmunoassays (New England Nuclear, Boston, MA) were 0·10–25·0 pmol cAMP and 0·05–10·0 pmol cGMP, per assay. Cross-reactivity of the cAMP antiserum (at 50 per cent displacement) was 100 per cent with cAMP and less than 0·0005 per cent with cGMP, AMP, ADP or ATP. Cyclic GMP antiserum was 100 per cent cross-reactive with cGMP and less than 0·007 per cent reactive with cAMP, ATP, GTP, GDP and GMP. Several pre- and postexposure urine samples were incubated with cyclic nucleotide phosphodiesterase (0·2 Units) or spiked with known quantities of cAMP or cGMP. Nucleotides present in the samples were degraded more than 93 per cent by the phosphodiesterase, and added nucleotides yielded measured values within 5 per cent of the predicted values.

Urinary creatinine was determined using the Gilford Diagnostics creatinine assay procedure, and the modified reagent system previously described by Fabiny and Ertingshausen (1971). Urine samples were diluted 1 : 20 (v/v) with distilled water and analysed on a programmed Gilford 2035 Clinical Chemistry Analyzer System (Gilford Diagnostics, Cleveland, OH). Some samples were also diluted 1 : 10, 1 : 30, or combined with known quantities of creatinine, as additional controls of assay performance.

Urine samples (2 ml) were prepared for prostaglandin analysis by organic extraction and purification on silica (SI) columns (Powell 1980, Siess and Drey 1982). Briefly, urines were acidified to pH 3·2 by the addition of 200 μl 2 M citric acid, and extracted with 4 ml ethyl acetate. Tubes were capped and mixed for 20 min on a shaker platform, then centrifuged at 1000 ***g*** for 5 min to separate phases. Two millilitres of the organic phase was applied to a pre-washed (methanol), equilibrated (benzene–ethyl acetate, 80 : 20 v/v) SI column. The columns were sequentially washed with: (a) benzene–ethyl acetate (80 : 20), (*b*) benzene–ethyl acetate (80 : 40), (*c*) benzene–ethyl acetate–methanol (60 : 40 : 2), and (*d*) benzene–ethyl acetate–methanol (60 : 40 : 10). Prostaglandins were eluted with a solvent mixture of

benzene–ethyl acetate–methanol (60 : 40 : 30), and evaporated to dryness under N_2. Representative urine samples spiked with radiolabelled PGE_2 and TxB_2 and processed by these methods revealed greater than 90 per cent recovery.

The dried column extracts were reconstituted in buffer (50 mM phosphate-buffered saline [pH 6·8] containing 1 per cent bovine gamma globulin and 0·05 per cent sodium azide). PGE_2 levels were determined using ^{125}I-radioimmunoassay kits. TxB_2 levels were determined with ^{3}H-TxB_2 tracer, TxB_2 antisera and TxB_2 standards (0·1 to 500 pg), prepared in buffer. The radioimmunoassay procedure was performed as described previously (Steel and Catravas 1982, Steel *et al.* 1983). TxB_2 antiserum specificity was previously reported (Steel and Catravas 1982).

For each cage of three mice, total urine volume was recorded in ml/24 h. Subsequent to analyses, each urinary biochemical parameter was first recorded in nmol/ml (cAMP, cGMP) picograms (pg)/ml (PGE_2, TxB_2) and mg/ml (creatinine) and then converted to nmol/24 h, pg/24 h and mg/24 h, respectively. For each cage (three animals), the seven-day, 24 h preirradiation values for each respective urinary parameter were averaged and this average served as baseline for that cage. Since each cage represents the combined contribution of three mice, it was also necessary to calculate the data on a per-animal basis to account for animal deaths following radiation exposure. This calculation assumes an equal sample contribution from each mouse, which may not be the case for those that were more severely injured by radiation exposure. Animals within each cage were earmarked for individual identification and the onset of morbidity (no food or water consumption, no defecation or urination, immobility) was recorded. In our experience, an animal which dies during the 24 h collection period does not contribute to the urine sample of its cage for that 24 h collection. Thus, the data point for the cage was calculated, per animal, on the basis of the number of surviving (excreting) mice (i.e. divided by 1, 2 or 3).

2.2. *Irradiations*

Mice were exposed within the array previously described (Stewart *et al.* 1982) using the AFRRI TRIGA Mark-F Reactor. Each mouse was restrained in a perforated aluminium cylinder and two cylinders were vertically stacked and rotated within the field at 1·5 r.p.m. on an aluminium rotator during the irradiation (Stewart *et al.* 1982). Irradiations to the whole body of up to 18 mice were delivered at a midline tissue (MLT) dose rate of 0·4 Gy/min. The total dose ranged from 2·0 to 5·0 Gy. A minimum of nine cages (three mice per cage) were employed at each dose.

Dosimetry was performed in the high neutron array (6 inch lead shield and 2 inch lead cave (Stewart *et al.* 1982) using the paired chamber technique described previously (ICRU Report 1976, Broerse *et al.* 1981, AAPM Report 1980). A 0·5 cm^3 Exradin model T-2 tissue equivalent (TE) chamber with methane-based TE gas, and a 0·5 cm^3 Exradin model M-2 magnesium chamber with argon gas (Meeker 1980) were placed inside tissue equivalent (A150 plastic) mouse phantoms (2·54 cm in diameter) at various positions in the array. All chamber calibrations are traceable to the National Bureau of Standards, and the compositions of A150 plastic and TE gas are cited elsewhere (ICRU Report 1976). The physical contents used in evaluating the chamber readings were calculated (Zeman and Ferlic 1984, Waterman *et al.* 1979) based on the available spectral data for this array (Verbinski *et al.* 1981). The absolute accuracy of the dose measurements is dependent on these constants and is considered to be between 5 and 10 per cent (Broerse *et al.* 1981). The variation

of neutron fluence across the array was determined by placing indium activation foils inside plastic mouse phantoms at each position. The precision of these measurements was approximately 2·5 per cent.

The results of the above dosimetry indicated a nominal MLT dose rate of 0·4 Gy/min at a reactor power of 4·5 kW, with a variation of −5 to +2 per cent across the array. The gamma component of the MLT dose was approximately 4·5 per cent of the total dose (neutron to gamma ratio of approximately 21). From the spectral information (Verbinski *et al.* 1981) the average neutron and gamma energies are estimated to be 0·68 MeV and 1·8 MeV, respectively (Zeman *et al.* 1984).

2.3. *Statistical analyses*

Irradiated animals were observed for 100 days. Survival fractions were constructed for each radiation dose and data examined by probit analysis (Finney 1971). Basal (preirradiation) excretion rates of urine volume and biochemical constituents were analysed for their degree of relationship by Spearman's rank (Rho) correlation (Conover 1980). A Student's *t* test for paired samples (Snedecor and Cochran 1980 a) was applied to determine significance between postirradiation values of each parameter and baseline values for each respective radiation dose. Groups in which two animals died were not included in tests for significance. Correlations across postirradiation time for the parameters, at each dose, were analysed by Spearman's rank correlation (Conover 1980). One-way analysis of variance (Snedecor and Cochran 1980 b) was applied to test for differences between the means within each parameter, across radiation doses, for each sampling day postirradiation. When variances between groups differed, Welch's Test (Welch 1951) was used instead of the one-way analysis of variance. A Newman–Keul's comparison test was used after each significant one-way analysis of variance, to distinguish between means.

3. Results

3.1. *Control excretion rates*

Daily control (preirradiation) excretion rates of urine volume, creatinine, cAMP, cGMP, TxB_2 and PGE_2 are presented in table 1. Analysis of the urinary parameters across time, for each day of the seven preirradiation samples (Spearman's rank (Rho) correlation (Conover 1980)) indicated a significant positive correlation between cGMP excretion and urine volume ($P \leqslant 0{\cdot}05$), and cGMP and cAMP excretion ($P \leqslant 0{\cdot}01$). No other relationships were significantly correlated ($P > 0{\cdot}05$). Urine volume ranged from 0·8 to 1·35 ml/mouse/24 h, with an overall average excretion rate of $1{\cdot}17 \pm 0{\cdot}05$ (11 experiments, 96 cages of three animals, and seven 24 h preirradiation collections). Other biochemical parameters ranged (and averaged) as follows: creatinine, 0·75–1·01 mg (average $0{\cdot}84 \pm 0{\cdot}03$ mg/mouse/24 h); cAMP, 14·07–21·08 nmol (average 16·47–0·73 nmol/mouse/24 h); 4·35–8·18 nmol (average $6{\cdot}47 \pm 0{\cdot}30$ nmol/mouse/24 h); PGE_2, 211·12–426·67 pg (average $311{\cdot}79 \pm 25{\cdot}65$ pg/mouse/24 h; and TxB_2, 390·67–643·17 pg (average $472{\cdot}86 \pm 29{\cdot}70$ pg/mouse/24 h). The average control excretion rates were relatively constant within each radiation group (see legends to figures 1–6).

A slight (albeit insignificant) seasonal variation was observed in the volume of urine, creatinine and cyclic nucleotide control excretion rates. Urine output and creatinine excretion tended to be lower during the winter months (November–January) and modestly higher ($P > 0{\cdot}05$, Snedecor and Cochran 1980 a) during the

Table 1. Preirradiation values of urine volume and biochemical constituents from B6D2F1 female mice†.

Indicator	Day preirradiation						
	−6	−5	−4	−3	−2	−1	0
Urine volume ml/24 h	1·16 ± 0·09‡	1·31 ± 0·06	1·21 ± 0·01	1·12 ± 0·06	1·11 ± 0·04	1·14 ± 0·11	1·12 ± 0·04
Creatinine mg/24 h	0·89 ± 0·03	0·89 ± 0·06	0·82 ± 0·04	0·84 ± 0·01	0·81 ± 0·02	0·84 ± 0·05	0·82 ± 0·02
cAMP nmol/24 h	17·34 ± 0·06	17·40 ± 0·45	15·69 ± 0·60	15·56 ± 0·82	15·43 ± 0·47	17·36 ± 0·87	16·47 ± 0·70
cGMP nmol/24 h	6·98 ± 0·16	7·06 ± 0·21	6·40 ± 0·04	5·82 ± 0·22	5·83 ± 0·11	6·83 ± 0·33	6·33 ± 0·36
TxB_2 pg/24 h	557·97 ± 6·15	530·88 ± 71·31	497·59 ± 23·23	512·72 ± 80·66	393·56 ± 29·07	389·64 ± 34·44	428·55 ± 51·59
PGE_2 pg/24 h	317·68 ± 35·25	343·50 ± 45·29	297·14 ± 24·09	254·11 ± 6·11	287·78 ± 16·76	314·07 ± 33·40	370·07 ± 47·02

† Each parameter was measured for 7 consecutive days prior to irradiation as described in the text.
‡ 24 h excretion rate per animal (mean ± s.e.m.; 11 experiments, 96 cages of three animals).

summer (June–September). Cyclic AMP and cGMP excretions were slightly higher during the winter and relatively constant during the other seasons (data not shown). The large variation in basal arachidonate metabolite excretion in the different groups of animals was similarly examined for seasonal influences. Urinary TxB_2 excretion was significant lower ($P<0{\cdot}001$; Snedecor and Cochran 1980 a) in experiments performed in December and January. Urinary PGE_2 concentrations were highest in December and January, and significantly lower ($P<0{\cdot}001$) August to November.

3.2. *Survival*

Deaths were recorded daily for 100 days following irradiation. Probit analysis was applied to obtain the best-fitting dose–mortality probit line and the 95 per cent confidence intervals (C.I.) were caclulated (data not shown). The estimated LD50/100 value is 3·97 Gy (95 per cent C.I., 3·92–4·02 Gy). The LD50/100 is identical to that obtained for an LD50/30. Examination of doses ranging from 3·85–4·25 Gy shows that each survival curve declines exponentially (graphs not shown). The dose range best representing haematopoetic failure for MST greater than 8 days was 3·85–4·25 Gy. A dose of 5 Gy, on the other hand, resulted in a MST of 6·4 days, a time frame characteristic of gastrointestinal complications. Of 72 animals receiving 5·0 Gy, 12 died on day 5, 34 on day 6, 19 on day 7 and 8 died eight days postexposure.

3.3. *Urinary changes after irradiation*

Whole-body exposure to an enhanced neutron field resulted in reduction in urine output (figure 1). Animals were observed to consume less water; however, precise measurements of consumption were not performed. Diarrhoea was also noted; its severity and duration were more pronounced with increasing radiation dose. The reduced urine output may be partially the consequence of reduced water intake and fluid loss from watery stools. A dose of 3·5 Gy or more resulted in significantly ($P<0{\cdot}005$) reduced urine volumes within the first 24 h; however, there was no significant difference (Snedecor and Cochran 1980 b) between the groups on the first day. Mice which received 2·0 Gy had separate and distinct patterns of urine output 5–7 days (analysis of variance; pw = 0·0001), compared to the marked reduction at all other doses. The nadir of excretion occurred 4–5 days postexposure for all groups. On days 5–8, animals given 5·0 Gy excreted very little urine ($<0{\cdot}05$ ml) and volumes could not be accurately quantitated or analysed for metabolites. In the remaining groups, urine volume gradually increased over the next 5 days, during which time animals that received 3·0 Gy exhibited excretion rates within normal limits ($P>0{\cdot}05$), while higher radiation doses resulted in persistent volume reductions (figure 1). Thirty days post-exposure, urine volumes from mice exposed to 3·85 and 4·0 Gy were distinct from those of lower doses (analysis of variance; $P<0{\cdot}0001$) with excretions of 65 and 57 per cent of control levels, respectively.

Postirradiation urinary creatinine excretion was significantly correlated across time (Spearman's Rho; $P<0{\cdot}05$) with urine volume for all doses (figures 1 and 2). Whereas the 2·0 Gy group did not reflect significantly altered creatinine levels throughout the study, higher doses significantly reduced its excretion (figure 2). Similar to urine output, urinary creatinine levels of the 2·0 Gy group were significantly different (analysis of variance; $P<0{\cdot}0001$) from excretion rates of higher doses 3–8 days postexposure. At 30 days, mice given 3·5, 3·85, or 4·0 Gy still had 20–30 per cent reductions in urinary creatinine levels.

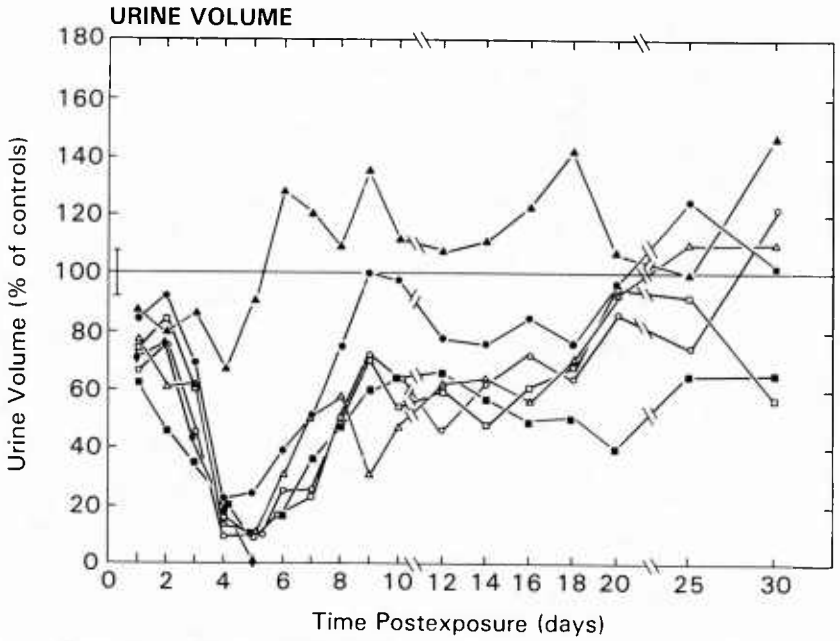

Figure 1. Changes in urine volume following whole-body exposure to an enhanced neutron field. 2·0 Gy, ▲——▲ (control: 0·80 ± 0·05 ml/24 h/mouse, $n = 9$ cages of three mice); 3·0 Gy, ●——● (1·18 ± 0·07 ml, $n = 9$); 3·5 Gy, ○——○ (1·29 ± 0·09 ml, $n = 18$); 3·67 Gy, △——△ (1·22 ± 0·08 ml, $n = 9$); 3·85 Gy, ■——■ (1·35 ± 0·11 ml, $n = 9$); 4·0 Gy, □——□ (1·12 ± 0·08 ml, $n = 18$); 5·0 Gy, ◆——◆ (1·16 ± 0·06 ml, $n = 24$); overall average preirradiation excretion illustrated at day 0; ↕ (1·17 ± 0·05 ml/24 h/mouse, $n = 96$ cages of three mice).

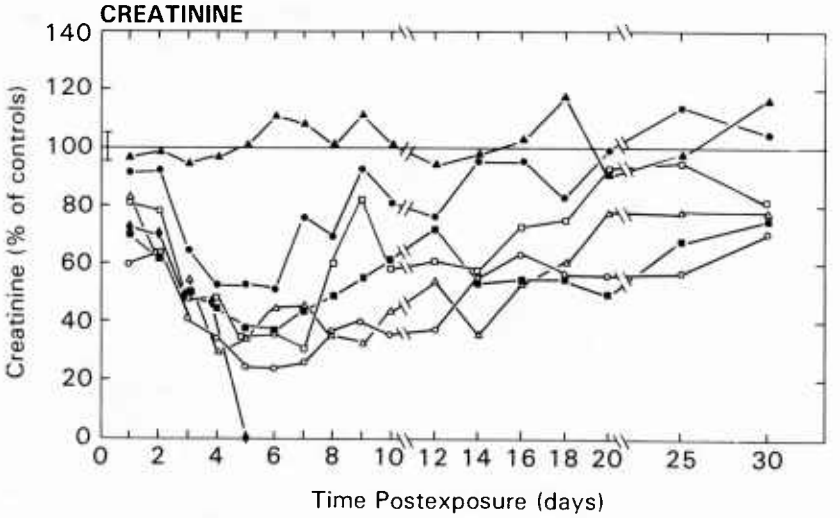

Figure 2. Changes in urinary excretion of creatinine following whole-body exposure to an enhanced neutron field. 2·0 Gy, ▲——▲ (control: 0·91 ± 0·04 mg/24 h/mouse, $n = 9$ cages of three mice; 3·0 Gy, ●——● (0·75 ± 0·04 mg, $n = 9$); 3·5 Gy, ○——○ (0·88 ± 0·03 mg, $n = 18$); 3·67 Gy, △——△ (1·01 ± 0·05 mg, $n = 9$); 3·85 Gy, ■——■ (0·98 ± 0·05 mg, $n = 9$); 4·0 Gy, □——□ (0·82 ± 0·04 mg, $n = 18$); 5·0 Gy, ◆——◆ (0·75 ± 0·02 mg, $n = 24$) overall average preirradiation excretion illustrated at day 0; ↕ (0·84 ± 0·03 mg/24 h/mouse, $n = 96$ cages of three mice).

Urinary excretion of cGMP from mice following exposure is presented in figure 3. With one exception (3·85 Gy), cGMP excretion was significantly correlated (Spearman's Rho, $P<0·05$) in a positive direction, to urine excretion across time (30 days) postirradiation. Similarly, cGMP correlated in a positive direction to creatinine levels in groups which received 3·0 Gy or more. Urinary cGMP excretion was similar to those of urine and creatinine profiles in nadir of excretion (days 4–5), significantly different excretion pattern from mice at 4–8 days after 2·0 Gy (analysis of variance, $P=0·0001$) and reduced cGMP excretion for 2 weeks after higher doses (figure 3). Three and four weeks following exposure, urinary cGMP attained or exceeded control levels.

The kinetics of postirradiation urinary cAMP excretion (figure 4) suggest a more complex situation. The initial response to radiation was characterized by elevated urinary cAMP during the first few days. Animals which received 2·0 Gy were distinctly different (analysis of variance) in cAMP excretion levels compared to those of higher radiation doses, at 1 ($P=0·0123$), 6 ($P=0·002$), and 7 ($P<0·0001$) days postexposure. A general trend toward increasing urinary cAMP excretion predominated 2–4 weeks after exposure. On day 30, all radiation groups except 4·0 Gy exhibited elevated cAMP levels in the urine (figure 4); however, no indications of a dose-relationship were apparent. Creatinine was significantly positively correlated with cAMP levels across time in dose groups of 2, 3, 3·67 and 4 Gy (Spearman's Rho, $P<0·05$). Cyclic GMP was positively correlated ($P<0·05$) to cAMP excretion in

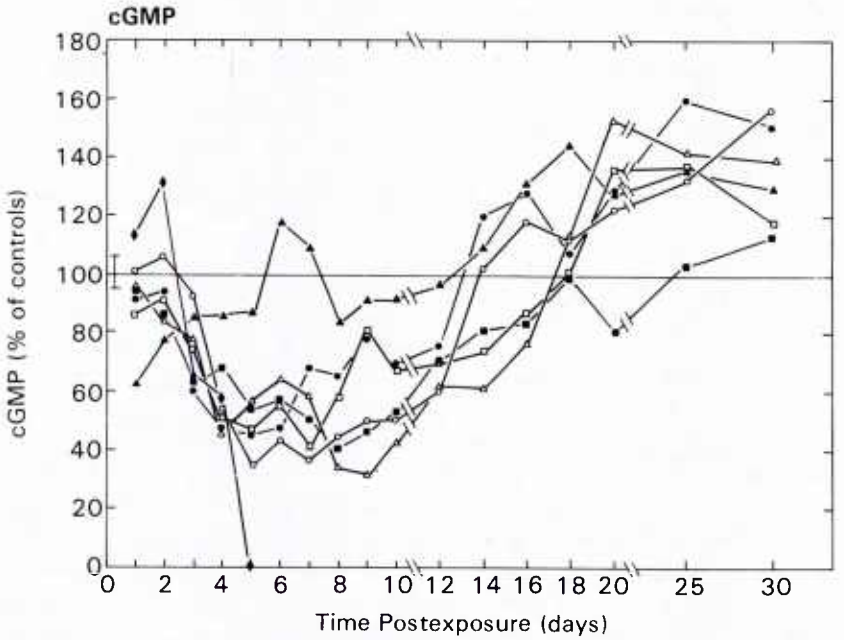

Figure 3. Changes in urinary excretion of cyclic GMP following whole-body exposure to an enhanced neutron field. 2·0 Gy, ▲——▲ (control: 8·18 ± 0·33 nmol/24 h/mouse, $n=9$ cages of three mice); 3·0 Gy, ●——● (4·35 ± 0·17 nmol, $n=9$); 3·5 Gy, ○——○ (6·55 ± 0·20 nmol, $n=18$); 3·67 Gy, △——△ (5·58 ± 0·17 nmol, $n=18$); 3·85 Gy, ■——■ (5·54 ± 0·33 nmol, $n=9$); 4·0 Gy, □——□ (6·81 ± 0·34 nmol, $n=18$); 5·0 Gy, ◆——◆ (6·94 ± 0·28 nmol, $n=24$); overall average preirradiation excretion illustrated at day 0, ↧ (6·47 ± 0·30 nmol/24 h/mouse, $n=96$ cages of three mice).

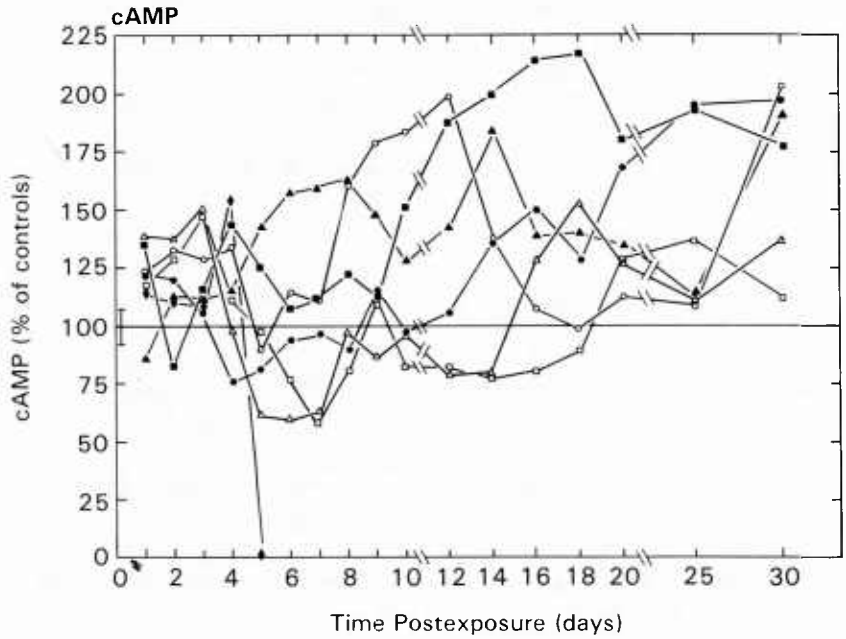

Figure 4. Changes in urinary excretion of cyclic AMP following whole-body exposure to an enhanced neutron field. 2·0 Gy, ▲——▲ (control: 21·08 ± 1·48 nmol/24 h/mouse, $n = 9$ cages of three mice), 3·0 Gy, ●——● (17·21 ± 1·20 nmol, $n = 9$); 3·5 Gy, ○——○ (14·79 ± 0·44 nmol, $n = 18$); 3·67 Gy, △——△ (15·50 ± 0·62 nmol, $n = 9$); 3·85 Gy, ■——■ (17·74 ± 1·06 nmol, $n = 9$); 4·0 Gy, □——□ (18·90 ± 0·94 nmol, $n = 18$); 5·0 Gy, ◆——◆ (14·07 ± 0·56 nmol, $n = 24$); overall average preirradiation excretion illustrated at day 0, I (16·47 ± 0·73 nmol/24 h/mouse, $n = 96$ cages of three mice).

groups which received 3, 3·67 or 4 Gy; and urine volume positively correlated to cAMP excretion ($P < 0·05$) in all groups except those which received 3·5 Gy.

Radiation-induced alterations in mouse urinary TxB_2 excretion are presented in figure 5. During the first few days postexposure, TxB_2 levels were unchanged or reduced (3·67 and 3·85 Gy), in relation to control (preirradiation) excretions. Days 4–8 reflected a continuation of unchanged levels in groups which received $\leqslant 3·5$ Gy; while the animals exposed to 3·67 and 3·85 Gy had reduced urinary TxB_2 levels on day 7, and days 4, 6, and 7, respectively. A modest (albeit significant) elevation in TxB_2 excretion occurred on days 4–6, in mice which received 4·0 Gy (figure 5). Analysis of variance across doses (Snedecor and Cochran 1980 b) showed no statistical difference in excretions on day 5 ($P = 0·2543$). The second week postexposure, transient elevations in urinary TxB_2 levels occurred in animals which received 2·0 Gy, while higher doses exhibited unchanged or transient reductions in urinary TxB_2. Patterns of excretion were not statistically different across doses 14–16 days postexposure ($P = 0·0674$ and $P = 0·1990$, respectively), and again on day 25 ($P = 0·0866$; Snedecor and Cochran 1980 b). Days 18–30 were characterized by variable, transient increases in TxB_2 excretion from mice exposed to 3·0 Gy or less. Animals which received 3·5 Gy or more exhibited unchanged or reduced (3·85 Gy) urinary TxB_2.

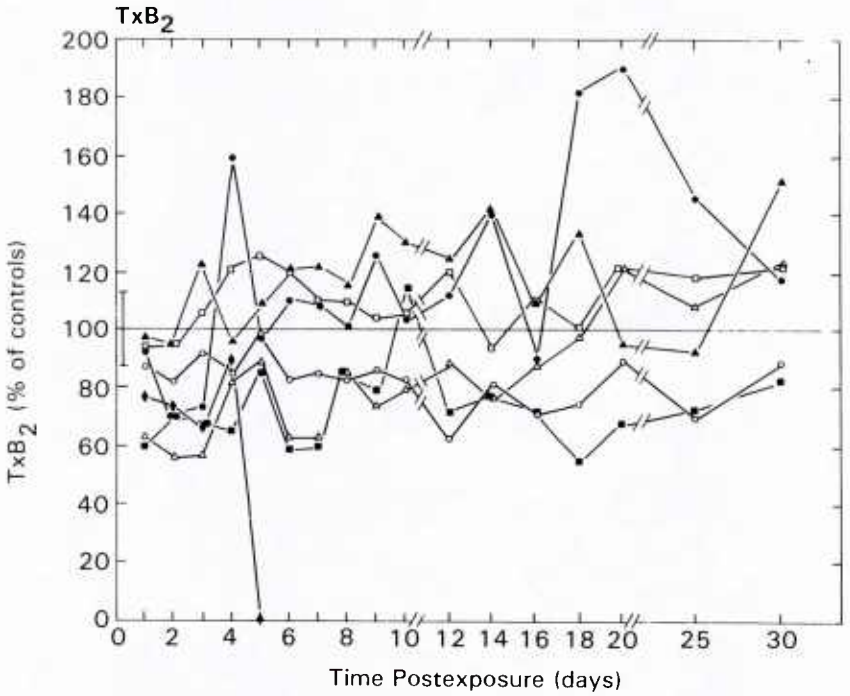

Figure 5. Changes in urinary excretion of thromboxane B_2 following whole-body exposure to an enhanced neutron field. 2·0 Gy, ▲——▲ (control: 390·67 ± 27·35 pg/24 h/mouse, $n=9$ cages of three mice), 3·0 Gy, ●——● (422·40 ± 54·91 pg, $n=9$); 3·5 Gy, ○——○ (462·95 ± 32·41 pg, $n=18$); 3·67 Gy, △——△ (643·17 ± 45·02 pg, $n=9$); 3·85 Gy, ■——■ (571·80 ± 45·74 pg, $n=9$); 4·0 Gy, □——□ (523·90 ± 20·96 pg, $n=18$); 5·0 Gy ◆——◆ (399·92 ± 20·0 pg, $n=24$); overall average preirradiation excretion illustrated at day 0, I (472·86 ± 29·70 pg/24 h/mouse, $n=96$ cages of three mice).

Thromboxane B_2 levels positively correlated (Spearman's Rho, $P<0·01$) with urine output and cyclic AMP excretion in animals given 2·0 Gy. Higher doses exhibited no such relationship with these parameters. Regardless of dose, postirradiation urinary levels of TxB_2 were unrelated to urinary levels of creatinine or cyclic GMP (P0·05).

Exposure to the neutron field resulted in biphasic elevations in PGE_2 excretion (figure 6, table 2). The first transient elevation occurred 2 or 3 days after irradiation. During this time PGE_2 levels were 1·5 to three times higher than their respective preirradiation excretions. One-way analysis of variance across doses (Snedecor and Cochran 1980 b) indicated no statistical difference between the radiation groups 2–5 days postirradiation. The second elevation in urinary PGE_2 excretion occurred 6–10 days postexposure. At this time, increases in dose up to 3·85 Gy were associated with increasingly elevated PGE_2 excretion. Although increases were still apparent on day 10, there was no significant difference in mean excretions (analysis of variance, $P=0·3973$) across radiation doses. PGE_2 excretion reached normal 18 days postexposure in groups which received 2·0, 3·0, 3·67 and 4·0 Gy. A transient elevation occurred on day 25 in the 3·0 Gy group. Animals given 3·5 or 3·85 Gy had reduced urinary PGE_2 18–25 days postexposure. By day 30, PGE_2 excretion was within (or below, for the 3·85 Gy group) normal excretion rates.

Table 2. Urinary excretion of PGE_2 (pg/24 h) from B6D2F1 female mice following whole-body exposure to an enhanced neutron field.

Day post-exposure	Means ± s.e.m. and Statistical Evaluation† Dose group (Gy)						
	2·0 ($n=9$)	3·0 ($n=9$)	3·5 ($n=18$)	3·67 ($n=9$)	3·85 ($n=9$)	4·0 ($n=18$)	5·0 ($n=24$)
(Control ‡)	426·7 ± 25·6	253·0 ± 22·8	389·9 ± 31·2	277·0 ± 16·6	334·5 ± 33·5	211·2 ± 23·2	312·1 ± 15·6
1	490·7 ± 46·9	194·8 ± 20·2 *a*	261·2 ± 23·4 *d*	379·5 ± 55·4	301·1 ± 30·1	302·0 ± 38·0 *a*	324·6 ± 34·3
2	665·6 ± 8·1 *a*	361·8 ± 53·1	682·3 ± 58·5 *d*	432·1 ± 47·1 *a*	582·0 ± 70·2 *b*	620·9 ± 99·3 *d*	630·4 ± 53·1 *d*
3	704·0 ± 64·0 *c*	384·6 ± 48·1 *a*	643·3 ± 58·5 *c*	714·7 ± 130·2 *b*	1003·5 ± 184·0 *b*	373·8 ± 27·5 *d*	508·7 ± 53·1 *c*
4	494·9 ± 38·4	217·6 ± 27·8	272·9 ± 31·2 *c*	205·0 ± 41·6	307·7 ± 26·8	179·5 ± 27·5	268·4 ± 25·0
5	635·7 ± 106·7	420·0 ± 53·1 *a*	448·4 ± 58·5	326·9 ± 149·6	384·7 ± 97·0	181·6 ± 31·7	ND§
6	610·1 ± 59·7 *a*	508·5 ± 96·1 *a*	717·4 ± 70·2 *d*	883·6 ± 191·1 *a*	1863·2 ± 2910 *c*	933·5 ± 304·1 *a*	—
7	635·7 ± 85·3 *a*	377·0 ± 58·2	1111·2 ± 191·1 *c*	1263·1 ± 196·7 *c*	1545·4 ± 438·2 *a*	842·7 ± 274·6 *a*	—
8	486·4 ± 46·9	404·8 ± 58·2 *a*	1080·0 ± 144·3 *d*	858·7 ± 193·9 *a*	1532·0 ± 381·3	798·3 ± 249·2 *a*	—
9	537·6 ± 51·2	442·8 ± 65·8 *a*	1009·8 ± 136·5 *d*	828·2 ± 326·9	1950·1 ± 304·4 *d*	851·1 ± 114·0 *d*	—
10	691·2 ± 136·5	407·3 ± 70·8	744·7 ± 85·8 *c*	548·5 ± 119·1	1264·4 ± 528·5	570·2 ± 101·4 *c*	—
12	413·9 ± 55·5	293·5 ± 50·6	612·1 ± 101·4 *a*	628·8 ± 119·1 *a*	528·5 ± 46·8 *c*	437·2 ± 52·8 *c*	—
14	349·9 ± 34·1	291·0 ± 45·5	444·5 ± 54·6	506·9 ± 69·3 *a*	274·3 ± 20·1 *a*	365·4 ± 52·8 *a*	—
16	345·6 ± 21·3 *b*	301·1 ± 38·0	378·2 ± 58·5	387·8 ± 41·6 *a*	207·4 ± 40·1 *a*	348·5 ± 33·8 *b*	—
18	465·1 ± 55·5	230·2 ± 58·2	276·8 ± 39·0 *a*	332·4 ± 52·6	227·5 ± 30·1 *b*	245·0 ± 27·5	—
20	435·2 ± 68·3	293·5 ± 43·0	206·6 ± 27·3 *d*	313·0 ± 44·3	137·1 ± 23·4 *d*	253·4 ± 31·7	—
25	384·0 ± 76·8	369·4 ± 43·0 *a*	214·4 ± 31·2 *d*	337·9 ± 49·9	224·1 ± 30·1 *b*	219·6 ± 40·1	—
30	469·3 ± 76·8	293·5 ± 43·0	331·4 ± 50·7	326·9 ± 49·9	194·0 ± 26·8 *d*	171·1 ± 19·0	—

† Significance between postirradiation values and control for each dose was determined by paired t-test (Snedecor and Cochran 1980 a). *a*, $P<0·05$; *b*, $P<0·01$; *c*, $P<0·005$; *d*, $P<0·001$.

‡ Control: calculated from the means of 7–24 h samples for each cage (n).

§ND, not done, urine volume less than 0·05 ml.

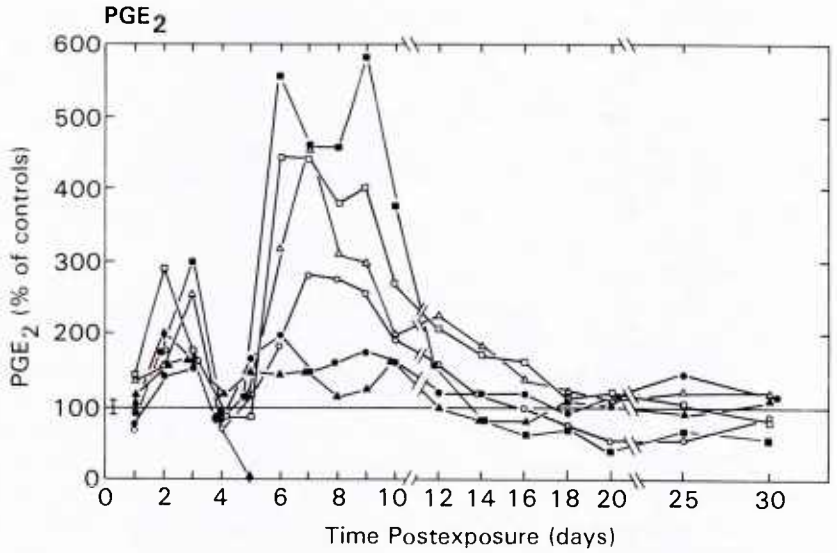

Figure 6. Changes in urinary excretion of PGE_2 following whole-body exposure to an enhanced neutron field. Control levels given in table 2. 2·0 Gy, ▲——▲; 3·0 Gy, ●——●; 3·5 Gy, ○——○; 3·67 Gy, △——△; 3·85 Gy, ■——■; 4·0 Gy, □——□; 5·0 Gy, ◆——◆; overall average preirradiation excretion illustrated at day 0, ŧ (311·79 ± 25·65 pg/24 h/mouse; $n = 96$ cages of three mice).

In general, urinary excretion of PGE_2 is negatively correlated with all other urinary parameters (Conover 1980). Doses of 2·0, 3·5 and 3·85 Gy elicited urinary PGE_2 levels which were significantly correlated in a negative direction to cyclic GMP excretion (statistics now shown.) Similarly, PGE_2 excretion was inversely related to creatinine levels of the 3·5 Gy group ($P < 0·05$), cyclic AMP levels of the 3·85 Gy group ($P < 0·01$) and TxB_2 excretion from animals given 3·67 Gy ($P < 0·05$). Other comparisons of PGE_2 excretion and urinary parameters (within each radiation dose and across time) revealed negative but insignificant correlations.

4. Discussion

4.1. *Cyclic nucleotides and creatinine*

In the present experiments, female mice were used in order to avoid the potential significant contribution of seminal cyclic nucleotides to urinary measurements in males (Gray 1970). A very slight increase in cAMP excretion has been reported to occur during the midportion of the menstrual cycle in human subjects (Taylor *et al.* 1970). In our studies, we did not establish the stage of oestrus cycle or examine sex-associated hormones which could potentially affect radiosensitivity or introduce variability in metabolic excretion.

We have found urinary cGMP excretion to be significantly associated with urine output and urinary cAMP levels in the nonirradiated mouse. Under normal metabolic conditions, approximately 60 per cent of the total urinary cAMP is derived from extrarenal sources by glomerular filtration (Pak 1980); the remainder being obtained from nephrogenous contributions (Broadus *et al.* 1971). Urinary cGMP is

derived largely from the plasma by filtration (Broadus *et al.* 1970). While the degree of hydration has no influence on the urinary excretion rates of cAMP and cGMP in man, dog or rat, over extreme ranges of urine flow (for review see Broadus *et al.* 1971), diet does appear to be a factor in cyclic nucleotide excretion, at least in the rat (Hardman *et al.* 1969). In the present studies we did not investigate the influence of food intake on urinary cyclic nucleotide excretion in the mouse. We did find that subtle changes in daily urine output and/or urinary cAMP excretion resulted in similar concomitant changes in urinary cGMP in the mouse. Dehydration and starvation studies coupled with measurements of plasma cyclic nucleotide levels may clarify these relationships.

Changes in urine volume and excretion of cAMP, cGMP, and creatinine were examined as potential measures of radiation damage. Because these assays do not involved sacrifice of the animal, it was also possible to assess mouse survival and urinary excretion of these parameters as a function of radiation dose. In general, urine volume and urinary cAMP, cGMP and creatinine were significantly, positively associated across time postexposure. However, none of these parameters suggest their use as an early (24–48 hr) prognostic indicator of the extent of radiation damage.

While the physiological role of cGMP is poorly characterized, the role of cAMP in mediating the actions of a variety of enzymes and hormones is recognized (Sutherland *et al.* 1967, Sutherland 1970). Several reports have shown altered cyclic nucleotide concentrations in a variety of tissues following irradiation (Catravas *et al.* 1981, Trocha and Catravas 1980, Hunt and Dalton 1980; Pausescu *et al.* 1976, Lipski 1976, Sobolev *et al.* 1984). It is possible that urinary cyclic nucleotide concentrations could reflect alterations of intracellular pools. This is supported by the observations that plasma concentrations exist in a steady-state relationship with the intracellular pool of these compounds (Broadus *et al.* 1970) and reflect changes in tissue levels (Strange and Mjos 1975). Experiments in which both plasma and urinary levels are examined may provide insight as to whether altered cyclic nucleotide excretion reflects changes in the nephrogenous contribution or changes in circulating concentration (derived from tissue intracellular pools and added to the urine by glomerular filtration).

Although haematological studies were not performed in this study, it is important to emphasize the fact that the cyclic nucleotides mediate the effects of a number of mediators and hormones which modulate haematopoietic proliferation and maturation (Lipski 1976). The decreased urinary cGMP during the first two weeks after irradiation may reflect reduced food intake, suppressed cell growth and proliferation, and reduced total cellularity. Increasing cellularity and resumption of radiation-suppressed mitotic activity (Daniel and Oleinick 1984) may correlate with normal and increasingly elevated urinary cGMP levels (3–4 weeks). The variable increases in cAMP excretion after irradiation may also reflect cell proliferation and increased DNA synthesis (Whitefield *et al.* 1972). However, the erratic nature of cAMP increases and lack of a correlation with radiation dose suggest other factors may have a causal role. Bacteria and their products can enhance the activity of cyclases or catalyse cAMP synthesis after entering the cell (for review see Burns 1984). Microorganisms repopulating or invading the body could, therefore, contribute to elevated cAMP levels. Necropsy of animals which succumbed following radiation exposure revealed haematopoietic depletion and frequently multifocal bacterial colony formations, primarily of cocci etiology, in several organs (lungs, liver, kidney). The mechanisms by which opportunistic organisms and their

toxins alter cyclic nucleotide synthesis/degradation is beyond the scope of this communication.

The daily excretion of creatinine has been used as a qualitative measure of kidney function and metabolic rate (Steinitz znd Turkland 1940). In these studies, kinetic procedures combined with the colorimetric assay permitted the direct determination of creatinine in the urine with minimal interference by other compounds ('pseudo-creatinines') which also react with picric acid in an alkaline solution. Representative samples with exogenously added creatinine yielded predicted values; however, the release of an endogenous substance into the urine postirradiation, which might alter the colorimetric detection of urinary creatinine, was not investigated. Urinary excretion of creatinine in X-irradiated rats (Thyagarajan *et al.* 1977, Nerurkar and Sahasrabudhe 1960) or dogs (Welbourne and Spurr 1971) was not significantly altered for 7 days. Three factors make it difficult to correlate the dramatic reductions in creatinine excretion reported herein with the aforementioned publications: method of calculating excretion rate, species employed, and radiation quality. Others (Welbourne and Spurr 1971, Thyagarajan *et al.* 1977) have taken into account the postirradiation reductions in body-weight, as well as urine volume, in determining total excretion. We have also measured body-weight and calculated the contribution of weight loss to the creatinine excretion rates. Animals which received 3·85 Gy or more suffered as much as 20–30 per cent reductions in body-weight. Analysis of creatinine excretion on the basis of animal weight, even under these extreme conditions of weight loss, still resulted in significantly reduced creatinine levels.

4.2. *Cyclo-oxygenase products*

Measurement of urinary PG excretion rate provides a non-invasive assessment of renal PG production. Urinary PGE_2 is primarily of renal medullary origin (Frölich *et al.* 1975), and experimental studies are generally performed in females because seminal PGs contribute significantly to urinary measurement in males (Gerber *et al.* 1982). TxB_2, the stable metabolite of the biologically active thromboxane A_2, is also present in kidney glomeruli, but may originate in part, from circulating platelets (Levenson *et al.* 1982). Opinion is still divided on the question of renal versus extra-renal origin of urinary TxB_2. Some studies suggest that urinary TxB_2 is a reflection of renal synthesis (Frölich *et al.* 1975, Patrono *et al.* 1983), however, in some disease states evidence for an extra-renal contribution exists (Foegh *et al.* 1981, Zipser and Smorlesi 1984).

In the present study, we have observed a seasonal influence on urinary PGE_2 and TxB_2 excretion in the mouse. Thromboxane levels were highest during the months of July–October, during which time daily excretion of PGE_2 was approaching its nadir. During the months of December and January, urinary PGE_2 concentrations were highest and TxB_2 levels lowest. These findings are particularly interesting in view of the fact that all the animals were purchased from the same source and subjected to identical housing conditions. The possibility that seasonal variation in arachidonate metabolite excretion may influence animal radiosensitivity was not pursued.

Exposure to ionizing radiation results in altered PG and TxB_2 levels in numerous tissues (for review see Steel and Catravas 1982) and bodily fluids (Donlon *et al.* 1983, Schneidkraut *et al.* 1983, 1984, Steel *et al.* 1984). The difficulty in interpreting the use of urinary levels as indicators of whole-body irradiation in the mouse partly

stems from the inability to distinguish between renal and extra-renal contributions. Williams and Denkamp (1983) have examined urine output in mice after X-irradiation of the kidneys and found dose-related increases in total urine volume beginning 17 weeks postexposure. Volume and urination frequency were unaltered for at least 5 months after localized bladder irradiation with 1·8 MeV electrons (Stewart *et al.* 1978, 1981). We have observed decreases in urine output during the first several weeks following whole-body exposure to a neutron-enriched field. An examination of urinary metabolite excretion following local irradiation to the bladder or kidneys is needed.

In the present experiments, biphasic increases in mouse urinary excretion of the vasodilator PGE_2 occurred following whole-body irradiation. The initial elevation, occurring 2–3 days postexposure, is of shorter duration and of lesser magnitude than that we observed in rats exposed to 9·0 Gy gamma radiation from a ^{60}Co source (Donlon *et al.* 1983, 1985). The reasons for this discrepancy between the two murine models is not clear. The rate seems to be an unusual species in that PGE_2 acts as a renal vasoconstrictor (Gerber and Nies 1979), while PGE_2 is a renal vasodilator in other mammals. Polyuria occurs in rats 1–24 h after exposure (Donlon *et al.* 1985, Kay and Entenman 1959), but in mice, urine output was unchanged or declined. This may relate to the observations that in hypercalcaemic rats, marked elevations of urinary PGE_2 excretion are associated with diuresis (Levi *et al.* 1983). Prostaglandins have been implicated in the regulation of renal water excretion (Anderson *et al.* 1976), and the stimulation of PG biosynthesis by calcium is well documented (for review see Hassid 1982). Hypercalcaemia (Vierling and Strike 1968) and elevations in urinary PGE_2 and TxB_2 (Donlon *et al.* 1983, 1985) also occur in the rat concomitant with postirradiation polyuria. In contrast, serum calcium levels were normal in female mice, or actually hypocalcaemic in males in the first 24 h after exposure (Fialkowska 1980). With the single exception of animals exposed to 4·0 Gy (PGE_2 elevated), urinary PGE_2 and TxB_2 levels were normal or reduced during the first 24 h after exposure. These findings suggest that hypercalcaemia and diuresis are associated with elevated arachidonate metabolite excretion during the first 24 h after exposure in the rat; while normal or reduced levels of calcium, urine output, and PGE_2 and TxB_2 excretion occur in the mouse during the same period.

Mouse urinary TxB_2 levels were unchanged or transiently elevated after neutron irradiation. Intermediate doses (3·5–3·85 Gy) resulted in transient reductions, and lethal exposure (5 Gy) also resulted in significantly reduced urinary TxB_2 excretion. These observations agree with the previous report in which whole-body irradiation of rats with 2 Gy ^{60}Co gamma radiation did not result in changes in urine TxB_2 levels 2–120 h postexposure (Schneidkraut *et al.* 1983). However, rat urinary TxB_2 is dramatically increased 4–120 h after 9 Gy (Donlon *et al.* 1985) or 10 Gy (Schneidkraut *et al.* 1984) gamma radiation. These differences may be due to the species employed but the quality of radiation may also be an important underlying factor. We have observed elevations in TxB_2 levels in parenchymal lung tissues of guinea pigs exposed to ^{60}Co gamma radiation (Steel *et al.* 1982). In contrast, tissue TxB_2 concentrations were reduced in guinea pigs exposed to an enhanced neutron field (Steel *et al.* 1983).

Mouse urinary PGE_2 concentrations are elevated 6–10 days after 2–4 Gy whole-body irradiation from an enhanced neutron field. Increases in radiation dose up to 3·85 Gy are associated with increasingly elevated PGE_2 excretion. Thus, urinary

PGE_2 may be a useful indicator of whole-body exposure to an enhanced neutron field, particularly at low and intermediate (potentially lethal) doses. In this context, it is important to emphasize that urinary PGE_2 is considered primarily to reflect renal PG production (Frölich *et al.* 1975). Therefore, the elevations observed following whole-body exposure may be an indicator only of the degree of kidney damage. We have recently reported elevations in plasma PGE_2 concentration in mice following 3·0 Gy whole-body dose from an enhanced neutron field (Ledney *et al.* 1985 a, b). Walker and Eisen (1979) have shown reductions in the enzyme 15-hydroxyprostaglandin dehydrogenase (PGDH) in kidney, spleen and jejunum tissues of irradiated mice. PGDH plays an important role in removing and inactivating PGs from the circulation. Impairment of this process, coupled with potential radiation damage to the transport mechanisms of PGs across cell membranes could contribute to increased levels in tissues and fluids. Elevated levels of circulating PGE_2 may escape uptake and inactivation, and thereby contribute extra-renally to urinary PGE_2. Examination of urinary PGE_2 excretion following local bilateral kidney irradiation may clarify renal versus extra-renal contributions.

Ongoing experiments of whole-body exposure to a gamma-enriched field also exhibit similar transient elevations in PGE_2 excretion 2–3 days after 5 Gy. However, the second rise in urinary PGE_2 concentration, apparent 6–10 days after neutron exposure, did not occur in mice irradiated with an enhanced gamma field. It is premature to draw any inferences regarding potential differences in mechanisms of action between the two qualities of radiation. It is possible that free radicals (Little 1968, Granger and Parks 1983) could potentiate changes in the synthesis of cyclo-oxygenase products. Lipid peroxides (Hemler *et al.* 1979), H_2O_2 and oxygen radicals (Taylor and Polgar 1980, Seregi *et al.* 1983, Taylor *et al.* 1983) have been shown to activate cyclo-oxygenase. These studies, as well as our observations, suggest that urinary prostaglandin and thromboxane levels may reflect increases in cyclo-oxygenase activity due to free radical formation after irradiation. We are currently examining free radical scavengers and cyclo-oxygenase inhibitors as potential modulators of these alterations, with the purpose of evaluating the role of free radicals, and possibly ameliorating radiation-induced changes in arachidonate metabolism.

Acknowledgments

Supported by the Armed Forces Radiobiology Research Institute, Defense Nuclear Agency, under Research Work Unit MJ00064. The views presented in this paper are those of the authors; no endorsement by the Defense Nuclear Agency has been given or should be inferred. Research was conducted according to the principles enunciated in the 'Guide for the Care and Use of Laboratory Animals', prepared by the Institute of Laboratory Animal Resources, National Research Council. The authors gratefully acknowledge the secretarial assistance of Mrs. Mariann Waldbillig.

Reference

AAPM, 1980, *Protocol for Neutron Beam Dosimetry Report* (New York, NY: American Association of Physicists in Medicine, American Institute of Physics).

Anderson, R. J., Bert, T., McDonald, K. M., and Schrier, R. W., 1976, Prostaglandins: Effects on blood pressure, renal blood flow, sodium and water excretion (editorial review). *Kidney International*, **10**, 205–215.

BOROWSKA, A., SIERAKOWSKI, S., MACKOWIAK, J., and WISNIEWSKI, K., 1979, A prostaglandin-like activity in small intestine and postirradiation gastrointestinal syndrome. *Experientia*, **35,** 1368–1370.

BROADUS, A. E., HARDMAN, J. G., KAMINSKY, N. I., BALL, J. H., SUTHERLAND, E. W., and Liddle, G. W., 1971, Extracellular cyclic nucleotides. *Annals of the New York Academy of Science*, **185,** 50–66.

BROADUS, A. E., KAMINSKY, N. I., HARDMAN, J. G., SUTHERLAND, E. W., and LIDDLE, G. W., 1970, Kinetic parameters and renal clearances of plasma adenosine 3′,5′-monophosphate and guanosine 3′,5′-monophosphate in man. *Journal of Clinical Investigation*, **49,** 2222–2236.

BROERSE, J. J., MIJNHEER, B. J., and WILLIAMS, J. R., 1981, European protocol for neutron dosimetry for external beam therapy. *British Journal of Radiology*, **54,** 882–898.

BURNS, D. L., 1984, In: J. Moss, moderator, Cyclic nucleotides: mediators of bacterial toxin action in disease. *Annals of Internal Medicine*, **101,** 653–666.

CATRAVAS, G. N., WRIGHT, S. J., TROCHA, P. J., and TAKENAGA, J., 1981, Radiation effects on cyclic AMP, cyclic GMP and amino acid levels in the CSF of the primate. *Radiation Research*, **87,** 198203.

CONOVER, W. J., 1980, *Spearman Rank Correlation and Practical Nonparametric Statistics*. Second edition (New York: John Wiley), pp. 250–256.

DANIEL, J. W., and OLEINICK, N. L., 1984, The participation of elevated levels of cyclic GMP in the recovery from radiation-induced mitotic delay. *International Journal of Radiation Biology*, **45,** 73–83.

DONLON, M., Steel, L., HELGESON, E. A., and CATRAVAS, G. N., 1983, Radiation-induced alterations in prostaglandin excretion in the rat. *Life Sciences*, **32,** 2631–2639

DONLON, M. A., STEEL, L. K., HELGESON, E. A., WOLFE, W. W., and CATRAVAS, G. N., 1985, WR 2721 inhibition of radiation-induced prostaglandin excretion in rats. *International Journal of Radiation Biology*, **47,** 205–212.

DUNN, M. J., and HOOD, V. L., 1977, Prostaglandins and the kidney. *American Journal of Physiology* F, **233,** 169–184.

FABINY, D. L., and ERTINGHAUSEN, G., 1971, Automated reaction rate method for determination of serum creatinine with Centrifichem. *Clinical Chemistry*, **17,** 391–395.

FIALKOWSKA, M., 1980, Diurnal fluctuations in calcium levels in the blood serum and homogenates of the kidney and small intestine of mice. I. Influence of X-rays. *Folia Biologia (Krakow)*, **28,** 273–285.

FINNEY, D. J., 1971, *Probit Analysis*. Third edition (New York, N.Y.: Cambridge University Press), pp. 50–80.

FOEGH, M., WINCHESTER, J. F., HELFRICH, G. B., ZMUDKA, M., COOLEY, C., RAMWELL, P. W., and SCHREINER, G. E., 1981, Urinary i-TxB_2 in renal allograft rejection. *Lancet*, **2,** 421–434.

FRÖLICH, J. C., WILSON, T. W., SWEETMAN, B., SMIGEL, M., NIES, A. S., CARR, K., WATSON, J. T., and OATES, J. A., 1975, Urinary prostaglandins. Identification and origin. *Journal of Clinical Investigation*, **55,** 763–770.

GERBER, G. B., and ALTMAN, K. I., 1970, Changes in the biochemistry of body fluids after irradiation. *Radiation Biochemistry*. Volume 2, edited by K. I. Altman, G. B. Gerber and S. Okada (New York: Academic Press), pp. 256–275.

GERBER, J. G., ANDERSON, R. J., SCHRIER, R. W., and NIES, A. S., 1982, *Prostaglandins and the Cardiovascular System*, edited by J. A. Oates (New York: Raven Press), pp. 227–254.

GERBER, J. G., and NIES, A. S., 1979, The hemodynamic effects of prostaglandins in the rat. Evidence for important species variation in renovascular responses. *Circulation Research*, **44,** 406–410.

GOODWIN, J. S., and WEBB, D. R., 1980, Regulation of the immune response by prostaglandins. *Clinical Immunology and Immunopathology*, **15,** 106–122.

GRANGER, D. N., and PARKS, D. A., 1983, Role of oxygen radicals in the pathogenesis of intestinal ischemia. *Physiologist*, **26,** 159–164.

GRAY, J. P. 1970, Adenosine 3′,5′-monophosphate and guanosine 3′,5′-monophosphate. Formation and occurrence in gametes and embryos Ph.D. Dissertation, Vanderbilt University, Nashville, Tennessee.

HANSON, W. R., and THOMAS, C., 1983, 16,16-dimethyl prostaglandin E_2 increases survival of murine intestinal stem cells when given before photon radiation. *Radiation Research*, **96,** 393–398.

HARDMAN, J. G., DAVIS, J. W., and SUTHERLAND, E. W., 1969, Effects of some hormonal and other factors on excretion of guanosine 3′,5′-monophosphate and adenosine 3′,5′-monophosphate in rat urine. *Journal of Biological Chemistry*, **244,** 6354–6362.

HASSID, A., 1982, Regulation of prostaglandin biosynthesis in cultured cells. *American Journal of Physiology* C, **243,** 205–211.

HEMLER, M. E., COOK, H. W., and LANDS, W. E. M., 1979, Prostaglandin biosynthesis can be triggered by lipid peroxides. *Archives of Biochemistry and Biophysics*, **193,** 340–345.

HUNT, W. A., and DALTON, T. K., 1980, Reduction in cyclic nucleotide levels in the brain after a high dose of ionizing radiation. *Radiation Research*, **83,** 210–215.

ICRU, 1976, *Neutron Dosimetry for Biology and Medicine Report*, No. 26 (Washington, D.C., International Commission on Radiation Units and Measurements).

KAY, R. E., and ENTENMAN, C., 1959, Polydipsia and polyuria by the x-irradiated rat. *American Journal of Physiology*, **197,** 169–172.

KUNKEL, S. L., CHENSUE, S. W., FANTONA, J. C., and WARD, P. A., 1984, Role of prostaglandins in macrophage cell function. *The Reticuloendothelial System, A Comprehensive Treatise.* Volume 7 *Immunology*, edited by J. A. Bellanti and H. B. Herscowitz (New York: Plenum Press), pp. 289–301.

LEDNEY, G. D., STEEL, L. K., EXUM, E. D., and GELSTON, H. M., 1985 a, Pathophysiologic responses in mice after neutron irradiation combined with either wound or burn trauma. *Proceedings of the Second International Symposium, Pathophysiology of Combined Injury and Trauma*, Wintergreen, VA, February 26–28.

LEDNEY, G. D., STEEL, L. K., GELSTON, H. M., and EXUM, D., 1985 b, Survival and pathophysiologic derangements in mice after enriched neutron field irradition or combined with burn or wound trauma. NATO Defense Research Group Panel VII: Physics and Medicine of Wound Ballistics/Casualty Care, Munich, Germany, September 23–27.

LEE, E. T., 1980, *Statistical Methods for Survival Data Analysis* (Lifetime Learning Publications), pp. 127–129.

LEVENSON, D. J., SIMMONS, C. E. JR., and BRENNER, B. M., 1982, Arachidonic acid metabolism, prostaglandins and the kidney. *American Journal of Medicine*, **72,** 354–362.

LEVI, M., ELLIS, M. A., and BERL, T., 1983, Control of renal hemodynamics and glomerular filtration rate in chronic hypercalcemia. Role of prostaglandins, renin-angiotensin system and calcium. *Journal of Clinical Investigation*, **71,** 1624–1632.

LIPSKI, S., 1976, Effects of 8-adrenergic stimulation on bone-marrow function in normal and sublethally irradiated mice. *International Journal of Radiation Biology*, **29,** 359–366.

LITTLE, J. B., 1968, Cellular effects of ionizing radiation. *New England Journal of Medicine*, **278,** 308–315.

MEEKER, R. D., 1980, Characteristics of a thimble type TE chamber manufactured by Exradin. *For Chambers for Neutron Dosimetry*, edited by J. J. Broerse (New York, N.Y.: Commission of the European Communities, Harwood Academic Publishers), pp. 43–46.

MENNIE, A. T., DALLEY, V. M., DINNEEN, L. C., and COLLIER, H. O. J., 1975, Treatment of radiation-induced gastrointestinal distress with acetylsalicylate. *Lancet*, **2,** 942–943.

MURAD, F., 1973, Clinical studies and applications of cyclic nucleotides. *Advances in Cyclic Nucleotide Research*, **3,** 335–342.

NERURKAR, M. K., and SAHASRABUDHE, M. B., 1960, Synthesis of creatine in X-irradiated rats. *International Journal of Radiation Biology*, **2,** 237–246.

NORTHWAY, M. G., EASTWOOD, G. L., LIBSHITZ, H. I., FELDMAN, M. S., MAMEL, J. J., and SZWARC, I. A., 1982, Antiinflammatory agents protect opossum esophagus during radiotherapy. *Digestive Diseases Science*, **27,** 923–928.

PAK, C. Y. C., 1980, Use of cyclic nucleotides in detection of disturbed parathyroid function. *Advances in Cyclic Nucleotide Research*, **12,** 393–403.

PATRONO, C., CIABATTONI, G., PATRIGNANI, P., FILABOZZI, P., PINCA, E., SATTA, M. A., VANDORNE, D., CINOTTI, G. A., PUGLISSE, F., PIERUCCI, A., and SIMONETTI, B. M., 1983, Evidence for a renal origin of urinary thromboxane B_2 in health and disease. *Advances in Prostaglandin, Thromboxane, and Leukotriene Research*, Volume II, edited by B. Samuelsson, R. Paoletti, and P. Ramwell (New York: Raven Press), pp. 493–498.

PAUSESCU, E., POPESCU, M., PAUN, C., and TEODOSIU, T., 1976, Dynamics of changes in the tissular levels of cyclic AMP after cobalt-60 gamma-irradiation. *Strahlentherapie*, **151,** 165–171.

POWELL, W. S., 1980, Rapid extraction of oxygenated metabolites of arachidonic acid from biological samples using octadecylsilyl silica. *Prostaglandins*, **20,** 947–957.

PRASAD, K. N., 1972, Radioprotective effect of prostaglandin and an inhibitor of cyclic nucleotide phosphodiesterase on mammalian cells in culture. *International Journal of Radiation Biology*, **22,** 187–189.

SCHNEIDKRAUT, M. J., KOT, P. A., RAMWELL, P. W., and ROSE, J. C., 1983, Urinary prostacyclin and thromboxane levels after whole-body gamma irradiation in the rat. *Advances in Prostaglandin, Thromboxane, and Leukotriene Research*, **12,** 107–112.

SCHNEIDKRAUT, M. J., KOT, P. A., RAMWELL, P. W., and ROSE, J. C., 1984, Thromboxane and prostacyclin synthesis following whole-body irradiation in rats. *Journal of Applied Physiology, Respiration, Environment and Exercise Physiology*, **57,** 833–838.

SEREGI, A., SERFOZO, P., and MERGL, Z., 1983, Evidence for the localization of hydrogen peroxide-stimulated cyclooxygenase activity in rat brain mitochondria: A possible coupling with monoamine oxidase. *Journal of Neurochemistry*, **40,** 407–413.

SIESS, W., and DREY, F., 1982, Very low levels of 6-keto-prostaglandin $F_{1\alpha}$ in human plasma. *Journal of Laboratory Clinical Investigation*, **99,** 388–398.

SNEDECOR, G. W., and COCHRAN, W. G., 1980a, The comparison of two samples; 1980b, Analysis of variance. *Statistical Methods* (Ames, Iowa: Iowa State University Press), pp. 85–86, 235–237.

SOBOLEV, A. S., TERTOV, V. V., and RYBALKIN, S. S., 1984, The cGMP system in irradiated animals. *Acta radiologica, Oncologica*, **23,** 367–373.

STEEL, L. K., and CATRAVAS, G. N., 1982, Radiation-induced changes in production of prostaglandins $F_{2\alpha}$, E, and thromboxane B_2 in guinea pig parenchymal lung tissues. *International Journal of Radiation Biology*, **42,** 517–530.

STEEL, L. K., SWEEDLER, I. K., and CATRAVAS, G. N., 1983, Effects of ^{60}Co radiation on synthesis of prostaglandins $F_{2\alpha}$, E and thromboxane B_2 in lung airways of guinea pigs. *Radiation Research*, **94,** 156–165.

STEEL, L. K., SWEEDLER, I. K., CATRAVAS, G. N., and WOLFE, W. W., 1984, Potential use of urinary cyclic nucleotides, prostaglandin E_2 and thromboxane B_2 levels in the evaluation of acute whole-body exposure to an enhanced neutron field. *Abstracts of Papers for 32nd Annual Meeting of Radiation Research Society* (Philadelphia, PA: Radiation Research Society), p. 134.

STEINER, A. L., PAGLIARA, A. S., CHASE, L. R., and KIPNIS, D. M., 1972. Radioimmunoassay for cyclic nucleotides. II. Adenosine 3′,5′-monophosphate and guanosine 3′,5′-monophosphate in mammalian tissues and body fluids. *Journal of Biological Chemistry*, **247,** 1114–1120.

STEINITZ, K., and TURKLAND, H., 1940, The determination of the glomerular filtration by the endogenous creatinine clearance. *Journal of Clinical Investigation*, **19,** 285–297.

STEWART, D. A., LEDNEY, G. D., BAKER, W. H., DAXON, E. G., and SHEEHY, P. A., 1982, Bone marrow transplantation of mice exposed to a modified fission neutron (N/G-30 : 1) field. *Radiation Research*, **92,** 268–279.

STEWART, F. A., MICHAEL, B. D., and DENEKAMP, J., 1978, Late radiation damage on the mouse bladder as measured by increased urination frequency. *Radiation Research*, **75,** 649–659.

STEWART, F. A., RANDHAWA, V. S., MICHAEL, B. D., and DENEKAMP, J., 1981, Repair during fractionated irradiation of the mouse bladder. *British Journal of Radiology*, **54,** 799–804.

STEWART, F. A., SORANSON, J. A., ALPEN, E. L., WILLIAMS, M. V., and DENEKAMP, J., 1984, Radiation-induced renal damage: The effects of hyperfractionation. *Radiation Research*, **98,** 407–420.

STRANGE, R. C., and MJOS, O. D., 1975, The sources of plasma cyclic AMP: Studies in the rat using isoprenaline, nicotinic acid and glucagon. *European Journal of Clinical Investigation*, **5,** 147–152.

SUTHERLAND, E. W., 1970, On the biological role of cyclic AMP. *Journal of the American Medical Association*, **214,** 1281–1288.

SUTHERLAND, E. W., BUTCHER, R. W., ROBINSON, G. A., and HARDMAN, J. G., 1967, The role of adenosine 3′,5′-monophosphate in hormone action. *Wirkungsmechanismen der Hormonen*, edited by P. Karlson (Berlin: Springer-Verlag), pp. 1–32.

TANNER, N. S. B., STAMFORD, I. F., and BENNETT, A., 1981, Plasma prostaglandins in mucositis due to radiotherapy and chemotherapy for head and neck cancer. *British Journal of Cancer*, **43**, 767–771.

TAYLOR, A. L., DAVIS, B. B., PAWLSON, L. G., JOSIMOVICH, J. B., and MINTZ, D. H., 1970, Factors influencing the urinary excretion of 3′,5′-adenosine monophosphate in humans. *Journal of Clinical Endocrinology*, **30**, 316–324.

TAYLOR, L., MENCONI, M. J., and POLGAR, P., 1983, The participation of hydroperoxides and oxygen radicals in the control of prostaglandin synthesis. *Journal of Biological Chemistry*, **258**, 6855–6857.

TAYLOR, L., and POLGAR, P., 1980, Stimulation of prostaglandin synthesis by ascorbic acid via hydrogen peroxide formation. *Prostaglandins*, **19**, 693–700.

THOMAS DE-LA VEGA, J. E., BANNER, B. F., HUBBARD, M., BOSTON, D. L., THOMAS, C. W., STRAUS, A. K., and ROSEMAN, D. L., 1984, Cytoprotective effect of prostaglandin E_2 in irradiated rat ileum. *Journal of Surgery, Gynecology, and Obstretrics*, **158**, 39–45.

THYAGARAJAN, P., VAKIL, U. K., and SREENIVASAN, A., 1977, Effects of whole body X-irradiation on the biogenesis of creatine in the rat. *Radiation Research*, **70**, 519–529.

TRANG, L. E., 1980, Prostaglandins and inflammation. *Seminars in Arthritis and Rheumatism*, **9**, 153–190.

TROCHA, P. J., and CATRAVAS, G. N., 1980, Variation in cyclic nucleotide levels and lysosomal enzyme activities in the irradiated rat. *Radiation Research*, **83**, 658–667.

URIBE, A., JOHANSSON, C., RUBIO, C., and ARNDT, J., 1984, Effects of 16,16-dimethyl prostaglandin E_2 on irradiation damage of the small intestine. *Acta radiologica, Oncology*, **23**, 349–352.

VERBINSKI, V. V., CASSAPAKIS, C. C., HAGAN, W. K., FERLIC, K., and DAXON, E., 1981, *Calculation of the Neutron and Gamma-ray Environment in and Around the Triga Reactor*. Volume 2, Defense Nuclear Agency 5793F-2.

VIERLING, A. F., and STRIKE, T. A., 1968, Plasma calcium concentrations in rats during postirradiation diuresis. *Armed Forces Radiobiology Research Institute Scientific Report SR68-21*, Defense Atomic Support Agency, Bethesda, Maryland.

WALKER, D. I., and EISEN, V., 1979, Effect of ionizing radiation on 15-hydroxy prostaglandin dehydrogenase (PGDH) activity in tissues. *International Journal of Radiation Biology*, **36**, 339–407.

WATERMAN, F. M., KUCHNIR, F. T., SKAGGS, L. S., KOUZES, R. T., and MOORE, W. H., 1979, Energy dependence of the neutron sensitivity of C-Co_2, Mg-Ar and TE-TE ionization chambers. *Physical and Medical Biology*, **24**, 721–733.

WELBOURNE, T. W., and SPURR, G. B., 1971, Mechanism of renal acid excretion following X-irradiation of the dog. *Radiation Research*, **47**, 472–479.

WELCH, B. L., 1951, On the comparison of several mean values: An alternate approach. *Biometrika*, **38**, 330–336.

WHITEFIELD, J. F., RIXON, R. H., MCMANUS, J. P., and BALK, S. D., 1972, Calcium, cyclic adenosine 3′,5′-monophosphate and the control of cell proliferation. A Review. *In Vitro*, **8**, 257–278.

WILLIAMS, M. V., and DENEKAMP, J., 1983, Sequential functional testing of radiation-induced renal damage in the mouse. *Radiation Research*, **94**, 305–317.

WILLIAMS, M. V., and DENEKAMP, J., 1984, Radiation induced renal damage in mice: Influence of fraction size. *International Journal of Radiation Oncology, Biology and Physics*, **10**, 885–893.

WILLS, E. D., and WILKINSON, A. E., 1967, The effect of irradiation on lipid peroxide formation in subcellular fractions. *Radiation Research*, **31**, 732–747.

ZEMAN, G. H., and FERLIC, K. P., 1984, Paired ion chamber constants for fission gamma-neutron fields. (Bethesda, MD, Armed Forces Radiobiology Research Institute) Technical Report TR84-8.

ZIPSER, R. D., and SMORLESI, C., 1984, Regulation of urinary thromboxane B_2 in man: Influence of urinary flow rate and tubular transport. *Prostaglandins*, **27**, 257–271.

Radiation Protection Dosimetry
Vol. 15 No. 2 pp 109–115 (1986)
Nuclear Technology Publishing

PERFORMANCE CHARACTERISTICS OF A HIGH-LEVEL SOLID-STATE PERSONNEL DOSIMETRY SYSTEM IN PULSED RADIATION ENVIRONMENTS

R. E. Swaja*, R. Oyan†, C. S. Sims* and M. A. Dooley‡
*Health and Safety Research Division
Oak Ridge National Laboratory
Oak Ridge, TN 37831, USA
†OECD Halden Reactor Project
PO Box 173, N-1751 Halden, Norway
‡Radiation Science Department
Armed Forces Radiobiology Research Institute
Bethesda, MD 20814-5145, USA

Received March 12 1986, Amended May 17 1986, Accepted May 24 1986

Abstract — The Health Physics Research Reactor at Oak Ridge National Laboratory was used to evaluate performance characteristics of a high-level, solid-state, personnel dosimetry system developed for the US Army for the rapid measurement of total (gamma plus neutron) radiation doses to soldiers in locations where tactical nuclear weapons could be used. The gamma sensitive element of the dosemeter consists of a silver-activated phosphate glass and the neutron detector is a silicon diode. Areas considered in this evaluation included pre-irradiation dose indication; accuracy and precision of gamma, neutron, and total dose measurements; time dependence; and temperature effects. Study results indicate that for doses above about 0.4 Gy, the system can provide rapid and accurate dose estimates within accuracy limits specified by several international regulatory and standards agencies for criticality accident dosimetry. However, theoretical and observed lower limits of detection for this system are somewhat higher than the 0.25 Gy minimum dose of interest for general accident dosimetry.

INTRODUCTION

At the request of the US Army, performance characteristics of a high-level, solid-state, personnel radiation dosimetry system were evaluated at the Oak Ridge National Laboratory (ORNL)[1]. The system considered in this study consisted of the US Army DT-236 personnel dosemeter, which uses radiophotoluminescent (RPL) glass and silicon diode detection elements, and the CP-696 reader[2]. This dosemeter was developed to measure total (gamma plus neutron) radiation doses to individual soldiers in locations where tactical nuclear weapons could be used. Although specifically designed for military applications, the DT-236 system could also be applied in situations where high-level gamma and/or neutron doses are possible, e.g.criticality accident dosimetry.

Performance characteristics of this system were evaluated in pulsed radiation environments to simulate battlefield exposure or criticality accident conditions. The source of radiation for this study was the Health Physics Research Reactor (HPRR) at ORNL operated in the pulse mode with and without spectrum-modifying shields[3]. Areas considered in this evaluation included pre-irradiation dose indication; accuracy and precision of gamma, neutron, and total dose measurements; time dependence; and temperature effects. The following text provides a summary of the results obtained during this study.

DESCRIPTION OF THE DT-236 DOSIMETRY SYSTEM

The DT-236 dosemeter badge, which is shown in Figure 1, consists of two independent solid-state detecting elements[4] used to measure gamma dose and fast neutron dose. A 12 × 15 × 3.5 mm^3 rectangular parallelepiped of silver-activated phosphate glass is used as the gamma sensitive element. Gamma dose estimation is based on radiophotoluminescent properties in which the phosphate glass fluoresces with an intensity proportional to the absorbed gamma dose when stimulated with ultraviolet (UV) light. The neutron detector is a wide-based silicon junction diode. When exposed to fast neutrons, the crystal lattice structure of the diode is damaged and the resistivity of the

Also published as Oak Ridge National Laboratory
Report Number ORNL-6265.

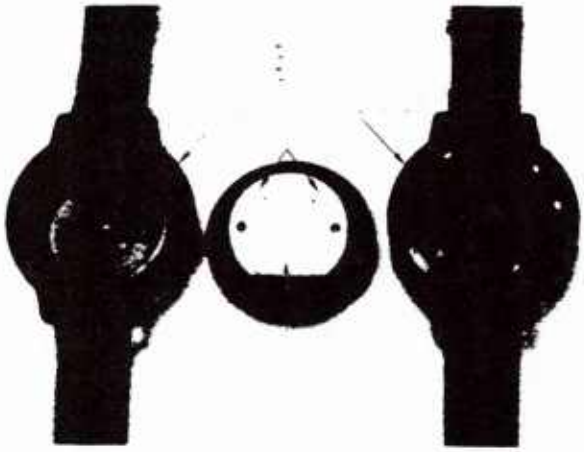

Figure 1. The DT-236 solid-state personnel dosemeter.

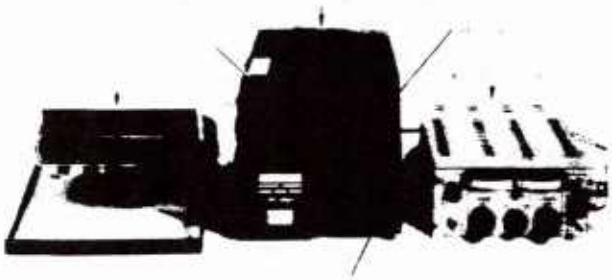

Figure 2. Experimental set-up used to evaluate the solid-state personnel dosemeters.

material increases. Neutron dose estimation is based on measuring the increase in voltage drop across the diode at constant current. For this system, gamma and neutron readings using these methods are non-destructible and the dosemeter will maintain the cumulative dose received by the individual. Both elements are packaged in a container of wristwatch size which can be worn on the wrist or on an identification tag chain.

In this study, dosemeters were evaluated using the instrument set-up shown in Figure 2 which includes a CP-696 reader, a power supply, and a digital voltmeter. The CP-696 reader consists of two separate evaluation circuits contained in one instrument. Dosemeters are read by placing the RPL-diode container on the dosemeter holder so that the diode contacts connect, depressing a 'read' switch, and observing the indicated dose on the analogue meter. The gamma portion of the reader is a UV flashtube source, optical filters, and a photodiode sensitive to the RPL glass fluorescent light. The neutron portion consists of a peak-reading voltmeter and a pulsed constant-current generator. The neutron and gamma channels have check standards to indicate proper reader operation. Power for the reader was supplied by a 24 volt DC power supply connected to the power input. Although the reader has analogue indication of radiation dose in tissue kerma, measurements in this study were based on digital indication from a voltmeter connected internally in parallel with the analogue meter. The use of the digital voltmeter permitted more accurate readings and allowed estimation of readings which were off scale on the analogue meter. To convert from indicated voltage to dose, a calibration curve was developed by comparing dose read from the analogue meter and digital readings[1]. Total and gamma doses were estimated directly from voltmeter readings, and neutron doses were obtained by subtracting the gamma components from the total indicated doses.

PRE-IRRADIATION CHARACTERISTICS

Prior to the HPRR exposures, 188 of the unirradiated DT-236 dosemeters were evaluated using the CP-696 reader. Since there was some variation between different readings of the same badge, the indicated dose was taken to be the middle value of three successive readings. The variation in successive readings for the same badge was approximately ± 3% about the middle value with most dosemeters being better than ± 2% for total, gamma, or neutron doses.

All unirradiated dosemeters gave non-zero dose readings. Total doses ranged from 0.26 to 0.66 Gy with a mean of 0.40 Gy and one standard deviation of 0.09 Gy (22% of the mean). Neutron doses varied between 0.02 and 0.38 Gy with a mean of 0.17 Gy and one standard deviation of 0.07 Gy (45% of the mean). Pre-irradiation gamma doses varied from 0.08 to 0.38 Gy with a mean of 0.23 Gy and one standard deviation of 0.08 Gy (34% of the mean). Based on the observed standard deviations and suggested calculational conventions[5], the theoretical lower limits of detection for this system are 0.41, 0.34, and 0.36 Gy for total, neutron, and gamma doses, respectively. It should be noted that these values are higher than the minimum dose of interest for accident conditions of 0.25 Gy[6]. In the subsequent analyses, unexposed dosemeter responses for each individual badge were recorded and subtracted from the exposed dosemeter indications for the same badge to account for background readings.

IRRADIATION CONDITIONS

The source of radiation for this evaluation was the

Health Physics Research Reactor operated in the pulse mode. The HPRR is a fast pulsed reactor which can be used to simulate nuclear battlefield conditions and provide acute, high-level, neutron and gamma doses. A variety of radiation fields with different neutron energy spectra and neutron to gamma dose ratios were produced by using spectrum-modifying shields to simulate various weapon and material attenuation spectra. The fields ranged from the unshielded reactor which has a hard (nearly ^{235}U fission) neutron energy spectrum with a low gamma component to a Lucite shielded condition which has a soft (hydrogen moderated) neutron spectrum with a relatively high gamma component.

A total of seven pulses was conducted for this study with fission yields ranging from 3.91 to 9.28 $\times$ 10^{16} fissions and corresponding pulse half-widths varying between about 120 and 65 μs, respectively. Associated neutron doses at 3 m from the HPRR vertical centreline varied from 0.40 to 3.10 Gy (tissue kerma), gamma doses varied from 0.12 to 0.50 Gy, and total doses varied from 0.77 to 3.60 Gy. Reference neutron doses, gamma doses, and fission yields were determined using standard HPRR reference dosimetry techniques[7,8] and recent neutron differential spectrum measurements. For these irradiations, the reactor was operated over the storage pit at a height of 1.4 m above the floor. Dosemeters were exposed in air (attached to ring stands) at a height of 1.4 m above the floor with at least five badges mounted side by side at each location.

ACCURACY AND PRECISION

Accuracy and precision associated with this solid-state system were determined by comparing measured and reference doses for a wide range of dose levels (0.04 to 13.98 Gy) and a variety of HPRR pulsed radiation fields. Accuracy is reflected by the mean of the individual measurements made at a particular location and precision is given by one standard deviation of the individual results about the mean. Dose measurements presented in the following text were made in air, and reference and measured results were reported in terms of tissue kerma.

Average measured doses (background corrected) divided by reference total, gamma, and neutron doses as a function of reference dose are shown in Figure 3 to 5, respectively. Most indicated results are for the unshielded HPRR with dosemeters placed at various distances from the reactor. Data for the steel, concrete, and Lucite shielded pulses are for the badges located at 3 m from the HPRR which is the distance at which the shielded reference doses are best known. Error bars represent one standard deviation about the mean.

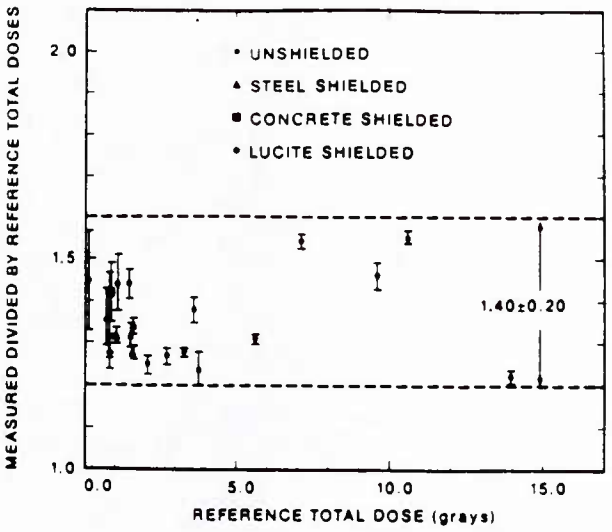

Figure 3. Measured divided by reference total doses as a function of reference dose.

Data shown in Figure 3 indicate that the DT-236 system over-estimates reference values by about 20 to 60% for total doses between approximately 0.2 to 14.0 Gy for all considered HPRR radiation fields. These over-estimates are expected based on RPL and diode performance observed during previous DT-236 dosemeter tests at pulsed reactor facilities[2]. The data also show that if the reader output is adjusted to indicate 40% lower total doses (i.e. decrease the calibration curves for digital readout or decrease the meter indication for analogue readout), measured results will be within $\pm$ 20% of reference results for a wide range of spectra and doses between about 0.2 and 14.0 Gy. The $\pm$ 20% limits about a measured to reference ratio of 1.4 are included in Figure 3. Although the figure indicates that this adjustment will provide $\pm$ 20% accuracy at total dose levels below 0.5 Gy, the practical system accuracy at low doses will still be limited by the 0.41 Gy theoretical lower limit of detection and the 0.09 Gy standard deviation observed for the unirradiated badges. A measurement accuracy of $\pm$ 20% would satisfy accuracy criteria specified by several regulatory and standards agencies[6,9,10] for criticality accident dosimetry systems.

With regard to measurement precision, single standard deviations were within 4% of the mean values for total doses greater than about 1.0 Gy. For doses below this value, standard deviations ranged from 4 to 12% of the means. These results are consistent with data obtained in previous DT-236 performance tests[11] which indicated a one standard deviation value of about 5% of the means for doses above 0.5 Gy.

Average measured divided by reference gamma doses as a function of reference dose are shown in Figure 4. The figure shows that, except for one measurement, the RPL system over-estimates gamma doses by about 20 to 60% for reference values above 0.35 Gy. This over-estimation is expected based on the observed over-response of the DT-236 gamma detection system to hard gamma rays and the neutron sensitivity of the RPL glass[2,6]. Below approximately 0.35 Gy, measured gamma doses show significant variations relative to reference values (between 0.5 to 1.9 times references) with relatively large standard deviations about the measured means. Thus, at gamma doses below about 0.35 Gy, which is very close to the theoretical lower limit of detection determined from unirradiated dosemeter results, the RPL system does not provide accurate gamma dose estimates in the fields considered in this study. Figure 4 also shows that by adjusting the reader output to indicate 40% lower, gamma doses between about 0.35 and 1.70 Gy can be measured to within ± 20% of the reference values.

Single standard deviations were within approximately 5% of the means for gamma doses above 0.50 Gy. Below this level, standard deviations ranged from about 5 to 31% of the means with most values being in the 15 to 25% range. These results are slightly more precise than results obtained in previous DT-236 performance tests[11] which indicated one standard deviation values of about 20% of the means for gamma doses above 0.50 Gy. Accuracy and precision of gamma measurements for doses above about 0.35 Gy are comparable with results obtained for other methods used to determine gamma doses under accident conditions[8]. However, theoretical and observed lower limits of detection for this system are higher than those observed for other gamma dosimetry techniques[6].

Measured divided by reference neutron doses as a function of reference dose are shown in Figure 5. Except for one point, average measured results over-estimate reference values by 20 to 60% over the entire range of reference doses and all HPRR spectra. Over-estimation is expected based on the observed over-response of the DT-236 silicon diode detection system to fast neutrons in air[2]. Figure 5 also shows that by adjusting the reader output to indicate 40% lower, neutron doses can be estimated to within ± 20% of reference values between about 0.20 and 12.00 Gy. At doses below about 0.20 Gy, neutron measurement accuracy is significantly affected by relatively large uncertainties in corresponding low gamma dose measurements which were subtracted from total dose readings.

Single standard deviations for the estimated neutron doses varied from 0.3 to 15.7% of the means over the entire range of reference doses. Most standard deviations were between 1 and 6% of the means, which is significantly more precise than the range of values obtained for the corresponding gamma measurements. These results are consistent with measurement precisions obtained in previous DT-236 dosemeter performance studies[11]. Neutron measurement accuracy and precision for the DT-236 system are comparable to values obtained for other methods used to estimate neutron doses under accident conditions[8].

TIME DEPENDENCE

Figure 6 shows measured total, neutron, and gamma doses at various times after exposure relative

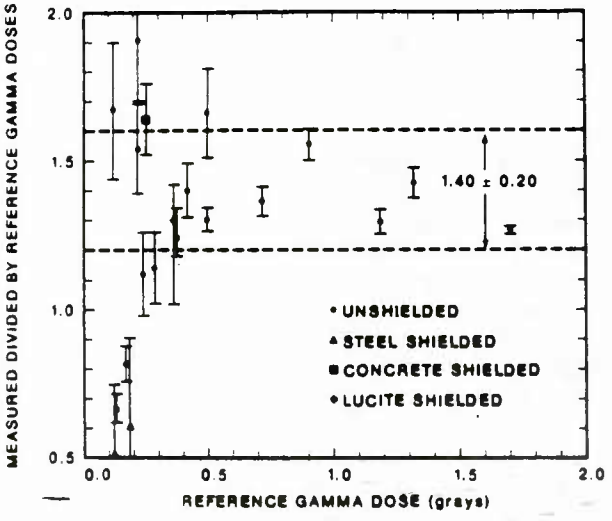

Figure 4. Measured divided by reference gamma doses as a function of reference dose.

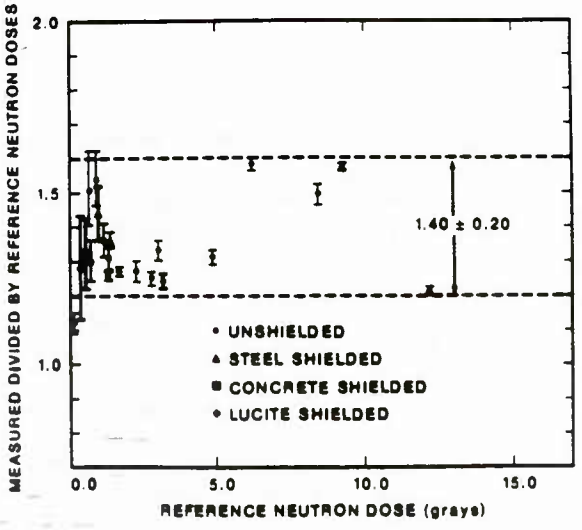

Figure 5. Measured divided by reference neutron doses as a function of reference dose.

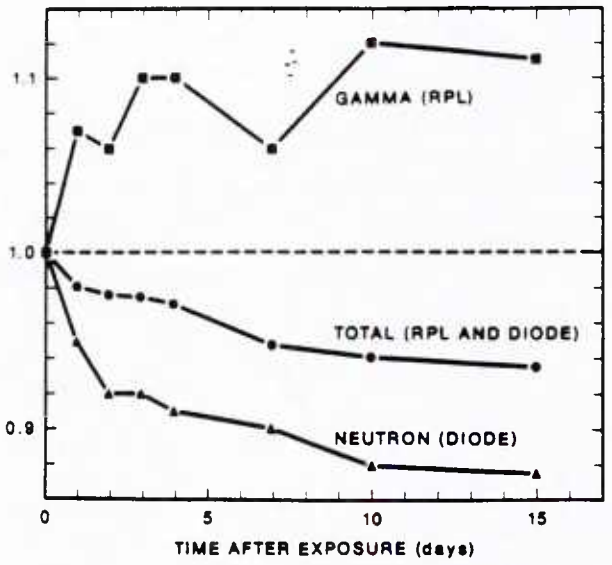

Figure 6. Total, gamma, and neutron dose indication as a function of time after exposure.

to the doses measured at two hours after irradiation for times up to 15 days. Each point represents the average result of five dosemeters irradiated to total, neutron, and gamma doses of 3.30, 2.88, and 0.42 Gy, respectively, in the unshielded HPRR spectrum. Single standard deviations associated with the indicated points are about 4%, 4%, and 10% about the means of the five readings for the total, neutron, and gamma measurements, respectively.

Over the 15 day evaluation period, the average total dose decreased by only about 7% relative to the value obtained two hours after exposure. Most of this decrease occurred within the first seven days after irradiation. Very little reduction was exhibited for total dose beyond the initial seven day period. Neutron dose results decreased by about 13% over the 15 day evaluation time with most reduction (approximately 8%) occurring in the first two days after irradiation. The RPL-measured gamma doses showed an increase of about 11% over initially measured results in 15 days. Most of this increase (approximately 7%) occurred in the first day after irradiation. The increased gamma response after exposure, which is characteristic of RPL materials[6], partly compensated for the decrease in neutron response to reduce the net decrease in total dose indication that might be expected in a strong neutron field.

TEMPERATURE EFFECTS

Effects of temperature changes on dosemeter response were evaluated by storing separate sets of badges exposed at room temperature (about 20°C) in cold (0°C) and in hot (45°C) environments for 24 hours and then reading the dosemeters while at the reduced or elevated temperatures and after return to room temperature. These cycles were repeated for three days to determine if observed changes were permanent. While part of the changes can be attributed to fading, magnitudes of some of the observed effects indicate definite temperature dependence. Temperature limits chosen for this test correspond with those specified in performance standards for routine personnel dosimetry systems[12].

Table 1 summarises results obtained for the cold and hot tests. Data shown in the table are average indicated total neutron and gamma doses relative to the values measured at room temperature two hours after exposure. Single standard deviations associated with these data are about ± 4% of the means for total and neutron values and about ± 10% of the means for gamma results. For total doses, the hot tests indicate that increasing from room temperature to

Table 1. Temperature effects on dosemeter response.

Condition	Time after exposure (hours)	Relative measured dose[a]					
		Total		Neutron		Gamma	
		Hot[b]	Cold[c]	Hot	Cold	Hot	Cold
Read at room temperature[d]	2	1.00	1.00	1.00	1.00	1.00	1.00
Stored and read at new temperature	24	0.77	1.00	0.76	1.00	0.84	1.22
Stored and read at room temperature	28	0.86	0.99	0.79	0.99	1.25	0.93
Stored and read at new temperature	48	0.77	1.01	0.76	0.98	0.81	1.13
Stored and read at room temperature	52	0.81	0.99	0.76	1.00	1.08	0.92
Stored and read at new temperature	72	0.77	1.03	0.75	0.97	0.85	1.27
Stored and read at room temperature	76	0.81	0.96	0.76	0.97	1.12	0.87

[a]Measured dose divided by the value measured at room temperature two hours after exposure
[b]Hot temperature = 45°C
[c]Cold temperature = 0°C
[d]Room temperature = 20°C

45°C for about 24 h causes a reduction of approximately 23% if the badges are read while hot. Allowing the badges to cool to room temperature before reading results in a 14 to 19% reduction in measured total dose. These data were consistent for all three hot temperature cycles. The cold tests showed only a 3% maximum increase in dosemeter response relative to the response after room temperature exposure when the badges were cooled to 0°C for 24 h and read cold. Reading the dosemeters after allowing them to return to room temperature resulted in decreases in average response of from 1 to 4% compared to the initial total dose.

Data for the neutron and gamma components of the dosemeter response showed that the RPL gamma system was more sensitive to temperature changes than the diode neutron detector. Considering the hot tests, neutron and gamma indications decreased by 24% and 16%, respectively, following heating to 45°C and reading at the elevated temperature. Subsequent heatings and coolings to room temperature produced almost no variation in neutron dose estimation following the initial decrease while the gamma dose estimates increased by about 25 to 40% between the hot and room temperature readings. Cold tests indicated that cooling the irradiated badges to 0°C and reading at cold or room temperature had almost no affect on neutron response. However, the gamma system was more sensitive to temperature variations in that the gamma dose estimate after the initial cooling and reading at 0°C increased by 22% relative to the original room temperature reading. Subsequent cooling and heating cycles produced approximately 20 to 40% variations in gamma response between 0°C and room temperature with a higher response obtained at the cold temperature.

SUMMARY

The following summary statements concerning performance of the DT-236 solid-state personnel dosimetry system are based on results presented in the preceding text:

1. There was about ± 3% variation in different readings of the same badge. The indicated dose was taken to be the middle value of three successive readings.
2. All unirradiated dosemeters gave non-zero dose readings. Theoretical lower limits of detection for this system based on the unirradiated readings are 0.41, 0.34, and 0.36 Gy for total, neutron, and gamma doses, respectively. These values are higher than the 0.25 Gy lowest dose of interest in accident dosimetry.
3. For the pulsed radiation environments and dose ranges considered in this study, the existing DT-236 dosimetry system over-estimated total, neutron, and gamma radiation doses in air by about 20 to 60% relative to reference values. By adjusting the reader output to indicate 40% lower total doses, measured results would be within ± 20% of reference values for a wide range of spectra and dose levels.
4. Measurement precisions for the DT-236 system were about 4%, 4%, and 5% for one standard deviation about the mean for total, neutron, and gamma doses greater than about 0.5 Gy, respectively. Below this value, standard deviations increased significantly for all three measurements. Also, precision for neutron measurements was generally better than that obtained for corresponding gamma measurements.
5. Observations of dosemeter response over a 15 day period indicated that the measured total dose decreased by approximately 7% relative to that obtained two hours after exposure. Neutron results decreased by about 13% while gamma measurements increased by 11% over the 15 day evaluation period.
6. Heating the dosemeter following exposure can result in a significant reduction in total and neutron response. Temperature variations below room temperature following irradiation produced relatively small effects on measured total and neutron doses. For the conditions considered in this study, the RPL gamma detector exhibited greater sensitivity to temperature changes than the neutron system.

Results of this study indicate that with some modification of existing reader calibration the DT-236 system can provide rapid and accurate estimates of total, neutron, and gamma radiation doses following acute, accident-level exposures for doses above about 0.4 Gy. In this range, measurement accuracies relative to reference values would be within limits specified by several international regulatory and standards agencies for criticality accident dosimetry. System accuracy and precision would also be comparable to performance characteristics of other methods presently used to determine radiation doses under accident conditions. However, theoretical and observed lower limits of detection for this system are higher than the 0.25 Gy minimum dose of interest for general accident dosimetry applications.

REFERENCES

1. Swaja, R. E., Oyan, R., Sims, C. S. and Dooley, M. A. *Evaluation of the U.S. Army DT-236 Battlefield Personnel Dosimetry System.* Oak Ridge National Laboratory Report ORNL-6265 (1986).
2. Basso, M. J. *Response of the UK DT-236 Personnel Dosimeter to a Fast Pulsed Nuclear Reactor Radiation Environment.* U.S. Army Report DEL CS-K (1982).
3. Sims, C. S. and Gilley, L. W. *Twenty Years of Health Physics Research Reactor Operation.* Nuclear Safety (5), 678-88 (1983).
4. Becker, K. *Solid State Dosimetry* (Cleveland, OH: CRC Press) pp. 141-173 and 225-231 (1973).
5. United States Nuclear Regulatory Commission. *Personnel Neutron Dosimeters.* Regulatory Guide 8.14 (1977).
6. International Atomic Energy Agency. *Dosimetry for Criticality Accidents – A Manual.* STI/DOC/10/211 (Vienna:IAEA) (1982).
7. Sims, C. S. and Ragan, G. E. *Health Physics Research Reactor Reference Dosimetry.* Oak Ridge National Laboratory Report ORNL-6240 (1986).
8. Swaja, R. E., Ragan, G. E. and Sims, C. S. *Twenty-First Nuclear Accident Dosimetry Intercomparison Study: August 6-10, 1984.* Oak Ridge National Laboratory Report ORNL-6173 (1985).
9. American National Standards Institute. *Dosimetry for Criticality Accidents.* ANSI Report N13.3-1969 (1969).
10. United States Atomic Energy Commission. *Nuclear Accident Dosimetry Program.* Manual AEC-0545 (1974).
11. Zeman, G. H., Brewer, R. A., Dooley, M. A. and Mohaupt, T. H. *Preliminary Evaluation of the U.S. Army Radiac Detector DT-236/PD and Radiac Computer CP-696/UD.* U.S. Armed Forces Radiobiological Research Institute Draft Report (1985).
12. American National Standards Institute. *Criteria for Testing Personnel Dosimeter Performance.* ANSI Report N13.11 (1980).

Prog. Lipid Res. Vol. 25, pp. 587–590, 1986
Printed in Great Britain

0163-7827/86/$0.00 + 0.50

DEVELOPMENT OF A MODEL SYSTEM TO STUDY LEUKOTRIENE-INDUCED MODIFICATION OF RADIATION SENSITIVITY IN MAMMALIAN CELLS

THOMAS L. WALDEN, JR.,* EUGENE V. HOLAHAN, JR. and GEORGE N. CATRAVAS
Departments of Biochemistry and Experimental Hematology, Armed Forces Radiobiology Research Institute, Bethesda, Maryland 20814-5145, U.S.A.

INTRODUCTION

Leukotrienes (LT) are an important class of biological mediators,[5] for which no information exists concerning their synthesis following a radiation insult, or on their ability to modify cellular response to a subsequent radiation exposure. LT are derived from arachidonic acid, as are prostaglandins, although by a separate enzyme system.[5] Prostaglandins are able to modify radiosensitivity of mammalian cells *in vivo*[3] and *in vitro*.[4] In addition, the cytoprotective effect induced by prostaglandins may have significance in cancer therapy since certain breast cancers which secrete elevated levels of prostaglandins are more resistant to therapy than similar tumors without the prostaglandin elevation.[1]

The objective of this study was to define a model system in which the metabolic fate of the LT could be monitored, and the effect of LT on the ionizing radiation sensitivity of mammalian cells *in vitro* could also be characterized.

METHODS

The Chinese hamster lung fibroblast cell line, V79A03, was selected for this model system because of its general use in radiobiology studies,[4,6] and because the radiosensitivity of this cell line has been shown to be modified by prostaglandin E_1.[4] This cell was derived from lung tissue, and has been continuously cultured for almost 37 yr. The monolayer cultures were grown in a CO_2 atmosphere of 3% in air, in a humidified incubator at 37°C. Cultures were maintained in α-MEM medium (Biofluids, Inc.) supplemented with Earle's salts, 25 mM Hepes buffer, 2 mM L-glutamine, 10% fetal bovine serum (Armour Pharmaceuticals) and an antibiotic mixture which typically included penicillin, streptomycin, gentamycin sulfate, and fungizone. Approximately 13 hr prior to the experiment, cells were trypsinized, resuspended in medium and plated as a single cell suspension in 4 ml of medium. No LT were detected in the fresh medium alone, or in untreated medium removed from flasks during passage of cells. LT were the generous gift of Dr. J. Rokach (Merck Frosst Laboratories). A 5 × concentration of LT was mixed with complete growth medium 5 min prior to addition to the flasks. The addition of 1 ml of filtered (0.22 μm filter) leukotriene-containing medium to the 4 ml already present in each flask, diluted the LT to the desired concentration.

Cells were irradiated using a 250 KVP Phillips X-ray machine at 13.5 mA. The beam was filtered with 0.26 mm Cu and 1 mm Al, with a target to object distance of 36.9 cm, at a dose rate of 1.7 Gray (Gy)/min to a total of 10 Gy. Drug toxicity and/or radiation sensitivity was determined 7 days later by the conventional survival assay based on colony formation as described by Sinclair and Morton.[6]

High performance liquid chromatography (HPLC) analyses were performed using an Ultrasphere C-18 column (Beckman, 4.6 × 250 mm). LT were eluted with an isocratic solvent system consisting of acetonitrile and 5 mM KH_2PO_4 in water, in a 1:2 ratio, at a flow rate of 1 ml/min, and detected by their absorbance at 280 nm wavelength.

*T. L. Walden is a National Research Council Associate.

RESULTS

Metabolism of LT by Tissue Culture Medium and by V79A03 Cells

2.5 μM LTC_4 in medium was incubated at 37°C for 0, 30, 60 and 120 min, and analyzed for metabolic breakdown at the indicated times. The fetal bovine serum used in the medium had detectable gamma glutamyl transpeptidase activity (data not shown), the enzyme which catalyzes the conversion of LTC_4 to LTD_4. This activity had minimal effects on the stability of LTC_4 levels in medium alone (Fig. 1). In a similar experiment examining the stability of LTD_4, 33% of the initial LTD_4 was converted to LTE_4 during the first 30 min, and 98% was converted to LTE_4 by 60 min. LTE_4 in medium was stable over this same time period.

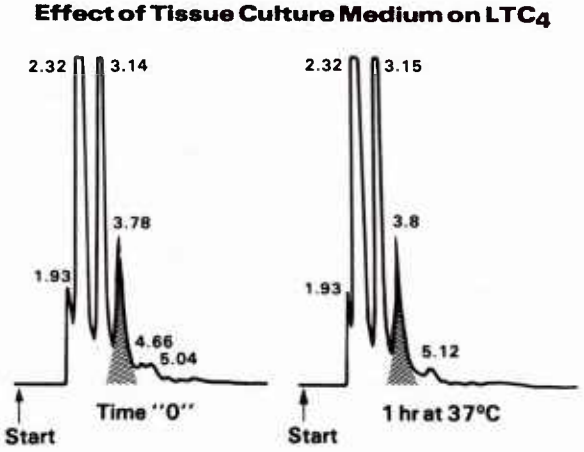

FIG. 1. Effect of tissue culture medium on LTC_4 stability. 2.5 μM LTC_4 in tissue culture medium was incubated for 0 and for 1 hr at 37°C. Aliquots were diluted 1:1 in HPLC buffer and 100 μl of this solution was analyzed by reverse-phase HPLC as described in Methods. The HPLC chromatograms shown indicate that LTC_4 (shaded peak at 3.78 or 3.8 min) was not degraded by medium alone over a 1 hr period.

Similar experiments were repeated in the presence of $3.5–4.0 \times 10^6$ V79A03 cells in exponential growth in a 100 mm petri dish. After incubating the cells for 2 hr at 37°C, only 23% of the initial LTC_4 remained, with 2% as LTD_4, 57% as LTE_4 and the remainder presumed attached to the cells or lost during recovery (Fig. 2A). No major unidentified peaks were observed after incubation, presumably indicating that LT metabolism stopped at LTE_4 without subsequent breakage of the thiolether bond. Similar results obtained with LTD_4 (Fig. 2B).

Recent studies have shown that trypsinization inactivated LT receptors found for each of the LT in V79A03 cells (to be reported later). In the experiments reported here, cells were permitted to recover from any trypsin-induced effect before initiating LT exposure.

Effect of LT on Radiation Sensitivity

V79A03 cells exhibited no toxicity following 7 day exposure to LTC_4 at 0, 0.5 and 2.5 μM (Fig. 3). LTD_4 and LTE_4 were also non-toxic at 2.5 μM (data not shown). Figure 3 also shows the results when cells are treated with LTC_4 at the indicated concentrations for 2 hr prior to exposure to 10 Gy of X-rays. Single cell survival was almost double for pretreated-irradiated cells (surviving fraction = 0.091 $\pm$ SEM of 0.006) compared to non-LT treated, irradiated cells (surviving fraction = 0.048 $\pm$ 0.002). This increase is statistically significant at the 0.001 level by a Student t-test comparison of the means. The LT-induced modification of radiosensitivity has been repeated with identical results, and has also been demonstrated for LTE_4 at 2.5 μM (surviving fraction = 0.071 $\pm$ 0.002, $p = 0.001$), but not for LTD_4.

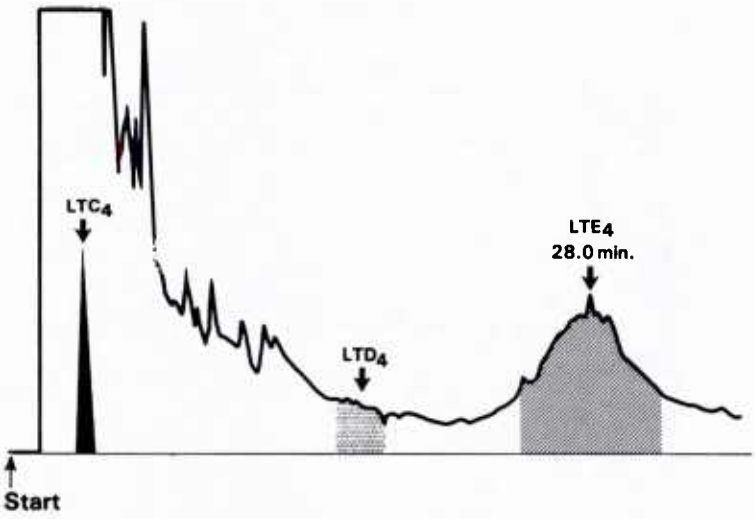

FIG. 2A. Metabolism of LTC_4 by V79A03 cells and by tissue culture medium. 2.5 μM LTC_4 was incubated in tissue culture medium placed in a 100 mm petri dish containing 3.5–4.0 $\times$ 10^6 cells in exponential growth. The medium was removed after 2 hr incubation at 37°C and analyzed by reverse-phase HPLC as described. The vertical scale of the HPLC chromatogram in the figure represents relative absorbance at 280 nm of the eluting peaks, while the horizontal axis represents elution time (not shown). The shaded areas show where LTC_4, LTD_4, and LTE_4 eluted. At the 0 incubation time, no peaks eluted in the areas where LTD_4 and LTE_4 are indicated.

FIG. 2B. Metabolism of LTD_4 by V79A03 cells and by tissue culture medium. V79A03 cells were incubated in medium containing 2.5 μM LTD_4 at 37°C for 2 hr, after which the medium was removed and analyzed by HPLC, as described for Fig. 2A. The arrow in the figure indicates where LTD_4 eluted in the 0 time chromatograph at ca. 20 ml, while the chromatogram in the figure shows that it was not present 2 hr later and had been shifted to the right (conversion to LTE_4).

DISCUSSION

A model system has been established to investigate the influence of leukotrienes, a class of biologically active mediators (1,6), on *in vitro* mammalian cell radiosensitivity. The V79A03 cell line appears to provide a good system for examining the cellular effects of LT, since the cells are responsive to LT and possess distinct LT receptors (Walden and Holahan, unpublished). Using this model system, the stability and metabolism of LT have been determined for α-MEM medium and by V79A03 cells. LTC_4 and E_4 are relatively stable in the medium alone, while LTD_4 breaks down to LTE_4 in a short period of time. This may reflect differences in the levels of the enzymes responsible, although we only examined the γ-glutamyl transpeptidase activity. V79A03 cells are capable of metabolizing LTC_4 and LTD_4 to LTE_4, and responses attributed to LTC_4 and LTD_4 will have to be examined carefully to ensure that any observed effects are not responses to LTE_4. The

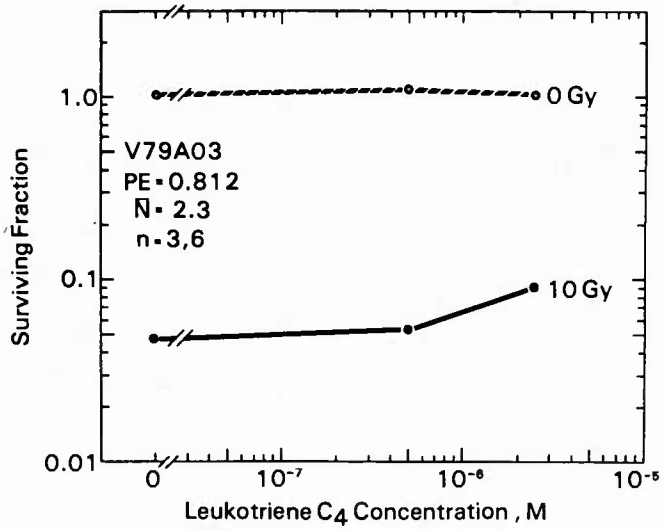

FIG. 3. Pretreatment with LTC_4 induces radioprotection in Chinese hamster V79A03 cells. V79A03 cells in exponential growth were placed in a 25 cm^2 flask. Thirteen hr later, the medium was removed and replaced with fresh medium containing LTC_4 at the indicated concentrations. Two hr after initiating chronic exposure of cells to either the control medium (without added LTC_4, or to LTC_4 supplemented medium), the flasks were divided into 2 groups of 3 or 6 flasks each for every concentration tested. Both groups were placed on ice for transportation to and from the radiation facilities. Group I represented by open circles was sham-irradiated (0 Gy) and indicates the toxicity of LTC_4 at the 3 concentrations shown: 0, 0.5, and 2.5 μM. Group I has an "n" of six. Group II represented by the solid circle received 10 Gy of X-irradiation. Reproductive viability was measured by counting the surviving colonies at day 7 post treatment, and correcting for multiplicity ($N = 2.3$) and the plating efficiency (PE = 0.812). Standard errors calculated for each point were within the size of the data point shown. Identical results were obtained when the experiment was repeated on a different day.

metabolic studies (Fig. 2A and B) were conducted with large populations of cells, while the radiation survival studies (Fig. 3) were conducted with much smaller cell populations, and as such, the stability of the LT in the radiation studies should be related primarily to medium effects.

Preliminary cell survival studies have shown a small but statistically significant decrease in cellular radiosensitivity when V79A03 cells are treated with LTC_4 2 hr before exposure to 10 Gy X-irradiation. The present study concentrated on examining only the effects with a single radiation exposure, because of the limited availability of LT. Experiments to optimize the dose and time of administration, as well as constructing a radiation dose response curve are in progress. The modification of radiosensitivity by LT was induced with continuous LT exposure. Future experiments will address the question of the necessity for continuous versus noncontinuous exposure to LT, as well as elucidating the mechanism(s) for the radio-/cytoprotection.

Acknowledgements—This work was supported by The Armed Forces Radiobiology Research Institute, Defense Nuclear Agency, under Research Work Units 00064 and 00104. The views presented in this paper are those of the authors. No endorsement by the Defense Nuclear Agency has been given or should be inferred.

REFERENCES

1. BENNETT, A., BERSTOCK, D. A., RAJA, B. and STAMFORD, I. F. *Br. J. Pharm.* **66,** 451P (1979).
2. DRAZEN, J. M., AUSTEN, K. F., LEWIS, R. A., CLARK, D. A., GOTO, G., MARFAT, A. and COREY, E. J. *Proc. Natl. Acad. Sci. U.S.A.* **77,** 4354–4358 (1980).
3. HANSON, W. R. and THOMAS, C. *Radiat. Res.* **96,** 939–948 (1983).
4. LEHNERT, S. *Radiat. Res.* **62,** 107–116 (1975).
5. SAMUELSSON, B. *Science* **220,** 568–575 (1983).
6. SINCLAIR, W. K. and MORTON, R. A. *Biophysics J.* **5,** 1–25 (1966).

Modelling of Biomedical Systems
J. Eisenfeld and M. Witten (editors)
Elsevier Science Publishers B.V. (North-Holland)
IMACS, 1986

STOCHASTIC MODELS FOR CELLS EXPOSED TO IONIZING RADIATION

Grace L. Yang and Charles E. Swenberg

Department of Mathematics, University of Maryland, College Park, Md. 20742, USA
and
Armed Forces Radiobiology Research Institute, Bethesda, Md. 20814, USA

The stochastic model for survivability of cells subjected to ionizing radiation initially formulated by Neyman and Puri [4] is modified to include both the plating time to cell proliferation and dose-saturation of potential lethal damage. This necessitates a reformulation of the cell survival and mutation probability. Based on the new model we derive the probability of occurrence for several experimental end points. The predictions of the model compare favorably to data for diploid yeast cells irradiated with 30 Mev electrons.

1. INTRODUCTION

In this paper we develop a stochastic model which quantitatively accounts for the effects of ionizing radiation on colonies of single cells. In addition to survival probability of single cells as a function of radiation dose, the stochastic model, by incorporating knowledge about the energy deposition characteristics, accounts for several experimental biological end points; in particular the effects of dose rate, radiation quality, delayed plating and split-dose reactivation on cell survivability can be explained. Survival is defined for a cell if it has the proliferative ability to form a colony. The model also predicts the time and dose dependence of the number of DNA strand breaks following irradiation and the number of phenotypically mutant (or transformed) cells as a function of dose and dose rate. Calculations using this model are compared to diploid yeast cells subjected to low energy electron irradiation.

There have been many mathematical models, mostly semi-deterministic, proposed for cell survivability [1-3]. The chance mechanism in cell survival deserves more emphasis but is often ignored in modeling. A major work on stochastic models for radiation dose-effect on single cells is the paper by Neyman and Puri [4] who developed a more detailed model by incorporating the chance mechanism into the biological responses of the cell to ionizing radiation. Two factors which appear to be important but not included in their paper are the time to plating and the possible "saturation of dose" in irradiated cell suspensions. Without including these factors the cell survival probability and mutation probability derived from the Neyman-Puri model are difficult to reconcile with experimental data (see eqs. (23) and (49) in [4]). That the mutation probability (eq. (49) in [4]) does not agree with the experiment was discussed by Neyman-Puri in [4].

In this paper, we modify the work of Neyman-Puri [4] by incorporating both the plating time to cell proliferation and dose-saturation effects. From this model we derive the cell survival probability and mutation probability among survivors. The predictions of the model satisfactorily fit the data on diploid yeast cells. By including the effects of dose saturation the observed "shoulder effect" in the graph of log survival probability versus dose and dose rate is explained.

Ionizing radiation can induce cell reproductive death (inactivation), non-fatal cell damage or no effect at all. Energy depositions in the cytoplasm have been shown experimentally not to alter cell survivability [5]. In general cell

inactivation and damage result from energy depositions within cell nuclei with DNA as the critical target. Three major classes of radiation-induced DNA damage can be recognized: (1) base damage, (2) single strand breaks and (3) double strand breaks. Although base damage prodominates over single strand breaks there is no direct evidence indicating that base damage is an important lesion in cell survival. DNA double strand breaks are believed to be responsible for both potentially lethal and sublethal damage [6] and if unrepaired, they will cause cell inactivation thereby decreasing survivability [2].

For modeling purposes, damage induced in a cell by ionizing radiation is measured by the number of lesions, a discrete unit. Cells have the ability to repair these lesions, but not with 100% efficiency. Some lesions will be correctly repaired (eurepair), while others may be misrepaired which presumably can result in transformed cells or cell inactivation. A transformed cell retains its reproductive ability, but its descendants are transformed cells which may be cancerous [7].

In controlled radiation experiments on single cell suspensions three distinct time periods can be recognized in the experimental setup: the irradiation period $(0,T)$, post-irradiation to time of cell plating (T,T_p) and post plating period (T_p,T_c). Cells of a given type, say yeast cells, are subject to irradiation by electrons or X-rays during $(0,T)$ with a specified dose rate. The initial sample size (number of cells) is known, typically about 10^6 per ml. The ionizing radiation may produce lesions which then activates the cell's repair mechanism. Thus during irradiation both lesion induction and repair go on simultaneously. After termination of the radiation the cells are placed in an environment which can be favorable for DNA repair but not for cell division. In this second time period (T,T_p) the cells continue to anneal the DNA strand breaks without producing a significant number of new lesions. The values of (T_p-T), the time to plating, cannot be made arbitrarily large since no nutrients are given to the cells; prolonged plating time will result in death. To actually count the number of survivors and the number of mutants, cells are plated in nutrients for colony forming ability at time T_p. The scoring time T_c is determined by the cell type and is selected such that the colonies have more than 50 cells. The number of colonies (assuming each colony originated from a single cell) determines the survival fractions and the mutation fractions for a given radiation dose.

In the model we assume that very little repair takes place after plating. This is not quite correct but constitutes a good first approximation [8]. Thus the status of the cell is fixed at the time of plating T_p, but the observation time T_c is much later. The experimental survival curve is constructed by plotting the log survival fraction against the dose, similarly for the mutation curve. For a given radiation dose (D) and plating time T_p the number of DNA strand breaks can also be measured using neutral and alkaline sucrose gradient velocity sedimentation techniques [9].

2. STOCHASTIC MODELING

We make the following assumptions on the initiation of lesions by irradiation and the repair-misrepair mechanism of the cell. Assumptions A1 and A2 pertain to the stochastic model of the evolution of cells during and after irradiation. Assumption A3 allows us to relate the model to experimental end points.

A1. Initiation of Lesions:

a. The primary radiation particles arrive at the cell according to a Poisson process with rate λ per unit time and unit volume. These primaries deposit their excess energy in discrete units thereby forming clusters of secondaries randomly distributed within the cell.

b. The number of secondaries, M, in a cluster is a random variable with probability generating function $g(\cdot)$. All particles act independently of one another. Each secondary particle can either induce a potentially lethal lesion or inactivate the cell or have no effect on the cell at all with respective probabilities π_1, π_2 and $1-\pi_1-\pi_2$. These probabilities may depend on time. Furthermore, there is a region, say nucleus, in the cell of size A such that radiation outside of this region does not affect survival of the cell [5].

A2. Repair-Misrepair Mechanism

Evolution of the cell during and after the radiation is described by a vector-valued stochastic process $\{(X_t,Y_t,Z_t);\ t\geq 0\}$, where

X_t = number of potentially lethal lesions that the cell has at time t,

Y_t = number of transformed lesions that the cell has at time t,

and

Z_t = number of inactivation events the cell has experienced up to time t.

A single inactivation event neutralizes the cell to the extent of destroying its dividing capability. Thus for the cell to maintain normal division rate, Z_t must be zero. The process $\{X_t,Y_t,Z_t;\ t\geq 0\}$ is a non-homogeneous Markov process.

A3.

The cell repair-misrepair process stops at the time of plating. For a cell to divide and grow into a visible colony at the time of scoring T_c it is necessary that all potentially lethal lesions are repaired by the time of plating.

Under assumptions A1 and A2, the joint probability generation function of X_t, Y_t and Z_t during irradiation $(0,T)$ and post irradiation (T,T_p) is given by

$$G(s_1,s_2,s_3;t) = \exp\{(s_3-1)\int_0^t \delta(v)dv - A\lambda\int_0^{t\wedge T}[1-g(h(s_1,s_2,s_3;v,t))]dv\}, \qquad (1)$$

where

$\delta(v) > 0$ is a natural death rate independent of irradiation,

$$h(s_1,s_2,s_3;v,t) = 1 + \sum_{i=1}^{3}\eta_i(v,t)(s_i-1), \quad |s_i|\leq 1, \qquad (2)$$

and

$\eta_i(v,t)$ are functions of π_1 and π_2.

Assumption A3 is introduced for mathematical simplification yet without deviating too much from reality. For example, diploid yeast cells do experience some repair after their reintroduction into a full growth medium [8]; however most of the reparable lesions occur prior to plating. Under assumptions A1, A2 and A3 the cell survival probability S(t) and transform probability C(t) can be derived:

$$S(t) = \exp\{-\int_0^t \delta(v)dv - \lambda A\int_0^{t\wedge T}[1-g(h(0,1,0;v,t))]dv\} \qquad (3)$$

where t is the time of plating, and the probability that the cell is alive and becomes a mutant by time t, for $t\geq T$, is

$$C(t) = S(t)\{1-\exp[-A\lambda\int_0^{t\wedge T}(g(h(0,1,0;v,t)) - g(h(0,0,0;v,t)))dv]\}. \qquad (4)$$

A general expression for the expected number of potentially lethal lesions is given by

$$E[X_t+cZ_t] = c\int_0^t \delta(v)dv + \lambda A g'(1)\,[\int_0^T \eta_1(v,t)dv + c\int_0^T \eta_3(v,t)dv], \qquad (5)$$

where c is the fraction of cell inactivations resulting from double strand breaks (see below).

3. APPLICATION TO LOW LINEAR ENERGY TRANSFER (LET) RADIATION

Radiation deposition of the primaries can be partially characterized by its energy loss per unit length along its trajectory. This is

called the LET of the radiation. For primaries interacting weakly with the environment the generating function of the cluster size is given by $g(s) = s$ to a good approximation. Suppose a total dose D is administered with a constant rate r, then T can be expressed as D/r. The survival probability $S(\cdot)$, mutation probability $C(\cdot)$ and the mean number of potentially lethal lesions can be thus written in terms of the dose D and dose rate r.

In Figure 1 is shown a comparison of theory with experimental results for the surviving fraction at two different plating times, immediately after irradiation and after 24 hours, as a function of dose for cells of the diploid strain 211*B of Saccharomyces cerevisiae irradiated in the stationary phase with 30 Mev electrons at a dose rate of 0.13 kGY/min. Parameters used to fit the experimental data are given in the figure caption. The probability π_1 of inducing a potentially lethal lesion varied with dose according to the relationship

$$\pi_1(D) = \pi_0(1 - \exp(-a\frac{D}{r})) \qquad (6)$$

whereas π_2 was taken to be independent of dose. Parameters determined from Figure 1 predict both the number of double strand breaks per cell as a function of dose for various plating times and the rate of annealing of double strand breaks after termination of the radiation. We have tacitly assumed that single cell critical lesions are DNA double strand breaks and have identified them as the potentially lethal lesions produced by ionizing radiation. Single strand breaks also occur and constitute major lesions in DNA. Their repair obeys first order kinetics, i.e., anneal exponentially with time; however, they do not inhibit cell proliferation and for this reason are not responsible for the increase in cell survivability as a function of time to plating (see Fig. 1). Nevertheless during the time period, $T_p - T$, single strand breaks are repaired and therefore constitute another measurable parameter not addressed here. These are illustrated in Figures 2 and 3, respectively. The dose dependence of the fraction of cell inactivations resulting from double strand breaks, c (see eq. (5)), has a form similar to eq. (6) but with $\frac{a}{r} = 2.7 \times 10^{-4}$/Gy. It is evident that agreement between theory and experiment is satisfactory. The kinetics of double strand break repair during liquid holding treatment according to eq. (5) is predicted to be an exponential decreasing function of time, $T_p - T$. With the Markov transition rates inferred from the surviving fraction of cells as a function of dose the number of double strand breaks as a function of time to plating (the holding time) can be calculated and as is evident from the results illustrated in Figure 3 agreement between theory and experiment is good. The explicit form of c in terms of known variables will be considered in a separate publication.

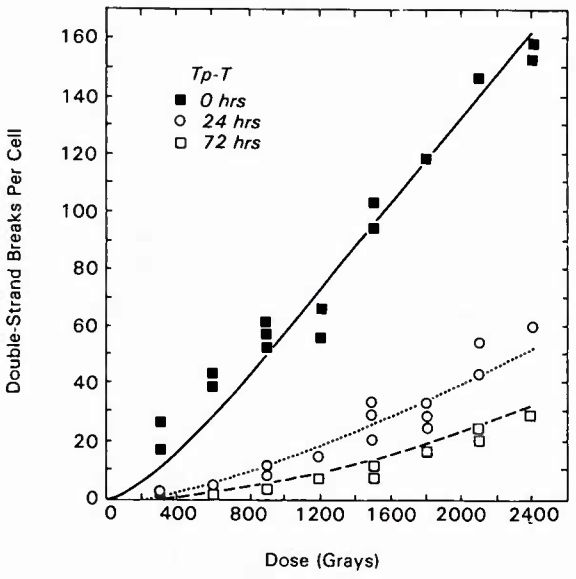

Fig. 2. Surviving fraction of cells as a function of dose. Lines denote theoretical fit with Markov transition rates $\alpha+\beta = 0.0457$/hr, $\gamma = 0.032$/hr, $a = 31.1$/hr, $\pi_0 = 0.46$, $\pi_2 = 1.3 \times 10^{-7}$, $\delta = 0.1 \times 10^{-6}$/hr and $A\lambda T/D = \theta = 0.01$ related to the process $\{X_t, Y_t, Z_t;\ t \geq 0\}$. (From Frankenberg-Schwager et al. [8].)

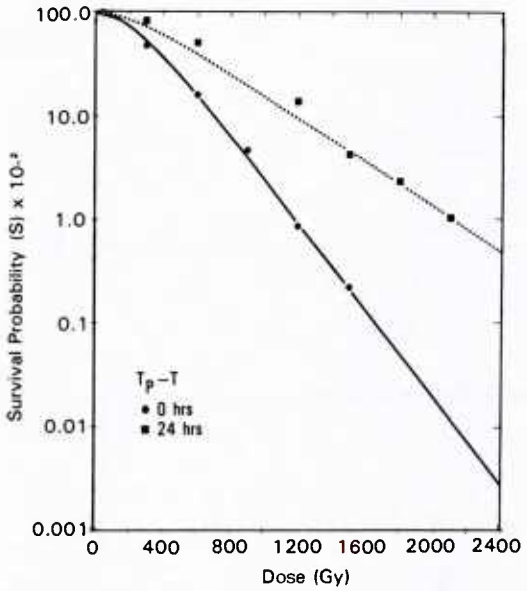

Fig. 1. Repair of double strand breaks under nongrowth conditions for different time to plating, T_p-T, as a function of dose. Lines denote theoretical fits with parameters as given in captcn to Figure 1. (From Frankenberg-Schwager et al. [8].)

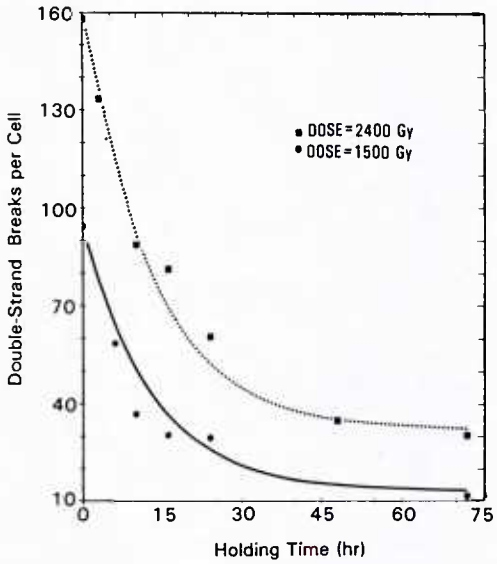

Fig. 3. Double strand breaks as a function of holding time (time to plating) for diploid yeast cells radiated with 30 Mev electrons. Lines denote theoretical fits using parameter as given in caption to Figure 1. (From Frankenberg-Schwager et al. [8].)

ACKNOWLEDGEMENT

We wish to thank Patrick Noon for numerous computer calculations.

REFERENCES

[1] Tobias, C.A., Blakely, E.A., Ngo, F.Q.H. and Yang, T.C.H. The repair-misrepair model of cell survival. In Radiation Biology In Cancer Research, ed. by Meyn, R.E. and Withers, H.R., Raven Press, New York, 195-230 (1980).

[2] Chadwick, K.H. and Leenhouts, H.P. The Molecular Theory of Radiation Biology, Springer-Verlag, Berlin (1981).

[3] Kappos, A. and Pohlit, W. A cybernetic model for radiation reactions in living cells: I. Sparsely-ionizing radiation; stationary cells. Int. J. Radiat. Biol. 22, 51-57 (1972).

[4] Neyman, J. and Puri, P.S. A hypothetical stochastic mechanism of radiation effects in single cells. Proc. R. Soc. Lond. B 213, 139-160 (1981).

[5] Von Borstel, R.C. and Rogers, R.W. Alpha-particle bombardment of the Habrobracon Egg II: Response of the cytoplasm. Radiat. Res. 8, 248-253 (1958).

[6] Frankenberg, D., Frankenberg-Schwager, M. and Harbich, R. Split-dose recovery is due to the repair of DNA double-strand breaks. Int. J. Radiat. Biol. 46, 541-553 (1984).

[7] Elkind, M.M. Repair processes in radiation biology. Radiat. Res. 100, 425-449 (1984).

[8] Frankenberg-Schwager, M., Frankenberg, D., Blöcher, D. and Adamczyk, C. Repair of DNA double-strand breaks in irradiated yeast cells under nongrowth conditions. Radiat. Res. 82, 498-510 (1980).

[9] See e.g. DNA Repair Mechanisms, ed. by Hanawalt, P.C., Friedberg, E.C. and Fox, C.F., Academic Press, New York (1978).

AFRRI TR86-3

TECHNICAL REPORT

Ionization chamber intercomparison in mixed neutron and gamma-ray radiation fields by National Bureau of Standards and Armed Forces Radiobiology Research Institute

M. Dooley
L. J. Goodman
G. H. Zeman
R. B. Schwartz
C. M. Eisenhauer
P. K. Blake

DEFENSE NUCLEAR AGENCY
ARMED FORCES RADIOBIOLOGY RESEARCH INSTITUTE
BETHESDA, MARYLAND 20814-5145

REVIEWED AND APPROVED

GARY H. ZEMAN
CDR, MSC, USN
Chairman
Radiation Sciences Department

LAWRENCE S. MYERS, Ph.D.
Scientific Director

RICHARD I. WALKER
CDR, MSC, USN
Acting Director

CONTENTS

INTRODUCTION

In 1983, the Radiological Physics Division at the Armed Forces Radiobiology Research Institute (AFRRI) embarked on an ambitious program aimed at upgrading the radiobiology dosimetry support at AFRRI. A key element in this upgrade was the evaluation of absorbed-dose measurements with ionization chambers in the mixed neutron and gamma-ray fields of the AFRRI TRIGA (Training Research Isotopes General Atomics) reactor. As part of the evaluation, an intercomparison of neutron dosimetry was carried out with the Nuclear Radiation Division of the National Bureau of Standards (NBS).

Before this effort, AFRRI had last compared its neutron ionization chamber measurements with other laboratories in 1973, when it participated in the International Neutron Dosimetry Intercomparison sponsored by the International Commission on Radiation Units and Measurements (1). Since that time, an increased interest in neutron radiotherapy has instigated the collection of considerable data on the basic physical parameters used for neutron dosimetry (2-6). Further, recent completion of the neutron spectral characterization of several AFRRI reactor fields (7,8) has enabled the calculation of the tissue-kerma factors needed for ionization chamber measurements in these fields (9). In conjunction with these efforts to improve the data base, protocols were established to standardize the methodology and terminology used in neutron dosimetry (10-12).

The availability of these physical data and the implementation of documented procedures made it essential for AFRRI to validate its mixed-field dosimetry techniques and to provide a foundation for future dosimetry programs between AFRRI and NBS. The intercomparison included measurements with ionization chambers in the NBS californium-252 facility and in four frequently used radiation fields of the AFRRI reactor. Scientists at AFRRI and NBS determined the tissue-kerma and absorbed-dose rates from the measurements and then compared results. In addition, the AFRRI chamber calibration procedures were examined through a comparison of chambers calibrated at the NBS and the AFRRI cobalt-60 facilities. This report summarizes the intercomparison, including a brief description of the sources, methods, results, special dosimetry problems, and accomplishments of the project.

MATERIALS AND METHODS

The intercomparison was accomplished through four sessions of measurement, with 2 weeks at the NBS radiation facilities and 2 weeks at the AFRRI reactor (see Appendix A).

The first set of measurements was performed in July 1983 at the NBS californium-252 irradiation facility, to take advantage of the well-known fission neutron spectrum and emission rate from the californium source (13,14). Free-in-air tissue-kerma rates were calculated from data that had been collected with ionization chambers exposed to an unmoderated californium-252 source and the same source moderated with a sphere of heavy water (D_2O). A second set of measurements was performed in November 1983 to resolve some ambiguous data

and discrepancies between AFRRI and NBS results. At that time, the calibration procedures of AFRRI were checked by calibrating four AFRRI chambers at the NBS cobalt-60 calibration facility.

Measurements were also performed in four configurations of the AFRRI reactor. Preliminary measurements were made in July 1983, followed by a definitive set of measurements completed in March 1984.

The Materials and Methods section provides a brief description of the sources, the instrumentation, and the measurement and calibration techniques used in the intercomparison.

RADIATION FACILITIES

NBS Californium-252 Facility

The NBS californium source used in this study is designated NS-100, and it was approximately 0.84 mg in July 1983. The source, fabricated for NBS by the Oak Ridge National Laboratories, is lightly encapsulated in about 3.2 mm of aluminum and 2.2 mm of stainless steel. With the moderator in place, the source was surrounded by a sphere of D_2O (radius 15.3 cm) covered with a thin sheet of cadmium (0.8 mm). The source was raised and lowered manually with a string from a shielded portion of the exposure facility. Each chamber was exposed individually in free air, at a nominal distance of 30 cm from the center of the source. When raised into position, the source was about 2.7 m from the concrete floor and 4 m from the nearest wall, making the contribution of room-backscattered neutrons negligible, i.e., less than a calculated value of 0.5% of the tissue-equivalent (TE) chamber response (14). Figure 1 diagrams the arrangement.

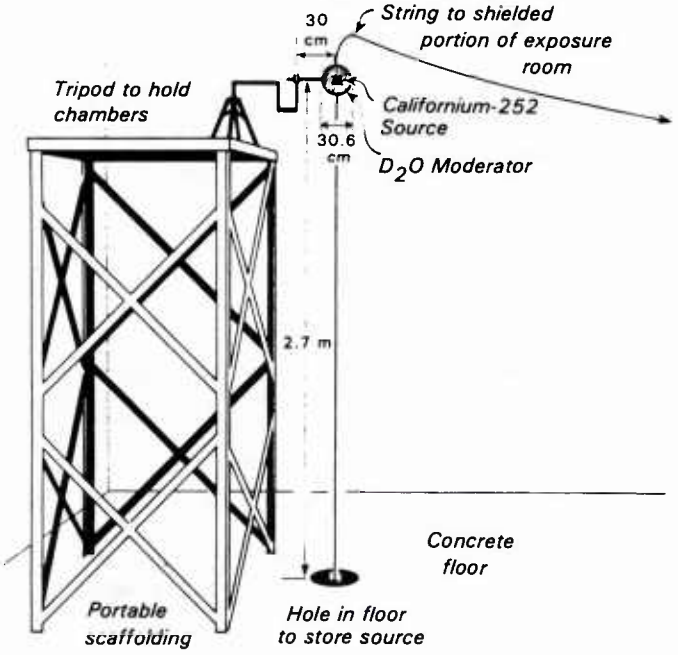

Figure 1. Arrangement of californium irradiation facility

AFRRI TRIGA Reactor

The AFRRI TRIGA reactor is described in reference 15. All measurements were performed in exposure room 1 (ER1) of the reactor facility. ER1 is approximately 6.1 m by 6.1 m by 2.6 m high, with a semicylindrical lobe of the reactor tank protruding into the south wall. The tank wall is covered with cadmium, and the exposure room surfaces (walls, floors, and ceiling) are coated with gadolinium paint to absorb thermal neutrons.

Measurements were conducted in four of the most frequently used reactor configurations (Table 1 and Figure 2), described in the following:

15-cm-Pb shield: A 15-cm-thick lead shield placed in front of the reactor tank wall to attenuate fission and fission product gamma radiation

Bare room: No shielding placed between the experiment and the reactor core

30-cm-water shield: Reactor core moved back 30 cm from its nominal position in the tank, creating a water shield to drastically reduce the neutron component of the radiation field

15-cm-Pb field with phantom: A 15-cm-diameter, 24-cm-high cylindrical phantom placed behind the lead shield (configuration 1). The phantom, shown in Figure 3, was constructed of plastic and filled with TE liquid (liquid number 33 in Appendix B of reference 10).

Table 1. Reactor Configurations

Number	Configuration	Meters From Core Center*
1	15 cm Pb	100, 235, 328, 401
2	Bare room	100, 235, 328, 401
3	30 cm water	130
4	15 cm Pb with phantom	100

*Nominal distance from front face of tank wall to core center was 30 cm.

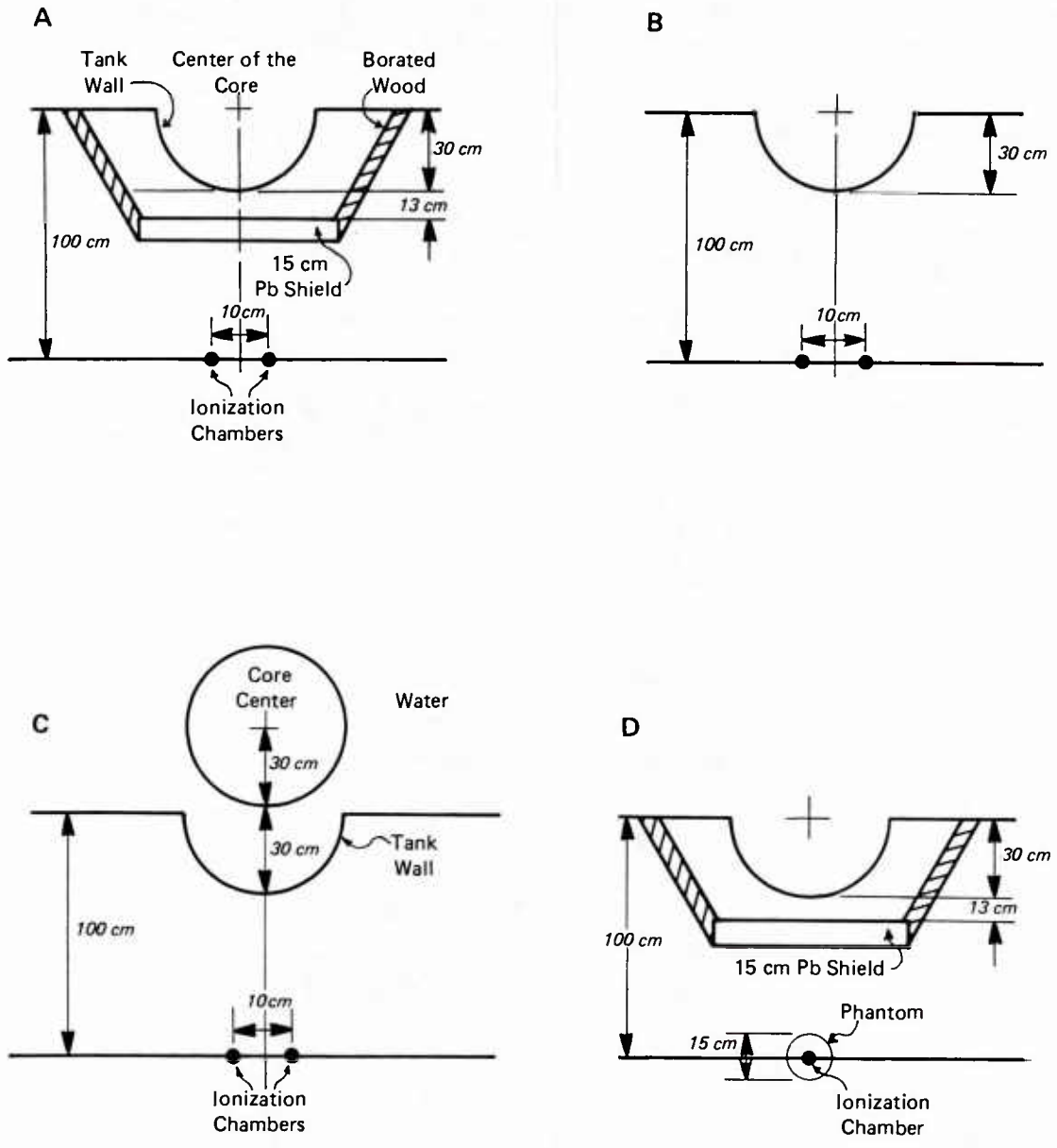

Figure 2. Reactor configurations: A, configuration 1; B, configuration 2; C, configuration 3; D, configuration 4.

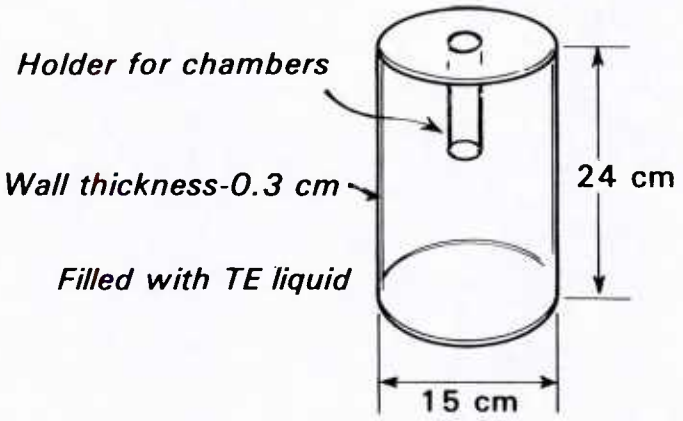

Figure 3. Plastic phantom used in intercomparison

In all configurations, measurements were made with the chambers 120 cm above the floor and 70 cm from the tank wall. This is a nominal distance of 100 cm from the reactor core center in configurations 1, 2, and 4, and 130 cm from the center of the core in configuration 3. To investigate the spatial variation within the exposure room, measurements were also performed in the lead-shielded and bare configurations at three additional distances ranging from 1 to 4 m from the core. AFRRI and NBS chambers were irradiated simultaneously, spaced about 10 cm apart and equidistant from the core centerline (see Figure 4) in all configurations except inside the phantom, where they were exposed individually. The neutron and gamma-ray spectra in each of these configurations are given in reference 7.

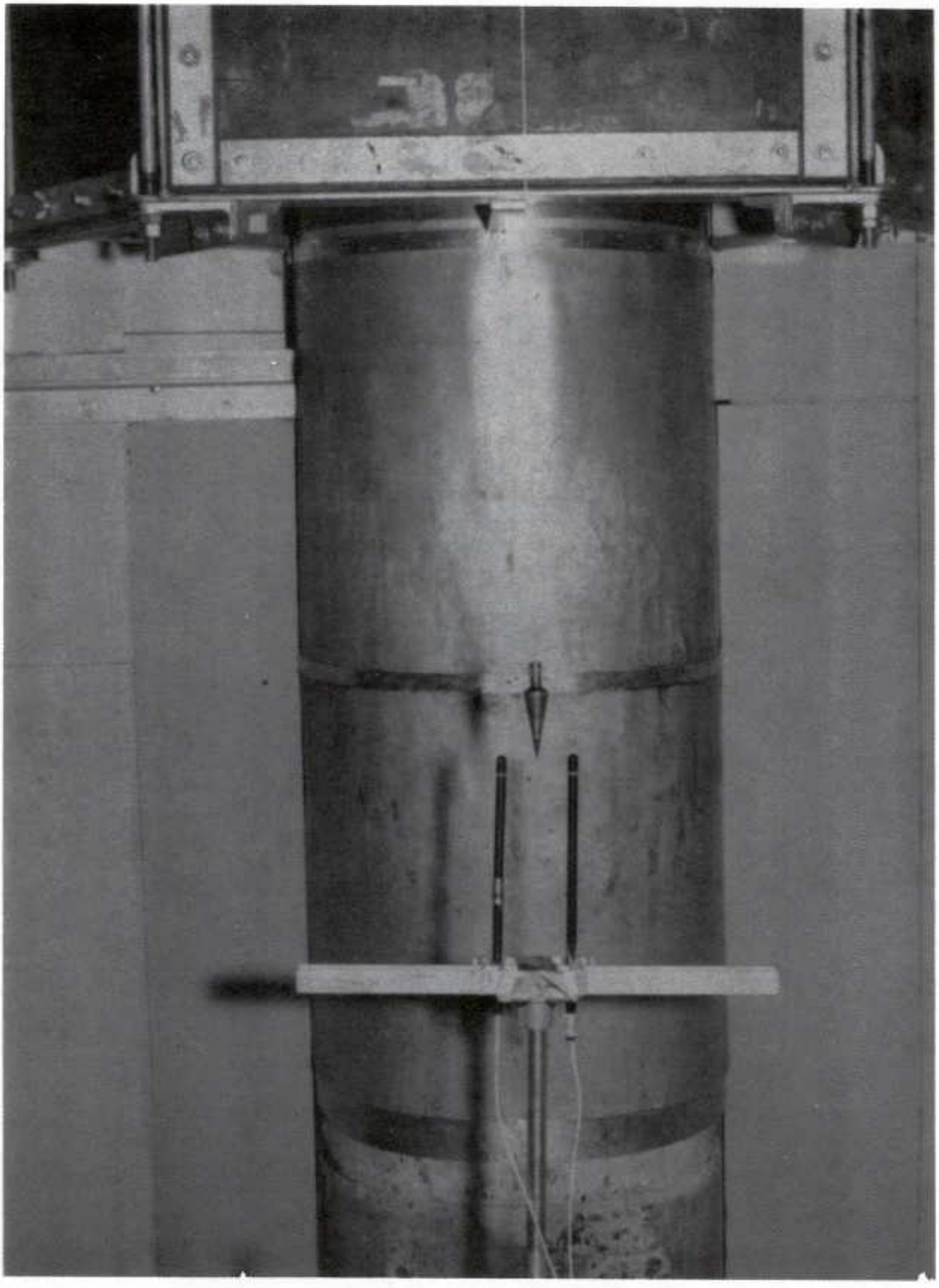

Figure 4. Two chambers set up in ER1 with no shield. (Note the plumb bob used for chamber positioning.)

DOSIMETRY SYSTEMS

The two-dosimeter method described in reference 10 was used to measure the neutron and gamma-ray tissue-kerma rates in free air and the absorbed-dose rate at the midline of a phantom. The NBS and AFRRI groups each used a pair of 0.5-cm^3 Exradin (Warrenville, IL) ionization chambers consisting of an A150 plastic TE chamber (Model T2) filled with methane-based TE gas (TE/TE chamber) and a magnesium chamber (Model MG2) with argon gas (Mg/Ar chamber). The gas flow rate through the chambers was approximately 30 cm^3/min. The composition of A150 plastic and TE gas are given in Appendix B of reference 10. In addition to the Mg/Ar chamber, the NBS dosimetrists substituted a Geiger Mueller (GM) proportional counter as the nonhydrogenous instrument of the dosimeter pair. The GM chamber was used in both configurations of the californium-252 facility, but was used only in the lead-shielded configuration of the reactor because the high background radiation from the core was too high for this sensitive dosimeter. The AFRRI group also used a second set of chambers in the californium-252 facility, consisting of two 50-cm^3 spherical chambers constructed at AFRRI (16). An A150 plastic chamber with TE gas provided the TE/TE portion of the pair, and a graphite chamber with carbon dioxide gas (Gr/C) served as the nonhydrogenous instrument. Both chambers used a gas flow rate of about 80 cm^3/min. Due to time constraints, the 50-cm^3 chambers were not used in the AFRRI reactor irradiations.

The NBS chambers were connected (via signal cables) to a Keithley Instruments, Inc. (Cleveland, OH) 642 electrometer through the accompanying remote preamplifier. The electrometer signal was fed to a scaler controlled by a timer. The collected counts per time interval were manually entered into a Hewlett-Packard (HP) (Corvallis, OR) 85 desktop computer, which calculated the charge per unit time. A collecting potential of + or - 400 volts was applied across the chamber through an Ortec, Incorporated (Oak Ridge, TN) high-voltage source.

The AFRRI chambers were connected to a Keithley 616 electrometer with the collecting potential (+ or - 400 volts for the 0.5-cm^3 chambers and + or - 1000 volts for the 50-cm^3 chambers) supplied by an Ortec high-voltage source. The system was semiautomated in that the electrometer signal was sampled at set time intervals by an HP 3421A data acquisition unit, which was controlled by an HP 85 desktop computer. The electrometer readings were stored by the computer and used to calculate the charge accumulated per time interval. Figure 5 is a photograph of the AFRRI data acquisition system.

CALIBRATIONS

Dosimetry using ionization chambers is generally based on the calibration of the ionization chambers in cobalt-60 or cesium-137 gamma-ray beams. The chambers used by the NBS group were calibrated using the standard cobalt-60 gamma-ray machine at NBS. AFRRI chambers were calibrated using the Theratron-80 cobalt-60 machine at AFRRI (17), which had been calibrated with an AFRRI ionization chamber calibrated in the standard NBS cobalt-60 beam. To verify that the traceability to the NBS standard had been properly transferred to AFRRI, four

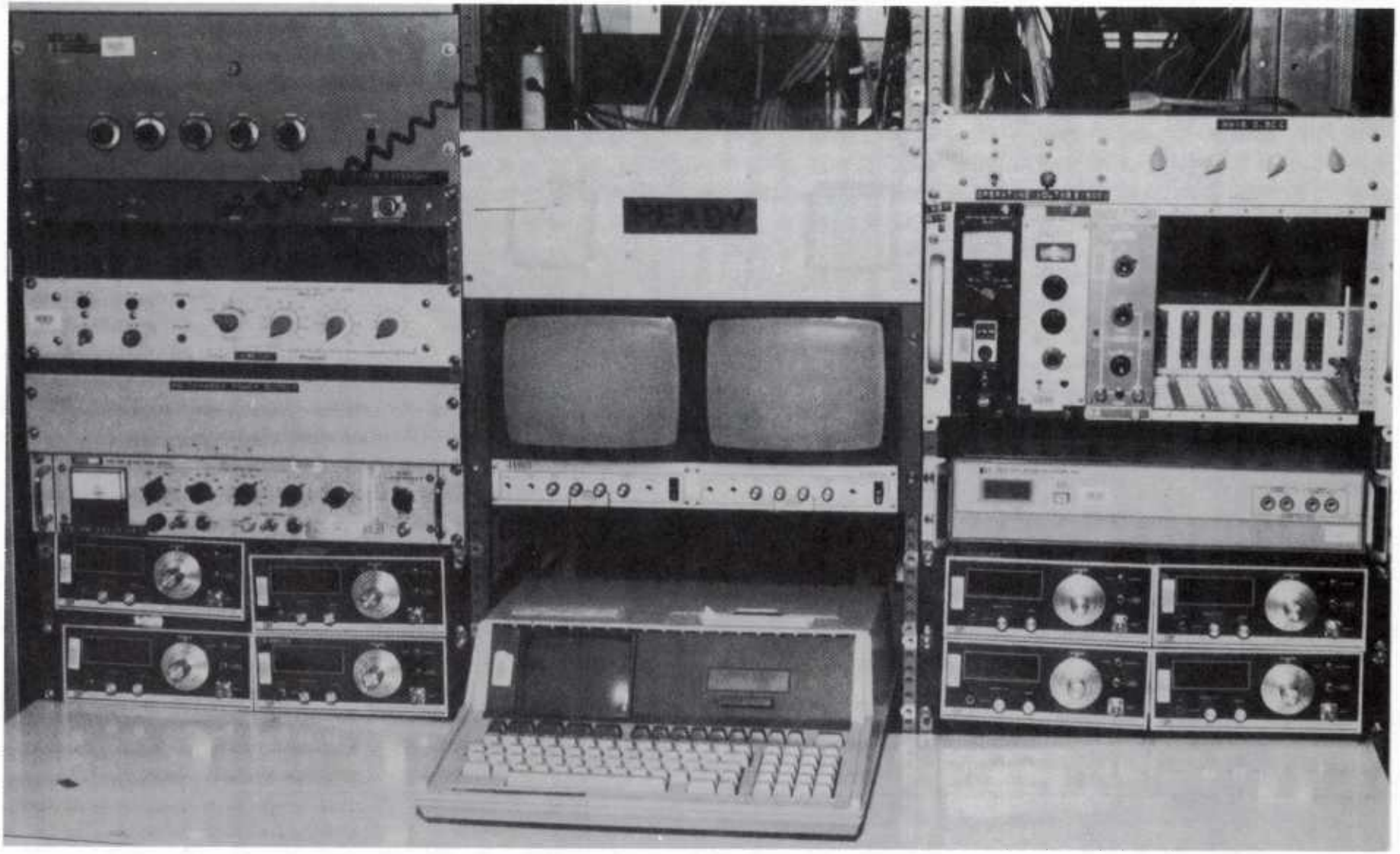

Figure 5. AFRRI data acquisition system

AFRRI chambers were calibrated directly in the NBS cobalt-60 beam. The calibration factors obtained at NBS for each chamber, N_X in roentgens per coulomb (R/C), were compared to the calibrations performed at AFRRI.

The absorbed-dose calibration factor, α_c (Gy/C), was calculated from the exposure calibration factor:

$$\alpha_c = N_X f_c K_W$$

where f_c = 9.62×10^{-3} Gy/R (reference 18) and represents the exposure-to-tissue absorbed-dose conversion factor for cobalt-60 photons

K_W = wall attenuation and scatter correction factor for the cobalt-60 beam

The wall correction factor (K_W) is necessary when measuring the tissue kerma in free air to determine the effect of the chamber wall. This factor need not be evaluated for in-phantom measurements because the chamber wall can be considered as part of the phantom if the composition of the chamber is similar to that of the phantom. In free air, the chamber wall both attenuates the incident radiation and scatters radiation into the sensitive volume of the chamber. Attenuation usually dominates over scatter; therefore, the response of the chamber decreases as the wall thickness increases past the thickness required for secondary particle equilibrium. To evaluate K_W, measurements were made with buildup caps of various thicknesses placed on the chamber. The chamber response with zero wall thickness was found by extrapolating the graph of response versus wall thickness to zero wall thickness. K_W was then computed as the ratio of the chamber response at the operating wall thickness to the theoretical response at zero wall thickness.

MEASUREMENTS

Paired-Chamber Equations

The measurement principles and techniques used throughout the intercomparison are described in reference 19. The neutron and gamma-ray kerma and absorbed-dose rates were calculated from the measured chamber responses using the following equations:

$$R_t' = k_t D_n + h_t D_g$$

$$R_u' = k_u D_n + h_u D_g$$

In these equations, known as the paired-chamber equations, the subscript t refers to the TE/TE chamber and u refers to the nonhydrogenous (Mg/Ar, GM, or Gr/C) chamber. The terms are defined as follows:

R_t', R_u' = Chamber response in the mixed field relative to its response to gamma rays used for calibration, cobalt-60 in this case (units: Gy [cobalt-60])

k_t, k_u = Response of each chamber to neutrons in the mixed field relative to its response to calibration gamma rays (units: Gy [cobalt-60]/Gy [mixed field])

h_t, h_u = Response of each chamber to gamma rays in the mixed field compared to the calibration gamma rays (units: Gy [cobalt-60]/Gy [mixed field])

D_n, D_g = Neutron and gamma-ray tissue kerma in free air or tissue-absorbed dose in Gy

By rearranging the above equations, the separate neutron and gamma-ray kerma or absorbed doses are given explicitly by:

$$D_n = \frac{h_u}{(h_u k_t - h_t k_u)} R_t' + \frac{-h_t}{(h_u k_t - h_t k_u)} R_u'$$

$$D_g = \frac{-k_u}{(h_u k_t - h_t k_u)} R_t' + \frac{k_t}{(h_u k_t - h_t k_u)} R_u'$$

The relative chamber responses (k_t, k_u, h_t, h_u) are spectrum dependent, and are discussed in detail in reference 19. The relevant physical parameters for each configuration are provided in Table 2, and the calculation of k_t is shown in Appendix B. Because the values of h_t and h_u are close to unity, the assumption $h_t = h_u = 1$ was made for all configurations.

Table 2. Values of Physical Parameters

Parameter	Californium-252	Californium-252 Moderated	15 cm Pb	Bare Room	30 cm Water
E_n (MeV)	2.7	2.6	1.7	2.6	4.8
W_n, MTE gas (eV)	31.6	32.5	32.2	32.0	31.7
W_n/W_c (W_c = 29.3 eV)	1.078	1.109	1.099	1.092	1.082
K ICRU* muscle (1E-11 Gy cm^2)	2.9	0.79	1.52	1.96	2.76
K A150 plastic (1E-11 Gy cm^2)	2.98	0.812	1.54	2.02	2.83
K MTE gas (1E-11 Gy cm^2)	2.95	0.803	1.54	2.00	2.80
k_t, TE/TE (0.5 cm^3)	0.948	0.922	0.922	0.939	0.943
k_t, TE/TE (50 cm^3)	0.944	0.917	0.922	0.934	0.938
k_u, Mg/Ar	0.033	0.005	0.01	0.02	0.025
k_u, GM	0.003	0.003	0.002	0.002	0.003
k_u, Gr/C	0.06	0.005	0.02	0.03	0.055
h_t, TE/TE	1.0	1.0	1.0	1.0	1.0
h_u, Mg/Ar, GM, Gr/C	1.0	1.0	1.0	1.0	1.0

*International Commission on Radiation Units and Measurements

Chamber Response

The relative chamber responses, R_t' and R_u', were computed from the chamber reading R, in coulombs (C), using:

$$R' = R \cdot \alpha_c \cdot K_{tp} \cdot K_s/K_w$$

where α_c (Gy/C) = the cobalt-60 tissue-absorbed dose calibration factor

K_{tp} = corrects ambient temperature and pressure to standard temperature and pressure:

$$K_{tp} = \frac{(T + 273.15)}{295.15} \times \frac{760}{P}$$

where T is temperature in Celsius and P is atmospheric pressure in mm of mercury

K_S = ion recombination (saturation) correction

K_W = chamber wall attenuation and scatter correction

The chamber reading R was measured by integrating the ionization charge for a set time interval (between 10 and 30 sec) while the source was in place and, in the case of the reactor, at power. The system noise, or drift, was measured both before and after the chamber was irradiated, and the mean of the pre- and postirradiation drifts was used to compensate the reading to determine the net charge accumulated during irradiation. That is,

$$R = R_c - R_d$$

where R = chamber reading compensated for drift

R_c = average charge collected with source on

R_d = average of pre- and postirradiation drifts

In the californium-252 facility, the drift charge was integrated with the source in its storage position. At the reactor, the drift was measured with the core in place but not at power, and it therefore included residual radiation from the power runs. Although at least some of the residual radiation is part of the measured gamma component of dose or kerma, it was subtracted to maintain consistency in the measurements. Several measurements of the drift and the ionization current were performed, using both positive and negative collecting potentials across the chamber. Measurements at the californium-252 facility were normalized to time, and all measurements in ER1 were normalized to the response of a 50-cm^3 air-filled TE monitor chamber fixed to the ceiling of the exposure room (shown in Figure 6).

The ion recombination correction was determined by measuring the chamber response at several values of collecting potential. For neutrons, initial (intratrack) recombination is usually dominant over general (intertrack) recombination, and the chamber response at an infinite collecting voltage is found by extrapolating the plot of 1/R against 1/V to 1/V = 0. At high dose rates, general recombination usually dominates, and then the plot of 1/R versus $1/V^2$ is extrapolated to $1/V^2 = 0$ (reference 20). Because the dose rates were very low in these measurements, the 1/V method was appropriate.

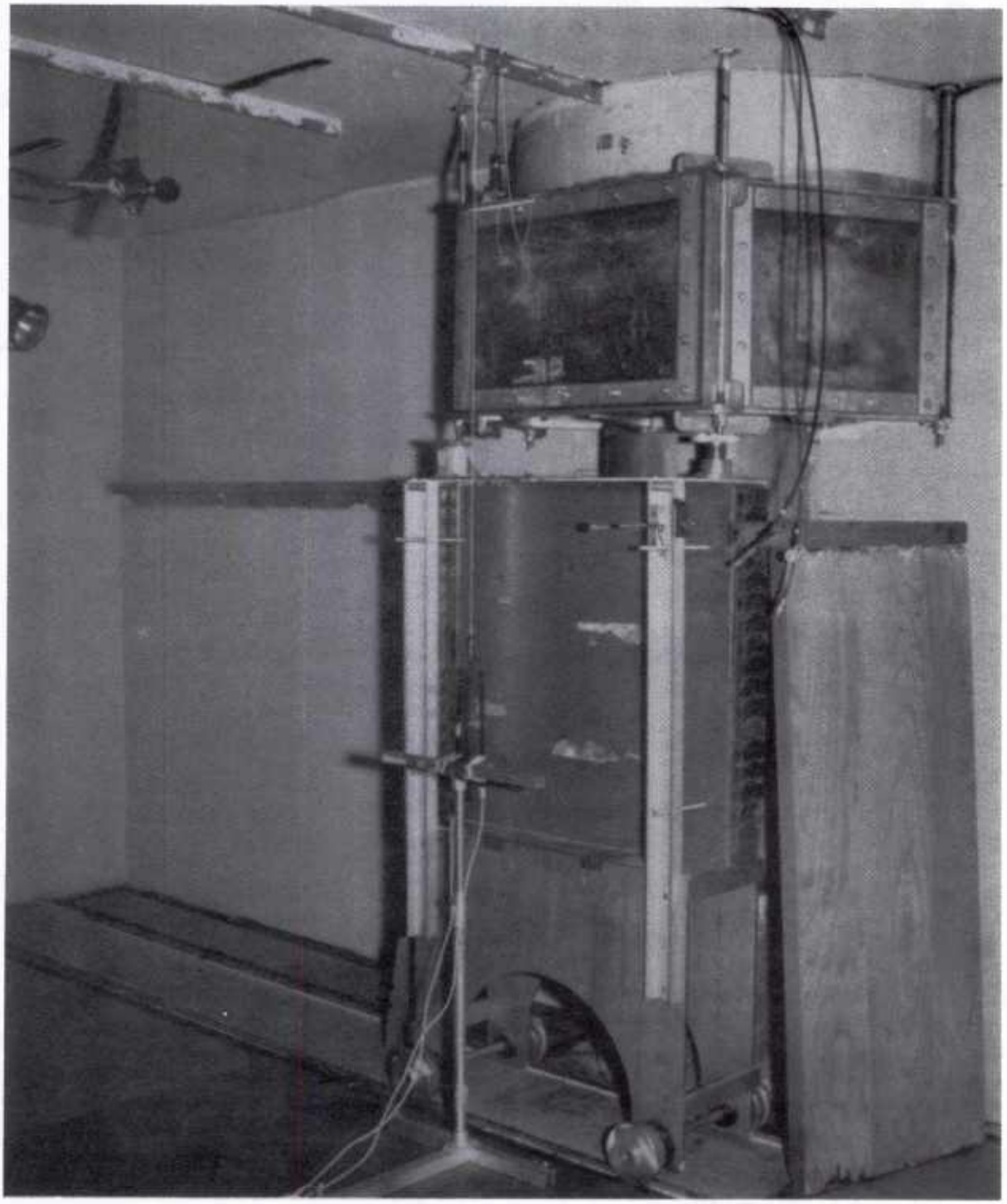

Figure 6. Ion chambers set up in ER1 with 15-cm-Pb shield. (Note the spherical monitor chamber mounted in the ceiling.)

The wall correction factors, K_W (discussed in section on Calibrations), were evaluated in the moderated californium-252 exposure field and in configurations 1, 2, and 3 of the AFRRI TRIGA reactor. Wall correction data were available from previous measurements for the 0.5-cm^3 Exradin chambers in the unmoderated californium-252 field (21), and these measurements were not repeated.

RESULTS

CHAMBER CORRECTION FACTORS

The chamber correction factors evaluated for this study are shown in Table 3. Note that all data were used except the wall data collected with the 0.5-cm^3 chambers using the moderated californium-252 source, which were inconclusive. As a result of these poor data, the kerma calculated from the 0.5-cm^3 chamber data could not be separated into the neutron and gamma-ray components.

Table 3. Chamber Correction Factors

Chamber	Factor	Co-60	Cf-252 Unmod	Cf-252 Mod	Reactor 15-cm Pb	Reactor Bare	Reactor 30-cm H_2O
TE/TE (0.5 cm^3)	K_W*	0.992 (2mm cap)	0.969	0.984	0.984	0.976 (3mm cap)	0.995 (5mm cap)
	K_S	1.00	1.002	1.002	1.002	1.002	1.000
Mg/Ar (0.5 cm^3)	K_W	0.989 (1mm cap)	0.961	0.725	0.988	0.986 (2mm cap)	0.995 (5mm cap)
	K_S	1.00	1.006	1.006	1.006	1.006	1.00
TE/TE (50 cm^3)	K_W	0.978	0.921	0.970	—	—	—
	K_S	1.00	1.00	1.00	—	—	--
Gr/C (50 cm^3)	K_W	0.979	0.959	0.973	—	—	--
	K_S	1.00	1.00	1.00	—	—	—

*Wall thicknesses of 0.5-cm^3 and 50-cm^3 chambers without buildup caps are approximately 1 and 7 mm, respectively.

COBALT-60 CALIBRATIONS

The results of the cobalt-60 calibration of the four AFRRI ionization chambers are shown in Table 4. The ratio of the calibration factors (AFRRI/NBS) determined at the two different cobalt-60 facilities varies from unity by 2% or less for three of

the four chambers, which is good precision for this comparison. However, for the 50-cm^3 chamber TE10, a difference of 5% in the calibration factors was obtained. The value in parentheses indicates that when the chamber was recalibrated at AFRRI, it differed with the NBS calibration by only 0.8%. Thus, the direct cobalt-60 calibration of AFRRI chambers with the NBS standard beam served not only to verify the correct calibration of the AFRRI machine but also to discover an inaccurately calibrated chamber.

Table 4. Calibration Results

Chamber	Exposure Calibration Factor (R/nC)	AFRRI/ NBS	K_W
TE 118 (0.5 cm^3)	5.473	0.993	0.992 (2-mm cap)
Mg 111 (0.5 cm^3)	3.740	1.019	0.989 (1-mm cap)
TE 10 (50 cm^3)	0.06114	1.054 (0.992)*	0.978 (no cap)
Gr1 A (50 cm^3)	0.04474	1.016	0.979 (no cap)

*Result of recalibration at AFRRI

CALIFORNIUM-252

Tissue-kerma rates measured by NBS and AFRRI at the NBS californium-252 facility are shown in Table 5. The measured total (neutron plus gamma ray) kerma rate, K_T, compared well in both the unmoderated and D_2O-moderated configurations. The measured neutron and gamma kerma rates (K_n and K_g) in the unmoderated field did not agree as well, with the largest discrepancies seen in the 50-cm^3 chamber results. However, in the moderated field, the 50-cm^3 chambers agreed very well with the NBS TE-GM dosimeter pair. Although the K_T measured with both the AFRRI and NBS TE-Mg dosimeter pairs agreed well with that measured with the 50-cm^3 chambers and the TE-GM pair, the two radiation components could not be resolved because of the extreme difficulty in measuring the low ionization current ($<10^{-14}$ A) produced in the small (0.5 cm^3) chambers.

The differences obtained in these measurements are reasonable, considering that the source intensity was insufficient to allow optimal precision of measurement. Table 5 implies that a precision of about 3% was achieved for the determination of the total kerma, and a precision of about 9% was achieved for the separate neutron and gamma-ray components.

Table 5. Californium-252 Results

Configuration	Dosimeter Pair	K_n (mGy/h)	K_g (mGy/h)	K_t (mGy/h)	K_g/K_t
Unmoderated	NBS TE-GM	19.2	9.6	28.8	0.33
	NBS TE-Mg	19.9	8.9	28.8	0.31
	AFRRI TE-Gr	18.5	10.4	28.9	0.36
	AFRRI TE-Gr*	20.2	9.8	30.0	0.33
	AFRRI TE-Mg	19.1	9.8	28.9	0.34
Moderated	NBS TE-GM	4.0	8.6	12.6	0.68
	NBS TE-Mg	—	—	12.4	—
	AFRRI TE-Gr	4.1	8.6	12.7	0.68
	AFRRI TE-Mg	—	—	12.7	—

*Second set of measurements

AFRRI TRIGA REACTOR

Table 6 gives the results of the measurements performed in ER1 of the AFRRI reactor. Although the chamber response was normalized to the response of the monitor chamber, the results are listed here in terms of integrated power (kilowatt · minute), a more meaningful term to most readers. The response of the monitor to reactor power is provided in Appendix C. Also in Appendix C are the relationships used to convert from μGy/pCm (microgray per picocoulomb monitor) to cGy/kW · min (centigray per kilowatt · minute). The precision of the chambers was better than 2% in almost all cases.

15-Cm-Pb Shield and 15-Cm-Pb Shield With Phantom

The effect of the 15-cm-Pb shield was to reduce the gamma-ray component of kerma to approximately 10% of the total. In this predominantly neutron field, the NBS- and AFRRI-measured neutron (K_n), gamma-ray (K_g), and total (K_T) kerma rates are in excellent agreement. The differences in K_T are all less than 1%, and the neutron and gamma-ray components differ by 3% or less. In the phantom, the measured neutron, gamma-ray, and total kerma rates of the two groups are within 1% of each other.

Table 6. Reactor Results

Reactor Configuration	Meters From Core Center	Group	cGy/kW · min K_n	K_g	K_T	K_g/K_T
15 cm Pb	1.00	NBS*	7.14	0.700	7.84	0.09
		NBS†	7.14	0.714	7.85	0.09
		AFRRI	7.17	0.700	7.87	0.09
	2.35	NBS†	0.742	0.560	1.30	0.43
		AFRRI	0.750	0.553	1.30	0.42
	3.28	NBS†	0.334	0.433	0.767	0.56
		AFRRI	0.333	0.428	0.761	0.56
	4.01	NBS†	0.199	0.373	0.571	0.65
		AFRRI	0.202	0.365	0.567	0.64
In phantom	1.00	NBS†	2.21	1.210	3.420	0.35
		AFRRI	2.19	1.220	3.400	0.35
Bare Room	1.00	NBS*	12.2	24.9	37.1	0.67
		NBS†	12.5	24.6	37.1	0.66
		AFRRI	12.2	24.6	36.8	0.69
	2.35	NBS†	1.88	5.09	6.97	0.73
		AFRRI	1.91	5.02	6.93	0.72
	3.28	NBS†	1.02	2.98	4.00	0.74
		AFRRI	0.99	2.96	3.95	0.75
	4.01	NBS†	0.476	2.36	2.84	0.83
		AFRRI	0.628	2.21	2.84	0.78
30 cm Water	1.30	NBS†	—	4.69	4.69	1.00
		AFRRI	—	4.67	4.67	1.00

*NBS pair T2-M2

†NBS pair T2-MG131

Bare Room

The bare-room field consists mainly of gamma rays, with the contribution of the neutrons ranging from about 30% at 1 m to less than 2% at 4 m from the reactor core center. In this field, better than 1% agreement was again seen between the NBS- and AFRRI-measured total kerma rates. The gamma-ray kerma rates, which constituted most of the total, also agreed to within 1% of each other at distances up to 3 m from the core center, but a 6% difference was seen at the 4-m position. Similarly, the neutron kerma rates compared well close to the core (1%-4% up to 3 m), but the measured values at 4 m differed by 30%.

30-Cm-Water Shield

With the reactor core moved back 30 cm, the neutron kerma was almost completely attenuated, and the two components of the kerma could not be resolved using the paired-chamber method. However, the agreement for the measured total kerma rates was within 1%. The wall attenuation and scatter data indicate that the radiation produced in this configuration consists predominantly of fairly hard gamma rays, resulting in part from neutron capture by hydrogen in the water ($H[n, \gamma]^2H$). The TE and Mg chambers both required a wall thickness of 6 mm to attain electronic equilibrium. (For comparison, a wall thickness of only about 3 mm is sufficient to attain electronic equilibrium for cobalt-60 photons.)

Summary of Reactor Results

NBS and AFRRI tissue-kerma and absorbed-dose rate measurements compared very well in all the reactor fields. The best comparisons were in the configurations where most of the kerma resulted from neutrons (configurations 1 and 4). In the predominantly gamma-ray fields, the total kerma compared well at all distances. Although the neutron and gamma-ray components also compared well at the 1-m and 2-m positions, these comparisons grew progressively poorer at larger distances from the core.

DISCUSSION

The results reviewed above show good agreement between NBS and AFRRI tissue-kerma rates measured at the NBS californium-252 facility, and excellent agreement of the measured tissue-kerma and absorbed-dose rates in the different fields of the AFRRI reactor. In addition to demonstrating sound dosimetry techniques, the intercomparison allowed the collection of much needed data pertaining to ionization chamber characteristics as well as the spatial variations in two configurations in ER1. Discussed below are some of the implications of the data and relevant lessons learned through the data-collecting process.

MODERATED CALIFORNIUM-252 SOURCE

The measurements of the ionization current from the D_2O-moderated californium-252 source stretched the capabilities of the 0.5-cm^3 chambers. In both sets of measurements, the wall attenuation and scatter data were inconclusive, and the precision in the second set of measurements was as poor as 20% due to unexplained system noise and instabilities. Under these measurement conditions, ionization currents less than about 10^{-13} A (~2 R/h) cannot be measured precisely with the 0.5-cm^3 chambers.

MG CHAMBER OVERRESPONSE TO NEUTRONS

During the course of measurements in the 15-cm-lead shield configuration, the NBS Mg/Ar chamber (designated MG2) consistently responded about 25% higher than did the AFRRI Mg/Ar chamber. An investigation of this discrepancy (involving interchanges of chambers, gas supplies, electrometers, and cables) led to the conclusion that the NBS chamber was in fact overresponding to the neutrons in this field. The response of the suspect chamber to gamma rays appeared to be correct, which was verified by checking the chamber calibration with the AFRRI Theratron-80 cobalt-60 source. Although the response of MG2 did not appear to be affected in the bare configuration, it was decided not to use the defective chamber at all. The manufacturer later stated that the inner surface of the chamber was probably contaminated.

This incident served as a reminder that, to ensure the proper operation and stability of ion chambers, it is essential to have some means (e.g., a neutron check source) of assessing the neutron sensitivity of TE as well as Mg chambers. Without a method of checking the neutron response, a defective chamber, such as MG2, could go undetected indefinitely because its unchanged response to cobalt-60 may give a false sense of security.

SPATIAL VARIATIONS IN ER1

Data were collected in the bare room and behind the 15-cm-Pb shield to evaluate how the neutron and gamma-ray kerma rates vary with distance from the reactor core. These measurements were also compared with the response predicted by the calculations in reference 7. (The calculations were performed only for the bare-room configuration using a one-dimensional ANISN code.) In Figures 7-9, the measured and calculated kerma rates multiplied by the square of the distance to the center of the core (Kr^2) are plotted as a function of the distance squared (r^2) in the bare and Pb-shielded configurations. A horizontal line on these plots would indicate $1/r^2$ behavior.

In Figure 7, the plots of Kr^2 versus r^2 for photons are shown for the 15-cm-Pb-shielded and the bare configurations. In both configurations, the data increase approximately linearly with distance squared. Also, the bare-room data agree reasonably well with the calculations for a spherical configuration (7).

Figures 8 and 9 show the variation of Kr^2 versus r^2 for neutron kerma in the Pb-shielded and bare configurations, respectively. In the Pb-shielded configuration, the measured data indicate a decrease with distance from the core center. The measured neutron kerma rate at the 1-m position is about 20% lower than the calculated value. In the bare room, the calculated neutron kerma rate at 1 m agrees well with the measured neutron kerma rate. However, in contrast to the measurements, the calculations predict a slow increase in Kr^2 with distance squared and only a slight deviation (<10%) from $1/r^2$ at 1 m.

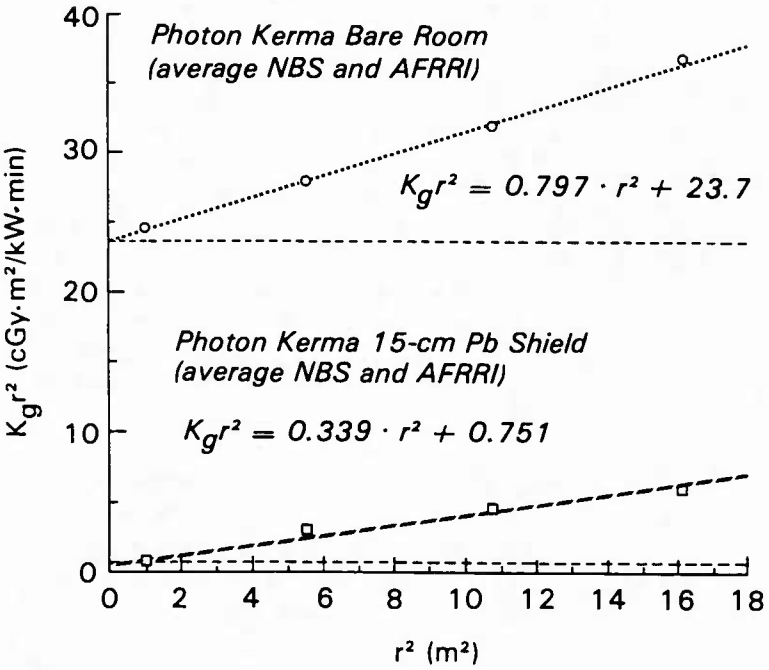

Figure 7. Photon $1/r^2$ measurements (with 15 cm Pb or bare room)

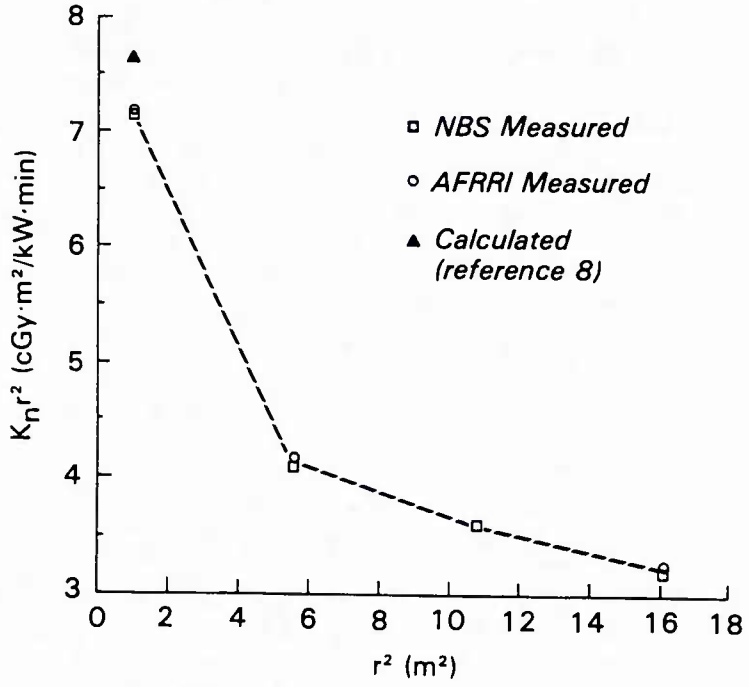

Figure 8. Neutron $1/r^2$ measurements with 15 cm Pb

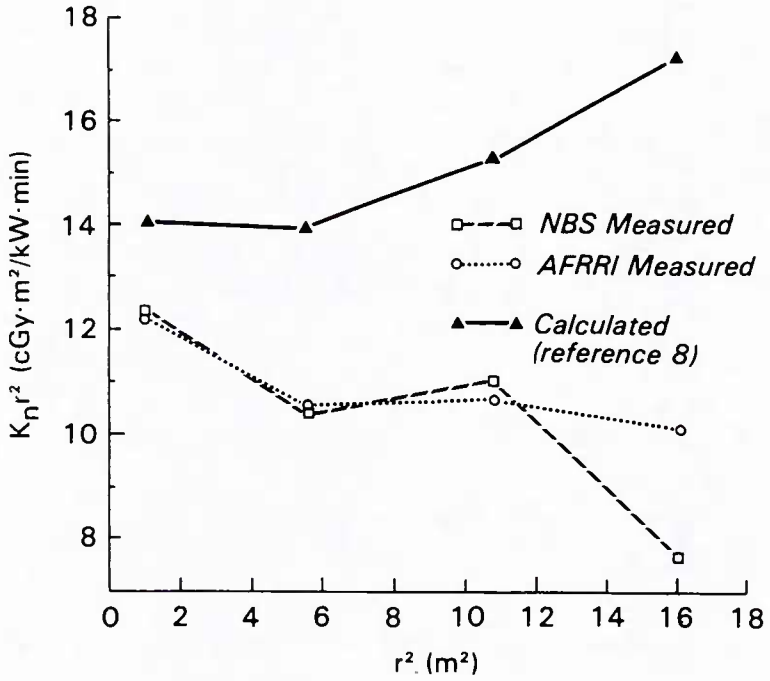

Figure 9. Neutron $1/r^2$ measurements with bare room

Clearly, the neutron kerma rates in the Pb-shielded and the bare configurations do not show $1/r^2$ behavior, if the reactor core center is taken to be the effective center of the source. The data are plotted in Figure 10 using the forward edge of the core as the effective center ([r - 0.3] m). For the 15-cm-Pb configuration, the graph is nearly flat, indicating consistency with an effective center at (r - 0.3) m. However, the data from the bare room do not show an obvious trend. At least one measurement may be inaccurate, or there may be some effects from the room-return neutrons that have not been characterized. The meaning of the data is not clear, and more measurements (with fission chambers and activation foils) may aid in the interpretation.

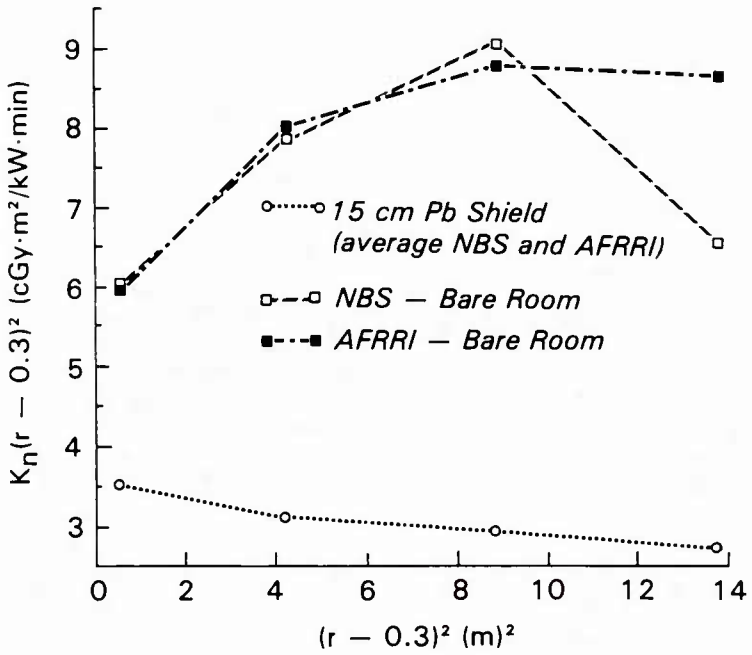

Figure 10. Neutron $1/(r-0.3)^2$ measurements (with 15 cm Pb or bare room)

POLARITY EFFECTS IN ER1

Appendix D provides the polarity data of the TE and Mg chambers from the measurements in ER1. In Appendix D, the ratio of +R to -R (+/-) is plotted for the TE and Mg chambers in the first and second sets of measurements. Differences of up to 30% in the chamber responses at opposite polarities were observed during the first set of measurements. Such large polarity effects are an indication of the presence of large spurious ionization currents from the cables and connectors. Before the second set of measurements, an attempt was made to reduce the polarity effect. The room was recabled, eliminating the patch panel inside the exposure room by running the signal cables straight to the readout room. In addition, lead bricks were used to shield the signal cables and the necessary connectors to the ionization chambers, but it was impractical to shield the cables immediately adjacent to the chambers. Although some improvement was seen in the AFRRI chambers, the recabling did not improve the large polarity differences of the NBS chambers. In fact, the NBS-observed polarity effects were even larger, and the effect was in the opposite direction for both groups. In spite of these large and inconsistent polarity effects, the average responses (average of +R and -R) of the AFRRI and NBS groups were in excellent agreement, indicating that averaging of the + and - chamber responses produces a reliable result.

However, the polarity problem should be considered when using small chambers to monitor experimental exposures. Generally, the polarity of the monitor chamber is not reversed, and therefore should be evaluated before each set of irradiations. If

significant changes are seen in the cable currents, then a correction should be applied. In any event, more work needs to be done to understand the cable-current problem and to reduce these sometimes anomalous effects.

DRIFT MEASUREMENTS

As discussed in the section on Chamber Response, the net chamber reading was determined by subtracting the average of the pre- and postirradiation drift readings from the chamber readings during irradiation. In the californium-252 facility, the drift readings were a measure of the system noise, but in the reactor facility the drift was actually a measure of the residual radiation in the exposure room. Although a portion of the residual radiation was a component of the measured gamma-ray kerma, it was subtracted to maintain consistency from day to day. This was necessary because the residual gamma radiation is, in some cases, very dependent on the core history.

The drift data for the AFRRI reactor exposures are summarized in Appendix E, where the drift data are plotted. These data indicate that with the lead shield in place, the residual radiation was a small percentage (~3%) of the total chamber reading, and the drift was not very dependent on core history. However, when the lead shield was moved away, the background radiation from the core constituted a much larger percentage of the total chamber reading (as high as 40%). Not only was the drift large in the unshielded configurations, but also it was very dependent on the core history. For example, the drift was lower at the beginning of the day and increased as the reactor core became more activated. In addition, the drift of the monitor chamber changed drastically in the unshielded configurations as the power increased from the very low levels (<0.1 kW) to the more routine power levels (>1 kW). One encouraging aspect of the unshielded data was that the monitor chamber and the measurement chambers (TE and Mg) showed similar patterns. That is, the changes in magnitude of the drift were about the same for the measurement and monitor chambers.

The drift data are tabulated in Appendix E, and the ratio of the postirradiation drift to preirradiation drift is shown for each chamber. For the lead-shielded configurations, the postirradiation drift was several times higher than the preirradiation drift (post/pre ranged from about 3 to 16), whereas this ratio was closer to 1 (1.1 to 4) for the unshielded radiations. Also, for all configurations, the ratio of post- to preirradiation drift increased as the chambers were moved farther from the core. This indicates that, closer to the core and without the lead shield, most of the drift results from the residual radiation of the core, whereas farther from the core or with the shield in place, the background radiation is mainly due to activation of products in the room (e.g., the lead shield, walls, and floor).

Although these observations are intuitive, they are important to remember when planning dosimetry for radiobiology experiments. Monitor chambers should be placed close to the subject of irradiation and should be filled with TE gas. This is to ensure that if the residual radiation changes significantly, the monitor chamber will in effect monitor the tissue kerma close to the experimental array. If several different dose rates (power levels) are to be used, the response of the monitor

compared to the dosimetry chambers should be evaluated at the different power levels. In addition, the residual radiation and its behavior with core history should be monitored closely for experiments in which the ratio K_g/K_T is crucial.

CONCLUSIONS

An extensive ionization-chamber intercomparison between NBS and AFRRI was completed using five radiation fields. The agreement between the two groups was good in the NBS californium-252 fields and excellent in the AFRRI reactor fields. Through the course of the study, the calibration procedures of AFRRI were validated, and many valuable data were collected concerning chamber characteristics and the spatial variation of tissue-kerma rates in two configurations of ER1.

In addition to these favorable results, the exercise itself proved to be an excellent opportunity for the AFRRI dosimetry program. Foremost was the valuable training experience afforded the AFRRI staff through the interaction with recognized experts in the radiation dosimetry field. Also, a guide to good dosimetry practices was prepared for AFRRI (19) as a direct result of the intercomparison. Finally, this work has resulted in the development of a long-term working relationship between the two groups, in which NBS will provide technical support to AFRRI in solving specific problems, and will assist AFRRI in maintaining continuity and reliability in its reactor dosimetry program.

APPENDIX A. RADIATION SCHEDULE

Date	Source
5-8 July 1983	NBS californium-252 source
18-22 July 1983	AFRRI TRIGA reactor
7 November 1983	NBS cobalt-60 source
8-11 November 1983	NBS californium-252 source
27 February- 7 March 1984	AFRRI TRIGA reactor

APPENDIX B. CALCULATION OF k_t

$$k_t = \frac{W_c}{W_n} \quad \frac{(s_{m,g})_c}{(r_{m,g})_n} \quad \frac{[(\mu_{en}/\rho)_t / (\mu_{en}/\rho)_m]_c}{(K_t/K_m)_n}$$

where c = calibration gamma rays (cobalt-60)

n = neutrons in the mixed field

W = average energy required to produce an ion pair in the cavity gas (Table 2)

$s_{m,g}$ = wall-to-gas restricted collision mass-stopping power ratio of 1

$r_{m,g}$ = gas-to-wall absorbed-dose conversion factor for the non-Bragg-Gray cavity conditions generally produced by neutrons of 0.99

$(K_t/K_m)_n$ = ratio of neutron kerma in tissue to the neutron kerma in the chamber materials

APPENDIX C. MONITOR CHAMBER RESPONSE

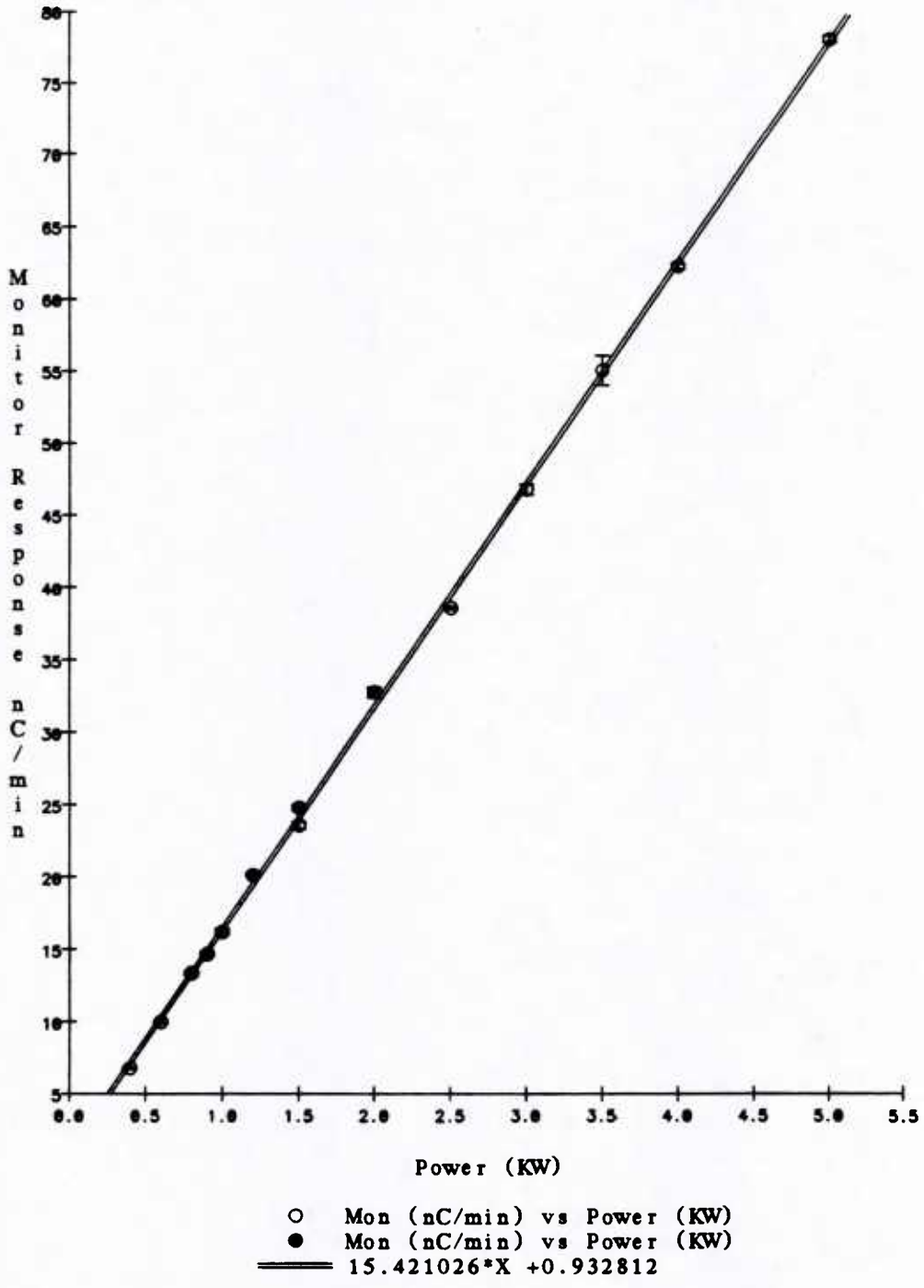

Figure 11. Monitor response in ER1 with 15-cm-Pb shield

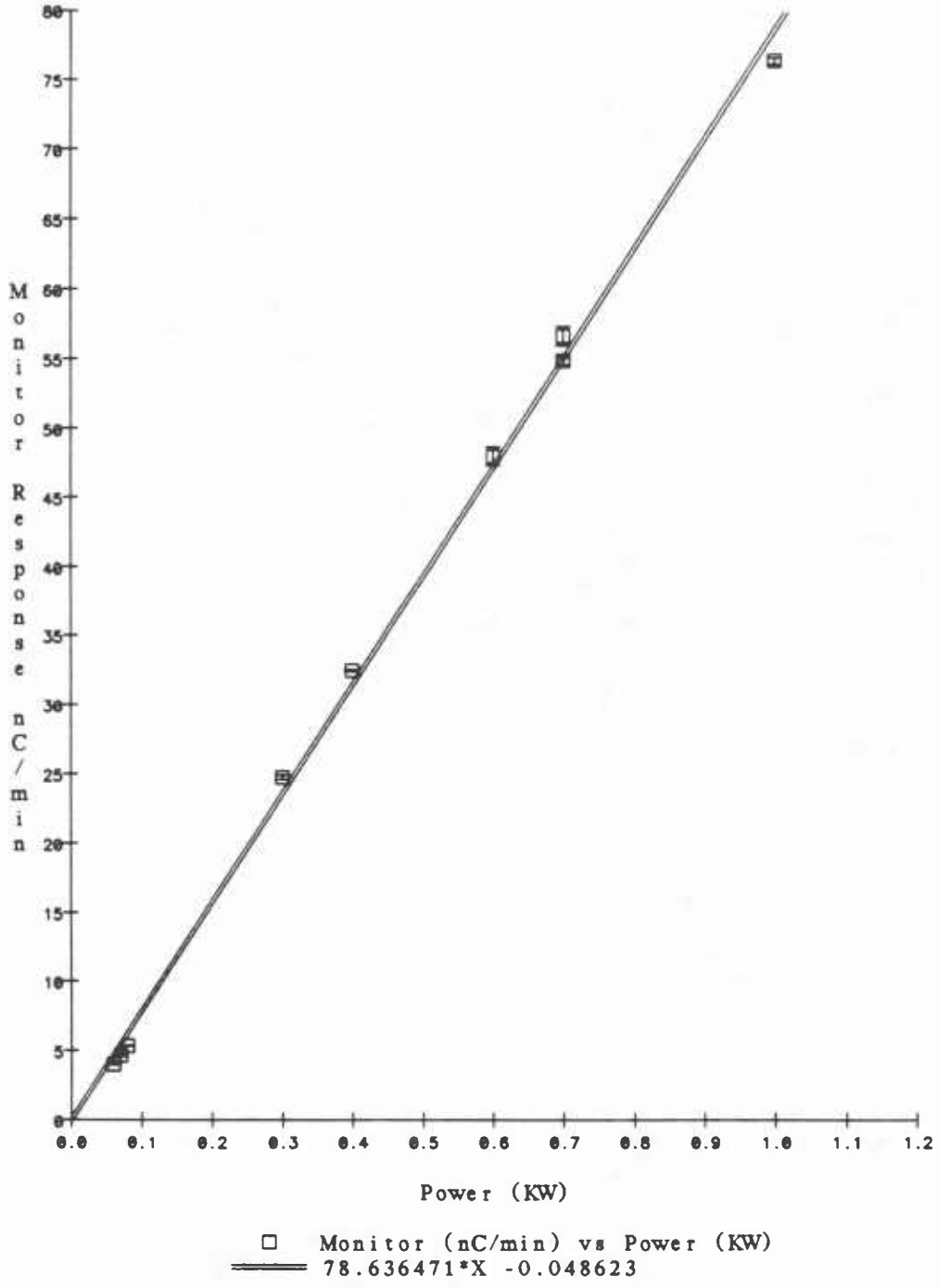

Figure 12. Monitor response in ER1 with no shield (bare room)

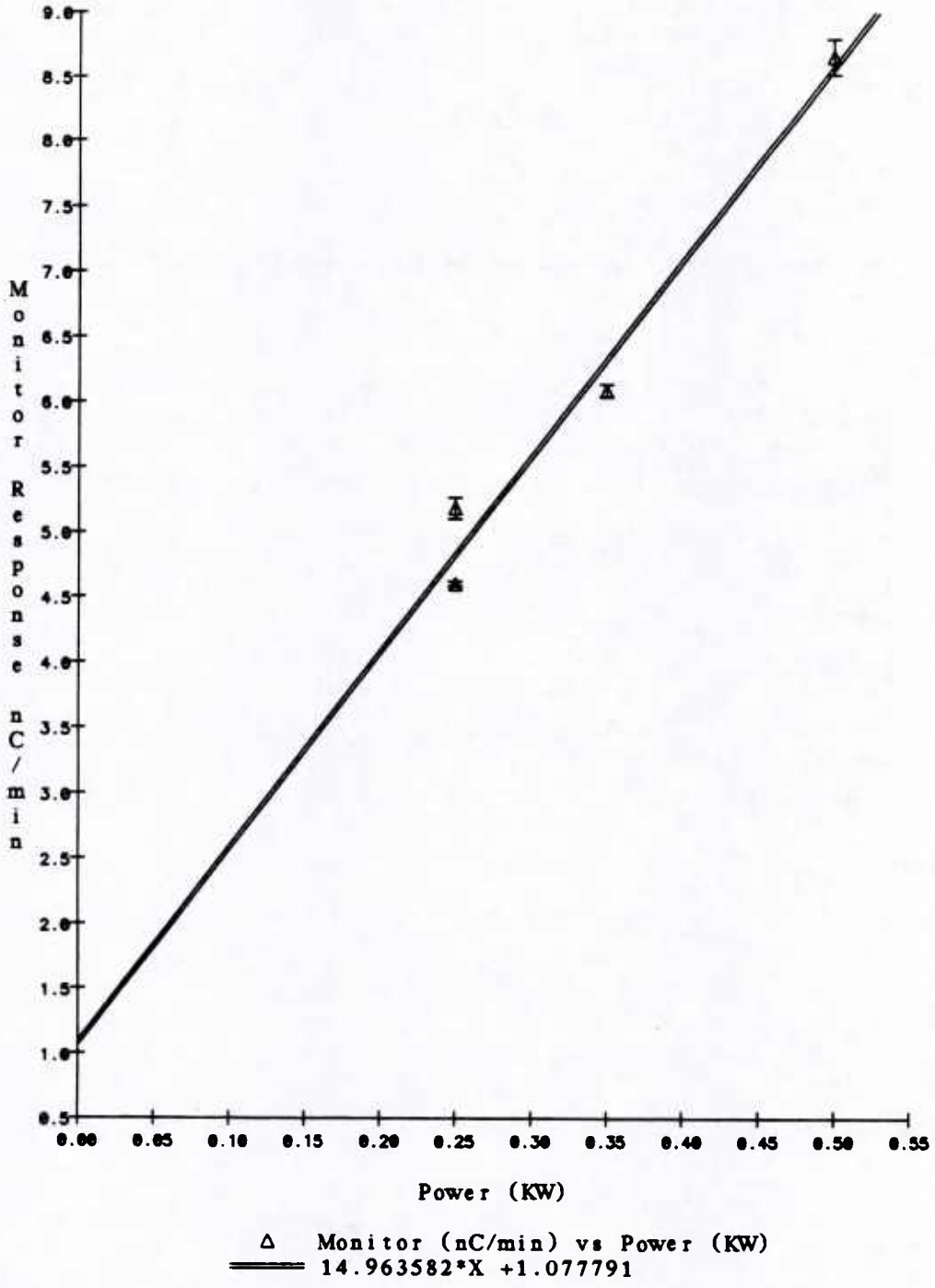

Figure 13. Monitor response in ER1 with 30-cm-water shield

Table 7. Conversion From Monitor Readings to cGy/kW · min

Configuration	Distance of Dosimetry Chambers From Tank Wall (cm)	Power (kW)	cGy/kW · min per μGy/pCm
15 cm Pb	70	0.4	1.775
	205	2.5	1.579
	298	3.5	1.568
	371	4.0	1.565
In phantom	70	1.0	1.636
Bare room	70	0.075	7.799
	205	0.350	7.850
	298	0.650	7.856
	371	0.850	7.856
30 cm water	70	0.500	1.730

APPENDIX D. POLARITY EFFECTS DATA

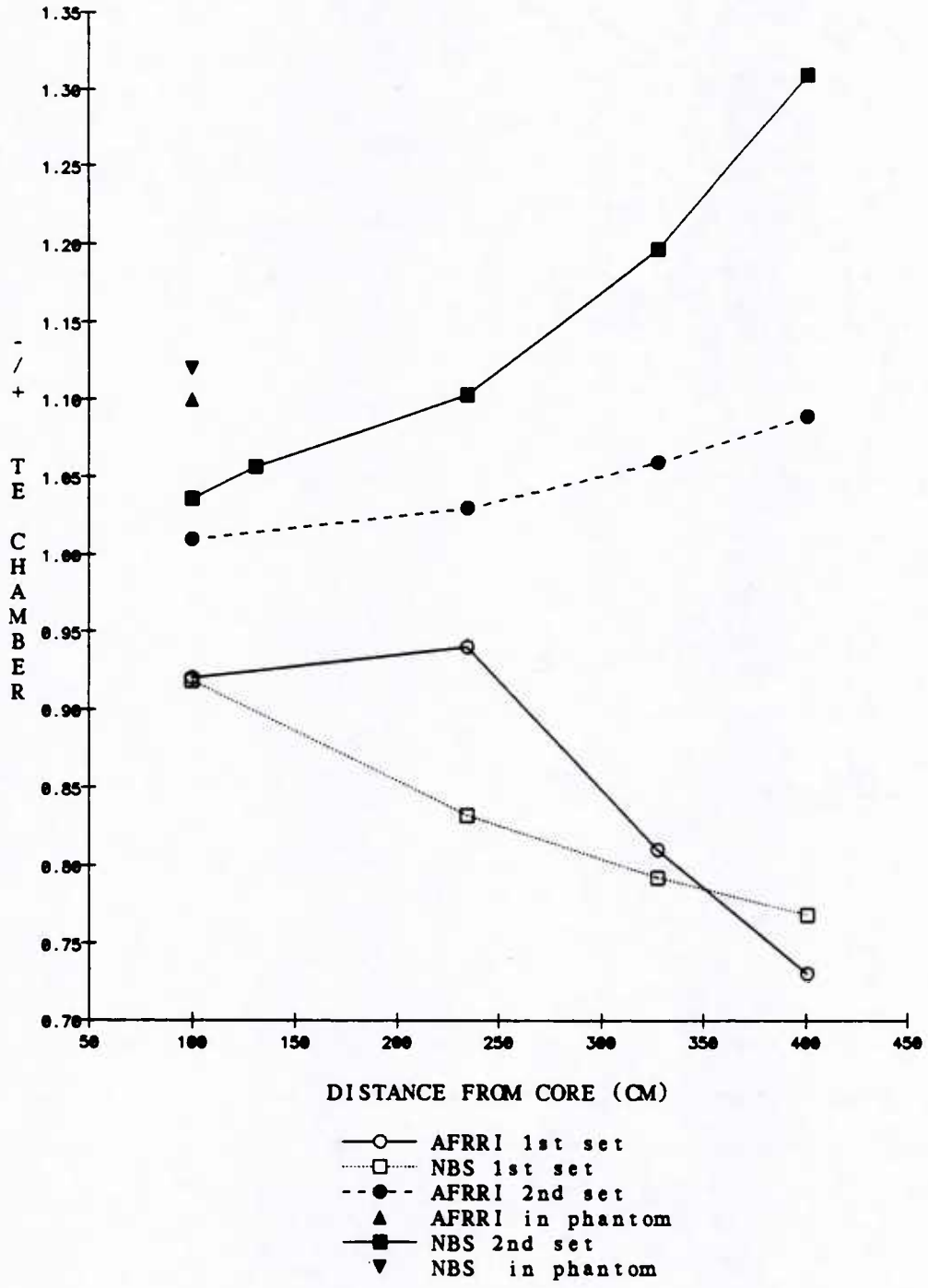

Figure 14. TE chamber polarity effects with 15-cm-Pb shield

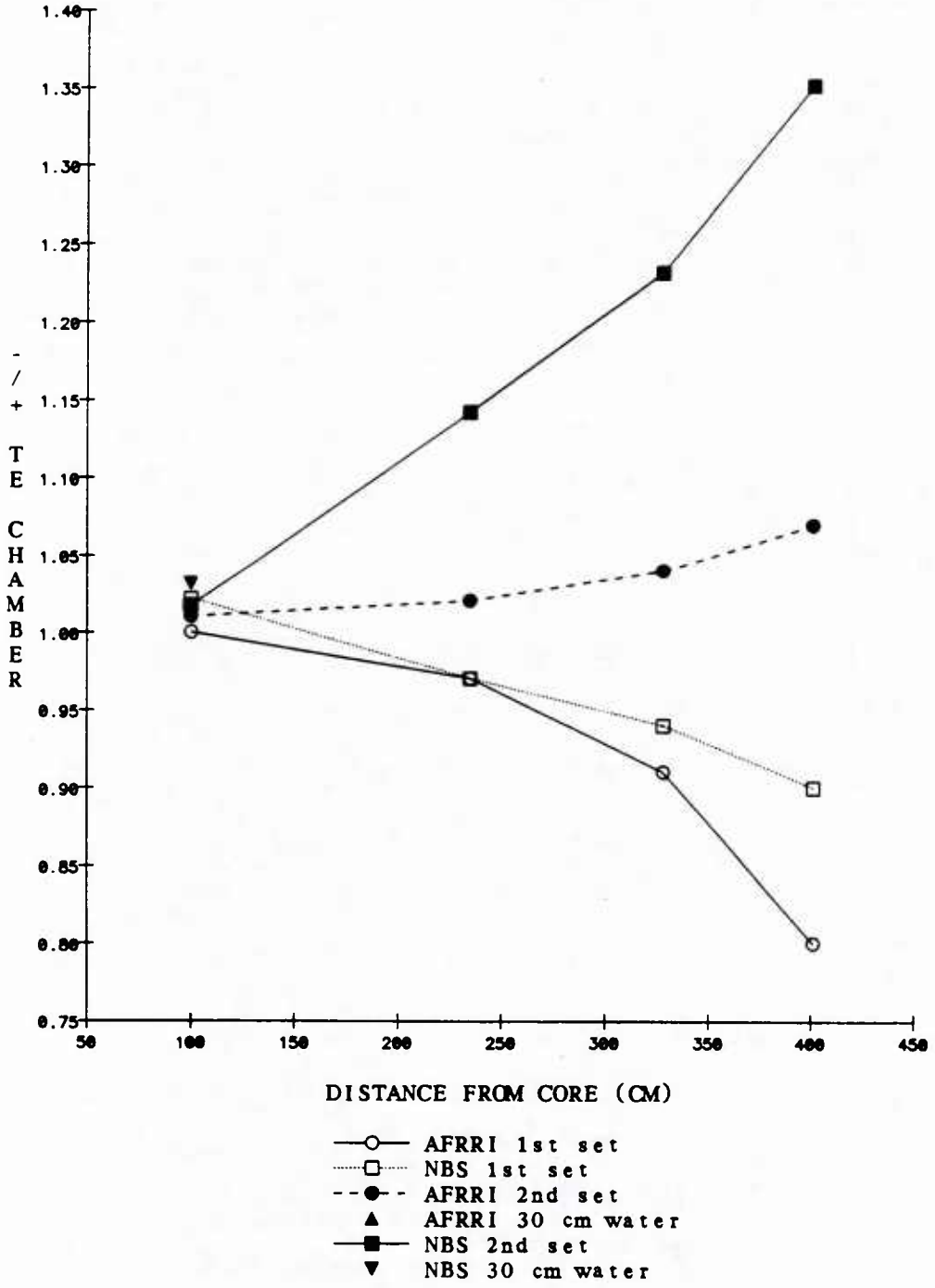

Figure 15. TE chamber polarity effects in bare room and with 30-cm-water shield

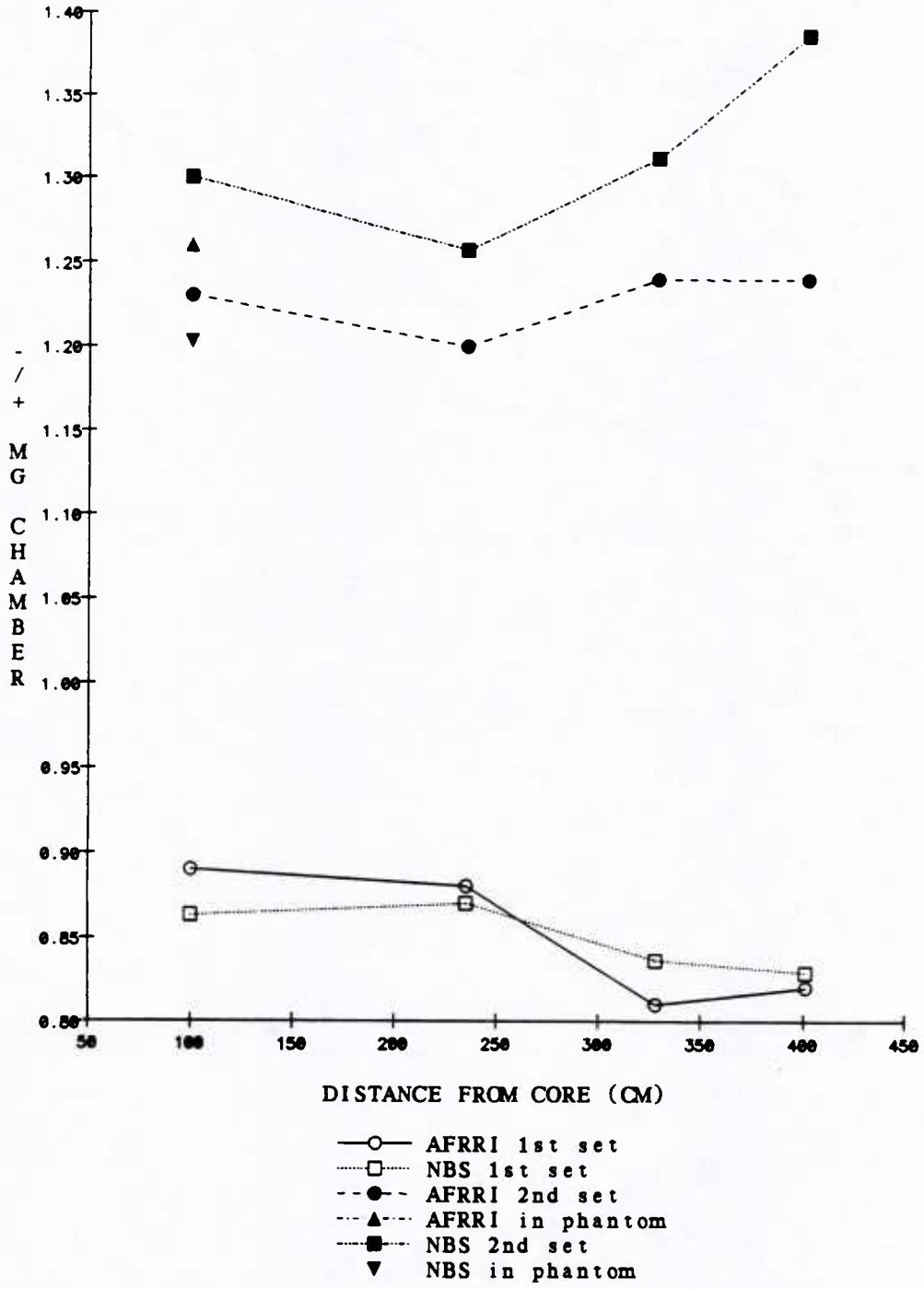

Figure 16. MG chamber polarity effects with 15-cm-Pb shield

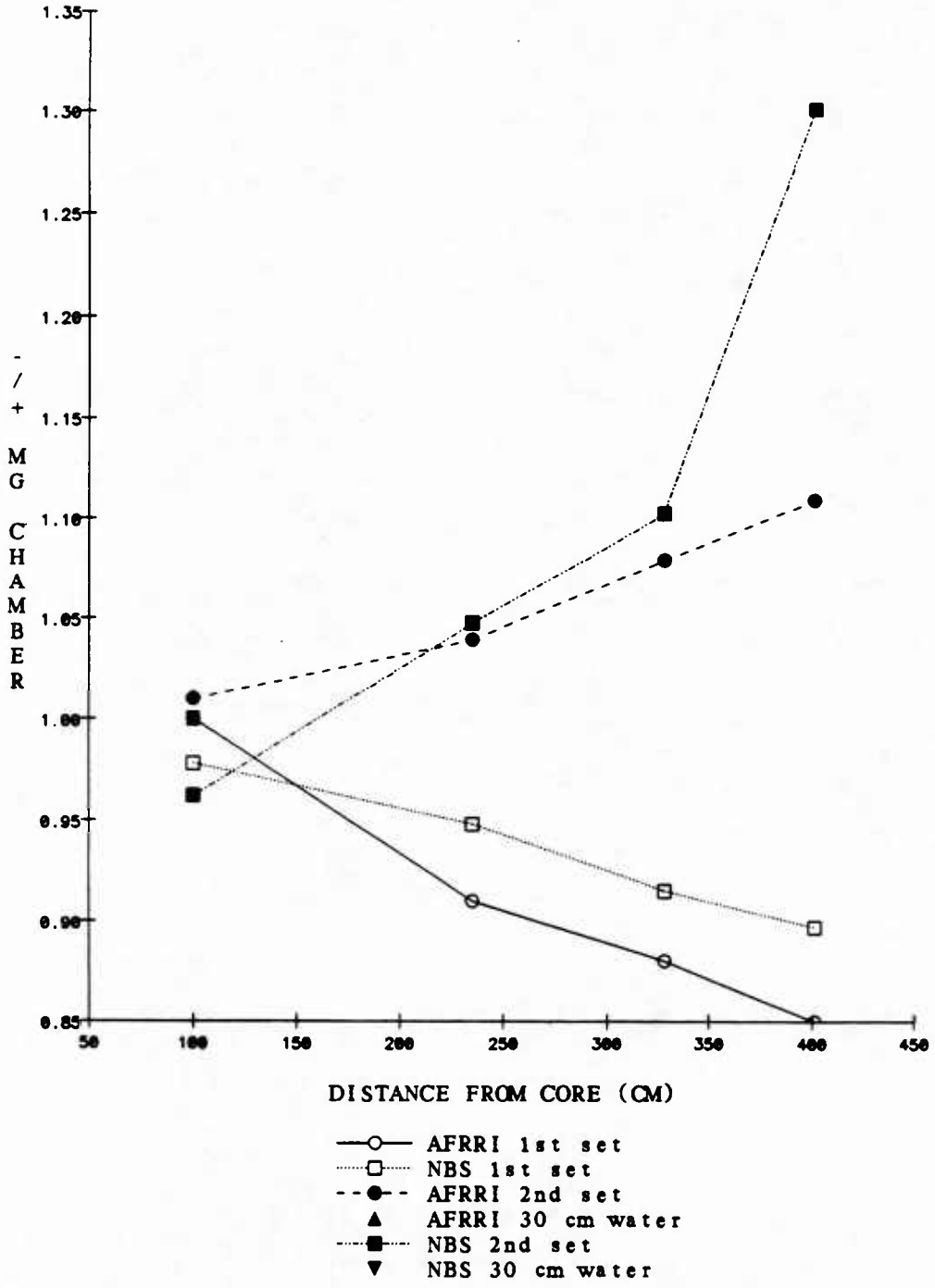

Figure 17. MG chamber polarity effects in bare room and with 30-cm-water shield

APPENDIX E. DRIFT DATA

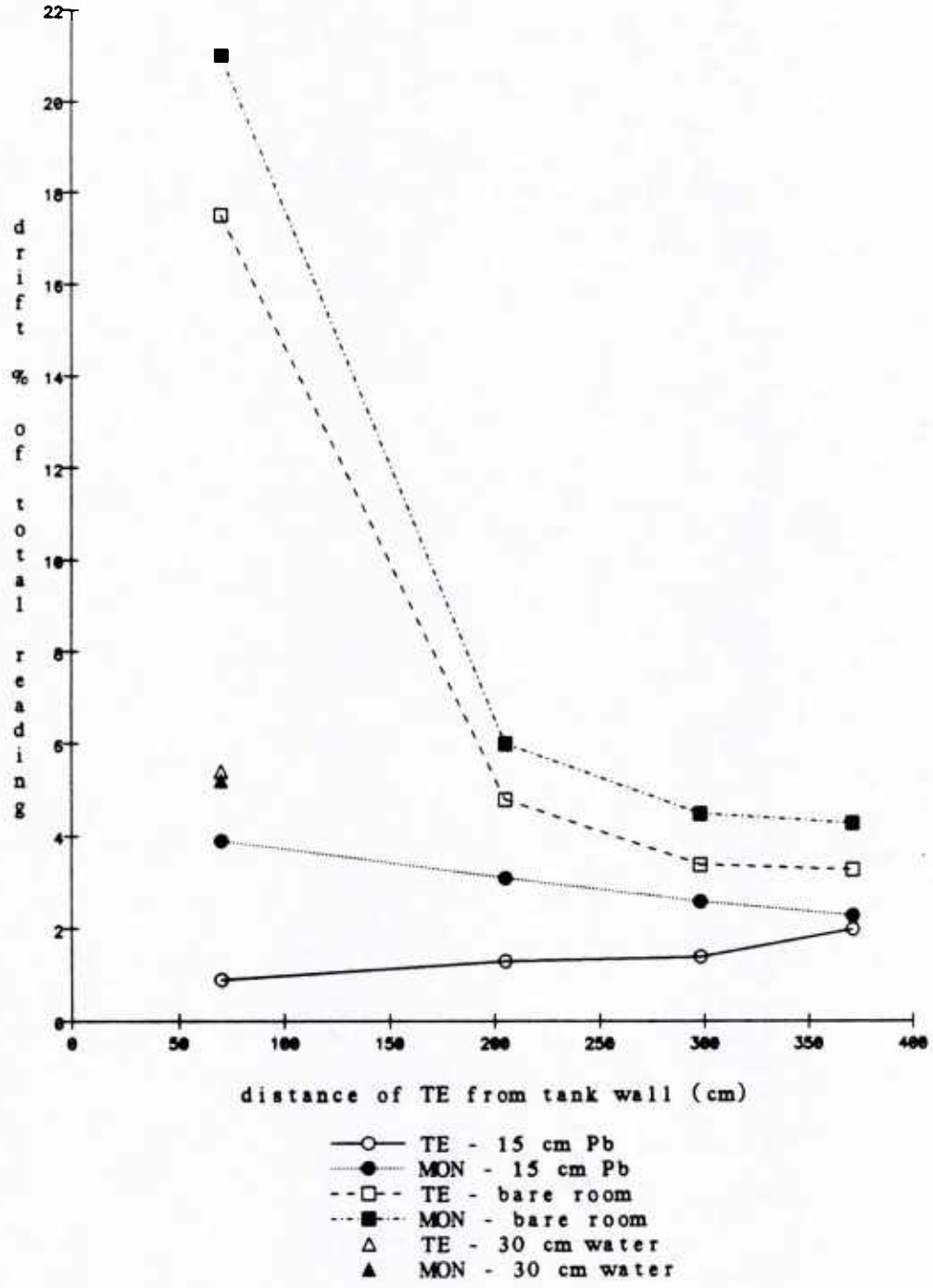

Figure 18. TE and monitor chambers drift data

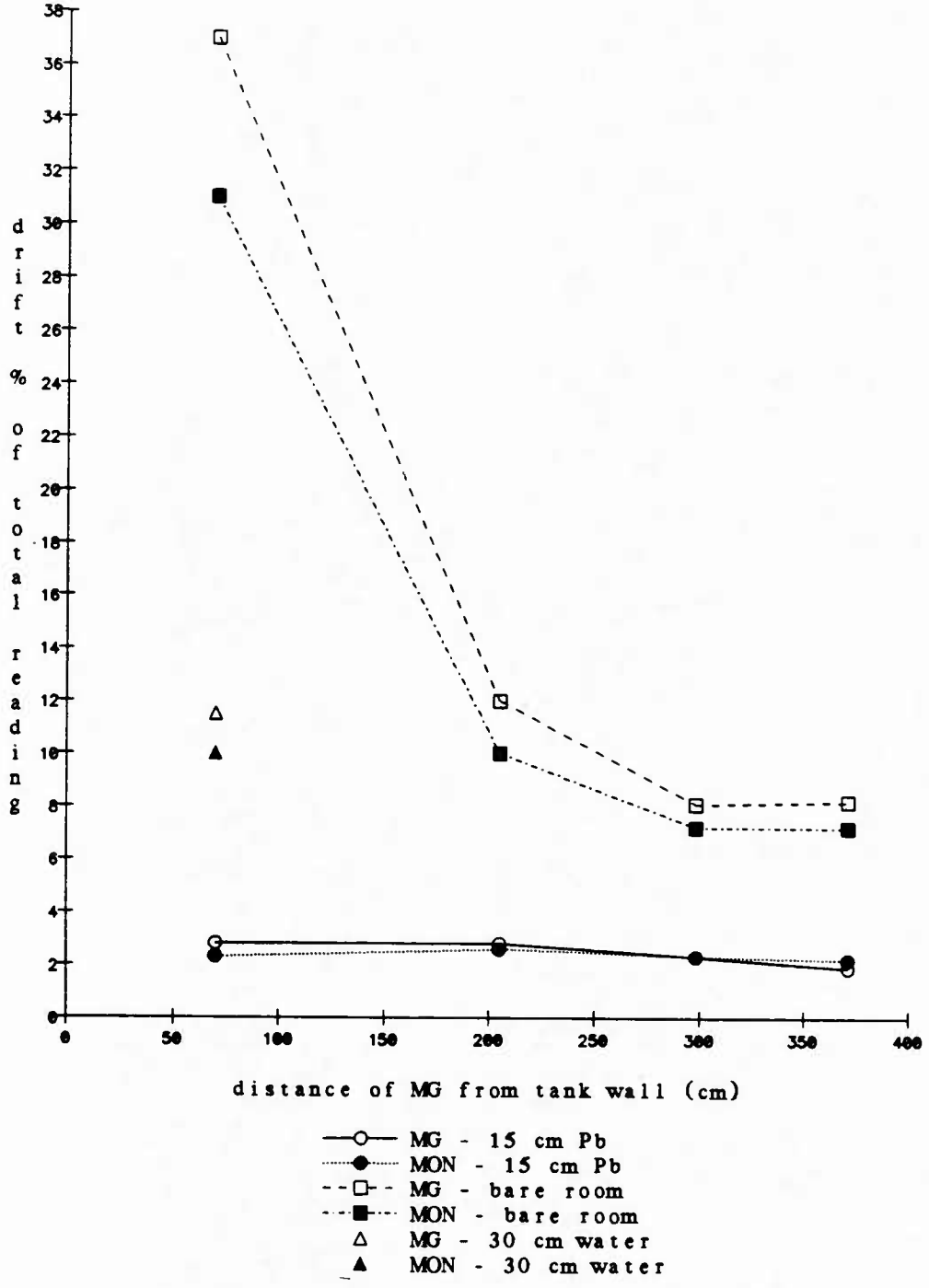

Figure 19. Mg and monitor chambers drift data

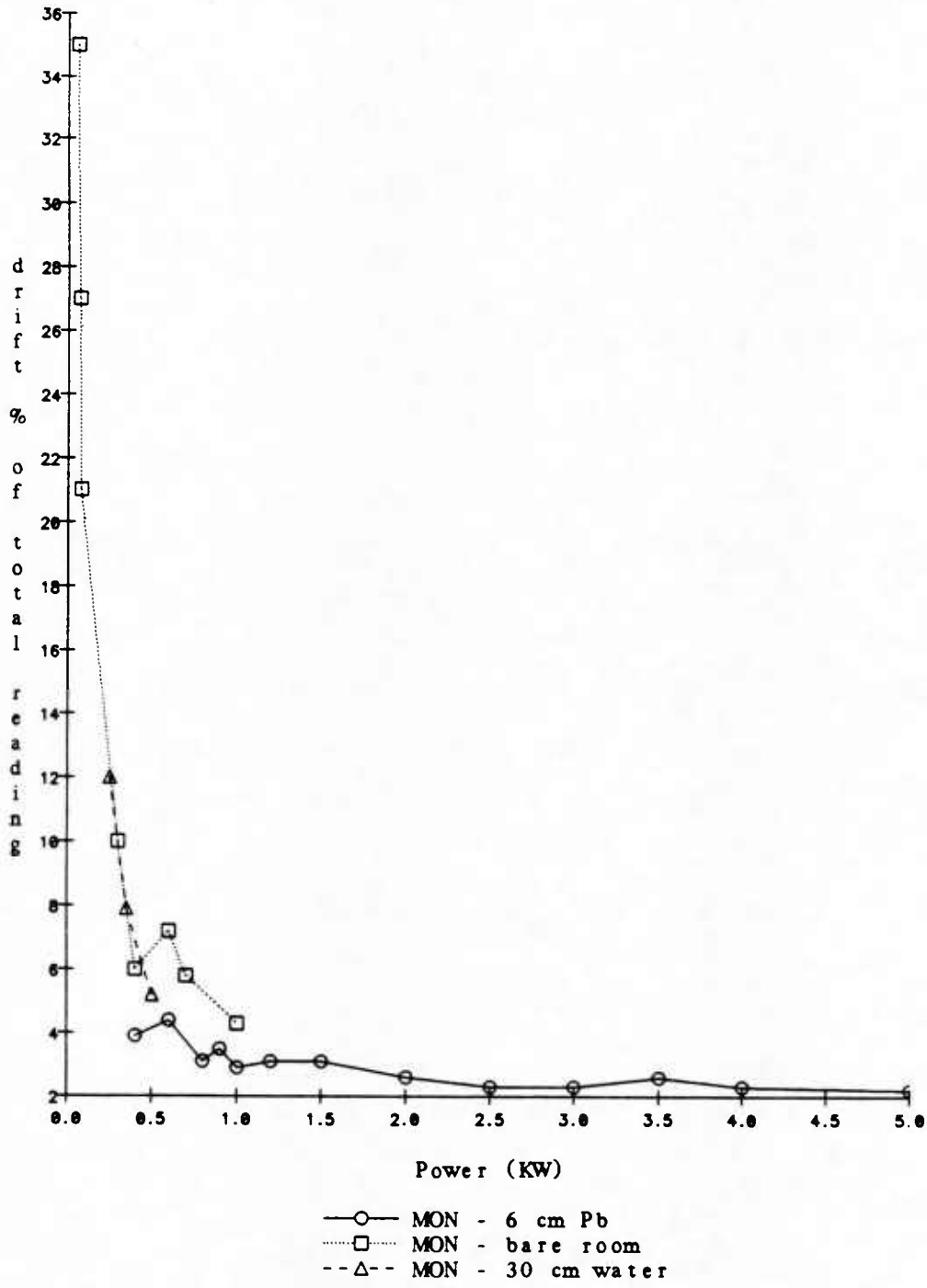

Figure 20. Monitor chamber drift versus reactor power

Table 8. Chamber Drift Data

Configuration	Distance From Tank Wall (cm)	Power (kW)	Drift (% of Total Reading)			Post/Pre*		
			TE	Mg	Monitor	TE	Mg	Monitor
15 cm Pb	70	0.4	0.9		3.9	5.0		2.8
	101	0.6	1.1		3.9	3.9		2.8
	205	1.5	1.3		3.1	4.1		4.0
	298	2.0	1.4		2.6	3.0		7.5
	371	3.0	2.0		2.3	2.3		9.3
In phantom	70	0.9	1.0		3.5	3.5		4.5
15 cm Pb	70	2.5		2.8	2.2		5.7	7.7
	205	3.5		2.8	2.6		11.0	9.7
	298	4.0		2.3	2.3		16.0	8.0
	371	5.0		1.9	2.2		7.4	10.0
In phantom	70	1.5		1.9	3.5		6.9	4.5
Bare room	70	0.08	18.0		21.0	1.2		1.2
	205	0.40	4.8		6.0	2.6		2.3
	298	0.70	3.4		4.5	3.4		3.0
	371	1.00	3.3		4.3	4.0		3.7
30 cm water	70	5.00	5.4		5.2	2.8		2.7
Bare room	70	0.06		41.0	35.0		1.1	1.1
	70	0.07		33.0	27.0		1.1	1.1
	205	0.30		12.0	10.0		1.6	1.7
	298	0.60		8.1	7.2		1.9	2.1
	371	0.70		8.2	7.2		1.8	2.1
30 cm water	70	0.25		14.0	12.0		1.5	1.5
	70	0.35		9.0	7.9		2.1	1.9

*Ratio of postirradiation drift to preirradiation drift

REFERENCES

1. An international neutron dosimetry intercomparison. ICRU Report 27. International Commission on Radiation Units and Measurements, Washington, DC, 1978.

2. Average energy required to produce an ion pair. ICRU Report 31. International Commission on Radiation Units and Measurements, Washington, DC, 1979.

3. Waterman, F. M., Kuchnir, F. T., Skaggs, L. S, Kouzes, R. T., and Moore, W. H. Energy dependence of the neutron sensitivity of C-CO_2, Mg-Ar, and TE-TE ionization chambers. Physical Medical Biology 24: 721-733, 1979.

4. Goodman, L. J., and Coyne, J. J. W_n and neutron kerma for methane-based tissue-equivalent gas. Radiation Research 82: 13-26, 1980.

5. Mijnheer, B. J. The relative neutron sensitivity, k_u, for non-hydrogenous detectors. In: Ion Chambers for Neutron Dosimetry. CEC Report EUR 6782 EN. Broerse, J. J., ed. Harwood Academic Publishers, New York, 1980.

6. Caswell, R. S., Coyne, J. J., and Randolph, M. L. Kerma factors of elements and compounds for neutron energies below 30 MeV. International Journal of Applied Radiation Isotopes 33: 1227-1262, 1982.

7. Verbinski, V. V., Cassapakis, C. C., Hagan, W. K., Ferlic, K., and Daxon, E. Radiation field characterization for the AFRRI TRIGA reactor. Vol. I: Baseline data and evaluation of calculational data. DNA Report No. 5793F-1. Defense Nuclear Agency, Washington, DC, 1981.

8. Verbinski, V. V., Cassapakis, C. C., Hagan, W. K., Ferlic, K., and Daxon, E. Calculation of the neutron and gamma-ray environment in and around the AFRRI TRIGA reactor, Vol. II. DNA Report No. 5793F-2. Defense Nuclear Agency, Washington, DC, 1981.

9. Ferlic, K. P., and Zeman, G. H. Spectrum-averaged kerma factors for reactor dosimetry with paired ion chambers. Technical Report TR83-2. Armed Forces Radiobiology Research Institute, Bethesda, Maryland, 1983.

10. Neutron dosimetry for biology and medicine. ICRU Report 26. International Commission on Radiation Units and Measurements, Washington, DC, 1977.

11. Protocol for neutron beam dosimetry. AAPM Report No. 7 of Task Group 18, Fast Neutron Beam Physics. Radiation Therapy Committee, American Association of Physicists in Medicine, 1980.

12. Broerse, J. J., Mijnheer, B. J., and Williams, J. R. European protocol for neutron dosimetry for external beam therapy. British Journal of Radiology 54: 882-898, 1981.

13. Grundl, J. A., and Eisenhauer, C. M. Fission spectrum neutrons for cross section validation and neutron flux transfer. Proceedings of Conference on Nuclear Cross Sections and Technology, NBS Special Publication 425, US Department of Commerce, Washington, DC, March, 1975.

14. Grundl, J. A., and Eisenhauer, C. M. Compendium of benchmark neutron fields for reactor dosimetry, standard neutron field entries. NBS IR 85-3151, US Department of Commerce, Washington, DC, January, 1986.

15. Sholtis, J. A., Jr., and Moore, M. L. Reactor facility at Armed Forces Radiobiology Research Institute. Technical Report TR81-2. Armed Forces Radiobiology Research Institute, Bethesda, Maryland, 1981.

16. Sayeg, J. A. Neutron and gamma dosimetry measurements at the AFRRI-DASA TRIGA reactor. Contract Report CR65-6. Armed Forces Radiobiology Research Institute, Bethesda, Maryland, 1965.

17. Zeman, G. H., and Dooley, M. A. Performance and dosimetry of Theratron-80 cobalt-60 unit at Armed Forces Radiobiology Research Institute. Technical Report TR84-1. Armed Forces Radiobiology Research Institute, Bethesda, Maryland, 1984.

18. Wycoff, H. O. Reply to corrected f factors for photons from 10 KeV to 2 MeV. Medical Physics 10: 715-716, 1983.

19. Goodman, L. J. A practical guide to ionization chamber dosimetry at the AFRRI reactor. Contract Report CR85-1. Armed Forces Radiobiology Research Institute, Bethesda, Maryland, 1985.

20. Boag, J. W. Ionization chambers. In: Radiation Dosimetry, Vol. II. Attix, R. H., Roesch, W. C., and Tochilin, E., eds. Academic Press, New York, 1966, pp. 11-41.

21. Goodman, L. J., Coyne, J. J., Zoetelief, J., Broerse, J. J., and McDonald, J. C. Dosimetry of a lightly encapsulated Cf-252 source. Radiation Protection Dosimetry 4(2): 91-96, 1983.